NOAA Technical Memorandum NMFS-AFSC-357
doi:10.7289/V5/TM-AFSC-357

Model-based Essential Fish Habitat Definitions for Bering Sea Groundfish Species

E. A. Laman, C. N. Rooper, S. C. Rooney, K. A. Turner,
D. W. Cooper, and M. Zimmermann

U.S. DEPARTMENT OF COMMERCE
National Oceanic and Atmospheric Administration
National Marine Fisheries Service
Alaska Fisheries Science Center

July 2017

NOAA Technical Memorandum NMFS

The National Marine Fisheries Service's Alaska Fisheries Science Center uses the NOAA Technical Memorandum series to issue informal scientific and technical publications when complete formal review and editorial processing are not appropriate or feasible. Documents within this series reflect sound professional work and may be referenced in the formal scientific and technical literature.

The NMFS-AFSC Technical Memorandum series of the Alaska Fisheries Science Center continues the NMFS-F/NWC series established in 1970 by the Northwest Fisheries Center. The NMFS-NWFSC series is currently used by the Northwest Fisheries Science Center.

This document should be cited as follows:

> Laman, E. A., C. N. Rooper, S. C. Rooney, K. A. Turner, D. W. Cooper, and M. Zimmermann. 2017. Model-based essential fish habitat definitions for Bering Sea groundfish species. U.S. Dep. Commer., NOAA Tech. Memo. NMFS-AFSC-357, 265 p.
>
> Document available: https://www.afsc.noaa.gov/Publications/AFSC-TM/NOAA-TM-AFSC-357.pdf

NOAA Technical Memorandum NMFS-AFSC-357
doi:10.7289/V5/TM-AFSC-357

Model-based Essential Fish Habitat Definitions for Bering Sea Groundfish Species

by
E. A. Laman, C. N. Rooper, S. C. Rooney, K. A. Turner,
D. W. Cooper, and M. Zimmermann

Resource Assessment and Conservation Engineering Division
Alaska Fisheries Science Center
7600 Sand Point Way NE
Seattle WA 98115

www.afsc.noaa.gov

U.S. DEPARTMENT OF COMMERCE
Wilbur L. Ross Jr., Secretary
National Oceanic and Atmospheric Administration
Benjamin Friedman, Acting Under Secretary and Administrator
National Marine Fisheries Service
Chris Oliver, Assistant Administrator for Fisheries

July 2017

This document is available to the public through:

National Technical Information Service
U.S. Department of Commerce
5285 Port Royal Road
Springfield, VA 22161

www.ntis.gov

ABSTRACT

Defining the essential habitat of federally managed fishes and invertebrates is an important step in managing groundfishes from Alaska. Species distribution models have been widely used in conservation biology and terrestrial systems to define the potential habitat for organisms of interest. The models themselves can take a number of forms, from relatively simple to more complex frameworks. We applied generalized additive and maximum entropy modeling to both fishery-independent and fishery-dependent data sets and defined the essential habitat of early (eggs, larvae, and pelagic juveniles) and later life stages (settled juveniles and adults) of over 30 federally managed species across all seasons in the eastern and northern Bering Sea. In general, sea surface temperature was an important predictor of ichthyoplankton distributions while geographic location and bottom depth were predominant habitat covariates describing the distribution of most crabs and adult fishes. Results from the species distribution models were used to synthesize maps identifying the spatial extent of essential fish habitat (EFH) for each species, life stage, and season. These maps represent quantitative links between species' distributions and their habitat, can be an aid to assessing anthropogenic impacts in Alaska's marine environment, and will be used for marine spatial planning.

CONTENTS

INTRODUCTION

The Magnuson-Stevens Fishery Conservation and Management Act (MSFCMA) mandates that the National Marine Fisheries Service (NMFS) identify habitats essential for managed species and conserve them from adverse effects of fishing and other anthropogenic activities. Essential fish habitat (EFH) is defined in the MSFCMA as "those waters and substrates necessary for fish to spawn, breed, feed or grow to maturity." As part of this mandate, EFH descriptions are necessary for all species listed under a Fishery Management Plan (FMP) in Alaska. In addition, these descriptions must be reviewed periodically to update species descriptions and EFH information from new data and research.

In Alaska, most EFH descriptions for groundfishes have been limited to qualitative statements on the distribution of adult life stages (i.e., based on presence-absence alone). These consist generally of EFH maps and written descriptions which can be improved by the use of species distribution models (SDM) that we detail here. The SDM approach demonstrated provides an opportunity to utilize previously unavailable data to create more empirically-derived and detailed maps depicting the distribution of species' life-history stages and season-specific habitat associations.

Species distribution models have been widely used in conservation biology and terrestrial systems to define the potential habitat for organisms of interest (e.g., Bio et al. 2002, Cutler et al. 2007, Elith et al. 2008, Kumar and Stohlgren 2009, Lozier et al. 2009), but have been less commonly applied in marine systems (e.g., DeLong and Collie 2004[1], Elith et al. 2011, Robinson et al. 2011, Sagarese et al. 2014). Recently, SDMs have been developed for coral and sponge species in the eastern Bering Sea, Gulf of Alaska, and Aleutian Islands (Rooper et al. 2014, Sigler et al. 2015, Rooper et al. 2016). These models can take a number of forms, from relatively simple frameworks such as generalized linear or additive

[1] DeLong, A. K., and J. S. Collie. 2004. Defining Essential Fish Habitat: A Model- Based Approach. Rhode Island Sea Grant, Narragansett, R.I. 4pp. Rhode Island Sea Grant Communications Office, University of Rhode Island Bay Campus, Narragansett, RI 02882-1197.

models to complex techniques like maximum entropy modeling. These SDMs can be used to predict potential habitat, probability of presence, or abundance.

In this study, the data used to parameterize the SDMs we employed shared common characteristics across the various models. The data consisted of independent predictor variables (habitat covariates) and a dependent response variables (e.g., larval presence, crab presence/absence, or fish abundance). Predictors were used to train the models and rasters of the habitat covariates were used to spatially predict abundance or probability of presence. Confidence bounds estimated around these predictions along with partitioning of the data produced test statistics used to evaluate the models' performance. The resulting maps, combined with the evaluation of the models' effectiveness, are important components of EFH descriptions that can pinpoint areas of high or low abundance, highlight local hotspots in the distributions, and inform future stock assessment models. Additionally, the formulation of the models provides a form of documentation that can frame the required text descriptions of EFH.

The objective of this study was to produce species distribution models for as many life stages and seasons as possible for all species of groundfishes and invertebrates subject to FMPs in the eastern Bering Sea (EBS) large marine ecosystem and the northern Bering Sea (NBS); accompanying reports will be generated for Aleutian Islands and Gulf of Alaska FMP taxa. The maps generated by these SDMs form the basis for describing EFH of FMP species in the EBS and NBS. We anticipate that the approach detailed here could form the basis for future EFH descriptions by providing a path to the integration of new data and studies while providing support for future stock assessments.

MATERIALS AND METHODS

Survey Area

The surveyed area described in this study is comprised of the eastern Bering Sea continental shelf and eastern Bering Sea upper continental slope, collectively known as the eastern Bering Sea large marine ecosystem (EBS), along with the northern Bering Sea (NBS) which is bounded by the shelf break and the U.S.-Russia Convention Line in the west, the Bering Strait in the north, Norton Sound in the east with its southerly extent just north of Nunivak Island (Fig. 1); the combination of these areas will be collectively referred to hereafter as the eastern Bering Sea (EBS). The continental shelf is shallow, flat, and comprised mostly of soft unconsolidated sediments with the majority of the seafloor at depths greater than 100 m. The upper continental slope (~200–1,200 m) is steep and encompasses five major canyon regions. The seafloor mosaic of the slope is more diverse than the shelf, with areas of rocky substrate (particularly in Pribilof Canyon) interspersed throughout the area which is otherwise dominated by soft unconsolidated sediments.

Survey Data

Data detailing the distribution and abundance of fishes and invertebrates in the EBS came from three different sources. The distribution data for the early life history stages (ELHS) of fishes (eggs, larvae, and pelagic juveniles) were supplied by the Ecosystems and Fisheries-Oceanography Coordinated Investigations (EcoFOCI) ichthyoplankton surveys from their ECODAAT database; species-specific ichthyoplankton data sets were separated into oceanographic seasons based on presence of ELHS in the water column. EcoFOCI is a joint research program between the Alaska Fisheries Science Center (AFSC) and Pacific Marine Environmental Laboratory (PMEL). Distributions of settled juvenile and adult stages were modeled using the AFSC's Resource Assessment and Conservation Engineering Division Groundfish Assessment Program's (RACE-GAP) summer bottom trawl surveys of the EBS from RACEBase database. The fall, winter, and spring distributions of what we assumed were primarily adult

animals were modeled using commercial catches from the Alaska Regional Office's (AKRO) fishery observer program VMS-Observer Enabled Catch-in-Areas database (VOE-CIA). Seasonal data were divided into fall (October-November), winter (December-February), spring (March-May), and summer (June-September). All fishes and invertebrates examined were separated into generic, species, or broader taxonomic groupings and then parsed into ontogenetic stages where prevalence and *a priori* sampling considerations were used to determine which species distribution modeling approach was applied to each data source, taxon, life stage, and season (Table 1).

Recruitment Processes Data

Ichthyoplankton catches at 24,505 EcoFOCI recruitment processes survey stations in the EBS (Fig. 2) were provided from the program's ECODAAT database were used in species distribution modeling. For our analyses, we included catches from 1991 through 2013. These data were collected in pursuit of a variety of survey objectives, often opportunistically, and on several different types of surveys (Matarese et al. 2003). Sampling design, gear type, mesh size, and seasonality varied during the history of these surveys as well. Collection methods included bongo nets, MOCNESS tows, Methot and Tucker trawls, egg pumps, and surface nets (De Forest et al. 2014). Over the years examined, all twelve months of the year were sampled. These ichthyoplankton collections were not uniformly spatially distributed and most samples came from the southwestern Bering Sea shelf which reflects the historic focus on pollock recruitment mechanisms during this time period. Additional factors such as weather and seasonal sea-ice extent likely also influenced the spatial sampling patterns observed in this time series. Inter-annual differences in survey design and coverage as well as species-season-life stage prevalence combined with our intent to generate a single ELHS EFH map for each species' life stages based on average conditions predicated combining all years of recruitment processes data for our analyses.

Temporal periodicity and prevalence of each taxon's ELHS was determined from the recruitment processes data (Table 2). Oceanographic seasonality for taxa and life stages present was defined by the months when they were present in the water column. Prevalence was used to determine whether there

were sufficient data to model distribution. There had to be 50 or more presence observations for a taxon-life stage combination to qualify for species distribution modeling.

Groundfish Bottom Trawl Survey Data

RACE-GAP has conducted fisheries-independent bottom-trawl surveys in the EBS since the 1940s, but the first systematic survey was conducted in 1975 (Lauth and Conner 2014); survey methodology and trawl gear became standardized in 1982. Since then, these bottom trawl surveys have been conducted annually during the summer under a rigorous and repeatable statistical sampling design. We included trawl survey data from 1982 through 2014 in our analyses, but the window of informative survey results varied by species due to the evolution of species identification and taxonomy. The eastern Bering Sea shelf survey has been conducted annually on a regular 20 nautical mile (nmi) grid that has recently (2010) been extended to include the northern Bering Sea and Norton Sound (Lauth 2011). The eastern Bering Sea slope survey began in 2000, is quasi-biennial (no survey took place in 2006 or 2014), and has been conducted on the upper continental shelf and slope at depths from 200 to 1,200 m (Hoff and Britt 2011). The slope survey randomly samples existing stations within depth and area strata and the sampling frame grows each survey year with the addition of new stations. RACE-GAP bottom trawl data were combined across the EBS for all survey years inclusive since 1982. This approach was driven by our desire to generate a single EFH map based on average conditions and representative of a wide range of conditions. When parameterizing the species distribution models from the groundfish bottom trawl data (except in the case of maximum entropy models), we used habitat covariates (e.g., depth and temperature) collected in association with the catch so that the best-fitting models were trained on local conditions and incorporated inter-annual variability in these predictors.

The eastern and northern Bering Sea shelf and the EBS Slope surveys were conducted in compliance with national protocols (Stauffer 2004), but different trawl nets were employed on the shelf and slope. The shelf surveys used an 83-112 Eastern otter trawl with a 25.3 m (83 ft) headrope and 34.1 m

(112 ft) footrope towed behind 816 kg, 1.8 × 2.7 m, steel V-doors and paired 54.9 m (30 fathom) dandylines. Each lower dandyline has a 61 cm chain extension connected to the lower wing edge to improve bottom-tending. The eastern Bering Sea slope bottom trawl survey deploys a poly Nor'Eastern high-opening bottom trawl with 27.2 m headrope and a 24.2 m footrope configured with roller gear comprised of 20 cm rubber bobbins separated by 10 cm rubber disks with "flying wing" sections outboard. Both surveys targeted trawl haul durations of 30 minutes in contact with the bottom (a.k.a. "on bottom" configuration). Bottom contact, distance fished, and net dimensions were recorded during each Bering Sea survey trawl haul.

Groundfish bottom trawl data records were screened for inclusion in the SDMs. To qualify in the initial cut, trawl performance was satisfactory and the geographic position, distance fished, average bottom depth, and water temperature were recorded. Trawl hauls were satisfactory if the net opening was within a predetermined "normal" range, the footrope maintained contact with the seafloor, and the net suffered little or no damage during towing. A total of 12,702 bottom trawl survey hauls from the EBS met the criteria for initial inclusion in our analyses.

Bottom trawl survey catch abundance was standardized as catch-per-unit-effort (CPUE in units of no. ha^{-1}) using the area swept method (Alverson and Pereyra 1969) and computational approach of Wakabayashi et al. (1985). For catch processing at sea, all fishes and invertebrates caught in the trawl during a survey tow were sorted either by species or into broader taxonomic groups and their total weight (kg) and number in the catch were determined and recorded. Effort in the form of area swept was calculated from measured net width averaged over the trawl haul duration and multiplied by the distance fished derived from positioning data collected with a vessel-mounted GPS receiver. For some species, both juvenile and adult sizes were captured in trawl catches. For our analyses, an approximate length at maturity taken from extant literature (Table 3) was used to apportion the catches into settled juvenile and adult stages using proportionality from the random length subsample taken from the catch. For some species, only a subset of the available years was used for modeling due to changing confidence in our

ability to distinguish taxa over the time series. For example, arrowtooth and Kamchatka flounder were not confidently distinguished from each other on Bering Sea shelf surveys until around 1992 (Stevenson and Hoff 2009); only data since and including 1993 surveys were used to parameterize models these two species.

Commercial Catch Data

Distribution data collected by fishery observers aboard commercial fishing vessels (2003-2013) and stored in the VOE-CIA database were used to parameterize species distribution models for species caught in commercial catches during the fall, winter, and spring seasons (Table 4). Summer VOE-CIA data were not included in our analyses because summer distributions were modeled from RACE-GAP groundfish bottom trawl survey data. The VOE-CIA data were provided by John V. Olson and Steve Lewis (AKRO). Species presence from observed catches, regardless of the type of fishing gear, was combined across years for our analyses. These presence-only data were used to parameterize maximum entropy species distribution models if the number of presence observations for a species exceeded 50. The fishes and invertebrates recorded by fishery observers were assumed to be adult life history stages since the commercial fisheries typically target mature animals. Because commercial fisheries by definition focus their effort on their target species, the distribution of catches is mainly dependent upon the fishing activity. In other words, instead of being a regular survey conducted over a regular grid, these catch presence observations are typically clustered around areas of high catches for a target species (e.g., walleye pollock). As such, the resulting species distribution models should be viewed with some caution compared to the models informed by fishery-independent data.

Habitat Covariates

The independent covariates used to parameterize and then select the best-fitting SDMs were chosen from a suite of habitat covariates typically collected on the bottom trawl survey plus some derived and modeled variables (Table 6, Figs. 3 and 4). Observed, derived, or modeled point values were

interpolated to regular spatial grids (rasters) on scales ranging from 100 × 100 m to 1 × 1 km using inverse distance weighting (Watson and Philip 1985) or ordinary kriging (Venables and Ripley 2002) with an exponential semi-variogram model. The potential for an independent habitat covariate to influence the distribution of the life stages of the fishes and invertebrates in the region was considered when identifying which predictors to include in the initial model formulations. For example, ELHS of *Atheresthes* spp. are released to and complete much of their development in the water column. Therefore, surface water temperature, surface current speed, and surface current direction were among the covariates chosen to parameterize the ELHS models. Additionally, surface current direction variability was considered an indication of potential eddy vorticity and was incorporated into these models. The covariates describing surface currents and temperature were derived from the regional ocean modeling system (ROMS) run for the period 1969-2005 (Danielson et al. 2011). Monthly data originated from a 10 × 10 km grid. The ROMS modeled data used were temporally synched to the months when the ELHS were present in the water column. For example, *Atheresthes* spp. larvae were collected on EcoFOCI ichthyoplankton surveys in the EBS from February until September, so the ROMS data from these months were input to the SDM.

We tested collinearity amongst the habitat covariates as a precursor to including them in the species distribution models (Table 5). The largest correlations between latitude and longitude ($r = 0.60$) resulted in combining geographic position into a bivariate interaction term for inclusion in the abundance models. Variance inflation factors were calculated using the method of Zuur et al. (2009) for each of the covariates considered as model inputs and they ranged from 1.05 to 3.41. These values were all acceptable (below 5.0) and the habitat covariates were included in the models of habitat suitability, presence or absence, and fish or invertebrate abundance in the EBS.

Ichthyoplankton Surveys

We used seven habitat descriptors to parameterize ELHS SDMs (Table 6). These independent predictors included environmental variables typically collected during oceanographic surveys as well as

derived and modeled covariates. The independent predictors in the SDMs were populated with measured, derived, and modeled covariates, but spatial predictions generated by the best-fitting models utilized derived or modeled raster surfaces as input. Derived habitat covariates consist of geo-referenced surfaces (rasters or maps) like local slope which is inferred from depth changes. These rasters generally consist of a matrix of cells organized into a grid where each cell contains a value representing information (e.g., local slope or surface current speed). Interpolated raster surfaces were based on extrapolation from point measures or modeled values such as satellite ocean color or maximum tidal current speed. The habitat covariates selected to parameterize the species distribution models were chosen both for their availability and for their potential influence on the distribution of fishes and invertebrates based on previous studies. Due to the pelagic nature of these ELHS, surface water temperature, surface current speed, and surface current direction were chosen as habitat covariates because of their potential to explain early life history distributions. Additionally, surface current direction variability was included as an indication of potential eddy vorticity or other current variability processes that might be present. All of these surface current-related variables were provided by A. Hermann and derived from ROMS model runs over the period 1969-2005 (in Danielson et al. 2011). The initial data values were derived monthly on a 10 km × 10 km grid and were then interpolated via inverse distance weighting to a 1 km × 1 km grid for our species distribution modeling and summarized by season (Fig. 3).

In addition to the ROMS current variables described above, depth, local slope, and ocean color were included when parameterizing distribution models for ichthyoplankton species (Fig. 3). Because ichthyoplankton samples were collected from a variety of different depths, we used a bathymetry raster produced by Steve Lewis (AKRO) and Zimmermann (unpublished data) for the eastern Bering Sea for both parameterization of the species distribution models and for prediction of habitat from the best-fitting models. Zimmermann derived bathymetric point data from soundings available on National Ocean Service (NOS) smooth sheets that were digitized and compiled according to the methods in Zimmermann and Benson (2013). These point data were linearly interpolated from a triangular irregular network (TIN)

layer to a 100 m × 100 m raster grid and empty spaces were filled using data from AKRO. This interpolation was conducted using the Spatial Analyst package in ArcMAP software[2]. Local slope was derived from this bathymetry raster and calculated for each raster grid cell as the maximum change in elevation over the distance between the cell and its eight neighbors using the slope tool from the Spatial Analyst package in ArcMAP. Local slope was also computed from the 100 m × 100 m bathymetry raster using the *raster* package[3] in R (R Core Development Team 2013) and these two layers were averaged to a 1 km × 1 km grid to parameterize and predict species distribution for ELHS.

To represent average ocean productivity ($g \cdot C \cdot m^{-2} \cdot day^{-1}$) at each of the ichthyoplankton survey sites, we employed satellite-based moderate-resolution imaging spectroradiometer (MODIS) ocean color data for the five spring-summer months (May-September) that encapsulated the spring-summer phytoplankton blooms from 2003 to 2011 in the eastern Bering Sea region (Behrenfeld and Falkowski 1997). These data were downloaded from the Oregon State University's (OSU) Ocean Productivity website[4], were averaged by grid cell and month, and then averaged again by cell and year (to account for differences in the number of samples within each cell). The averages were then interpolated to a 1 km × 1 km raster grid using inverse distance weighting using the *raster* package[5] in R (R Core Development Team 2013).

Bottom Trawl Survey

Vessel position, bottom depth, and bottom temperature were collected at each bottom trawling site. A start and end position for the vessel during the on-bottom portion of the trawl were collected using the vessel-mounted GPS receiver. Vessel position was corrected for the position of the bottom trawl itself by triangulating how far the net was behind the vessel (based on the seafloor depth and the wire out) and

[2] ArcMap Desktop. Environmental Systems Research Institute. 2009. Redlands, CA:
[3] R v3.0.1; Hijams, R.J., J. van Etten, M. Mattiuzzi, M. Sumner, J.A. Greenberg, O.P., Lamigueiro, A. Bevan, E.B. Racine, and A. Shortridge. 2015. Geographic data analysis and modeling: package 'raster' version 2.3-24. 232 p.
[4] http://www.science.oregonstate.edu/ocean.productivity/
[5] R v3.0.1; Hijams, R.J., J. van Etten, M. Mattiuzzi, M. Sumner, J.A. Greenberg, O.P., Lamigueiro, A. Bevan, E.B. Racine, and A. Shortridge. 2015. Geographic data analysis and modeling: package 'raster' version 2.3-24. 232 p.

subtracting this distance from the vessel position in the direction of the bottom trawl haul. We assumed that the bottom trawl was directly behind the vessel during the tow and that all bottom trawl hauls were conducted in a straight line from the beginning point to the end point. The mid-point of the start and end positions of the trawl haul was used as the location variable in the modeling. The longitude and latitude data for each tow (and all other geographical data including the raster layers described below) were projected into Alaska Albers Equal Area Conic projection (center latitude = 50° N and center longitude = 154° W) and degrees of latitude and longitude were transformed into 100 m × 100 m square grids of eastings and northings for modeling. The location variable was used to capture any significant spatial trends in bottom trawl survey catches across the EBS.

Bottom depth and temperature were routinely collected for each trawl haul on the eastern Bering Sea bottom trawl surveys between 1982 and 2014, but different instruments were used to measure these values through the years (Buckley et al. 2009). From 1982 to 1990, depth and temperature were recorded as point values measured with expendable bathythermographs (XBTs). In 1993, the XBTs were replaced by the Brancker XL200 digital bathythermographic data logger (Richard Brancker Research, Ltd., Kanata, Ontario, Canada) which was mounted on the trawl net. With the advent of continuous temperature and depth recording at the trawl net, the survey began reporting on-bottom depth and temperature averaged over the trawl haul duration. Starting in 2004, the Brancker data logger was replaced by the SeaBird SBE-39 microbathythermograph (Sea-Bird Electronics, Inc., Bellevue, WA). The SBE-39 is attached to the headrope of the net and the averaged gear depth is added to the averaged measured net height to come up with average bottom depth during the trawl haul.

Depth and temperature measured at the trawl net were used as independent habitat covariates to parameterize the SDMs while rasters of these and other features (e.g., bathymetry, temperature, and local slope) were used primarily for prediction but occasionally for parameterization. The estimated slope derived from the bathymetry raster at each bottom trawl haul location was used as a habitat variable in the SDM, but the slope raster derived from bathymetry was used for prediction. Mean bottom temperatures

from each trawl haul were also interpolated to the 100 × 100 m grid of the eastern Bering Sea region using ordinary kriging (Venables and Ripley 2002) with an exponential semi-variogram model. The result was a single temperature raster layer that reflects the average temperature conditions on the bottom trawl surveys from 1982 to 2014. This raster layer of average temperature was used for prediction.

Two measures of water movement and its potential interaction with the seafloor were included as habitat covariates for modeling and prediction from the bottom trawl survey data. One variable was the maximum tidal current speed at the site of each bottom trawl haul. Tidal speeds were estimated for 368 consecutive days (January 1st, 2009 to January 3rd, 2010) using a tidal inversion program parameterized for the eastern Bering Sea on a 1 km × 1 km grid (Egbert and Erofeeva 2002). Their tidal prediction model was used to produce a series of one lunar year tidal currents for spring and neap cycles at each bottom trawl survey location. The maximum predicted tidal current speed for the series at the bottom trawl survey haul site was extracted and used to parameterize the distribution models. Maximum tidal current speed at each bottom trawl survey site was also interpolated over the EBS using ordinary kriging and an exponential semi-variogram (Venables and Ripley 2002) to interpolate a raster of maximum tidal current speed values on a 1 km × 1 km grid that was used for predictions. The second water movement variable was the predicted bottom water layer current speed from ROMS model runs from 1969-2005 (Danielson et al. 2011). This long-term current speed and direction were available as points on a 10 km × 10 km grid. The ROMS model was based on a three-dimensional grid with 60 depth tiers for each grid cell. For example, a point at 60 m water depth would have 60 depth bins at 1 m intervals, while a point at 120 m depth would have 60 depth bins at 2 m depth intervals, etc.). The bottom current speed and direction for the deepest depth bin at each point (closest to the seafloor) was used in our analyses. These regularly spaced data were interpolated to a 100 m × 100 m raster grid covering the EBS using inverse distance weighting (Fig. 4). Point values of bottom current speed were extracted from this raster layer at each of the bottom trawl survey haul locations and the mean current speed value computed for the

path of each bottom trawl survey tow. The interpolated bottom current speed raster was also as input to the best-fitting species distribution models for spatial predictions.

Average ocean productivity ($g \cdot C \cdot m^{-2} \cdot day^{-1}$) at each of the bottom trawl survey sites was extracted from the ocean color raster to parameterize the SDMs. Similar to its inclusion in the ELHS models above, we used MODIS ocean color data for 5 spring-summer months (May-September) that encompassed the spring and summer phytoplankton blooms over 8 years (2003-2011) for the EBS (Behrenfeld and Falkowski 2007). The ocean color data downloaded from OSU's Ocean Productivity website were averaged by cell and month and then averaged again by cell and year (to account for differences in the number of samples within each cell). The averages were then interpolated to a 1 km × 1 km raster grid using inverse distance weighting using the *raster* package[6] in R (R Core Development Team 2013; Fig. 4). The complete raster of ocean productivity was the input to the best-fitting species distribution models when producing spatial predictions.

Sediment grain size from the Eastern Bering Sea Sediment Database (EBSSED; Smith and McConnaughey 1999) and the National Geophysical Data Center Seafloor Sediment Grain Size database[7] was used as a predictor variable for the bottom trawl survey catches, but not for the ELHS models. Mean grain size (mm) is expressed as "phi" which is a negative $\log_2$-transform of grain size (e.g., a large phi-value indicates fine grains). The sampling tools for this sediment information are bottom grabs and corers which do not distinguish boulder or bedrock habitat. A consequence of this sampling program is that boulder and bedrock habitats are implicitly excluded from our analyses. The grain size and sorting values from the sediment data (n = 803) were kriged using an exponential model (Venables and Ripley 2002) which was the best fit to the semi-variogram of both grain size and sorting values.

[6] R v3.0.1; Hijams, R.J., J. van Etten, M. Mattiuzzi, M. Sumner, J.A. Greenberg, O.P., Lamigueiro, A. Bevan, E.B. Racine, and A. Shortridge. 2015. Geographic data analysis and modeling: package 'raster' version 2.3-24. 232 p.
[7] ngdc.noaa.gov/geosamples/metadata.jsp?g=G00127.

The biogenic habitat covariates included in bottom trawl survey SDMs were the concurrent catches of structure forming invertebrates (corals, sponges, and pennatulaceans). The binomial (presence or absence) factor for each of these categories of invertebrates was a used as a habitat covariate in the models. Complete raster surfaces from distribution models for each of these structure-forming invertebrates (Rooper et al. 2016) were used as input to the best-fitting species distribution models for spatial predictions.

Commercial Fisheries VOE-CIA Observer Data

Species distributions were also described from presence-only data collected by NMFS's Observer Program in Alaska. The same habitat covariates used to parameterize models based on the bottom trawl survey data were used to parameterize the observer catch data (VOE-CIA) models. The exception to this rule was that the structure forming invertebrate presence-absence factors were not included in commercial observer data models.

Modeling Methods -- Recruitment Processes Data

Maximum entropy modeling (MaxEnt; Phillips et al. 2006, Elith et al. 2011) was used to predict species distribution for ELHS of fishes collected on EcoFOCI ichthyoplankton surveys of the EBS. MaxEnt modeling was implemented in R software using the *dismo* package[8]. A minimum prevalence of 50 presence observations was required to use the MaxEnt model. These models used only presence observations and predicted the probability of suitable habitat from raster grids of habitat covariates and point observations of presence (i.e., given the depth, temperature, slope, and current speed at a grid cell where the species and life-stage of interest was present – what is the probability that these were suitable conditions for that species?). Note that since predictions are made from a raster grid that geographic location is implicit in the results from MaxEnt models.

[8] R, v3.0.1; Hijams, R.J., S. Phillips, J. Leathwick, and J. Elith. 2014. Species distribution modeling: package 'dismo' version 1.0-5. 65 p.

Modeling Methods -- Bottom Trawl Survey Data

Three types of distribution modeling were used to predict species distribution from RACE-GAP summer bottom trawl survey data. The choice of model was based on the prevalence of each species in the overall survey. For species that occurred in greater than 30% of bottom trawl hauls, such as arrowtooth flounder (Table 3), the best-fitting standard generalized additive model (GAM; Hastie and Tibshirani 1990) describing the 4^{th}-root transformed CPUE was identified through backward stepwise term selection and the resulting model was used to make spatial predictions of species distribution. Generalized additive models were applied to the trawl data using the *mgcv* package[9] in R. For each habitat covariate, the basis degrees of freedom used in the smoothing function were limited to ≤ 4 for univariate variables and ≤ 30 for the bivariate term (geographic location). To identify the best-fitting GAM, insignificant terms were sequentially removed until the Akaike Information Criterion (AIC) was minimized (Wood 2006). For each species, the formulation with the lowest AIC score was deemed the best-fitting model and used for further prediction and validation. For species where frequency of occurrence was between 10% and 30%, a hurdle model (hGAM) was used (Cragg 1971, Potts and Elith 2006) to predict species distribution. Hurdle models predict the spatial distribution of abundance in three stages: 1) probability of presence is predicted from presence-absence data using the best-fitting GAM and binomial distribution for each species; 2) a threshold presence probability is determined that defines presence or absence of the species; and 3) a conditional GAM is constructed that predicts a species' abundance by modeling the fourth-root transformed CPUE data from the bottom trawl survey at locations where the probability of presence was predicted to meet or exceed the threshold established in step 2 above. As was done for the standard GAM's above, the basis degrees of freedom used in the smoothing function were limited and insignificant terms were sequentially removed to minimize the AIC and

[9] R, v3.0.1; Wood, S. 2014. Mixed GAM computation vehicle with GCV/AIC/REML smoothness estimation: package 'mgcv' version 1.8-4. 243 p.

determine the best-fitting model. For species with less than 10% frequency of occurrence, but greater than 50 presence observations, the MaxEnt model was used to describe the probability of suitable habitat.

For all species distribution models, separate training (80%) and testing (20%) data sets were randomly selected from the data. The training and testing data sets were selected before modeling began and remained the same during analyses of each data class. The larger (80%) segment of data was used to train the model of choice while the remaining 20% was used to test and validate the model fit.

Modeling Methods -- Commercial Catch (Observer) Data

MaxEnt modeling was used to estimate species distribution from commercial fishery catch observer data from the VOE-CIA database. As above, MaxEnt was implemented in R software (R Core Development Team, 2013) using the *dismo* package. MaxEnt models use only presence observations and are based on raster grids of habitat covariates and point observations of presence so that geographic location is implicit in the MaxEnt results. As with the other models, separate training (80%) and testing (20%) data were randomly selected for MaxEnt model and the testing data were used to assess model performance.

Modeling Methods -- Model Validation

To test the performance of the best-fitting models, the predictions were compared to the observations. For presence and presence-absence models the area under the receiver operating characteristic curve (AUC) was computed to judge model performance. The AUC calculates the probability that a randomly chosen presence observation would have a higher probability of presence than a randomly chosen absence observation using rank data. We used the scale of Hosmer and Lemeshow (2005)**,** where AUC value greater than 0.5 is estimated to be better than chance, a value greater than 0.7 is considered acceptable, and values greater than 0.8 and 0.9 are excellent and outstanding; we considered AUC values less than 0.5 to indicate models with

questionable predictive ability. Confidence intervals for the AUC (95%) were calculated according to the methodology of DeLong et al. (1988). The performance of abundance models (i.e., generalized additive models) was directly tested by correlating predictions with observations; correlations less than 0.5 were considered to be marginal and less than 0.3 were considered poor. Model testing was also performed on 20% of the data withheld at random, using the same metrics. Because of space limitations, figures displaying the model validation results were not shown here. Deviations from assumptions or models with questionable predictive power were highlighted and considered to be loci where the robustness of model predictions was uncertain.

Modeling Methods -- Essential Fish Habitat Maps

Maps of essential fish habitat were produced for each species, life history stage, and season from predictions of the distribution of suitable habitat (for species where MaxEnt was used) or predictions of the distribution of abundance (for species where CPUE was modeled using either a GAM or hGAM). These maps were produced as quantiles of the population of predictions. For each map, 300,000 model prediction points were randomly sampled from the raster surface. These values were then ordered by cumulative distribution and zero abundance values and probabilities of suitable habitat less than 0.05 were removed. Four population quantiles were selected from these cumulative distributions (5%, 25%, 50%, and 75%). These quantiles were then used as break points to translate the model predictions (maps of suitable habitat or abundance) to map the distribution of categories of the amount of the species abundance or suitable habitat. For example, where the 5% quantile of species A was 0.024 individuals/ha, this meant that 95% of the population occurred at values greater than 0.024. Similarly, a 75% quantile of species A at 2.1 individuals/ha meant that values above 2.1 represented the top 25% of the

population proportion, or the predicted highest abundance areas. The four categories for each species, life history stage, and season were mapped to show the distribution of the areas containing 95%, 75%, 50%, and 25% of the population. It is important to note that these values were chosen somewhat arbitrarily (except 95% which is the current definition of EFH in Alaska), and other values could be equally appropriate.

Table 1. -- Life history stages of fishes and invertebrates collected on Ecosystems and Fisheries-Oceanography Cooperative Investigations ichthyoplankton surveys (EcoFOCI) and NMFS Alaska Fisheries Science Center Resource Assessment and Conservation Engineering-Groundfish Assessment Program summer bottom trawl surveys (RACE-GAP) of the eastern and northern Bering Sea indicating the species distribution modeling technique used to describe their distributions.

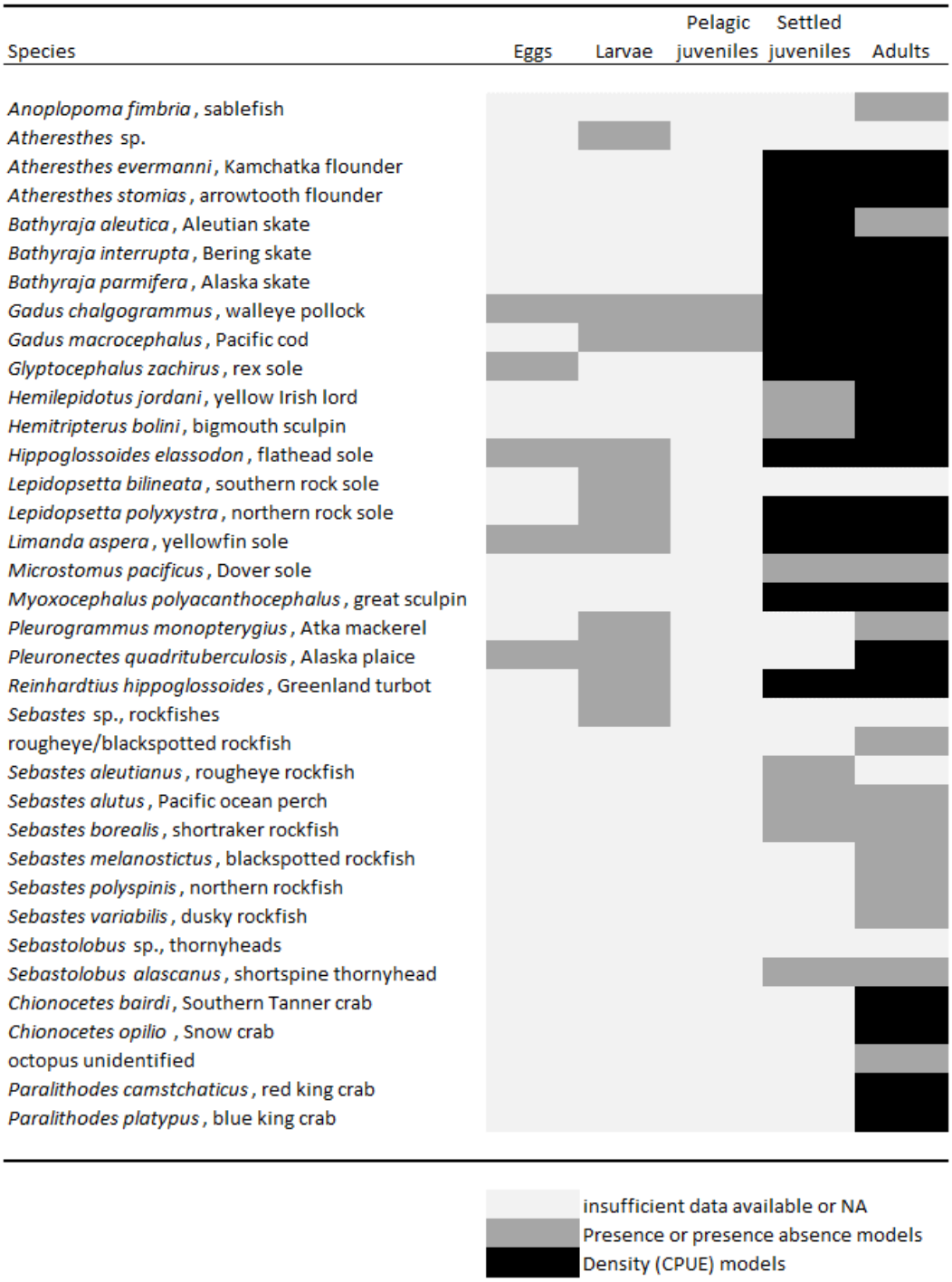

Table 2. -- Oceanographic seasons for early life history stages of taxa collected during Ecosystems and Fisheries-Oceanography Cooperative Investigations ichthyoplankton surveys (EcoFOCI) of the eastern and northern Bering Sea (1991-2013) were defined by months present in the water column; prevalence (number of presence observations) are indicated in parentheses.

Species	Eggs	Larvae	Pelagic juveniles
Atheresthes spp.	Feb - May (45)	Feb - Sept (537)	Jul - Sept (13)
rex sole (*Glyptocephalus zachirus*)	Feb - Sept (380)	Jun - Sept (34)	--
Dover sole (*Microstomus pacificus*)	Apr - Sept (31)	Jul (5)	--
flathead sole (*Hippoglossoides elassodon*)	Apr - Sept (1459)	Apr - Oct (718)	Jul - Sept (10)
yellowfin sole (*Limanda aspera*)	May - Oct (783)	Jul - Oct (481)	Sept (2)
southern rock sole (*Lepidopsetta bilineata*)	--	May - Sept (107)	--
northern rock sole (*Lepidopsetta polyxystra*)	--	April - Oct (1016)	Sept (2)
Alaska plaice (*Pleuronectes quadrituberculatus*)	Feb - Sept (1082)	May - Sept (275)	--
Greenland turbot (*Reinhardtius hippoglossoides*)	Feb - Mar (43)	Feb - Sept (235)	Jul - Sept (3)
walleye pollock (*Gadus chalcogramma*)	Feb - Oct (2646)	Feb - Sept (2145)	May - Oct (542)
Pacific cod (*Gadus macrocephalus*)	Apr - Jul (29)	Feb - Oct (376)	Jul - Sept (122)
sablefish (*Anoplopoma fimbria*)	Feb - May (16)	Feb - Aug (34)	Jul - Sept (6)
Atka mackerel (*Pleurogrammus monopterygius*)	--	Feb - Sept (151)	--
yellow Irish lord (*Hemilepidotus jordani*)	--	Feb - Sept (25)	May - July (25)
great sculpin (*Myoxocephalus polyacanthocephalus*)	--	July (1)	--
bigmouth sculpin (*Hemitripterus bolini*)	--	April (1)	--
rockfishes *(Sebastes* spp.)	--	Feb - Sept (738)	Sept (30)
thornyheads *(Sebastolobus* spp.)	June - Aug (5)	Aug (2)	--

Table 3. -- Taxa from RACE-GAP summer bottom trawl surveys that were used for species distribution modeling: the years included in the modeling efforts, the prevalence of settled juveniles and adults (frequency of occurrence) in the bottom trawl hauls, and the length at first maturity (presented here as the maximum juvenile length) with sources indicated; "All" years modeled = 1982-2014.

Species	Years modeled	% Prevalence of settled juveniles	% Prevalence of adults	Maximum juvenile length (cm)	Length@Maturity Source
Alaska plaice (*Pleuronectes quadrituberculatus*)	All	--	54.97	28	Tenbrink and Wilderbuer 2015
Alaska skate (*Bathyraja parmifera*)	1999-	69.68	52.22	92	Matta 2006
Aleutian skate (*Bathyraja aleutica*)	1999-	12.34	2.35	132	Ebert et al. 2007
arrowtooth flounder (*Atheresthes stomias*)	1992-	36.20	45.12	35	Zimmermann 1997
Atka mackerel (*Pleurogrammus monopterygius*)	All	--	0.48	25	Cooper et al. 2010
Bering skate (*Bathyraja interrupta*)	1999-	14.08	15.38	69	Ebert et al. 2007
bigmouth sculpin (*Hemitripterus bolini*)	All	5.06	8.90	51	Tenbrink and Hutchison (NPRB)
snow crab (*Chionoecetes opilio*)	All	--	68.94		Bush et al. 2013
blackspotted rockfish (*Sebastes melanostictus*)	2006-	1.21	1.52	43	Rooper 2008
southern Tanner crab (*Chionoecetes bairdi*)	All	--	59.40		Bush et al. 2013
red king crab (*Paralithodes camtschaticus*)	All	--	21.35		Bush et al. 2013
blue king crab (*Paralithodes platypus*)	All	--	10.70		Bush et al. 2013
Dover sole (*Microstomus pacificus*)	All	0.94	0.96	38	Abookire and Macewicz 2003
dusky rockfish (*Sebastes variabilis*)	1996-	--	0.39	29	Chilton 2010
flathead sole (*Hippoglossoides elassodon*)	All	50.43	66.19	25	Stark 2004
great sculpin (*Myoxocephalus polyacanthocephalus*)	2002-	31.53	21.39	51	Tenbrink and Hutchison 2009
Greenland turbot (*Reinhardtius hippoglossoides*)	All	19.00	11.70	65	Cooper et al. 2007
Kamchatka flounder (*Atheresthes evermanni*)	1992-	39.35	18.81	52	Stark 2012a
northern rock sole (*Lepidopsetta polyxystra*)	1996-	52.59	74.94	24	Stark 2012b
northern rockfish (*Sebastes polyspinis*)	All	--	0.54	25	Chilton 2007
octopus unidentified	All	--	4.05		
Pacific cod (*Gadus macrocephalus*)	All	72.46	80.43	46	Stark 2007
Pacific ocean perch (*Sebastes alutus*)	All	0.99	3.82	25	Rooper 2008
rex sole (*Glyptocephalus zachirus*)	All	5.45	15.40	24	Abookire 2005
rougheye rockfish (*Sebastes aleutianus*)	2006-	1.56	0.62	43	Rooper 2008
sablefish (*Anoplopoma fimbria*)	All	0.26	4.87	40	Hanselman pers comm
shortraker rockfish (*Sebastes borealis*)	All	0.69	1.19	44	Rooper 2008
shortspine thornyhead (*Sebastolobus alascanus*)	All	1.93	5.05	21	Rooper 2008
southern rock sole (*Lepidopsetta bilineata*)	1996-	0.22	0.36	24	Stark 2012b
walleye pollock (*Gadus chalcogramma*)	All	68.47	84.90	25	Stahl and Kruse 2008
yellow Irish lord (*Hemilepidotus jordani*)	All	1.09	5.44	22	Tenbrink and Buckley 2013
yellowfin sole (*Limanda aspera*)	All	53.64	60.74	25	Wakabayashi 1989

Species distribution modeling approach used:

Standard GAM model
Hurdle GAM model
Maximum entropy model

Table 4. -- Number of presence records by species and season in the VMS-Observer Enabled Catch-in-Areas commercial database (VOE-CIA) for the eastern and northern Bering Sea.

Species	Fall	Winter	Spring
Alaska plaice (*Pleuronectes quadrituberculatus*)	1236	10440	5388
Alaska skate (*Bathyraja parmifera*)	9427	11410	18391
Aleutian skate (*Bathyraja aleutica*)	1741	567	1776
arrowtooth flounder (*Atheresthes stomias*)	12572	10630	23700
Atka mackerel (*Pleurogrammus monopterygius*)	519	1027	1490
bigmouth sculpin (*Hemitripterus bolini*)	3469	2170	4479
blackspotted, rougheye rockfish (*Sebastes aleutianus, S. melanostictus*)	164	148	230
blue king crab (*Paralithodes platypus*)	225	91	86
Dover sole (*Microstomus pacificus*)	51	77	75
dusky rockfish (*Sebastes variabilis*)	446	238	467
flathead sole (*Hippoglossoides elassodon*)	12920	20231	34782
great sculpin (*Myoxocephalus polyacanthocephalus*)	738	1722	2437
Greenland turbot (*Reinhardtius hippoglossoides*)	2253	1599	1279
Kamchatka flounder (*Atheresthes evermanni*)	4123	3260	4182
northern rock sole (*Lepidopsetta polyxystra*)	3549	20079	20004
northern rockfish (*Sebastes polyspinis*)	557	359	429
octopus unidentified	823	626	1939
Pacific cod (*Gadus macrocephalus*)	14187	23888	38312
Pacific ocean perch (*Sebastes alutus*)	778	915	1966
red king crab (*Paralithodes camtschaticus*)	311	508	1669
rex sole (*Glyptocephalus zachirus*)	1659	4002	9469
sablefish (*Anoplopoma fimbria*)	693	545	770
shortraker rockfish (*Sebastes borealis*)	171	474	738
shortspine thornyhead (*Sebastolobus alascanus*)	174	811	1632
snow crab (*Chionoecetes opilio*)	4132	6390	6320
southern rock sole (*Lepidopsetta bilineata*)	267	3712	4899
southern Tanner crab (*Chionoecetes tanneri*)	1867	5601	6406
walleye pollock (*Gadus chalcogramma*)	15838	27189	44786
yellow Irish lord (*Hemilepidotus jordani*)	266	1412	1406
yellowfin sole (*Limanda aspera*)	4411	14134	15491

Table 5. -- Variance inflation factors amongst habitat covariates from the eastern and northern Bering Sea NMFS Alaska Fisheries Science Center Resource Assessment and Conservation Engineering-Groundfish Assessment Program summer bottom trawl surveys (RACE-GAP), VMS-Observer Enabled Catch-in-Areas commercial catch observations (VOE-CIA), and Ecosystems and Fisheries-Oceanography Cooperative Investigations ichthyoplankton surveys (EcoFOCI).

	Variance Inflation Factors (VIF)		
Variable	RACE-GAP	VOE-CIA	EcoFOCI
Depth	2.79	2.73	3.23
Slope	2.10	2.12	1.63
Temperature	1.65	1.73	
Ocean color	2.01	1.73	1.11
Current speed	1.68	1.23	
Tidal current	3.41	2.35	2.08
Phi	3.24	2.62	
Coral	1.10		
Sponge	1.17		
Sea whips	1.05		
Surface temperature			1.30
Surface current speed			1.38
Surface current variability			1.41

Table 6. -- Habitat covariates used to model the distributions of fishes and invertebrates in the eastern and northern Bering Sea.

Variable	Unit	Definition	Interpolation method	Source	
Position	eastings, northings	Latitude and longitude of bottom trawl hauls in Alaska Albers projection corrected for the position of the trawl net relative to the vessel	--	DGPS collected at bottom trawl hauls	
Depth	m	Bathymetry of the seafloor based on digitized and position corrected NOS charts	Linear interpolation	Mean depth of bottom trawl hauls (modeling), Zimmermann, M, unpublished data (prediction)	
Slope	percent	Maximum difference between a depth measurement and its adjoining cells	--	Zimmermann, M, unpublished data	
Bottom temperature	°C	Mean summer bottom temperature for the region measured during bottom trawl surveys from 1996-2010	Ordinary kriging	Temperature data collected at bottom trawl hauls	2
Surface temperature	°C	Ocean current speed predicted from the ROMS model during the years 1970-2004 and averaged on a 10 km by 10 km grid	Inverse distance weighting	Danielson et al. 2011	1
Ocean color	Carbon*m^{-2}*day^{-1}	Net primary production in surface waters in May to September averaged by 1080 by 2160 grid cells then averaged across years (2002-2011)	Inverse distance weighting	Behrenfeld and Falkowski 1997	
Mean bottom ocean current	m*sec^{-1}	Seafloor ocean current speed predicted from the ROMS model during the years 1970-2004 and averaged on a 10 km by 10 km grid	Inverse distance weighting	Danielson et al. 2011	2
Maximum tidal current	cm*sec^{-1}	Maximum of the predicted tidal current at each bottom trawl location over a 1-year cycle	Ordinary kriging	Egbert and Erofeeva 2002	2
Mean surface ocean current speed	m*sec^{-1}	Surface ocean current speed predicted from the ROMS model during the years 1970-2004 and averaged on a 10 km by 10 km grid	Inverse distance weighting	Danielson et al. 2011	1
Mean surface ocean current direction	angle	Surface ocean current direction predicted from the ROMS model during the years 1970-2004 and averaged on a 10 km by 10 km grid	Inverse distance weighting	Danielson et al. 2011	1
Surface ocean current direction variability	--	Variability in surface ocean current direction predicted from the ROMS model during the years 1970-2004 and averaged on a 10 km by 10 km grid	Inverse distance weighting	Danielson et al. 2011	1
Sediment grain size (phi)	--	Sediment grain size derived from historical bottom sampling in the eastern Bering Sea compiled in the EBSSED database	Ordinary kriging	Smith and McConnaughey 1999	2
Coral presence or absence	--	Coral presence or absence in bottom trawl catch and raster of predicted presence or absence of coral	--	Catch data from bottom trawl hauls (modeling), Rooper et al. 2016 (prediction)	2
Sponge presence or absence	--	Sponge presence or absence in bottom trawl catch and raster of predicted presence or absence of Sponge	--	Catch data from bottom trawl hauls (modeling), Rooper et al. 2016 (prediction)	2
Pennatulacean presence or absence	--	Pennatulacean presence or absence in bottom trawl catch and raster of predicted presence or absence of Pennatulacean	--	Catch data from bottom trawl hauls (modeling), Rooper et al. 2016 (prediction)	2

[1] Used to model egg, larval and early juvenile stages only

[2] Used to model bottom trawl survey data only

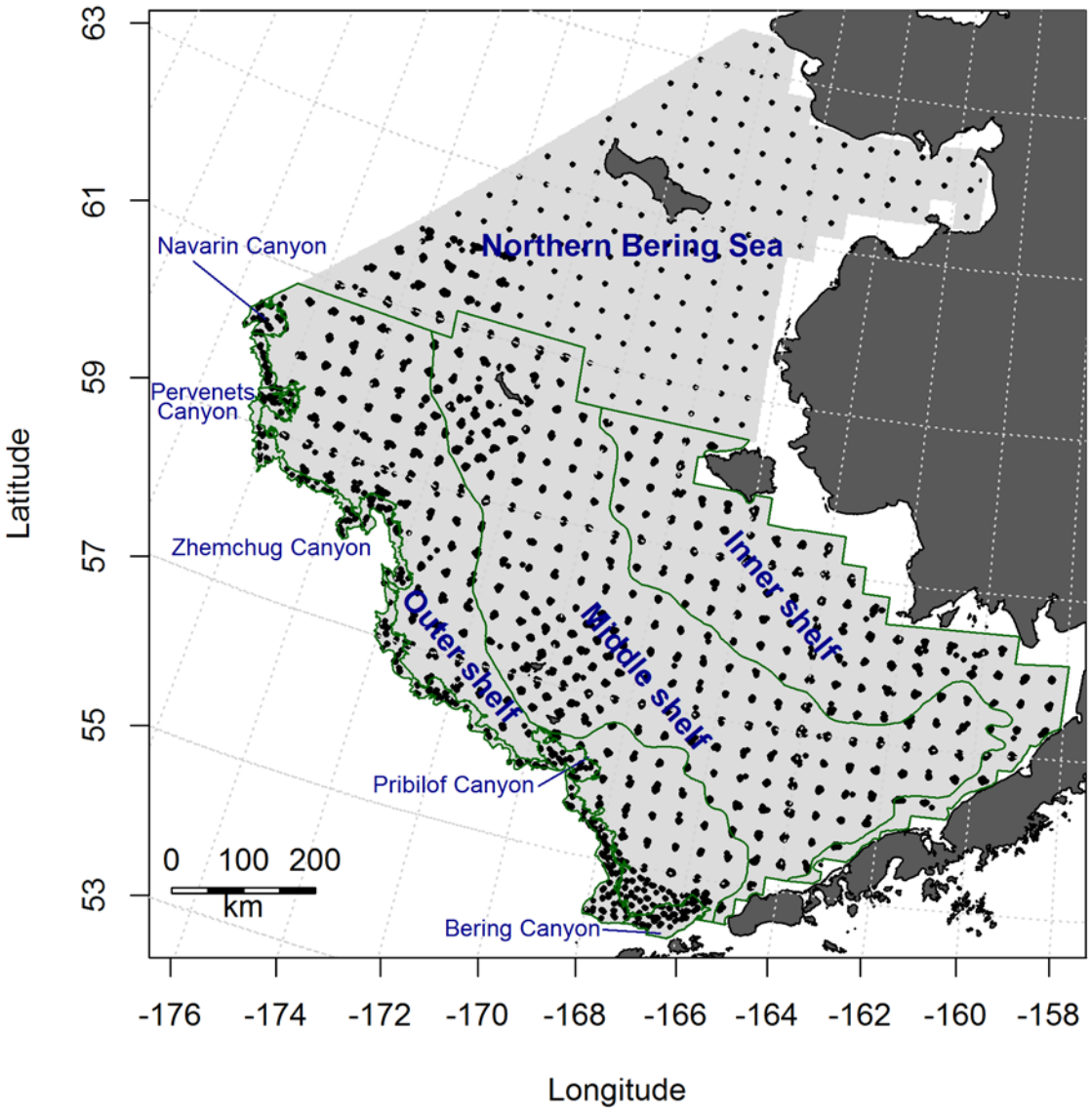

Figure 1 -- Locations ($N_{stations}$ = 12,702) of stations sampled on RACE-GAP summer bottom trawl surveys of the eastern Bering Sea shelf (1982-2014) and upper continental slope (2002-2012) and the northern Bering Sea (2010).

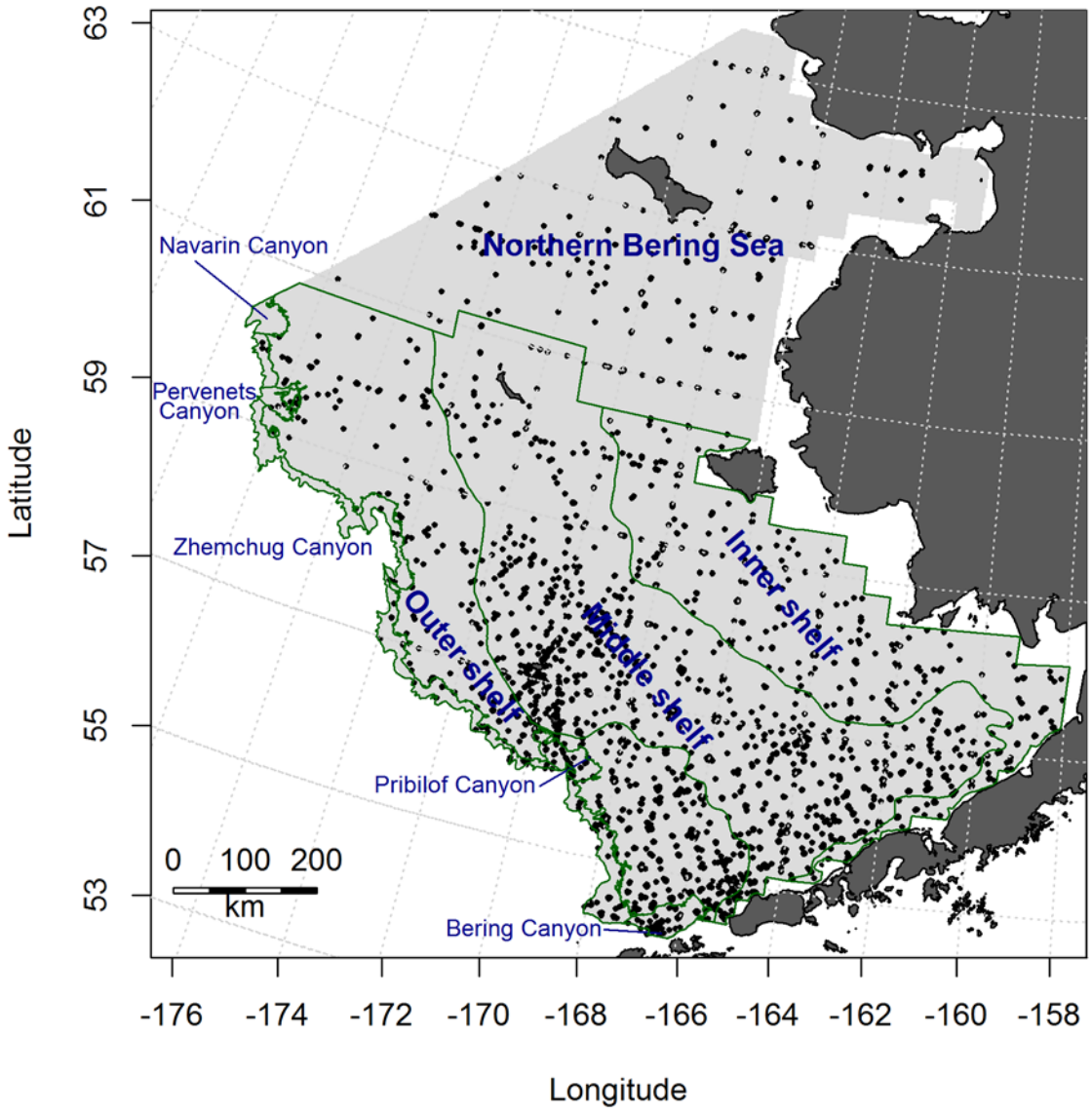

Figure 2. -- Locations ($N_{stations}$ = 24,505) of ichthyoplankton sampling stations in the eastern and northern Bering Sea (1991-2013) from the EcoFOCI ECODAAT database.

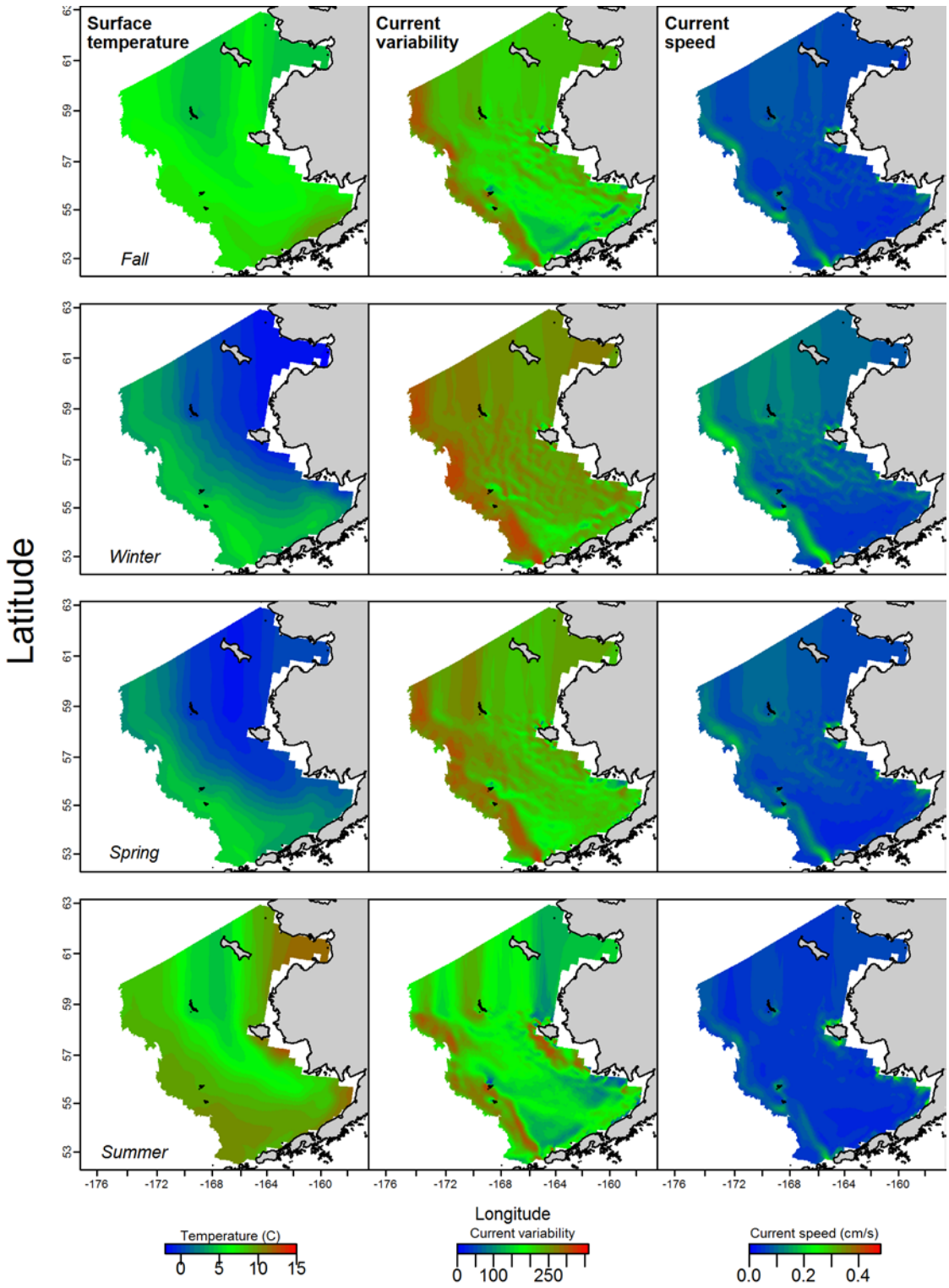

Figure 3. -- Habitat covariate rasters of surface temperature, surface current variability, and surface current speed from ROMS model runs (1969-2005; Danielson et al. 2011) for the eastern and northern Bering Sea used in species distribution models for the early life history stages (ELHS) of species collected from EcoFOCI ichthyoplankton surveys.

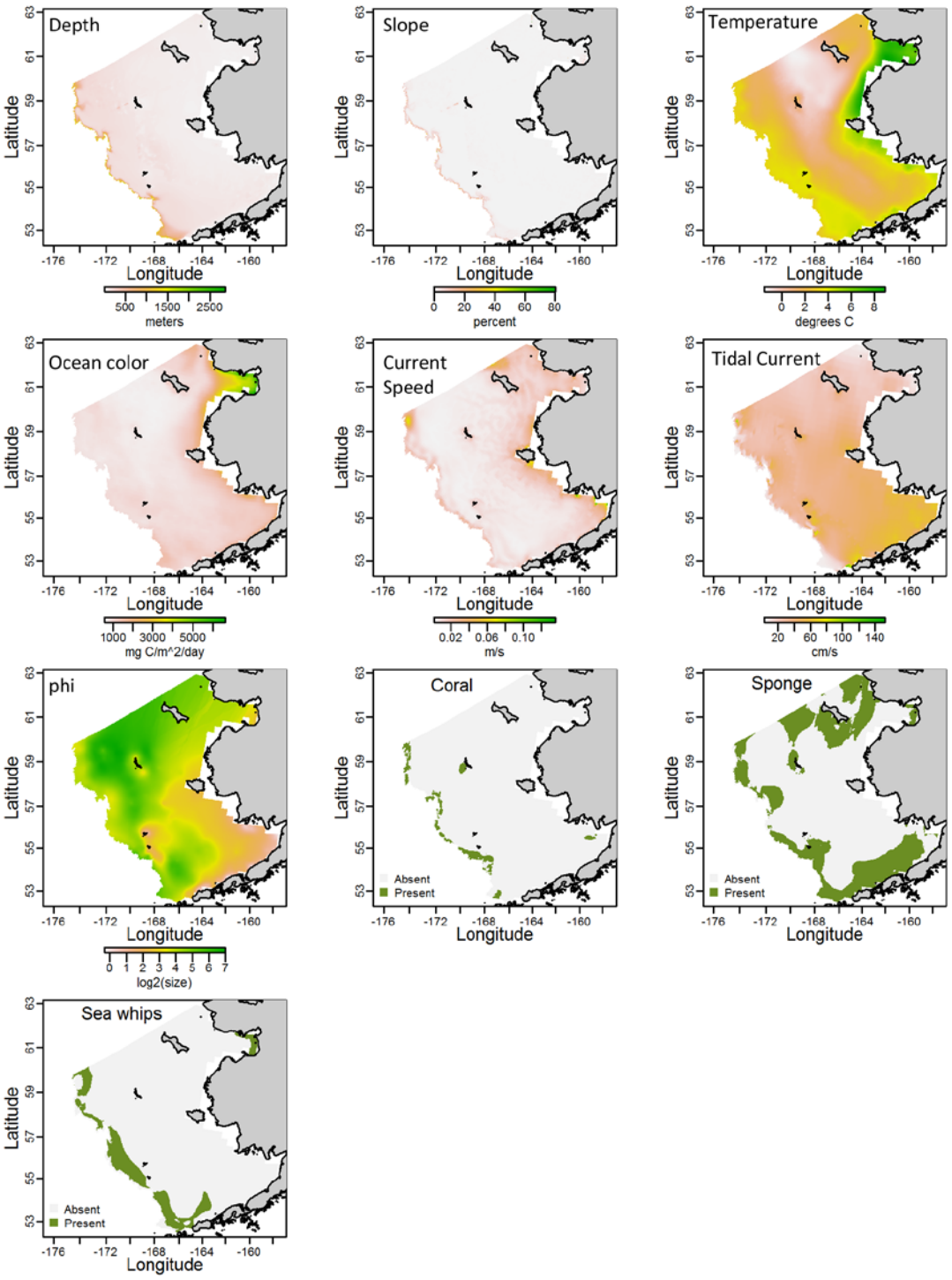

Figure 4. -- Habitat covariate rasters used in species distribution models for the settled juvenile and adult stages of fishes and invertebrates collected from RACE-GAP summer bottom trawl surveys in the eastern and northern Bering Sea (Depth = bottom depth, Slope = kriged local slope, Temperature = bottom temperature, Ocean color = ocean productivity, Current speed = bottom current speed, Tidal current = tidal maxima, phi = sediment grain size; Coral, Sponge, and Sea Whips are presence-absence).

RESULTS

Flatfishes

Atheresthes spp.

Distribution of *Atheresthes* spp. early life history stages from EcoFOCI ichthyoplankton surveys of the eastern Bering Sea -- There were 45 occurrences of *Atheresthes* spp. eggs reported from EcoFOCI ichthyoplankton surveys of the EBS (Fig. 5). The eggs were collected between February and May during the survey years examined (Table 2). All occurrences of *Atheresthes* spp. eggs but one occurred over the Bering Canyon.

Atheresthes spp. larvae were collected on EcoFOCI ichthyoplankton surveys between February and September with the greatest prevalence in the southwest portion of the EBS over waters deeper than 100 m (Fig. 6). They occurred less commonly in the NBS and across the middle and outer shelf of the central region of the EBS. Distribution of *Atheresthes* spp. larvae was modeled from presence-only data using the MaxEnt SDM. Suitable larval *Atheresthes* spp. habitat predicted by the MaxEnt model was primarily found on the outer and middle shelf of the southwestern portion of the EBS. The most important variable for predicting distribution of suitable larval *Atheresthes* spp. habitat was sea surface temperature (relative importance = 82.3%). The next most important predictor was bottom depth (8.0%). The model fits were outstanding to the training data (AUC $\geq$ 0.97) and excellent to the testing data (AUC $\geq$ 0.92) indicating successful validation of the model. The percent of cases correctly classified was high for both data sets (90% for the training data and 92% for the test data).

Pelagic juvenile *Atheresthes* spp. were observed in the water column between July and September at just 13 ichthyoplankton survey stations (Fig. 7). Most of these occurrences were over the middle and outer shelf north of the Pribilof Canyon in the vicinity of the Pribilof Islands. The prevalence of pelagic juvenile *Atheresthes* spp. was too low to parameterize a MaxEnt distribution model for this life stage.

Bering Sea *Atheresthes* spp. essential larval habitat maps and conclusions -- Essential habitat for *Atheresthes* spp. larvae was widely dispersed across the EBS (Fig. 8). Core EFH (the shape encompassing the top 25% of predictions) for larval *Atheresthes* spp. was located between the Pribilof Islands and the Alaska Peninsula in waters deeper than 100 m on the outer shelf of the EBS. Egg and pelagic juvenile stages of *Atheresthes* spp. were not prevalent enough to model essential habitat for these life stages.

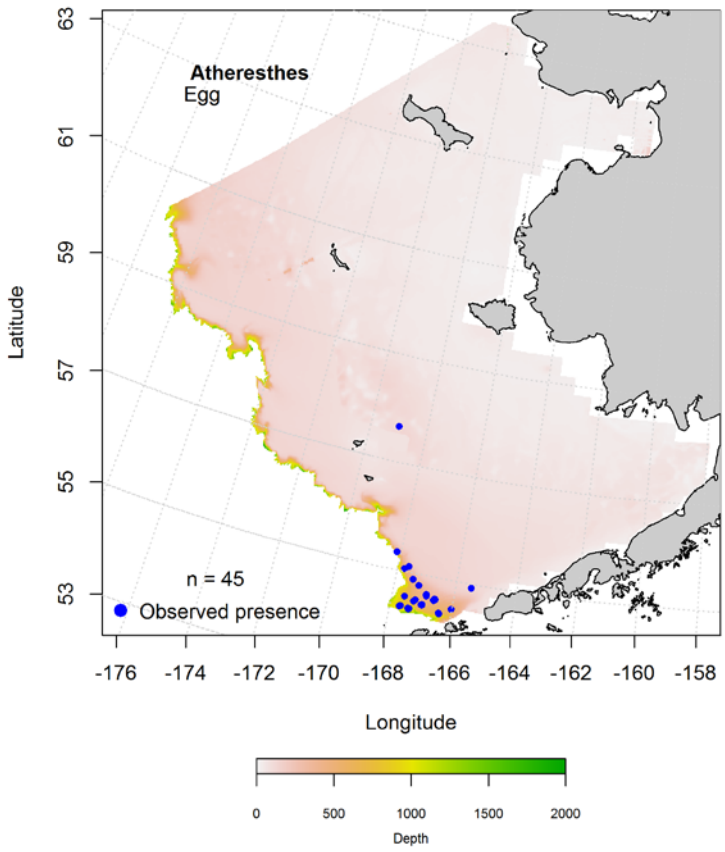

Figure 5. -- Presence of *Atheresthes* spp. eggs in EcoFOCI ichthyoplankton surveys of the eastern Bering Sea (1991-2013).

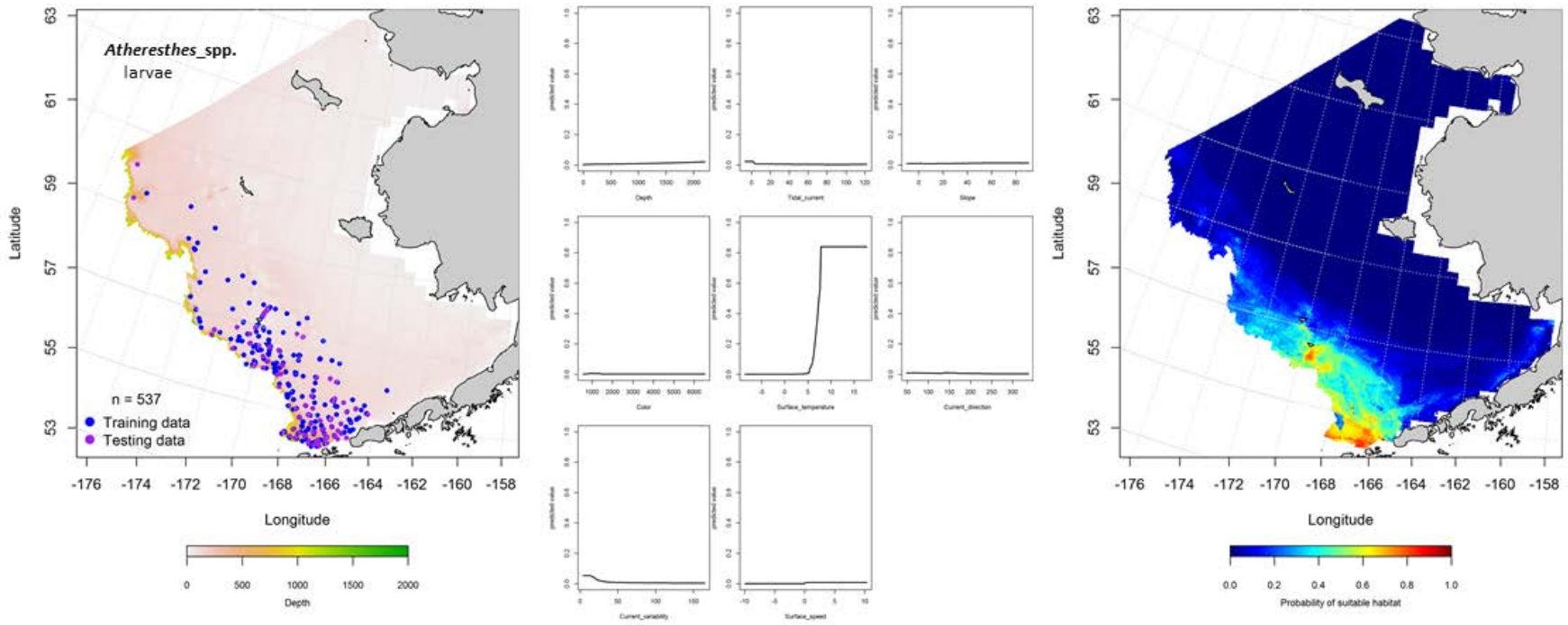

Figure 6. -- Presence of *Atheresthes* spp. larvae in EcoFOCI ichthyoplankton surveys of the eastern Bering Sea (left panel) with training (blue dots) and testing (purple dots) data sets indicated alongside the maximum entropy model (MaxEnt) effects (center panel) and the MaxEnt spatial predictions of the probability of suitable larval *Atheresthes* spp. habitat (right panel).

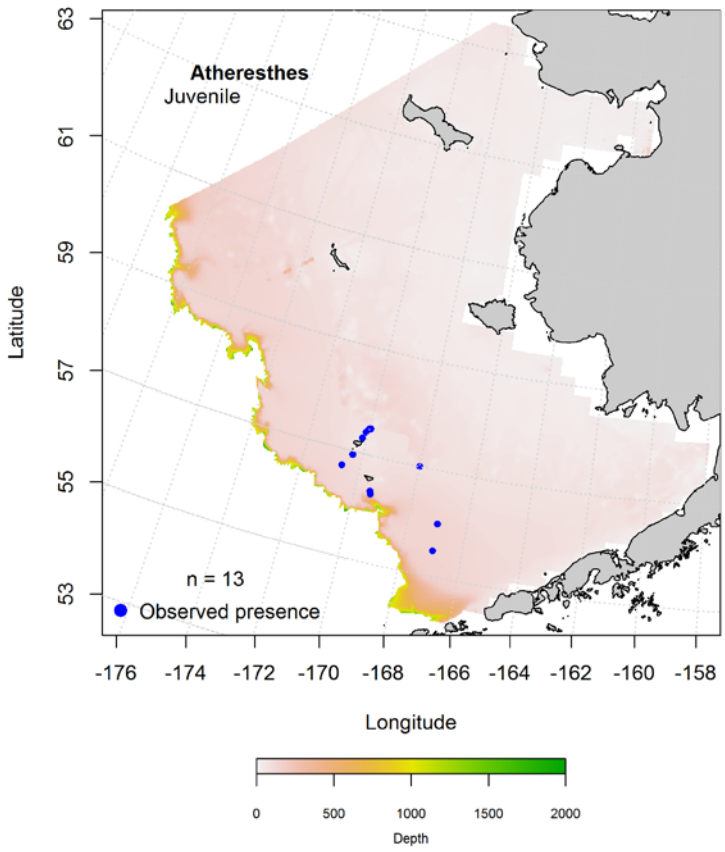

Figure 7. -- Presence of pelagic juvenile *Atheresthes* spp. in EcoFOCI ichthyoplankton surveys (1991-2013) of the eastern Bering Sea.

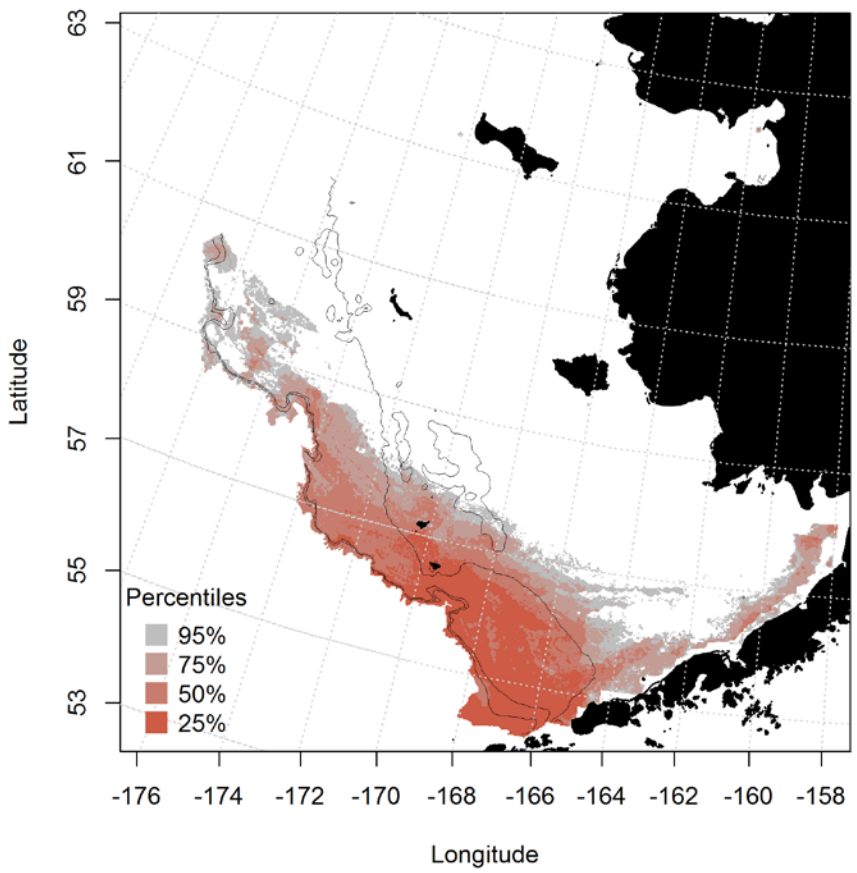

Figure 8. -- Essential habitat of larval *Atheresthes* spp. predicted from EcoFOCI ichthyoplankton surveys of the eastern Bering Sea (1991-2013).

Arrowtooth Flounder (*Atheresthes stomias*)

Summertime distribution of settled juvenile and adult arrowtooth flounder (*Atheresthes stomias*) from RACE-GAP bottom trawl surveys of the eastern Bering Sea -- Generalized additive models predicting the abundance of settled juvenile arrowtooth flounder from bottom trawl survey catches across the EBS (Fig. 9) explained 67.2% of the deviance in the bottom trawl CPUE data. Geographical location, bottom temperature, bottom depth, and tidal current speed were the most significant variables explaining their distribution. Model effects on the y-axis are relative to zero and indicated by the solid line on the graph; shaded areas around the effects line are confidence limits. When the model effect line is above zero, the habitat covariate (magnitude indicated on the x-axis) has a positive

effect on the model prediction and vice-versa; model effects are neutral at zero. The GAM predictions indicate that settled juvenile arrowtooth flounder abundance would be greatest in the central and southern domains of the EBS over the middle and outer shelves. The model also indicates that their abundance would decrease as bottom depth increases and increase with increasing temperature and maximum tidal current speed. The correlation coefficient of the model for the training ($r^2 = 0.67$) and test ($r^2 = 0.65$) data sets indicates an acceptable fit and moderately successful model validation. The area with the highest predicted abundance of settled juvenile arrowtooth flounder was centered near the Bering Canyon over the outer shelf and slope edge.

Adult arrowtooth flounder were collected from bottom trawl surveys throughout the EBS (Fig. 10). The best-fitting GAM explained 73.8% of the deviance in bottom trawl CPUE estimates and showed that geographical location, bottom depth, and bottom temperature were the most important habitat covariates for predicting adult arrowtooth abundance. Predicted abundance was greatest over the outer shelf of the eastern Bering Sea extending from the Bering Canyon in the southern domain to the northern extent of the survey area. Modeled abundance was also greatest in depths around 300 m and increased with increasing bottom temperature. The model fit for the training ($r^2 = 0.74$) and test ($r^2 = 0.72$) data was good.

Distribution of arrowtooth flounder (*Atheresthes stomias*) in commercial fishery catches from the eastern Bering Sea -- Arrowtooth flounder were not routinely distinguished from Kamchatka flounder in commercial catches until 2007 (Spies et al. 2014). Their presence in commercial fishery catches since 2007 were used to model the probability of suitable habitat for this species using MaxEnt modeling (Fig. 11). Depth and bottom temperature were consistently the dominant habitat covariates in the MaxEnt models describing the seasonal probability of suitable arrowtooth flounder habitat in the EBS. In fall, the distribution of suitable arrowtooth flounder habitat predicted from commercial catches extended over the outer and middle shelf of the EBS from the Bering Canyon in the southern domain to the northern extent of the survey area. Depth and bottom temperature were the dominant habitat

covariates predicting the probability of suitable habitat and comprised 90.2% of the relative importance of the six habitat covariates included in the model formulation. The model fits to the training and test data were excellent (AUC = 0.88) and acceptable (AUC = 0.80); 80% of cases in both data sets were correctly classified by the model. From winter commercial catches, the predicted distribution of suitable arrowtooth flounder habitat was similar to that in fall (i.e., over the outer shelf from Bering Canyon to the northern extent of the survey area) with an eastward extension of habitat into the southern half of Bristol Bay. Depth and bottom temperature provided 93.1% of the leverage of all habitat covariates in the model. The model fits to the training and test data were outstanding (AUC = 0.93) and excellent (AUC = 0.85); 86% of the cases were correctly classified in the model using the training data and 85% were correctly classified with the test data. Spring distribution of suitable arrowtooth flounder habitat predicted from commercial catches extended over the outer shelf and the middle shelf from the Bering Canyon in the southern domain of the eastern Bering Sea to the northern extent of the survey area. Depth and bottom temperature comprised 85.4% of the leverage from habitat covariates in the model. The model fits to the training and test data were outstanding (AUC = 0.93) and excellent (AUC = 0.85). The model correctly classified 86% of predicted cases from the training data and 85% of the cases from the test data.

Eastern Bering Sea arrowtooth flounder (*Atheresthes stomias*) essential fish habitat maps and conclusions -- Essential fish habitat for *Atheresthes* spp. ELHS as well as settled juvenile and adult arrowtooth flounder was widely dispersed across the EBS (Fig. 12). Egg and pelagic juvenile stages of *Atheresthes* spp. were not prevalent enough to model essential habitat for these life stages. The rough correspondence of SDM predictions from three different sources of distribution data strongly suggests that the core habitat for this species (top 25% of predictions) is along the middle and outer shelves of the EBS ranging from the Alaska Peninsula northward to the northern extent of the survey area. There is little difference among the spatial predictions of EFH from the commercial catches comparing fall, winter, and spring which suggests that the spatial extent of ATF habitat is a consistent property of the sampling area. Essential habitat for the life stages considered and contained within the bounds of the top 95% of

predictions extends over the majority of the eastern EBS from the Alaska Peninsula and Bristol Bay to Norton Sound and the northern Bering Sea and westward on the Bering Sea Slope.

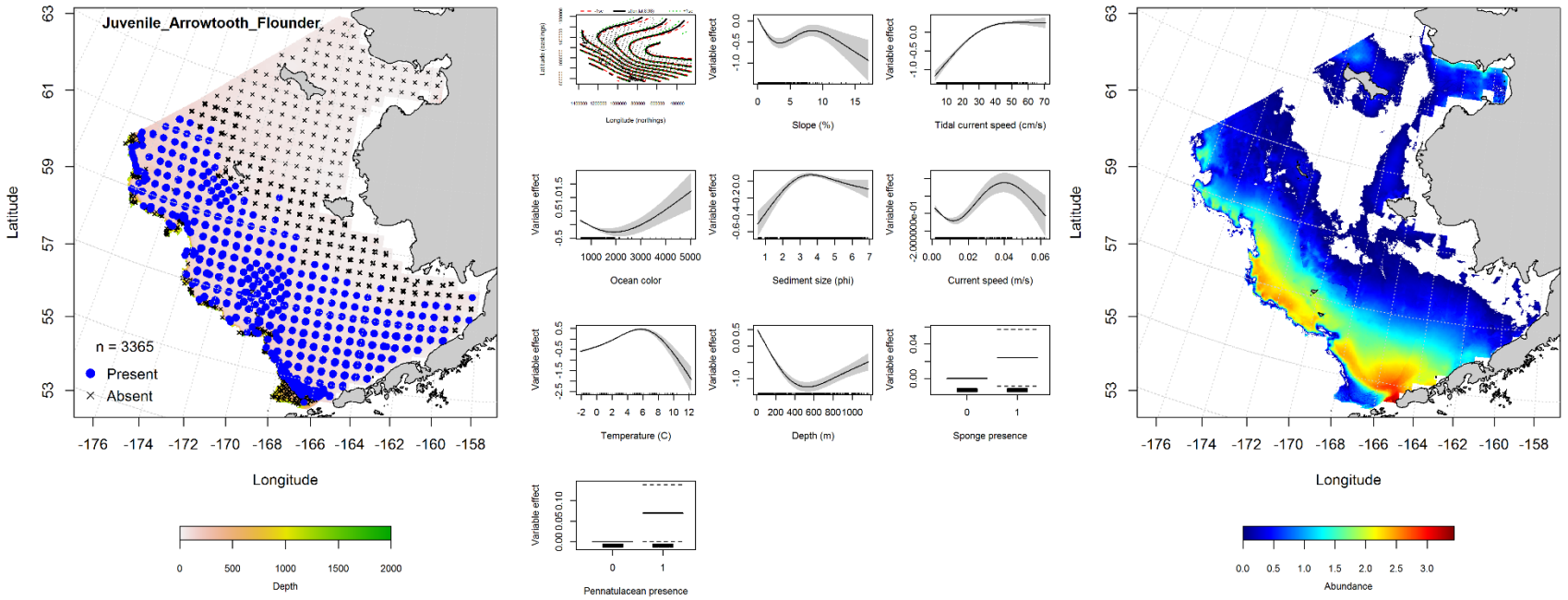

Figure 9. -- Distribution of settled juvenile arrowtooth flounder in 1993-2014 RACE-GAP summer bottom trawl surveys (left panel) alongside effects of retained habitat covariates in the best-fitting generalized additive model (GAM; center panel) predicting spatial distribution of abundance (CPUE, right panel) across the eastern Bering Sea.

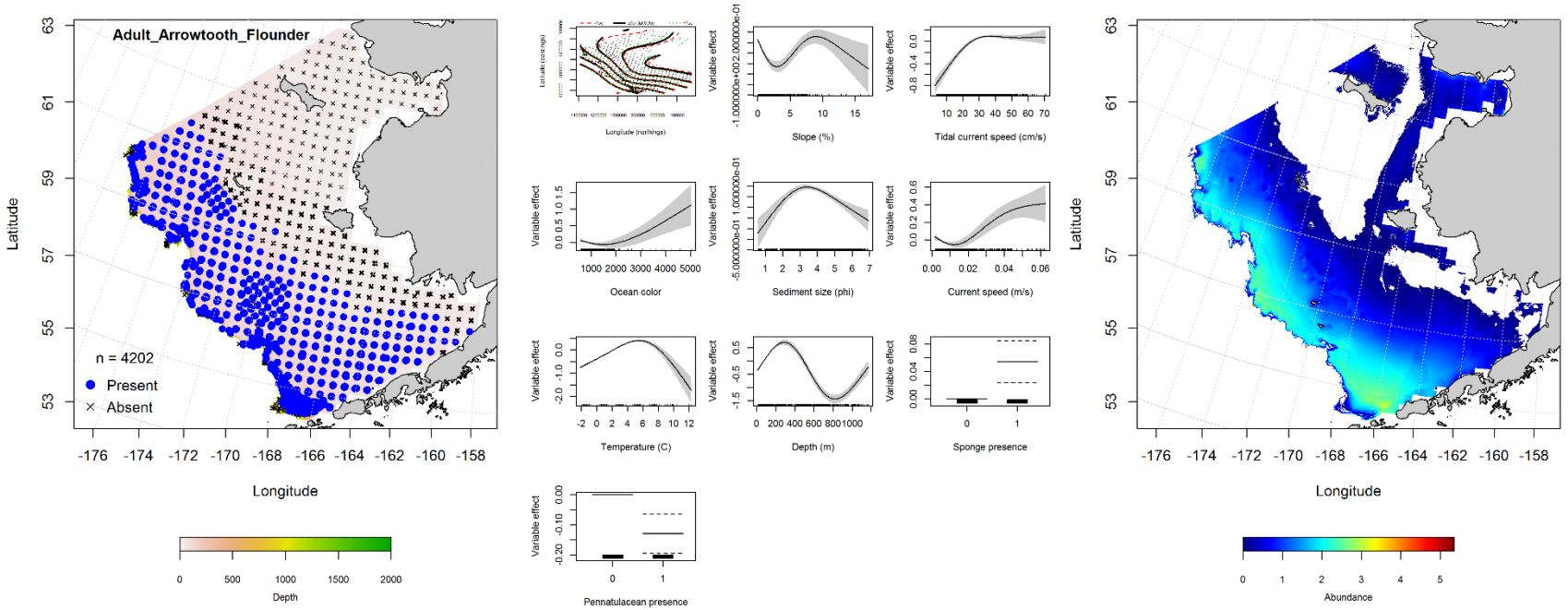

Figure 10. -- Distribution of adult arrowtooth flounder catches in 1993-2014 RACE-GAP summer bottom trawl surveys (left panel) alongside effects of retained habitat covariates in the best-fitting generalized additive model (GAM; center panel) predicting spatial distribution of abundance (CPUE, right panel) across the eastern Bering Sea.

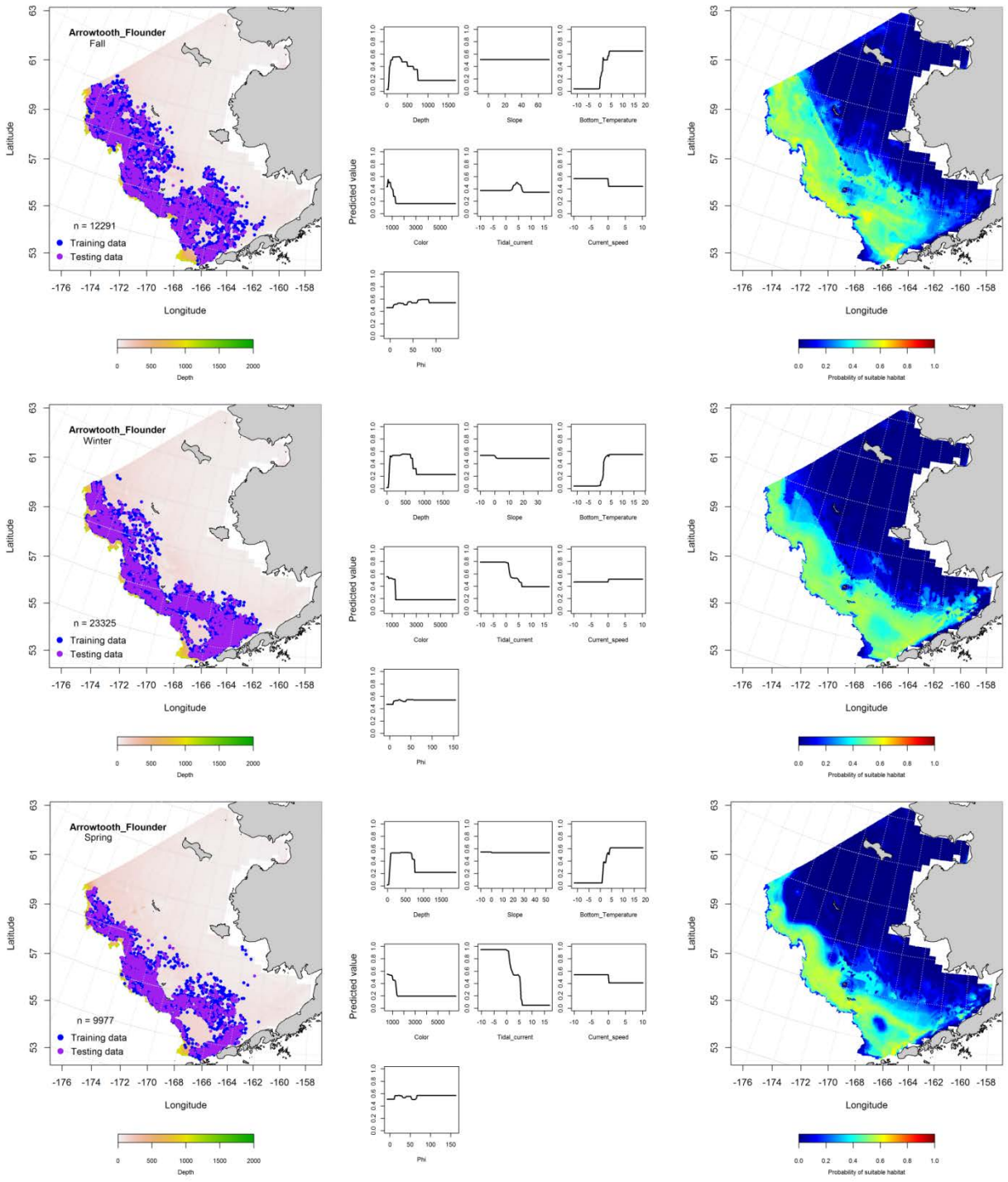

Figure 11. -- Locations of arrowtooth flounder in fall (October-November; top row), winter (December-February; middle row), and spring (March-May; bottom row) commercial fisheries catches (2003-2013) from the eastern Bering Sea (left-hand column). Blue points were used to train the MaxEnt model (center column) predicting the probability of suitable habitat (right-hand column) and the purple points were used to validate the model.

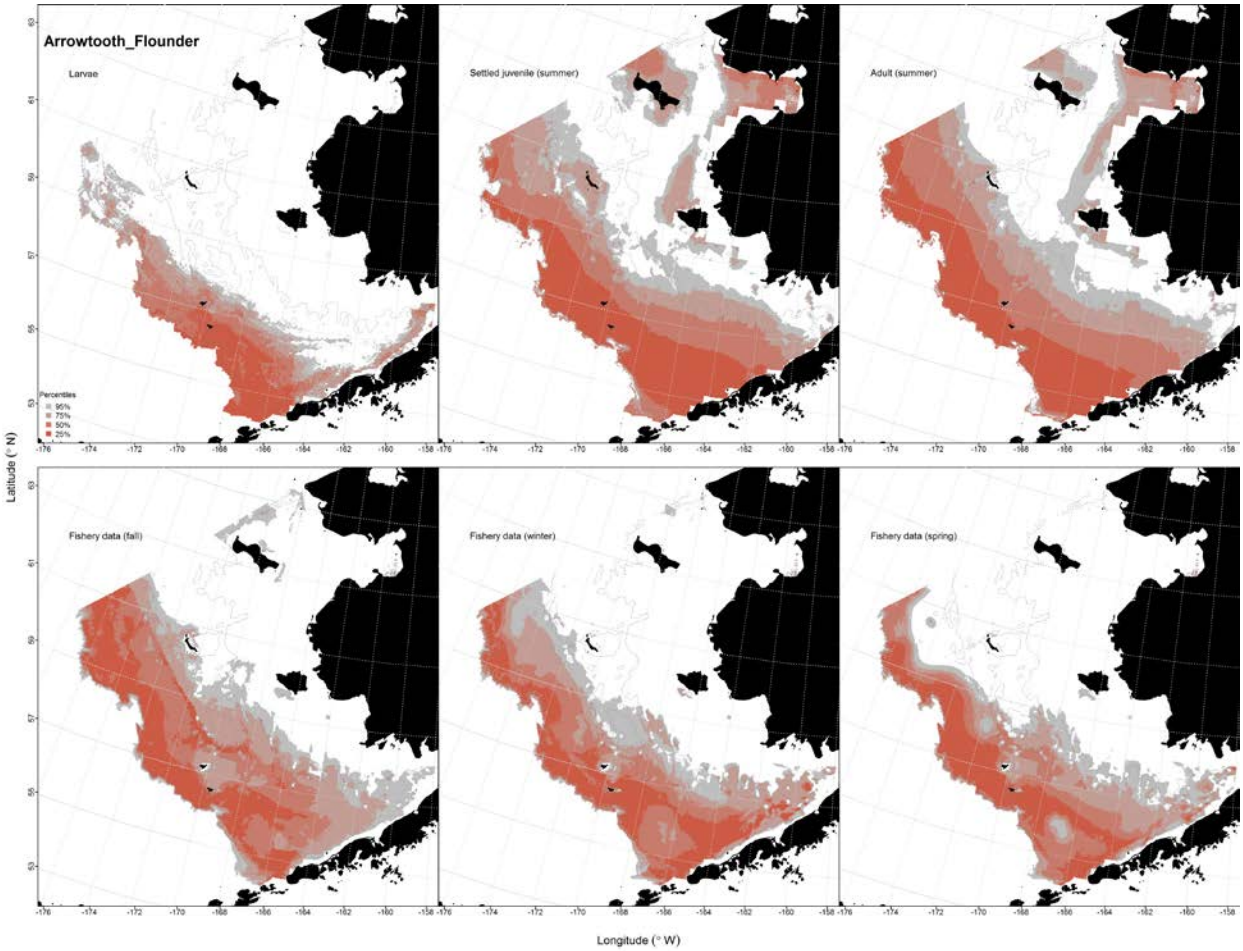

Figure 12. -- Essential fish habitat predicted for *Atheresthes* spp. larvae (upper left panel), settled juvenile arrowtooth flounder settled juveniles and adults (upper middle and right panels) from RACE-GAP summertime bottom trawl surveys (1993-2014), and from presence in commercial fishery catches (2003-2013) from fall, winter, and spring in the eastern Bering Sea (bottom panels).

Kamchatka Flounder (*Atheresthes evermanni*)

Summertime distribution of settled juvenile and adult Kamchatka flounder (*Atheresthes evermanni*) from RACE-GAP bottom trawl surveys of the eastern Bering Sea --

Settled juvenile Kamchatka flounder from summer RACE-GAP bottom trawl surveys were distributed from the EBS middle shelf onto the continental slope from the U.S.-Russia Convention Line to the Alaska

Peninsula and eastward into Bristol Bay (Fig. 13). The areas with the highest predicted abundance of settled juveniles Kamchatka flounder were on the outer shelf of the EBS in the Bering Canyon in the southern domain and between Pribilof and Zhemchug Canyons in the central domain. The best-fitting GAM explained 60.6% of the deviance in settled juvenile Kamchatka flounder CPUE from the bottom trawl survey. Geographic location, bottom depth, and bottom temperature were the most important covariates predicting their abundance. Predicted abundance increased in the southwest portion of the southern region and increased with increasing temperature and depth. Sea pens were also an important covariate in the model and juvenile abundance was predicted to be higher when they were present. The model fit to the training and test data was acceptable (r^2 = 0.61 and 0.60 for each). Catches of settled juveniles were more widely distributed than adults during the summer with catches coming from well east into Bristol Bay.

An hGAM was used to describe the distribution and abundance of adult Kamchatka flounder in RACE-GAP summer bottom trawl survey catches (Fig. 14). The presence-absence model results corroborated our empirical observations from summertime surveys that adult Kamchatka flounder have the highest probability of occurrence in continental shelf edge and upper slope waters (200–1,000 m) of the EBS. The six habitat covariates retained in the best-fitting presence-absence GAM explained 46.6% of the deviance in adult Kamchatka flounder distribution. The most important covariates leveraging the presence-absence model were bottom depth, bottom temperature, and geographic location. Probability of encountering adult Kamchatka flounder was greatest in the western EBS at depths around 600 m with bottom temperatures above 6° C and the model fit to the training data was outstanding (AUC = 0.92) and correctly classified 84% of presence-absence cases. Using the test data, the best-fitting presence-absence model was validated with an outstanding fit (AUC = 0.93) and 85% of cases correctly classified. Abundance of adult Kamchatka flounder was predicted at locations where the threshold probability of occurrence (0.23) established in the presence-absence GAM above was met or exceeded. This conditional abundance GAM explained 42.8% of the deviance in the CPUE data. Highest predicted abundances were

on the EBS outer shelf and upper continental slope around the heads of submarine canyons. The most important habitat covariates retained in the model were bottom depth, geographical location, and coral presence and abundance was generally predicted to be higher in the southwest EBS at depths ca. 550 m in the presence of corals. This GAM fit to the training data ($r^2 = 0.43$) and test data ($r^2 = 0.42$) was marginal.

Seasonal distribution of Kamchatka flounder (*Atheresthes evermanni*) in commercial fishery catches from the eastern Bering Sea -- Kamchatka flounder presence in commercial fishery catches was used in a MaxEnt model to predict the probability of suitable habitat in the EBS (Fig. 15). Most of the commercial catches of this species occurred on the middle and outer shelves of the EBS. In fall, winter, and spring, bottom depth and bottom temperature comprised the most important (greatest leverage) habitat covariates in the MaxEnt model predicting probability of suitable Kamchatka flounder habitat in the EBS. Their combined relative importance ranged from 83.5% in the fall to 91.4% in the spring. Model fits to the training data were outstanding in all seasons, ranging from AUC = 0.90 and 85% of cases correctly predicted in the fall to AUC = 0.95 and 87% in the spring.

Eastern Bering Sea Kamchatka flounder (*Atheresthes evermanni*) essential fish habitat maps and conclusions -- Essential habitat in the EBS of *Atheresthes* spp. ELHS, settled juvenile and adult Kamchatka flounder from summer RACE-GAP bottom trawl surveys, and from commercial catches in fall, winter, and spring was primarily found over the outer shelf and upper continental slope of the EBS (Fig. 16). Larval EFH was restricted to the central and southern domains of the EBS over the middle and outer shelves. Summer distribution of settled juvenile Kamchatka flounder extended from the Alaska Peninsula to the U.S.-Russia Convention line and inshore into Bristol Bay and Norton Sound. Adult EFH from the summer bottom trawl surveys was largely restricted to deeper waters off of the shelf break and along the upper continental slope as well as on the middle and outer shelves extending from north of the Pribilof Islands northward to the convention line. Essential habitat based on presence of Kamchatka flounder in commercial catches was primarily distributed along the outer and middle shelves between the Alaska Peninsula and the Convention Line and into Bristol Bay in the winter and spring.

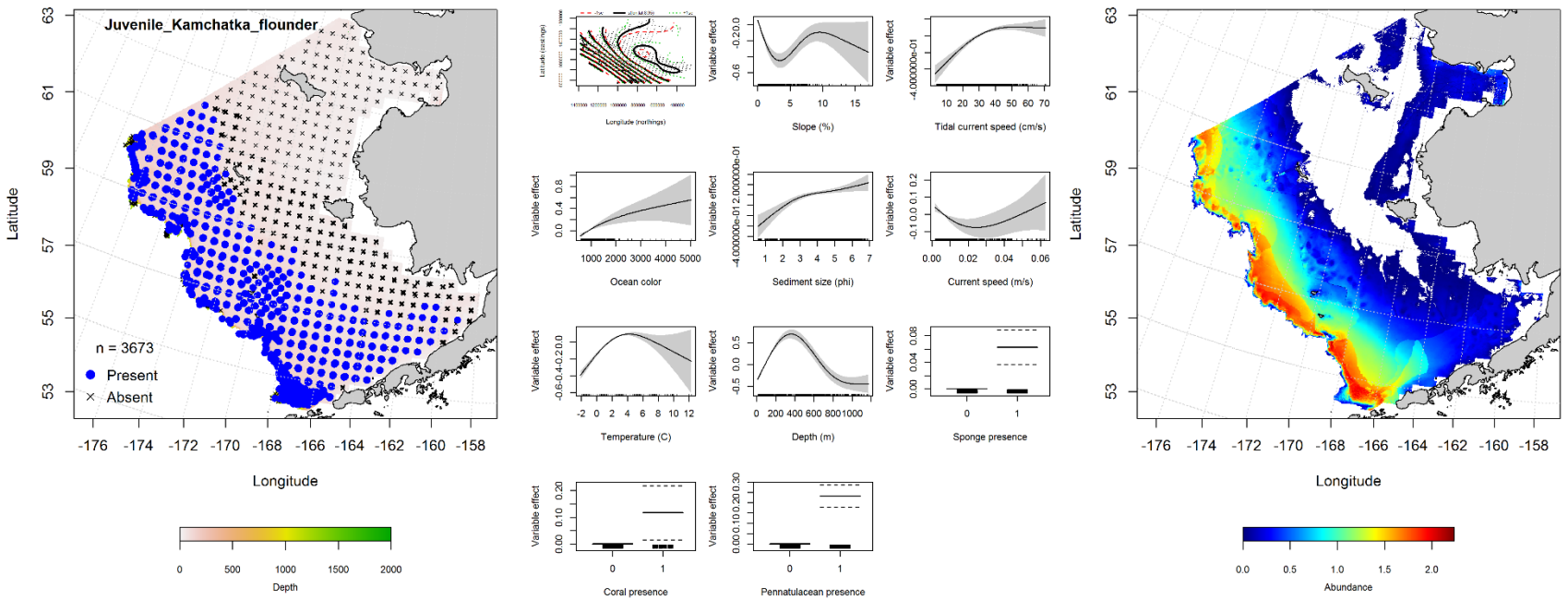

Figure 13. -- Distribution of settled juvenile Kamchatka flounder in 1993-2014 RACE-GAP summer bottom trawl surveys (left panel) alongside effects of retained habitat covariates in the best-fitting generalized additive model (GAM; center panel) predicting spatial distribution of abundance (CPUE, right panel) across the eastern Bering Sea.

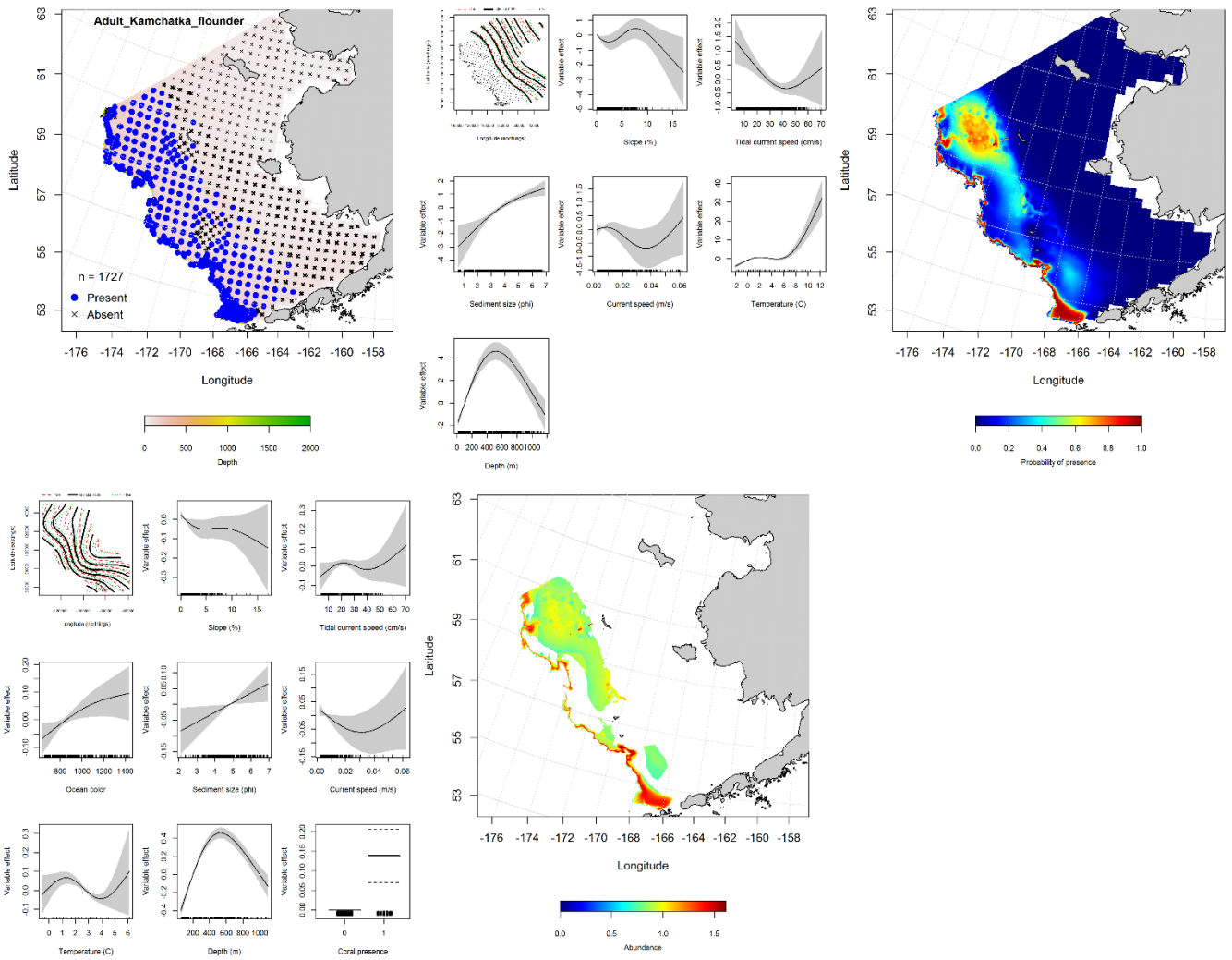

Figure 14. -- Distribution of adult Kamchatka flounder in 1993-2014 RACE-GAP summer bottom trawl surveys conducted in the eastern Bering Sea (upper left panel) and the effects of retained habitat covariates in the best-fitting generalized additive model (GAM) of presence-absence (upper center panel) spatially predicting the probability of their presence (upper right panel); the best-fitting abundance GAM (lower left panel) conditionally predicts adult Kamchatka flounder catch-per-unit-effort (CPUE) at sites where the optimum threshold for probability of presence (0.23) was met or exceeded (lower center panel).

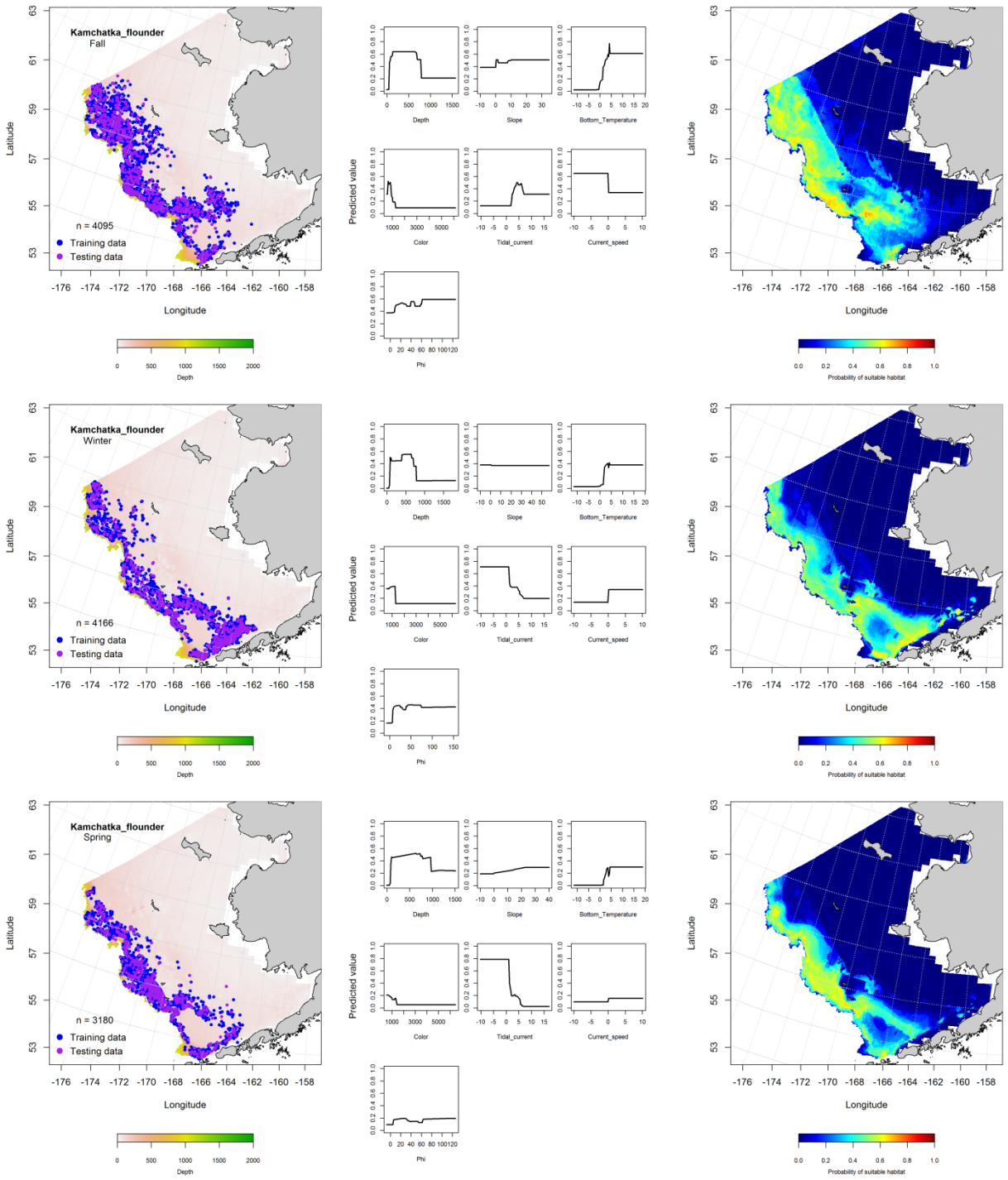

Figure 15. -- Locations of Kamchatka flounder in fall (October-November; top row), winter (December-February; middle row), and spring (March-May; bottom row) commercial fisheries catches (2003-2013) from the eastern Bering Sea (left-hand column). Blue points were used to train the MaxEnt model (center column) predicting the probability of suitable habitat (right-hand column) and the purple points were used to validate the model.

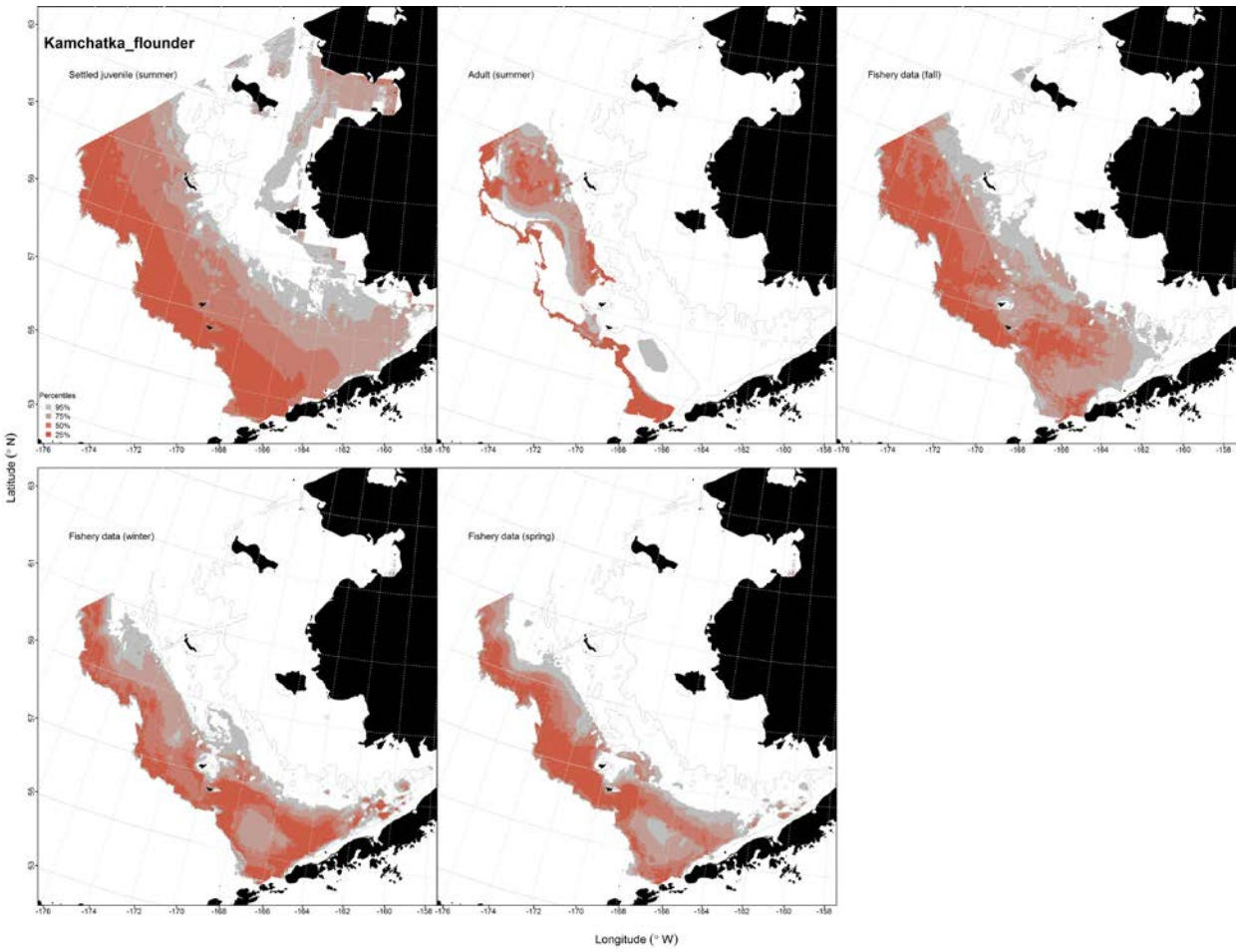

Figure 16. -- Essential fish habitat (EFH) predicted for settled juvenile (upper left panel) and adult Kamchatka flounder (upper center panel) from RACE-GAP summertime bottom trawl surveys (1993-2014) and predicted from presence in commercial fishery catches (2003-2013) from fall (upper right panel), winter, and spring (bottom panels) in the eastern Bering Sea.

Rex Sole (*Glyptocephalus zachirus*)

Distribution of rex sole (*Glyptocephalus zachirus*) early life history stages in EcoFOCI ichthyoplankton surveys of the eastern Bering Sea -- Rex sole eggs were collected on EcoFOCI ichthyoplankton surveys of the EBS between February and September (Table 2; Fig. 17); pelagic juvenile stages of rex sole were not reported. They primarily occurred over deeper waters of the outer shelf and slope (> 100 m) in the southwestern portion of the EBS. The most important habitat covariate in the

MaxEnt model of rex sole egg presence was sea surface temperature with a relative importance of 78.9% and the predicted probability of suitable rex sole egg habitat increased with increasing sea surface temperature. The next most important term in the MaxEnt model was ocean productivity (relative importance = 8%). The model fit to the training data was outstanding (AUC = 0.95) and it correctly classified 88% of predicted cases. Model validation returned an excellent fit to the test data (AUC = 0.85) where 85% of predicted cases were correctly classified. The highest predicted probabilities of suitable rex sole egg habitat were located over the Bering Canyon north of Unimak Pass and in Pribilof Canyon.

Rex sole larvae were collected on EcoFOCI ichthyoplankton surveys between June and October (Table 2; Fig. 18). They occurred over the outer shelf (100 to 200 m) from near the head of the Bering Canyon in the southern domain of the EBS northward to around Zhemchug Canyon in the central domain. There were not enough records of rex sole larvae (n = 34) to model their distribution.

Summertime distribution of settled juvenile and adult rex sole (*Glyptocephalus zachirus*) from RACE-GAP bottom trawl surveys of the eastern Bering Sea -- Settled juvenile rex sole were distributed from the inner shelf in Bristol Bay across the middle and outer shelf along the Alaska Peninsula and northward to the U.S.-Russia Convention Line in summer RACE-GAP bottom trawl surveys of the EBS (Fig. 19). Rex sole also occurred in deeper waters over the Bering Slope. An hGAM was used to describe settled juvenile rex sole distribution and abundance based on habitat covariates. The best-fitting presence-absence GAM describing settled juvenile rex sole distribution in the eastern Bering Sea indicates that the highest probability locations for juvenile rex sole to occur are along the continental shelf edge and slope. This model explained 44.1% of the deviance in their distribution with the covariates of geographical location, bottom temperature, and the presence of sea pens among the most important variables retained in the model. The probability of settled juvenile rex sole presence was high at around 4°C bottom temperatures and in the presence of sea pens and low in the northeast portion of the survey area. Both the training and test data models correctly classified 88% of predicted cases. The model fit to the training data and to test data in the model validation step was outstanding (AUC = 0.94). Conditional

juvenile rex sole abundance predicted from the best-fitting CPUE GAM where their probability of presence met or exceeded the optimum threshold determined from the presence-absence GAM (0.09) returned an abundance map constrained to the outer shelf of the eastern Bering Sea. This conditional abundance model explained just 13% of the deviance in the settled juvenile rex sole CPUE data and retained geographic location and slope as the most significant predictors in the relationship. Model fits to the training and test data sets were minimal and poor (r^2 = 0.13 and 0.08).

An hGAM was also used to describe adult rex sole distribution and abundance from RACE-GAP summer bottom trawl surveys of the eastern Bering Sea. The presence-absence GAM describing distribution of rex sole adults explained 56.5% of the deviance in the data (Fig. 20). The most important predictors in this model were geographical location, bottom depth, and bottom current speed. Model effects increased from north to south over the survey area and increased with increasing bottom depth and bottom current speeds. The highest probability of adult rex sole presence occurred in waters greater than 200 m deep on the outer shelf and slope edge. The model was an outstanding fit to the training data and to the test data in model validation (AUC = 0.96 for both data sets) and correctly classified 89% of predicted cases for both data sets. The best-fitting GAM for adult rex sole abundance predicted the highest conditional abundances over the Bering Canyon near Unimak Pass and along the shelf edge north of Pribilof Canyon. This model explained 45.5% of the deviance in the CPUE data. Geographical location and bottom depth were the most significant covariates retained, but model fits to the training and test data were marginal (r^2 = 0.44 and 0.36).

Seasonal distribution of rex sole (*Glyptocephalus zachirus*) in commercial fishery catches from the eastern Bering Sea -- There were seasonal differences in the distribution of rex sole in commercial catches from the eastern Bering Sea (Fig. 21). In general, rex sole were caught over the outer shelf and upper slope edge from the Bering Canyon northward to the U.S.-Russia Convention Line. It is unclear whether the seasonal differences observed were the result of changes in rex sole distribution across the region or changes in fishing activities during those seasons. In fall, the highest probability

habitats were in the southern domain of the eastern Bering Sea over the Bering Canyon and near the head of Pribilof Canyon. The most important covariates predicting probability of suitable rex sole habitat from the MaxEnt model were bottom depth and bottom temperature (combined relative importance of 89.3%). The model fit to the training data was outstanding (AUC = 0.97); it correctly classified 91% of predicted cases. Model validation with the test data was successful (AUC = 0.90); correctly classifying 90% of cases. During the winter, rex sole catches were centered over the Bering Canyon eastward into Bristol Bay. The most important covariates predicting probability of suitable wintertime rex sole habitat from the MaxEnt model were bottom depth, ocean productivity, and bottom temperature (combined relative importance of 90.1%). The model fit to the training data was outstanding (AUC = 0.99); it correctly classified 94% of predicted cases. Model validation with the test data set was successful (AUC = 0.94), correctly classifying 94% of cases. In the spring, the pattern of commercial catches containing rex sole resembled that of the fall and high probability areas of suitable habitat were predicted over Bering Canyon near the Alaska Peninsula and around the head of Pribilof Canyon. The most important covariates predicting probability of suitable rex sole habitat from the MaxEnt model were bottom temperature and bottom depth (combined relative importance of 90.1%). The model fit to the training data was outstanding (AUC = 0.96); it correctly classified 90% of predicted cases. Model validation with the test data set was successful and the fit was excellent (AUC = 0.89), correctly classifying 89% of cases.

Eastern Bering Sea rex sole (*Glyptocephalus zachirus*) essential fish habitat maps and conclusions -- Essential habitat for different life stages of rex sole in the eastern Bering Sea varied by life stage and season (Fig. 22). For res sole ELHS, larval and pelagic juvenile presence were too low to model their habitat distributions, but the prevalence of their eggs in EcoFOCI ichthyoplankton survey samples was high enough to predict EFH for this life stage. Core EFH for rex sole eggs extended from Bristol Bay westward onto the EBS shelf in waters deeper than 100 m and then extended northward around the head of Pribilof Canyon to around St. George Island. The distribution of summertime EFH was similar for settled juvenile and adult life stages of rex sole with core EFH constrained to the outer shelf and Bering

Canyon. The settled juveniles occurred exclusively in waters greater than 100 m while adults in summer RACE-GAP survey trawls occurred over a wider range of depths. Rex sole EFH predictions based on commercial fishery activity corresponded to EFH predicted from other sources, but also extended further over the inner shelf than seen in EcoFOCI ichthyoplankton or RACE-GAP summer bottom trawl surveys. It is likely that the spatial variation of rex sole EFH predicted from commercial catches is the result of seasonal changes in fishing effort.

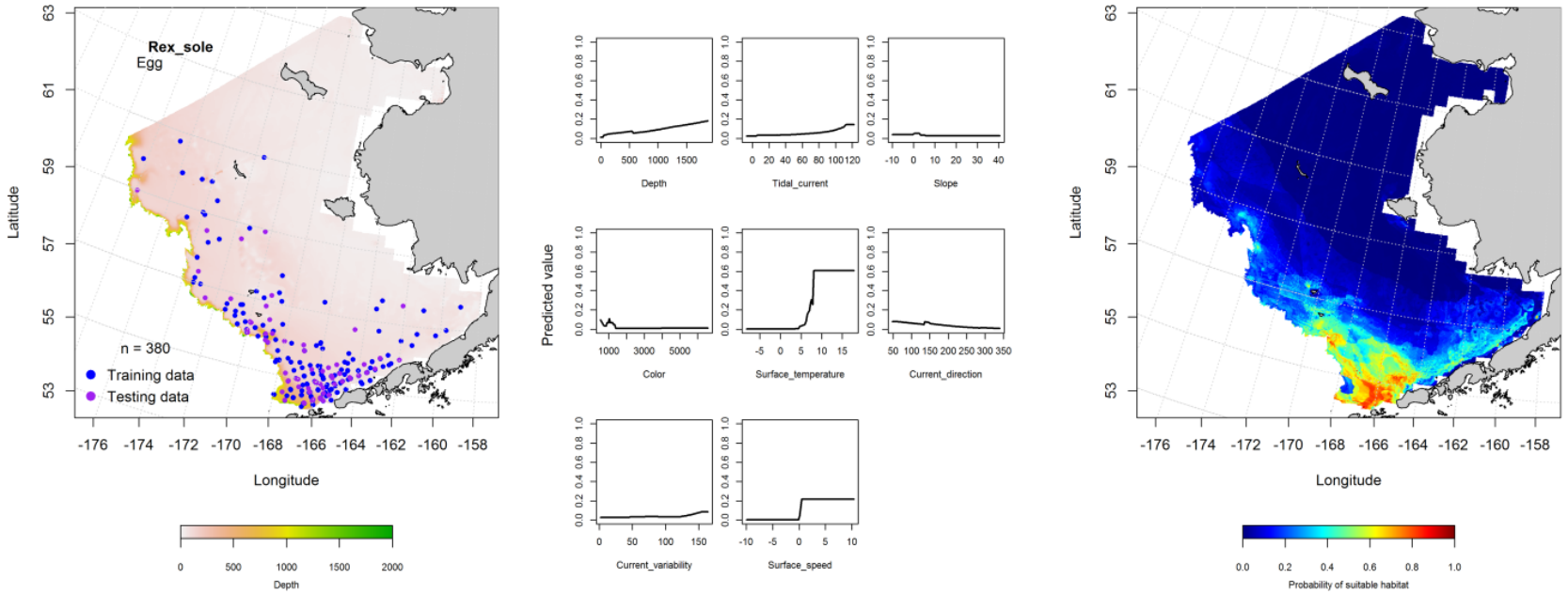

Figure 17. -- Presence of rex sole eggs in EcoFOCI ichthyoplankton surveys of the eastern Bering Sea (left panel) with training (blue dots) and testing (purple dots) data sets indicated alongside the maximum entropy model (MaxEnt) effects (center panel) and the MaxEnt spatial predictions of the probability of suitable rex sole egg habitat (right panel).

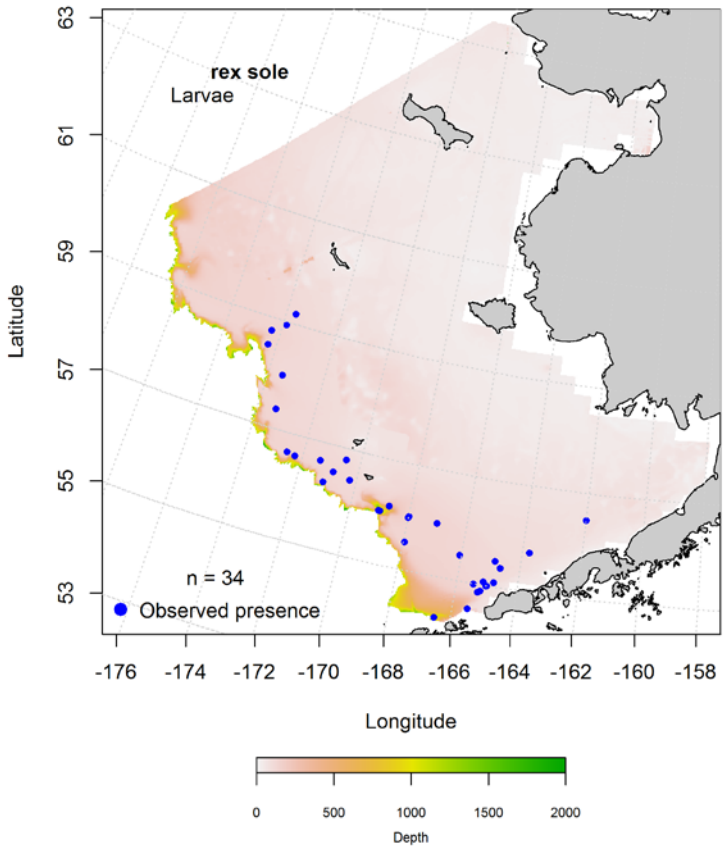

Figure 18. -- Presence of rex sole larvae in EcoFOCI ichthyoplankton surveys of the eastern Bering Sea (1991-2013).

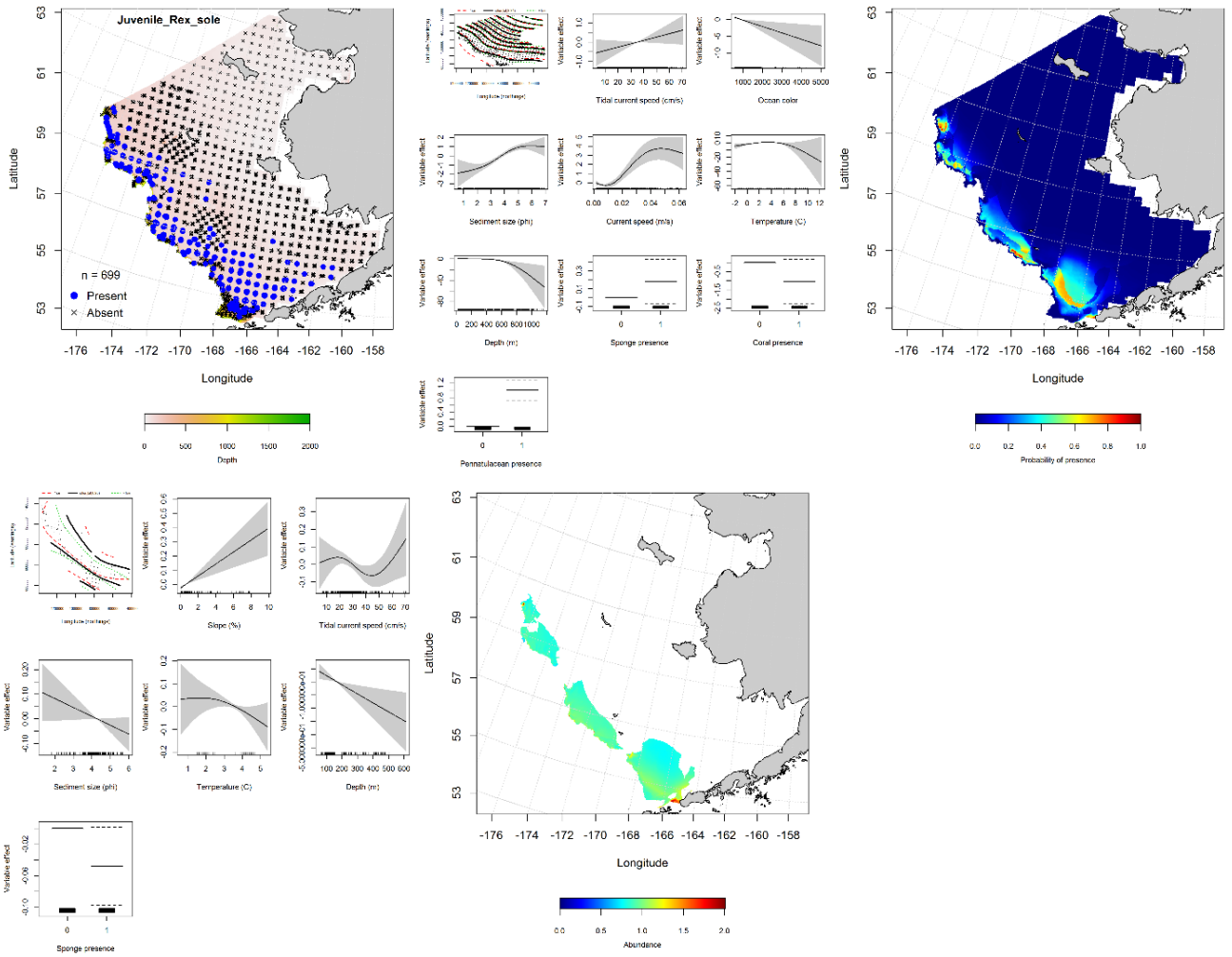

Figure 19. -- Distribution of settled juvenile rex sole in 1982-2014 RACE-GAP summer bottom trawl surveys conducted in the eastern Bering Sea (upper left panel) and the effects of retained habitat covariates in the best-fitting generalized additive model (GAM) of presence-absence (upper center panel) spatially predicting the probability of their presence (upper right panel); the best-fitting abundance GAM (lower left panel) conditionally predicts adult Kamchatka flounder catch-per-unit-effort (CPUE) at sites where the optimum threshold for probability of presence (0.09) was met or exceeded (lower center panel).

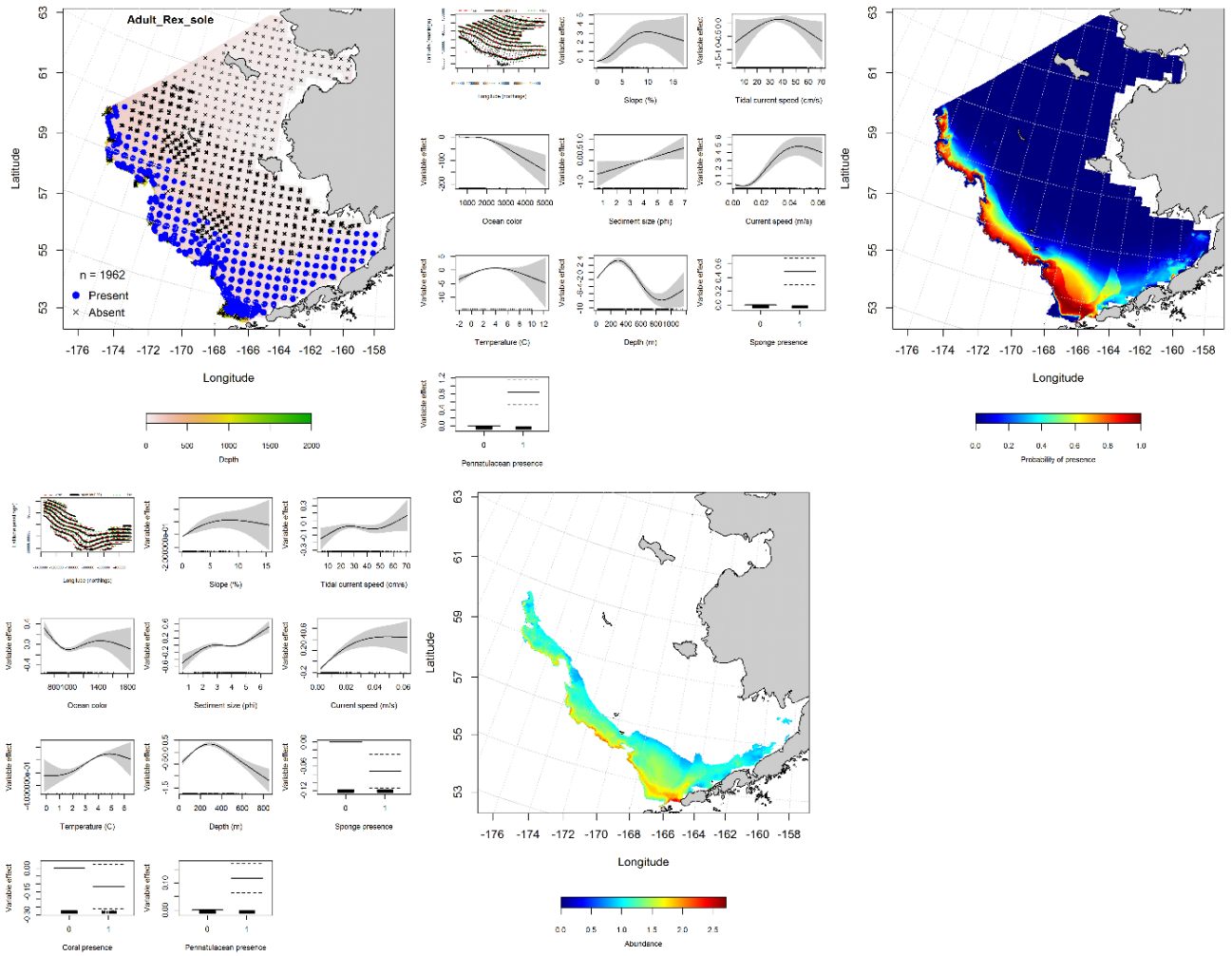

Figure 20. -- Distribution of adult rex sole in 1982-2014 RACE-GAP summer bottom trawl surveys conducted in the eastern Bering Sea (upper left panel) and the effects of retained habitat covariates in the best-fitting generalized additive model (GAM) of presence-absence (upper center panel) spatially predicting the probability of their presence (upper right panel); the best-fitting abundance GAM (lower left panel) conditionally predicts adult Kamchatka flounder catch-per-unit-effort (CPUE) at sites where the optimum threshold for probability of presence (0.21) was met or exceeded (lower center panel).

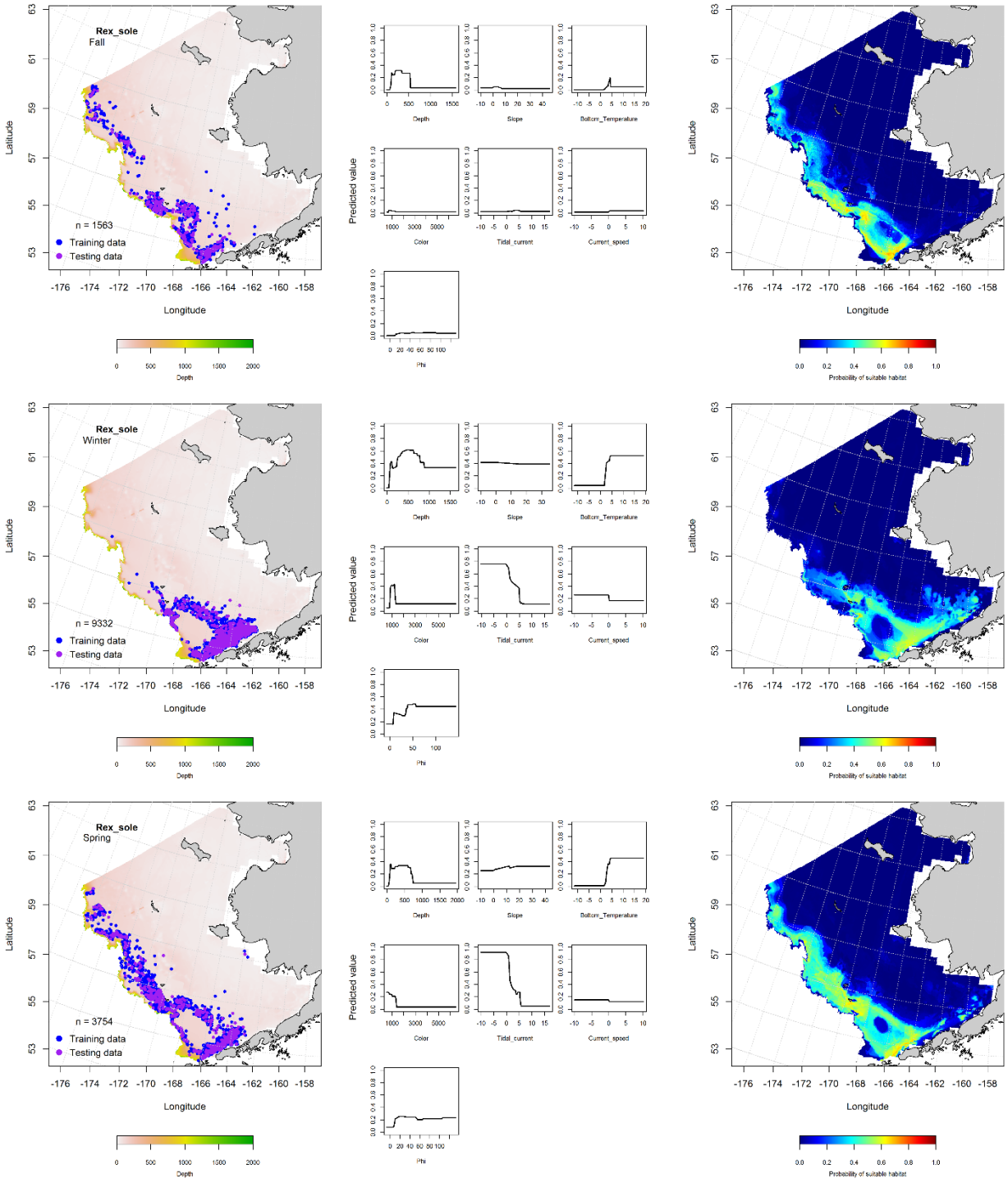

Figure 21. -- Locations of rex sole in fall (October-November; top row), winter (December-February; middle row), and spring (March-May; bottom row) commercial fisheries catches (2003-2013) from the eastern Bering Sea (left-hand column). Blue points were used to train the MaxEnt model (center column) predicting the probability of suitable habitat (right-hand column) and the purple points were used to validate the model.

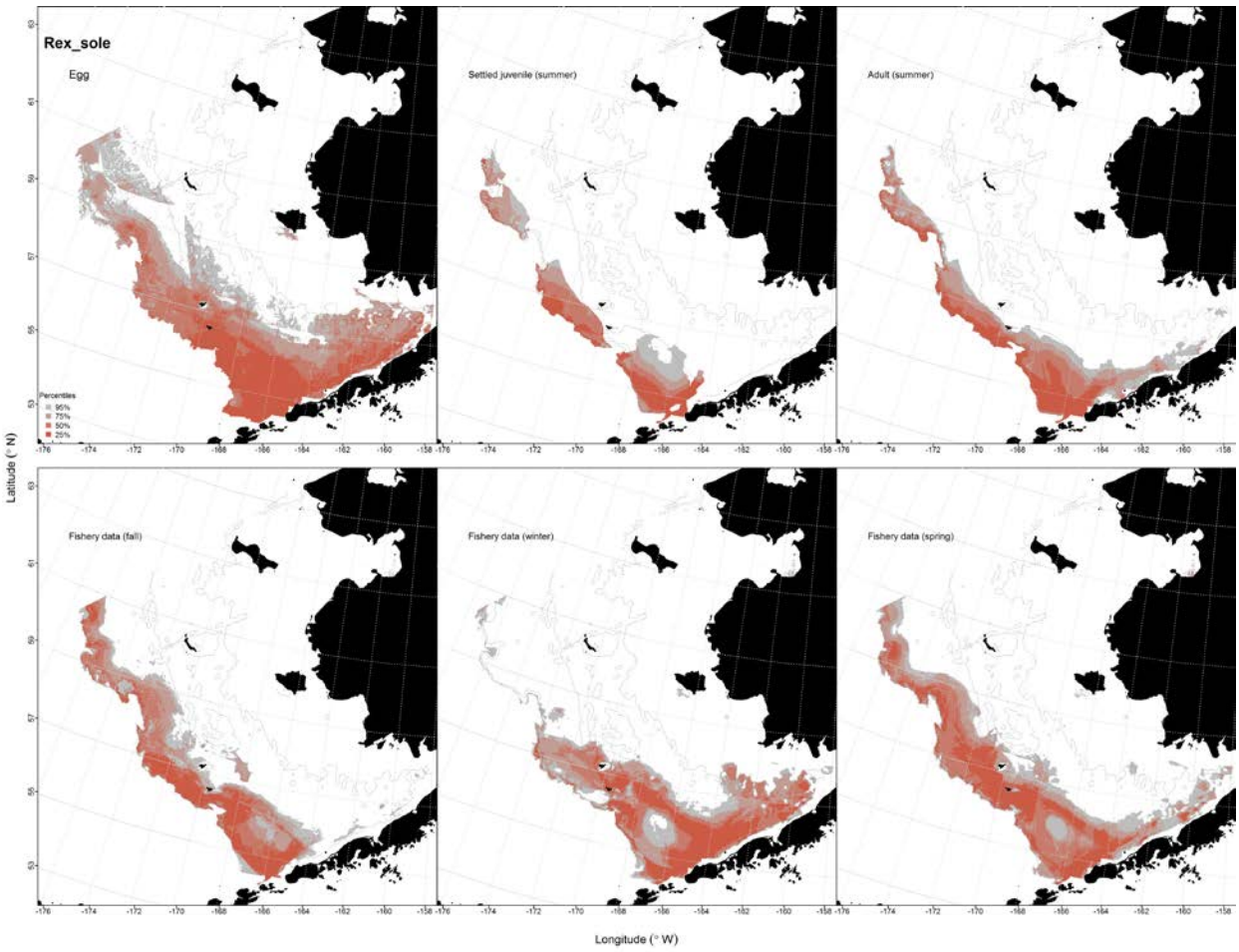

Figure 22. -- Essential habitat (EFH) predicted for rex sole eggs (upper left panel) from EcoFOCI ichthyoplankton surveys (1991-2013), settled juveniles and adults (upper center and right panels) from RACE-GAP summertime bottom trawl surveys (1982-2014), and predicted from presence in commercial fishery catches (2003-2013) from fall, winter, and spring in the eastern Bering Sea (bottom three panels).

Dover Sole (*Microstomus pacificus*)

Distribution of early life stages of Dover sole (*Microstomus pacificus*) in EcoFOCI ichthyoplankton surveys of the eastern Bering Sea -- Early life history stages of Dover sole were not common in EcoFOCI ichthyoplankton surveys (1991-2013) of the eastern Bering Sea (Fig. 23). Eggs were present between April and September, but larvae were collected only during the month of July

(Table 2). There were 31 instances of Dover sole egg and 5 instances of Dover sole larval collections. This prevalence was too low to support modeling distribution of essential habitat for these two life stages.

Summertime distribution of settled juvenile and adult Dover sole (*Microstomus pacificus*) from RACE-GAP bottom trawl surveys of the eastern Bering Sea -- Settled juvenile Dover sole were collected on RACE-GAP summer bottom trawl surveys conducted in the EBS (Fig. 24). A MaxEnt model was used to describe their distribution. The most important covariates for predicting the probability of settled juvenile Dover sole suitable habitat were, in order of importance, bottom depth, ocean productivity, and bottom temperature. Combined, these three terms accounted for 88.5% of the leverage provided by all covariates in the model. The region predicted to have the most suitable habitat for settled juvenile Dover sole was in the southern domain of the eastern Bering Sea along the 200 m isobath and in deeper waters over the Bering Canyon. The model fit to the training data was outstanding (AUC = 0.97), correctly classifying 93% of predicted presence-absence cases. Model validation using the test data was acceptable (AUC = 0.79) and correctly classified 79% of the predicted cases.

A MaxEnt model was also used to describe distribution and to predict suitable adult Dover sole habitat (Fig. 25). The most important habitat covariates predicting the probability of suitable adult Dover sole habitat were, in order of importance, bottom depth, slope, and ocean productivity. Combined, these three terms accounted for 97.1% of the leverage provided by all covariates in the model. The areas predicted to have the most suitable habitat for adult Dover sole were in the southern domain of the eastern Bering Sea in waters greater than 200 m over the Bering Canyon, near the head of Pribilof Canyon, and below the southern arm of Zhemchug Canyon. The model fit to the training data was outstanding (AUC = 0.99), correctly classifying 94% of predicted cases. Model validation using the test data also outstanding (AUC = 0.98) and correctly classified 98% of the predicted cases.

Seasonal distribution of Dover sole (*Microstomus pacificus*) in commercial fishery catches from the eastern Bering Sea -- The occurrence of Dover sole in commercial catches from the eastern Bering Sea varied seasonally (Fig. 26). In fall, they occurred in the southern domain of the eastern Bering

Sea primarily in the Bering Canyon and near the head of Pribilof Canyon, but not with sufficient prevalence to warrant modeling habitat distribution in this season. During wintertime, the most important covariates predicting suitable habitat from the MaxEnt model were, in order of importance, slope, bottom temperature, and bottom depth (combined relative importance of 60.2%). High probability winter Dover sole habitat extended eastward from the Bering Canyon into Bristol Bay and was also found at the head of Pribilof Canyon. The model fit to the training data was outstanding (AUC = 0.99); it correctly classified 96% of predicted cases. Model validation with the test data set was also outstanding (AUC = 0.96), correctly classifying 96% of cases. In the spring, the most important covariates predicting probability of suitable Dover sole habitat from the MaxEnt model were, in order of importance, bottom slope, bottom depth, and ocean productivity (combined relative importance of 83.8%). The predicted probability of suitable habitat in springtime was highest over the Bering Canyon and at the head of Pribilof Canyon. The model fit to the training data was outstanding (AUC = 0.99); it correctly classified 94% of predicted cases. Model validation with the test data set was excellent (AUC = 0.80), correctly classifying 80% of cases.

Eastern Bering Sea Dover sole (*Microstomus pacificus*) essential fish habitat maps and conclusions -- Predicted Dover sole EFH varied amongst seasons and data sources (Fig. 27). For settled juvenile Dover sole from summer surveys, EFH was widely spread across the southern domain of the eastern Bering Sea. Adult Dover sole EFH was constrained to waters greater than 200 m deep on the outer shelf and upper slope and this area of core EFH was shared by the settled juveniles. EFH predicted from commercial fishery catches shared most areas in common with EFH predicted from the summer surveys. Where EFH from the VOE-CIA data was predicted in shallower waters around the Pribilofs and in Bristol Bay it is likely that this reflects fishing activity and not Dover sole movement into those shallower waters.

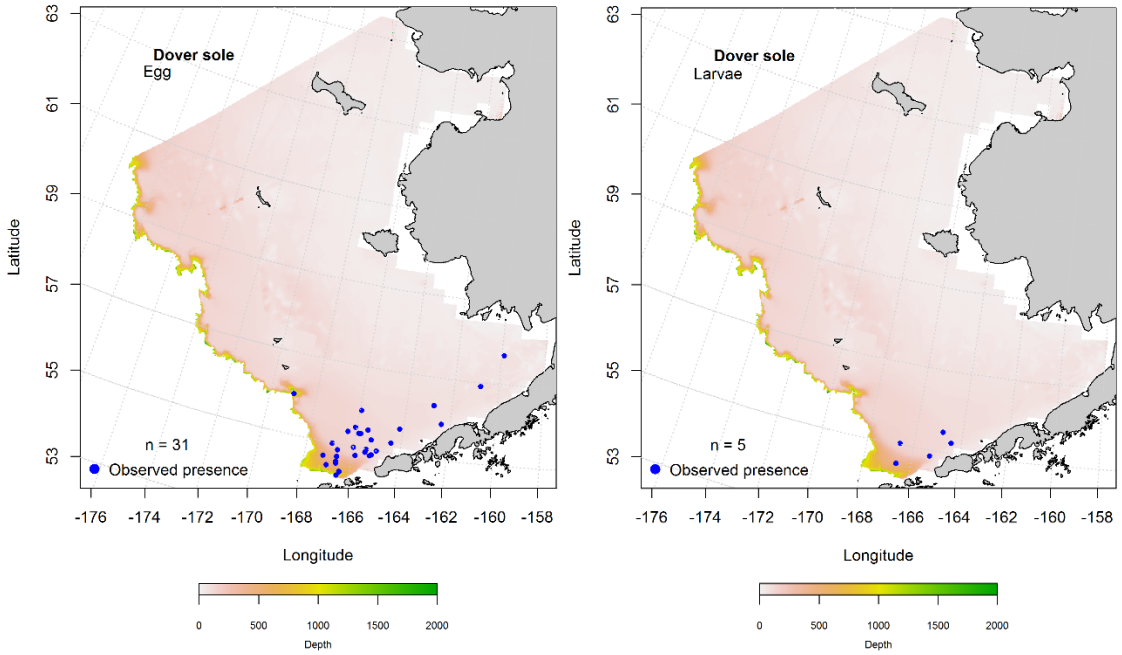

Figure 23. -- Presence of Dover sole eggs (left panel) and larvae (right panel) in EcoFOCI ichthyoplankton surveys of the eastern Bering Sea (1991-2013).

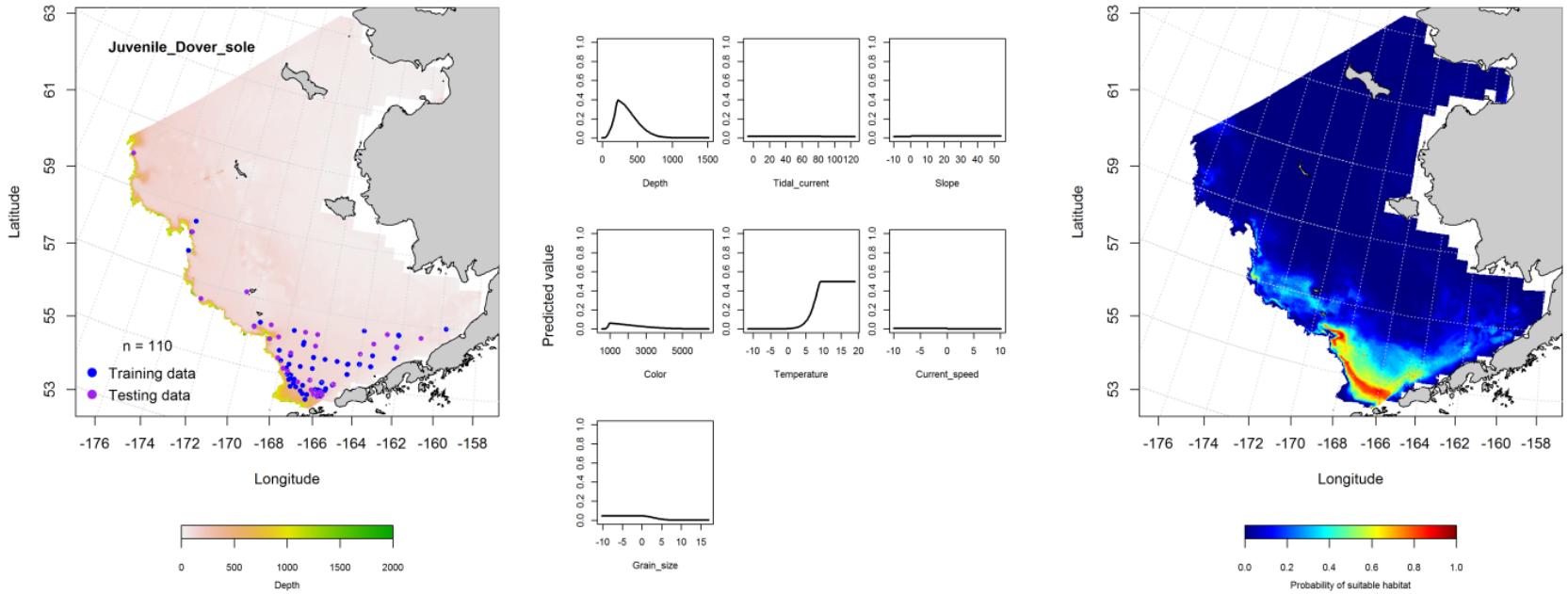

Figure 24. -- Presence of settled juvenile Dover sole in RACE-GAP summer bottom trawl surveys (1982-2014) of the eastern Bering Sea (left panel) with training (blue dots) and testing (purple dots) data sets indicated alongside the maximum entropy model (MaxEnt) effects (center panel) and the MaxEnt spatial predictions of the probability of suitable settled juvenile Dover sole habitat (right panel).

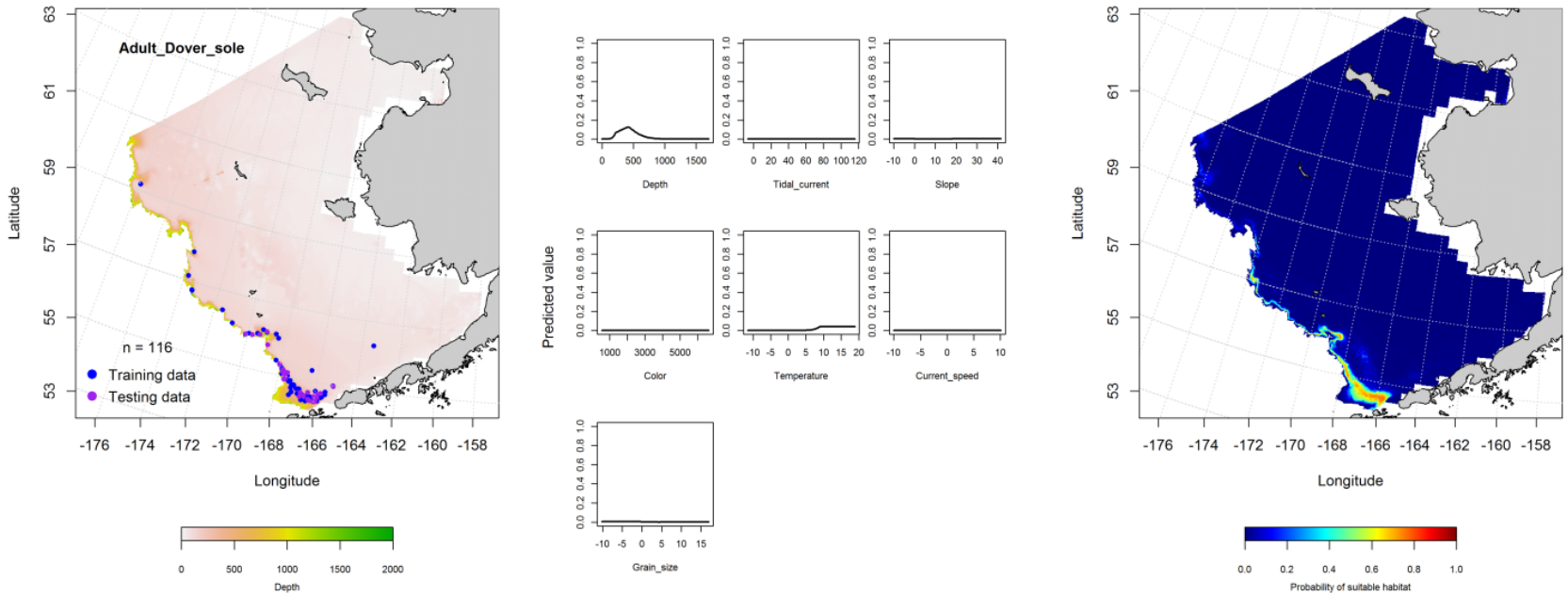

Figure 25. -- Presence of adult Dover sole in RACE-GAP summer bottom trawl surveys (1982-2014) of the eastern Bering Sea (left panel) with training (blue dots) and testing (purple dots) data sets indicated alongside the maximum entropy model (MaxEnt) effects (center panel) and the MaxEnt spatial predictions of the probability of suitable adult Dover sole habitat (right panel).

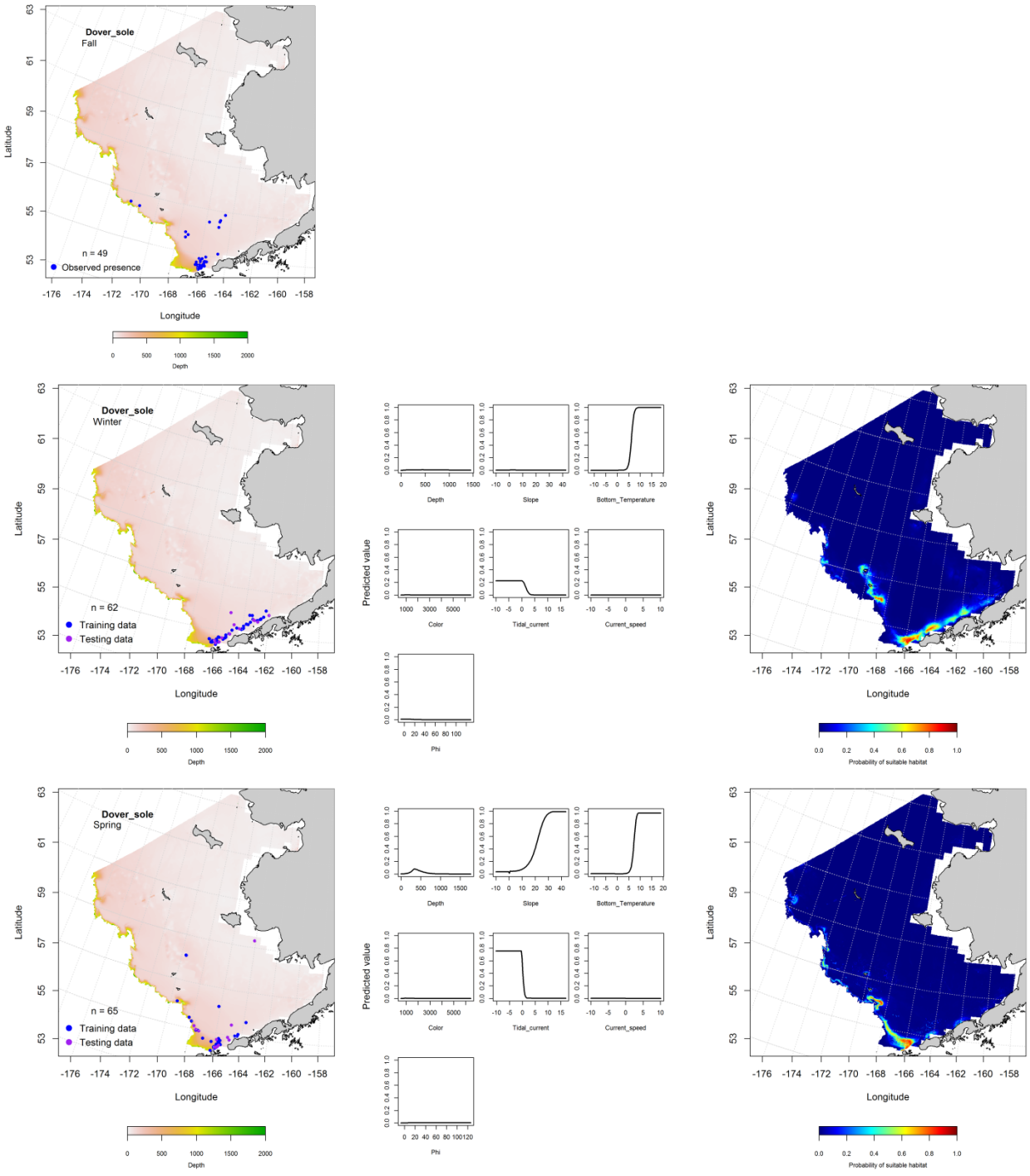

Figure 26. -- Locations of Dover sole in fall (October-November; top row), winter (December-February; middle row), and spring (March-May; bottom row) commercial fisheries catches (2003-2013) from the eastern Bering Sea (left-hand column). Blue points were used to train the MaxEnt model (center column) predicting the probability of suitable habitat (right-hand column) and the purple points were used to validate the model.

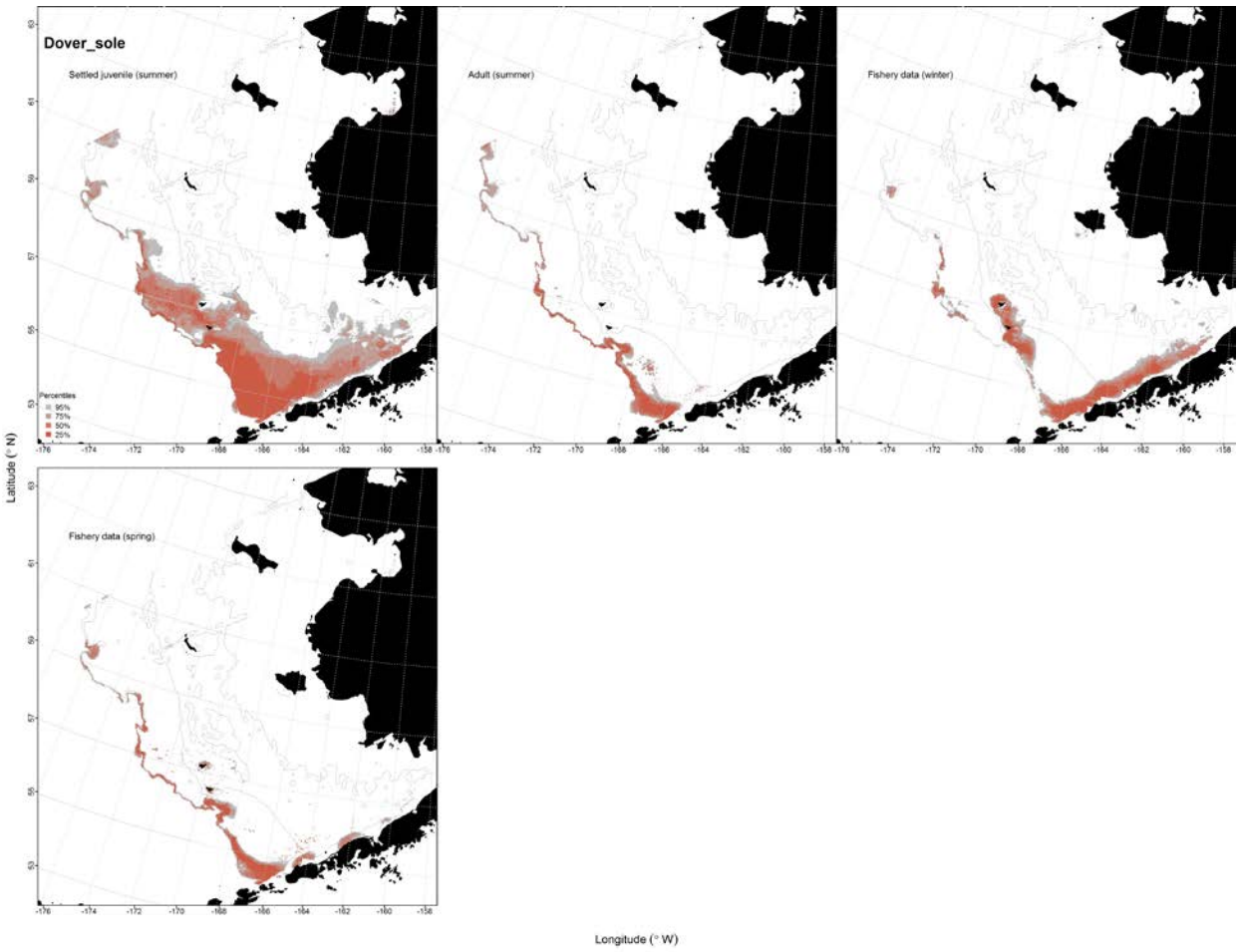

Figure 27. -- Essential fish habitat (EFH) predicted for settled juvenile (upper left panel) and adult Dover sole (upper right panel) from RACE-GAP summertime bottom trawl surveys (1982-2014) and predicted from presence in commercial fishery catches (2003-2013) from winter (upper right panel) and spring (lower left panel) in the eastern Bering Sea.

Yellowfin Sole (*Limanda aspera*)

Distribution of early life history stages of yellowfin sole from EcoFOCI ichthyoplankton surveys of the eastern Bering Sea -- Early life history stages of yellowfin sole were present in EcoFOCI ichthyoplankton surveys of the EBS between May and October (1991-2013; Table 2). Eggs and larvae were prevalent on the inner and middle shelves of the eastern Bering Sea and extended into Norton Sound. Pelagic juvenile yellowfin sole were not common in these surveys (Fig. 35) and, consequently, their distribution was not modeled.

Yellowfin sole eggs were present in 1991-2013 EcoFOCI ichthyoplankton survey samples between May and October (Fig. 36). The most important habitat covariates in the model were bottom depth, ocean productivity, and surface temperature (combined relative importance = 36%). The MaxEnt model fit to the egg presence training data was outstanding (AUC = 0.90) and the model correctly classified 82% of the predicted cases. Model validation was successful (AUC = 0.80) correctly classifying 80% of the predicted cases.

Larval yellowfin sole were present in 1991-2013 EcoFOCI ichthyoplankton survey samples between July and October (Fig. 37). The most influential habitat covariates in the summer MaxEnt model were bottom depth and ocean productivity (combined relative importance = 79.2%). The model fit to the yellowfin sole larval presence data was outstanding (AUC = 0.90) and it correctly classified 82% of the cases it predicted. Model validation produced a fit to the test data (AUC = 0.69) that was better than chance with 69% of predicted cases correctly classified.

Summertime distribution of settled juvenile and adult yellowfin sole from RACE-GAP bottom trawl surveys of the eastern Bering Sea -- Settled juvenile and adult yellowfin sole were collected on RACE-GAP summer bottom trawl surveys throughout the EBS. Historically, yellowfin sole catch rates have been highest on the inner shelf of the EBS (< 50 m deep) in Bristol Bay (Lauth and Conner 2014). They were also one of the most abundant flatfishes collected in the NBS (Lauth 2011).

Settled juvenile yellowfin sole collected during RACE-GAP summer bottom trawl surveys were distributed throughout the EBS on the inner, middle, and outer shelf from the Alaska Peninsula to the U.S.-Russia Convention Line (Fig. 38). The best-fitting GAM predicted the highest settled juvenile yellowfin sole abundance along the inner shelf in the central domain of the EBS south of Nunivak Island where sediment grain size was small and currents were low. The most influential habitat covariates retained in the model were geographic location, sediment grain size, bottom and tidal current speeds, and ocean productivity. This GAM explained 80.3% of the deviance in juvenile yellowfin sole CPUE and was

a good fit to the training data ($r^2 = 0.80$); model validation using the test data had an identical fit ($r^2 = 0.80$).

Adult yellowfin sole were collected over a similar range to that observed for juvenile yellowfin sole collected during RACE-GAP summer bottom trawl surveys (Fig. 39). The best-fitting GAM predicting adult yellowfin sole abundance maps their highest abundance on the inner shelf of the EBS south of Nunivak Island where sediment grain size was small and current speeds were low. The most influential habitat covariates retained in the model were geographic location, sediment grain size, ocean productivity, tidal current speed, and bottom depth. This model explained 81.6% of the variability in the adult yellowfin sole CPUE data and was a good fit to both the training ($r^2 = 0.82$) and test data ($r^2 = 0.81$).

Seasonal distribution of yellowfin sole in commercial fishery catches from the eastern Bering Sea -- Yellowfin sole observed in fall, winter, and spring commercial catches from the EBS primarily came from the central and southern domains on the middle and outer shelf of the eastern Bering Sea (Fig. 40). In contrast to fall and winter, it appears that a portion of the commercial fishing effort moved inshore into shallow waters along continental Alaska in spring. The most important fixed habitat covariates in the MaxEnt model for predicting probability of suitable yellowfin sole habitat from their presence in commercial catches were sediment grain size and bottom depth. The combined relative importance of these two covariates was 66.8% in fall, 73.1% in winter, and 61.2% in spring. Also important in fall and winter were ocean productivity (12.4% and 18.8%); in springtime bottom temperature accounted for 17.4% of the relative importance of habitat covariate predictors in the model. In all three seasons, model effects were highest in depths less than 100 m and where sediment grain sizes decreased. Model fits to the training data were excellent (AUC > 0.90) and the models correctly classified 83-90% of predicted cases. Model validation was successful, AUC ranged from outstanding (0.83) to excellent (0.90) and correctly classified between 83% and 90% of predicted cases.

Essential fish habitat maps and conclusions for yellowfin sole (*Limanda aspera*) from the eastern Bering Sea -- Yellowfin sole EFH in the EBS is centered in nearshore areas along the Alaska

Peninsula and continental shore (Fig. 41). Essential yellowfin sole egg and larval habitat was primarily found between the 50 and 100 m isobaths from Bristol Bay north into the NBS. Settled juveniles and adults in RACE-GAP summer bottom trawl surveys displayed similar distributions of EFH. The pattern of nearshore EFH demonstrated in ELHS and RACE-GAP data sets was not duplicated in the MaxEnt predictions of EFH from fall and winter commercial fisheries data suggesting that fishing activity was not directed into nearshore areas during those seasons. In springtime, more observations of yellowfin sole in commercial catches came from nearshore areas which helped to extend the EFH map based on these data in shore.

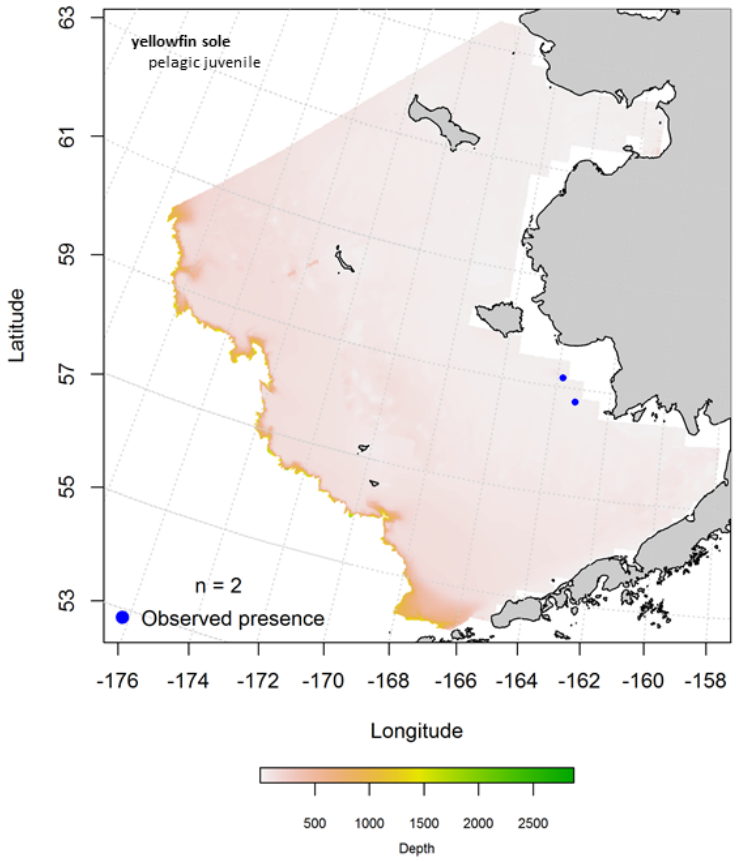

Figure 28. -- Presence of pelagic juvenile yellowfin sole in EcoFOCI ichthyoplankton surveys of the eastern Bering Sea (1991-2013).

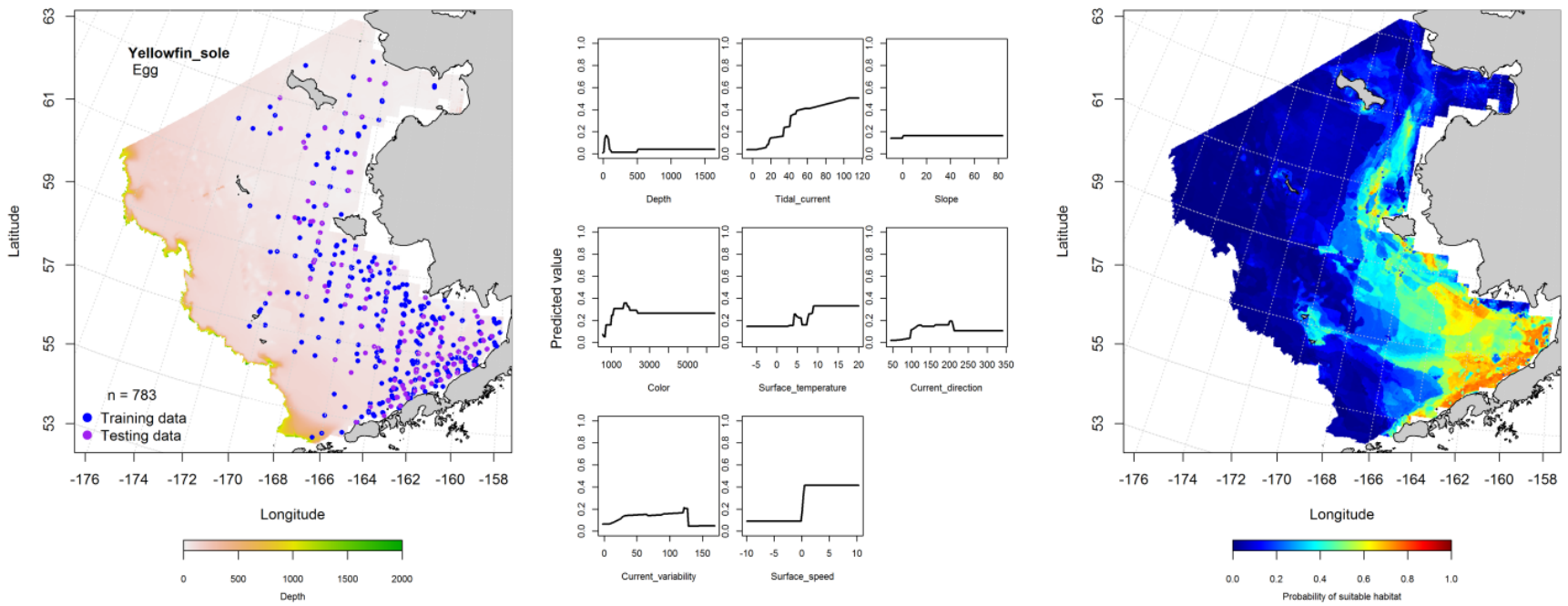

Figure 29. -- Presence of yellowfin sole eggs in EcoFOCI ichthyoplankton surveys of the eastern Bering Sea (left panel) with training (blue dots) and testing (purple dots) data sets indicated alongside the maximum entropy model (MaxEnt) effects (center panel) and the MaxEnt spatial predictions of the probability of suitable yellowfin sole egg habitat (right panel).

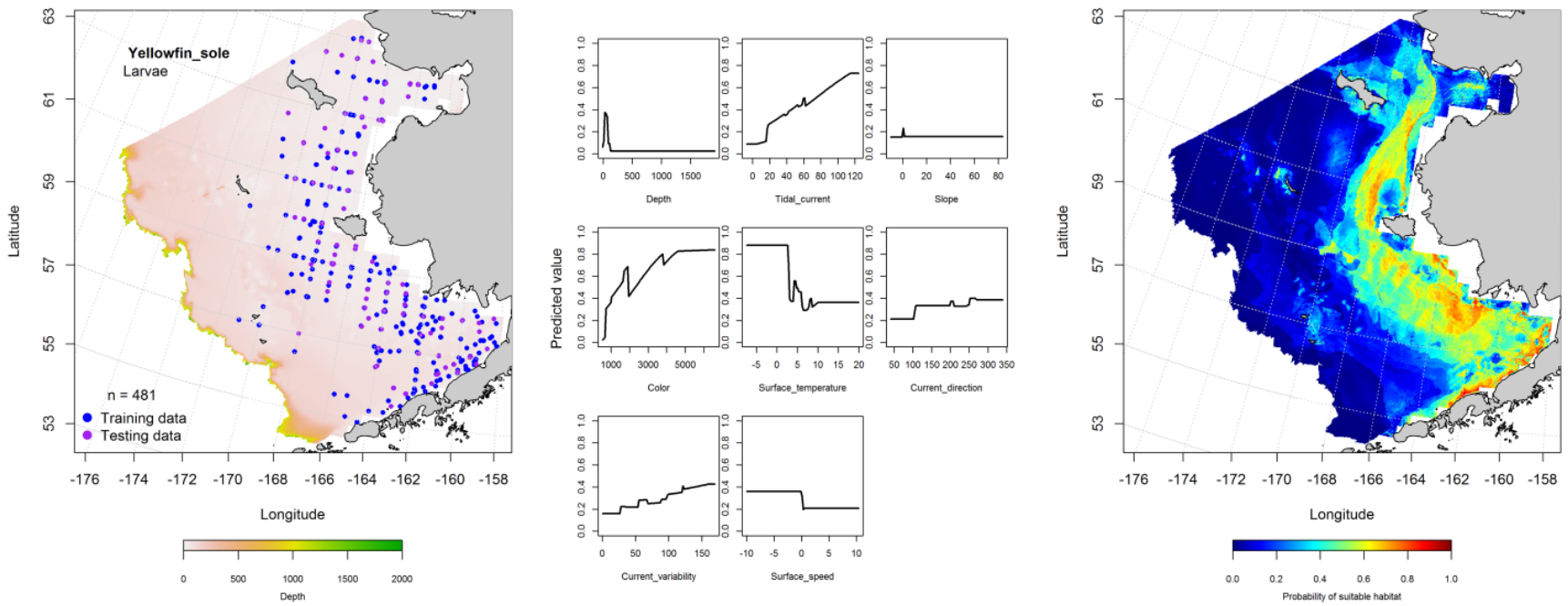

Figure 30. -- Presence of yellowfin sole larvae in EcoFOCI ichthyoplankton surveys of the eastern Bering Sea (left panel) with training (blue dots) and testing (purple dots) data sets indicated alongside the maximum entropy model (MaxEnt) effects (center panel) and the MaxEnt spatial predictions of the probability of suitable larval yellowfin sole habitat (right panel).

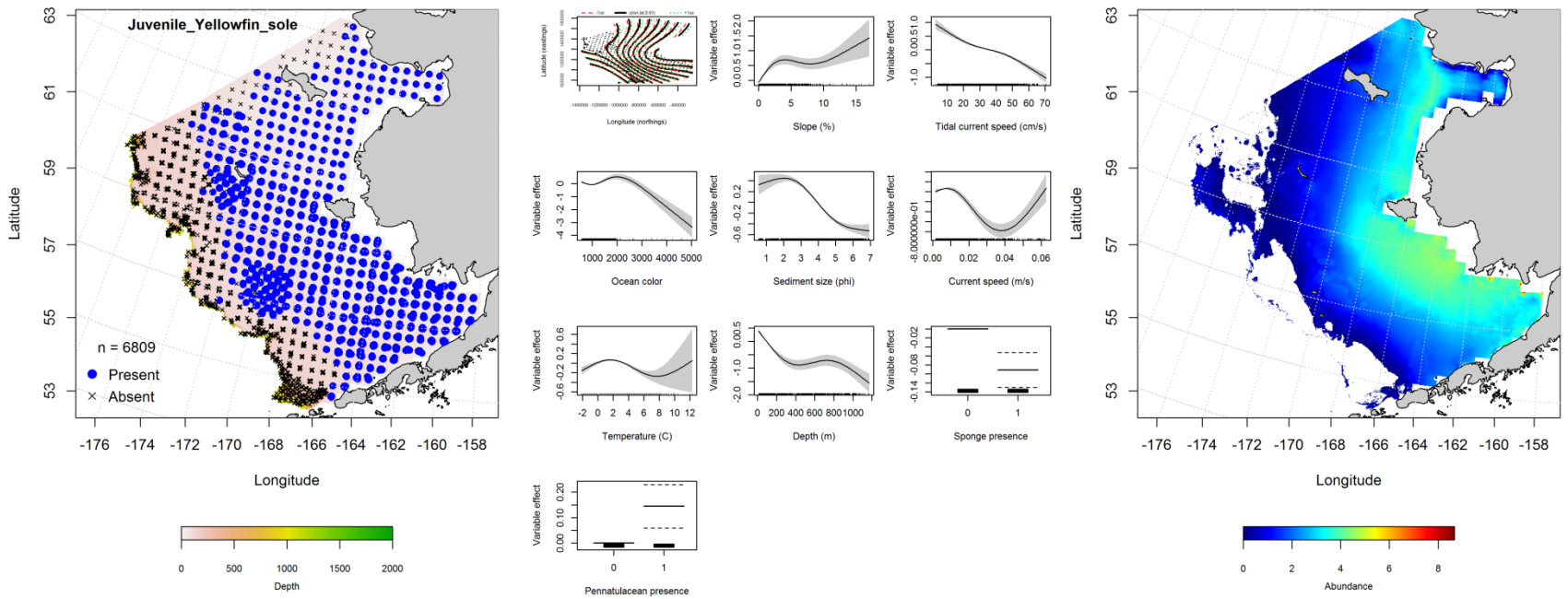

Figure 31. -- Distribution of settled juvenile yellowfin sole in 1982-2014 RACE-GAP summer bottom trawl surveys (left panel) alongside effects of retained habitat covariates in the best-fitting generalized additive model (GAM; center panel) predicting spatial distribution of abundance (CPUE, right panel) across the eastern Bering Sea.

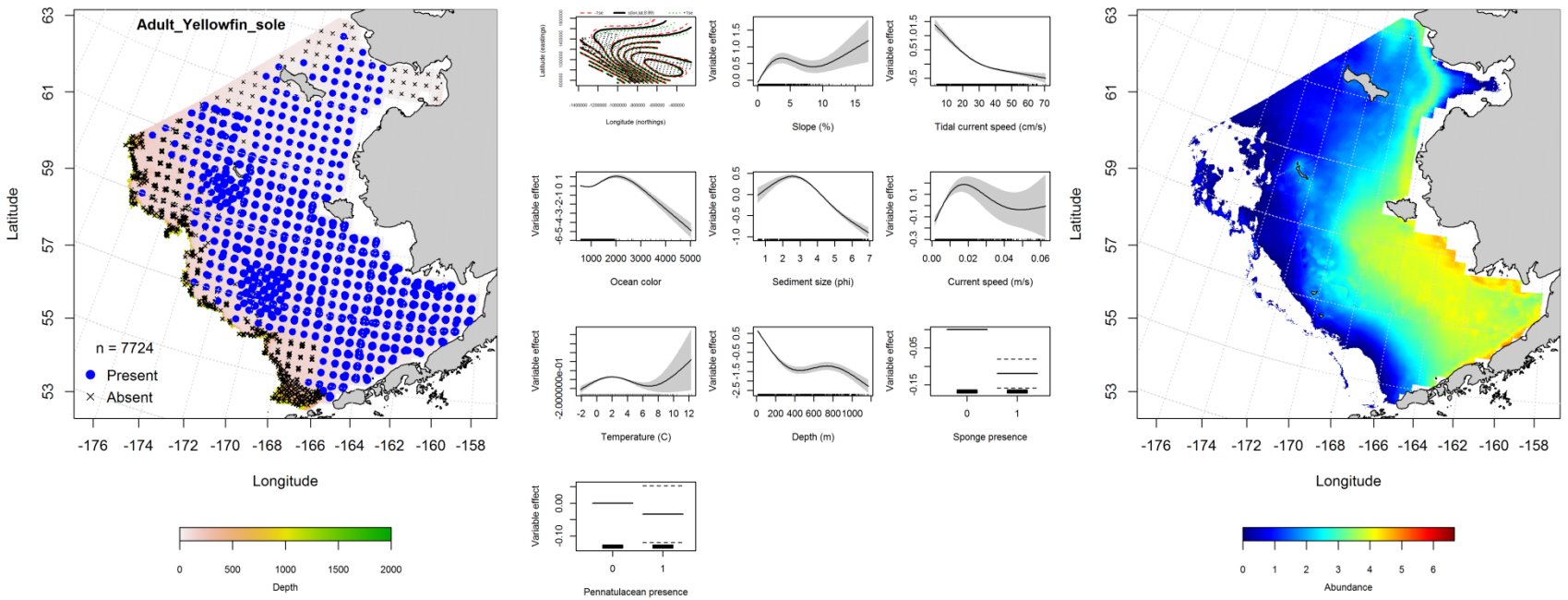

Figure 32. -- Distribution of adult yellowfin sole in 1982-2014 RACE-GAP summer bottom trawl surveys (left panel) alongside effects of retained habitat covariates in the best-fitting generalized additive model (GAM; center panel) predicting spatial distribution of abundance (CPUE, right panel) across the eastern Bering Sea.

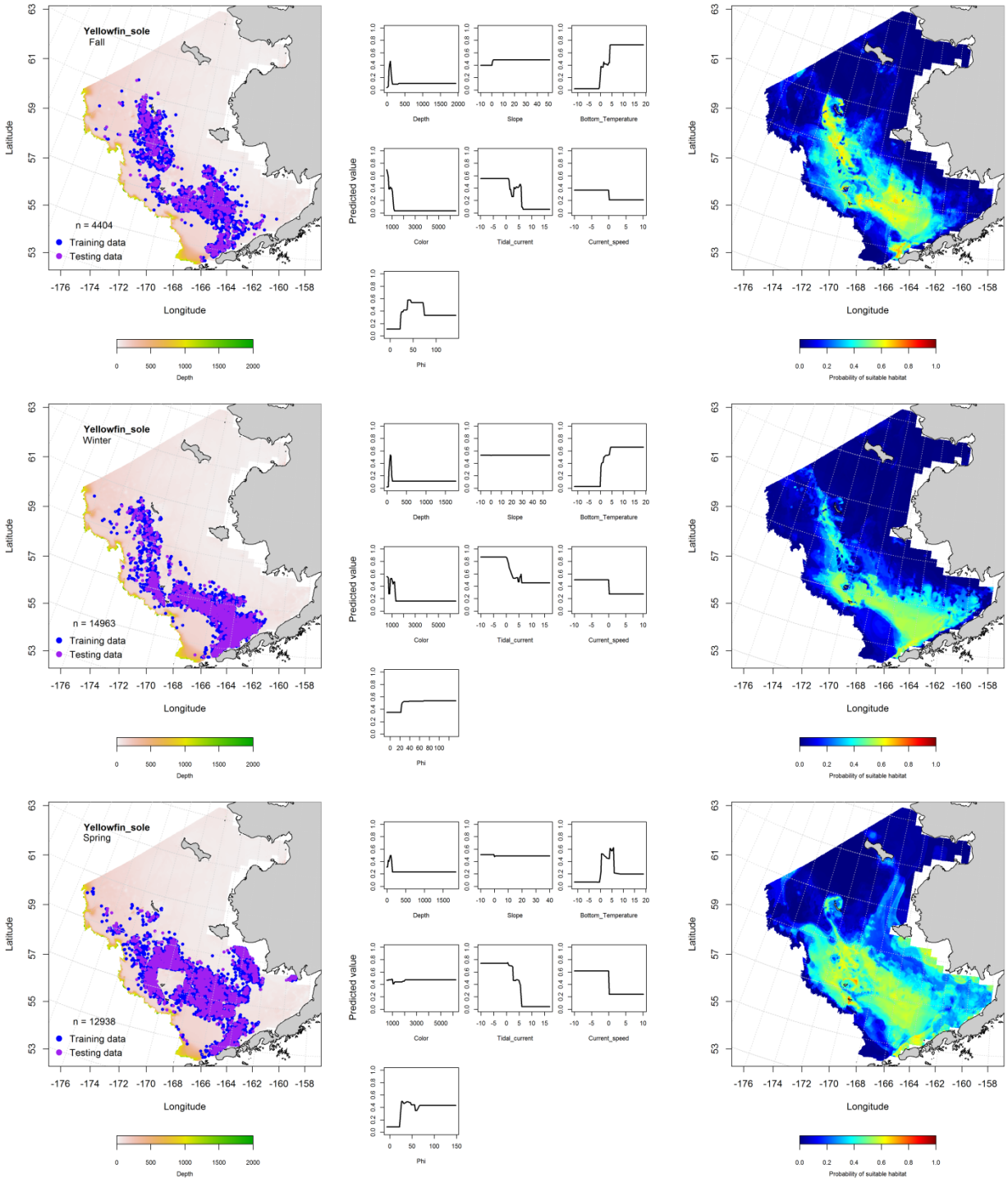

Figure 33. -- Locations of yellowfin sole in fall (October-November; top row), winter (December-February; middle row), and spring (March-May; bottom row) commercial fisheries catches (2003-2013) from the eastern Bering Sea (left-hand column). Blue points were used to train the MaxEnt model (center column) predicting the probability of suitable habitat (right-hand column) and the purple points were used to validate the model.

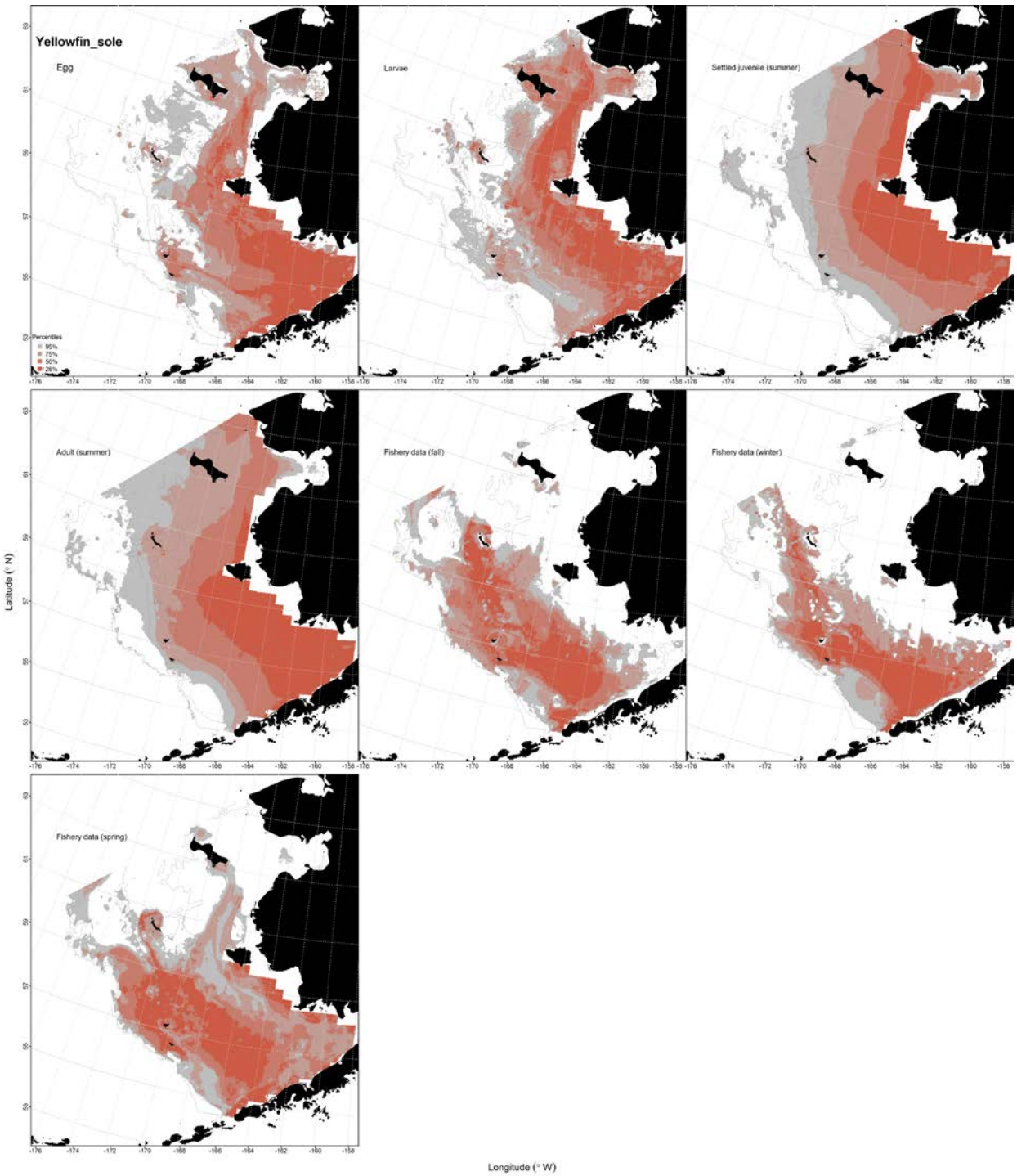

Figure 34. -- Essential habitat (EFH) predicted for yellowfin sole eggs and larvae (upper left and center panels) from EcoFOCI ichthyoplankton surveys (1991-2013), settled juveniles and adults from the RACE-GAP summer bottom trawl surveys (1982-2014; upper right and middle left panels), and predicted from their presence in commercial fishery catches (2003-2013) from fall and winter (middle center and right panels), and spring (bottom left panel) from the eastern Bering Sea.

Flathead Sole (*Hippoglossoides elassodon*)

Distribution of early life history stages of flathead sole from EcoFOCI ichthyoplankton surveys of the eastern Bering Sea -- Flathead sole eggs, larvae, and pelagic juveniles can be distinguished from ELHS of other flatfish species in EcoFOCI ichthyoplankton samples. These early life stages are generally observed in the southern domain of the eastern Bering Sea but their distribution varies seasonally.

Flathead sole eggs were primarily reported from EcoFOCI ichthyoplankton samples collected between April and September (Table 2) from the central and southern domains of the eastern Bering Sea (Fig. 28). Flathead sole eggs were present on the inner shelf (< 50 m) out to the shelf edge and beyond (200 to 3,000 m). There were also a few clusters of flathead sole egg observations from the northern Bering Sea around St. Matthew's Island and Pervenets Canyon. The highest MaxEnt-predicted probability for suitable flathead sole egg habitat was located along the northern side of Unimak Pass near the Bering Canyon and extending eastward into Bristol Bay. The most influential habitat covariate in this model was surface temperature (relative importance of 76.7%) followed by bottom depth (8.9%) and ocean productivity (6.6%). The model fit to the training data was excellent (AUC = 0.93) and it correctly classified 87% of predicted cases. Model validation with the test data was successful (AUC = 0.88) and correctly classified 88% of cases.

Flathead sole larvae were collected on EcoFOCI ichthyoplankton surveys between April and October (Table 2) primarily from the central and southern domains of the eastern Bering Sea (Fig. 29). The larvae were more dispersed than across the EBS than were the eggs. The most important covariate in the MaxEnt model describing larval flathead sole habitat was surface temperature (relative important = 59.8%) followed by ocean productivity (15%) and bottom depth (9.1%). The areas with the highest predicted probabilities of suitable habitat for this ELHS were centered around the Pribilof Islands and the northern margin of Unimak Pass. The model fit to the training data was excellent (AUC = 0.90)

and it correctly classified 82% of predicted cases. Model validation with the test data was successful (AUC = 0.84) and correctly classified 84% of cases.

Pelagic juvenile stage flathead sole were not common in EcoFOCI ichthyoplankton samples of the eastern Bering Sea (Fig. 30). The 10 occurrences reported were spread from the Alaska Peninsula to the Pribilof Islands. These did not provide sufficient data for distribution modeling.

Summertime distribution of late-juvenile and adult flathead sole from RACE-GAP bottom trawl surveys of the eastern Bering Sea -- Settled juvenile and adult flathead sole catches in RACE-GAP summer bottom trawl surveys of the eastern Bering Sea were spread from the northern to southern extent of the survey area from the inner to the outer shelf. Historically, high flathead sole CPUEs have been recorded on the middle shelf around the Pribilof Islands (Lauth and Conner 2014).

The best-fitting GAM for settled juvenile flathead sole abundance in the EBS explained 57.2% of the deviance in the CPUE data (Fig. 31). Geographical location, sediment grain size, and bottom depth were the most important predictors amongst the 10 habitat covariates retained in the GAM. Juvenile flathead sole abundance decreased from southwest to northeast across the survey area with decreasing bottom depth and increased with decreasing sediment grain size. The fit of this model was better than chance ($r^2 = 0.57$). The fit to the test data in the model validation step was similar ($r^2 = 0.57$).

The best-fitting GAM describing adult flathead abundance explained 58.9% of the deviance in the CPUE data from the EBS (Fig. 32). Geographical location, bottom depth, and sediment grain size were the most influential habitat covariates retained in the model. Model effects on abundance were highest in the southeast portion of the survey area and decreased to the north and northeast. Modeled abundance increased over finer sediments and warmer temperatures and decreased with increasing bottom depth. The GAM fit to the training data was acceptable ($r^2 = 0.59$). The fit to the test data in the model validation step was slightly better ($r^2 = 0.61$).

Seasonal distribution of flathead sole in commercial fishery catches from the eastern Bering Sea -- Flathead sole observed in commercial catches from the eastern Bering Sea primarily occurred on the middle and outer shelves from the U.S.-Russia Convention Line to the Alaska Peninsula in all three seasons considered (Fig. 33). The most important covariates predicting suitable habitat from the MaxEnt model in fall, winter, and spring were bottom depth and bottom temperature; combined relative importance for these two terms ranged from a low in springtime of 78.4% to a high in fall of 91%. The areas with the highest probability to provide suitable flathead sole habitat based on these commercial observer data varied with season, but were generally found in waters deeper than 100 m. MaxEnt model fits ranged from excellent in winter (AUC = 0.93) where 86% of predicted cases were correctly classified to outstanding in fall; AUC = 0.89 and 82% of cases were correctly classified. Model validation was successful with outstanding AUC's of 0.80 and 0.85 in fall and winter resulting in correctly classified cases of 80 and 85%, respectively.

Essential fish habitat maps and conclusions for flathead sole from the eastern Bering Sea -- Much of the core EFH for the flathead sole life stages collected in different seasons and predicted from different data sources overlapped across the EBS (Fig. 34). Core essential habitat of flathead sole eggs was primarily found across the shelf from Bristol Bay to Bering Canyon along the Alaska Peninsula. Core larval habitat mirrored that of flathead sole eggs, but extended farther northward past St. Paul in the Pribilof Islands. Summertime EFH of late-juvenile and adult flathead sole was spread across the outer and middle shelf from the southern domain of the eastern Bering Sea to the U.S.-Russia Convention Line to the north with distinct areas of core EFH in each of the three domains. There were some notable areas of EFH for settled juvenile flathead sole in Norton Sound as well. In general, EFH predicted from flathead sole observed in the commercial fisheries demonstrated little difference amongst seasons and was similar to that seen for other life stages from other data sources. However, core EFH predicted from commercial fisheries appears to be constrained more to the outer shelf than either the ELHS EFH or the summertime EFH.

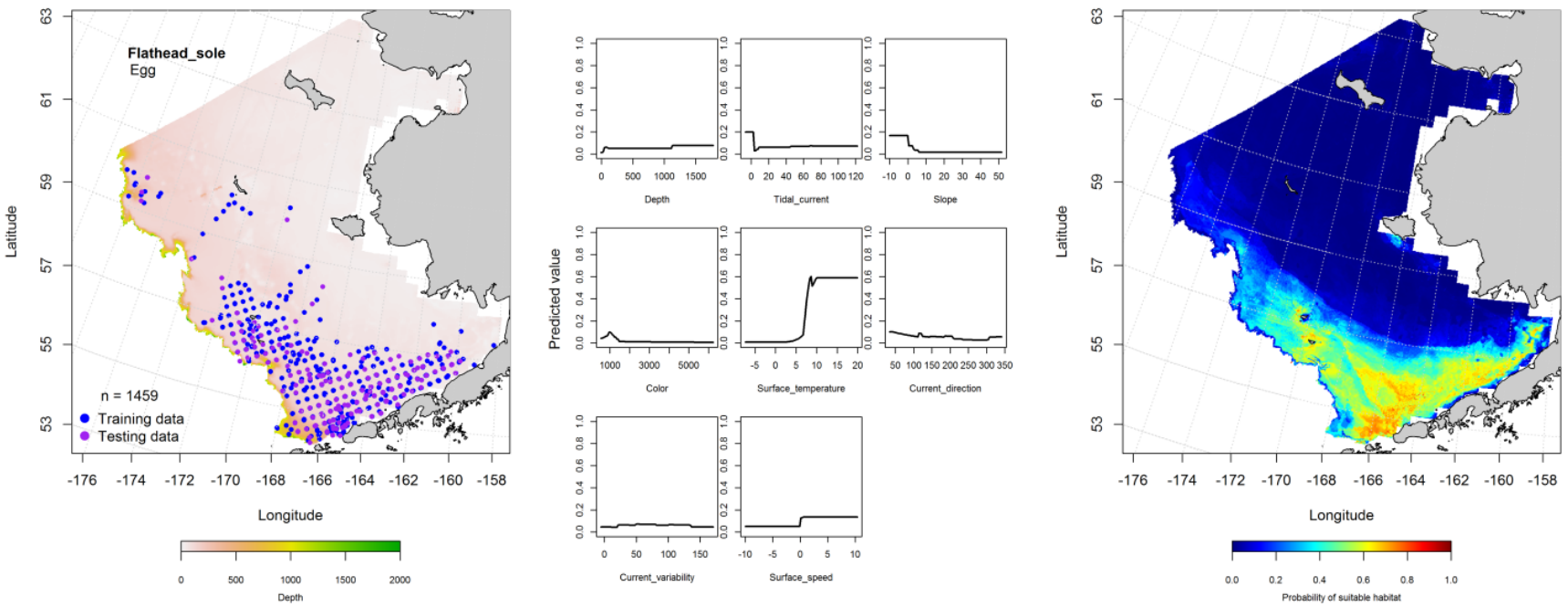

Figure 35. -- Presence of flathead sole eggs in EcoFOCI ichthyoplankton surveys of the eastern Bering Sea (left panel) with training (blue dots) and testing (purple dots) data sets indicated alongside the maximum entropy model (MaxEnt) effects (center panel) and the MaxEnt spatial predictions of the probability of suitable flathead sole egg habitat (right panel).

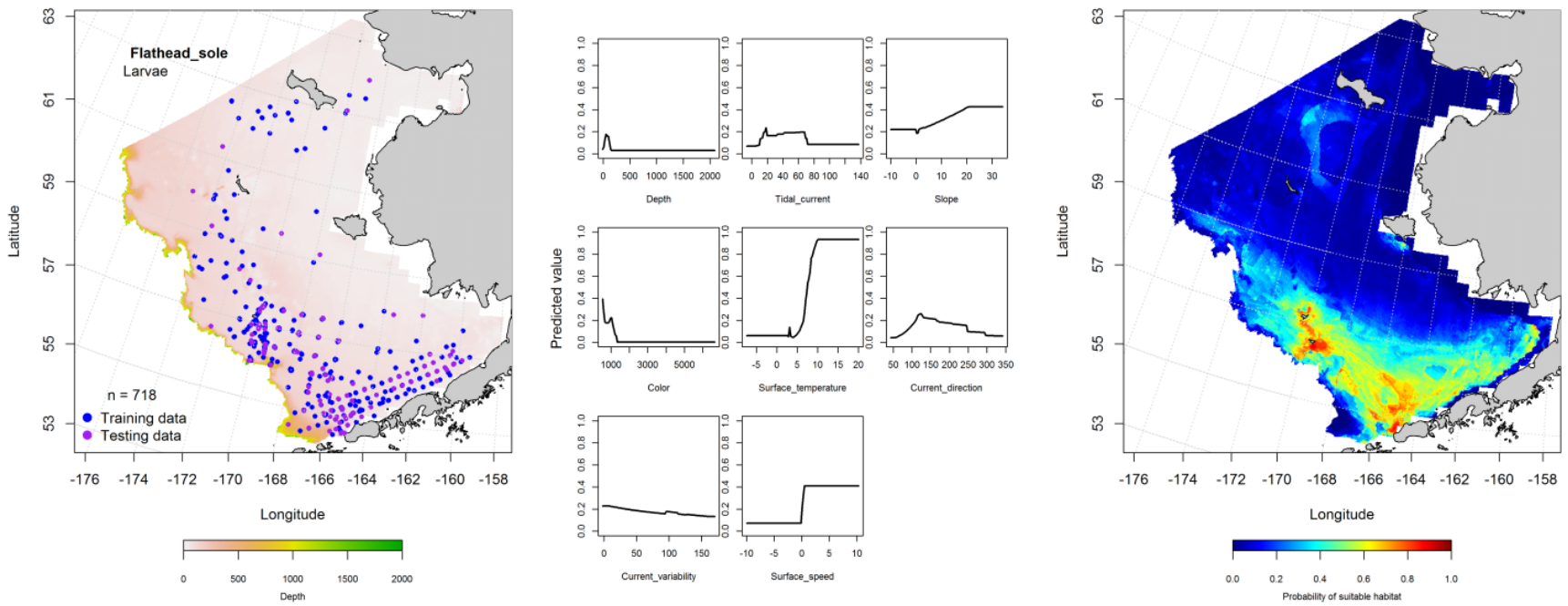

Figure 36. -- Presence of flathead sole larvae in EcoFOCI ichthyoplankton surveys of the eastern Bering Sea (left panel) with training (blue dots) and testing (purple dots) data sets indicated alongside the maximum entropy model (MaxEnt) effects (center panel) and the MaxEnt spatial predictions of the probability of suitable larval flathead sole habitat (right panel).

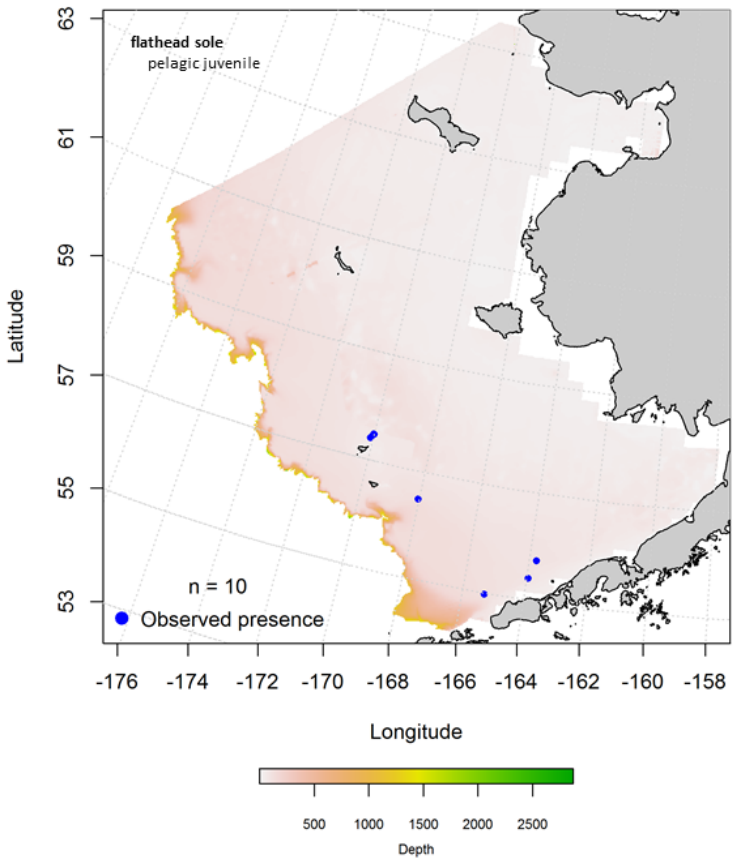

Figure 37. -- Presence of pelagic juvenile flathead sole in EcoFOCI ichthyoplankton surveys of the eastern Bering Sea (1991-2013).

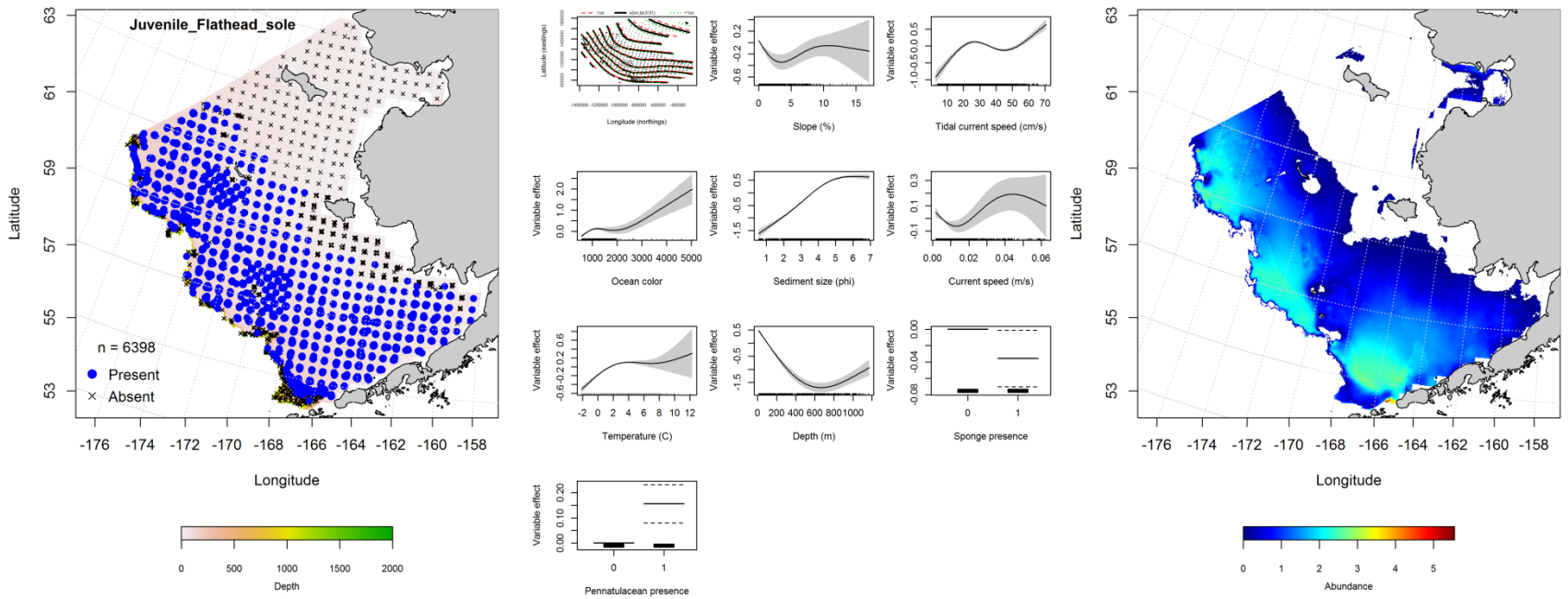

Figure 38. -- Distribution of settled juvenile flathead sole in 1982-2014 RACE-GAP summer bottom trawl surveys (left panel) alongside effects of retained habitat covariates in the best-fitting generalized additive model (GAM; center panel) predicting spatial distribution of abundance (CPUE, right panel) across the eastern Bering Sea.

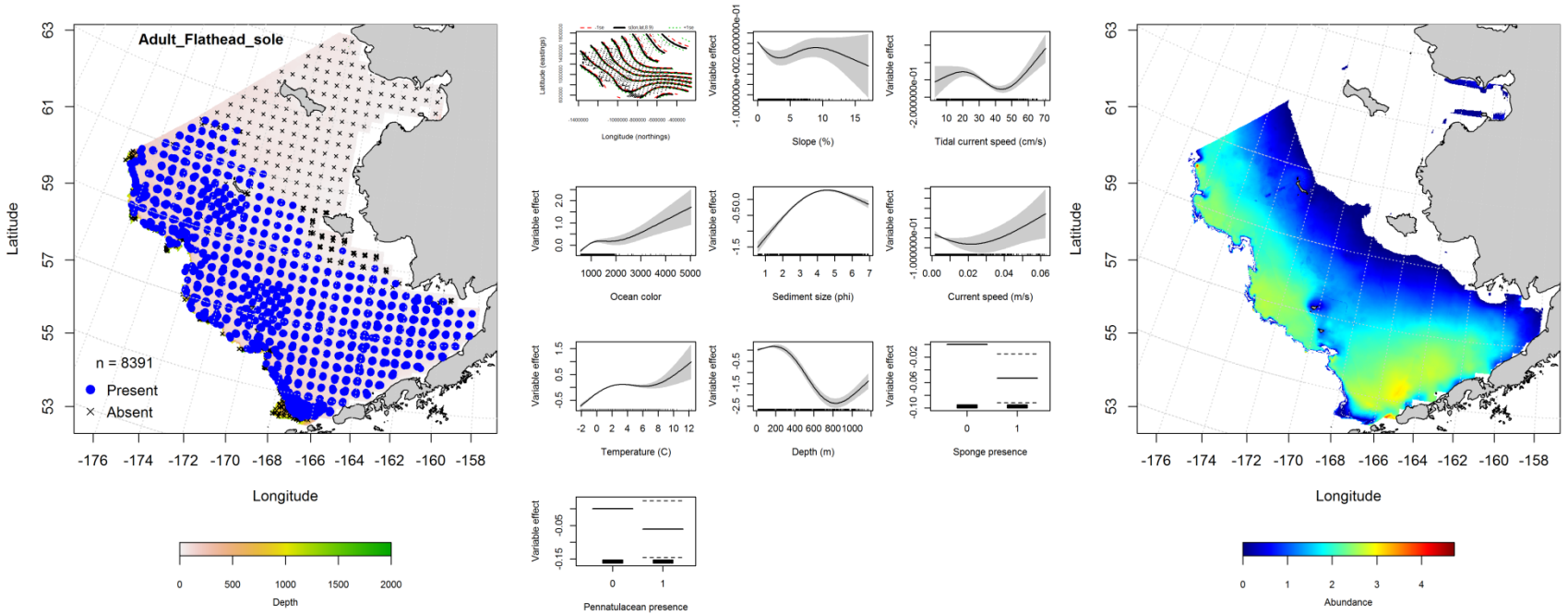

Figure 39. -- Distribution of adult flathead sole in 1982-2014 RACE-GAP summer bottom trawl surveys (left panel) alongside effects of retained habitat covariates in the best-fitting generalized additive model (GAM; center panel) predicting spatial distribution of abundance (CPUE, right panel) across the eastern Bering Sea.

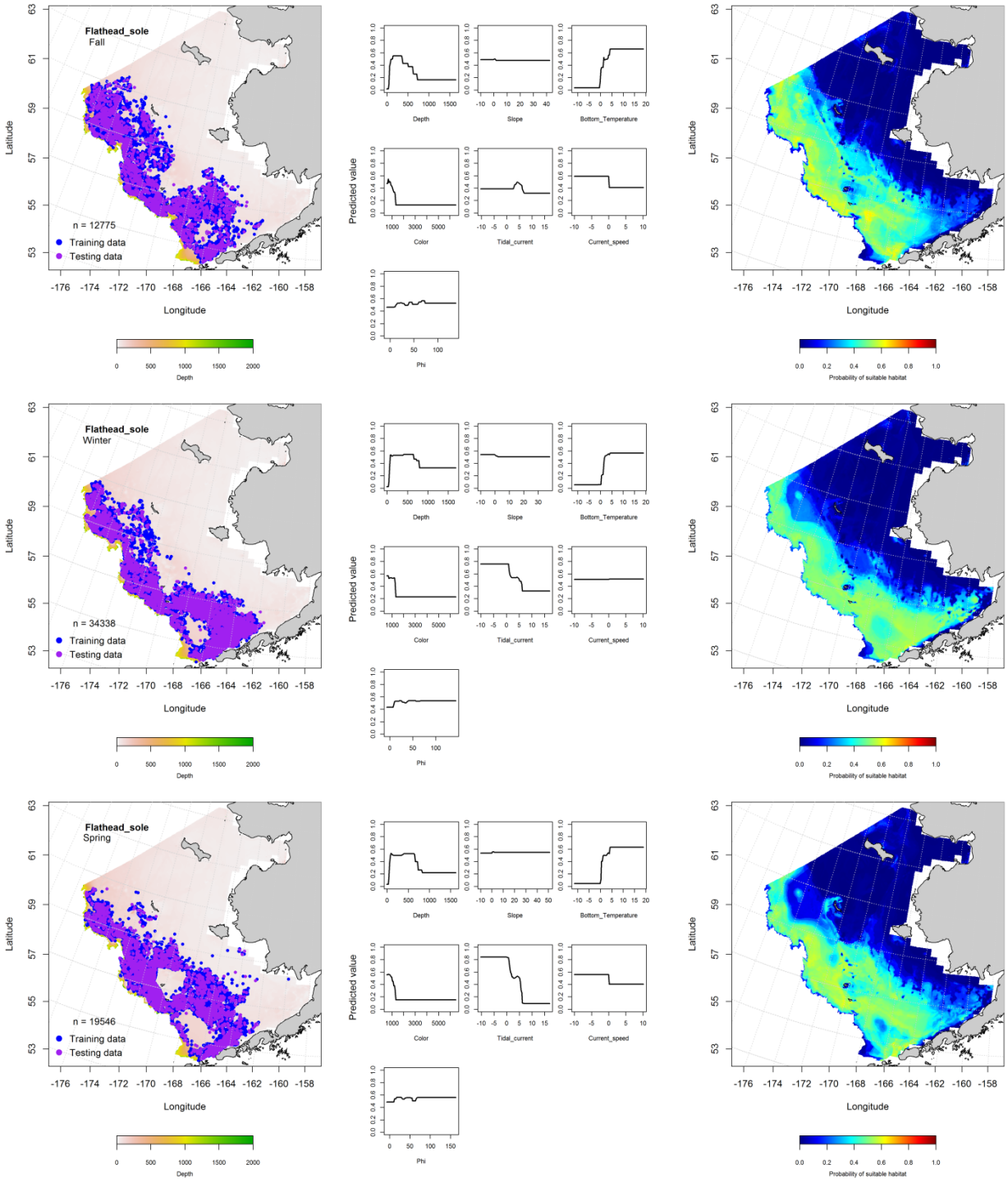

Figure 40. -- Locations of flathead sole in fall (October-November; top row), winter (December-February; middle row), and spring (March-May; bottom row) commercial fisheries catches (2003-2013) from the eastern Bering Sea (left-hand column). Blue points were used to train the MaxEnt model (center column) predicting the probability of suitable habitat (right-hand column) and the purple points were used to validate the model.

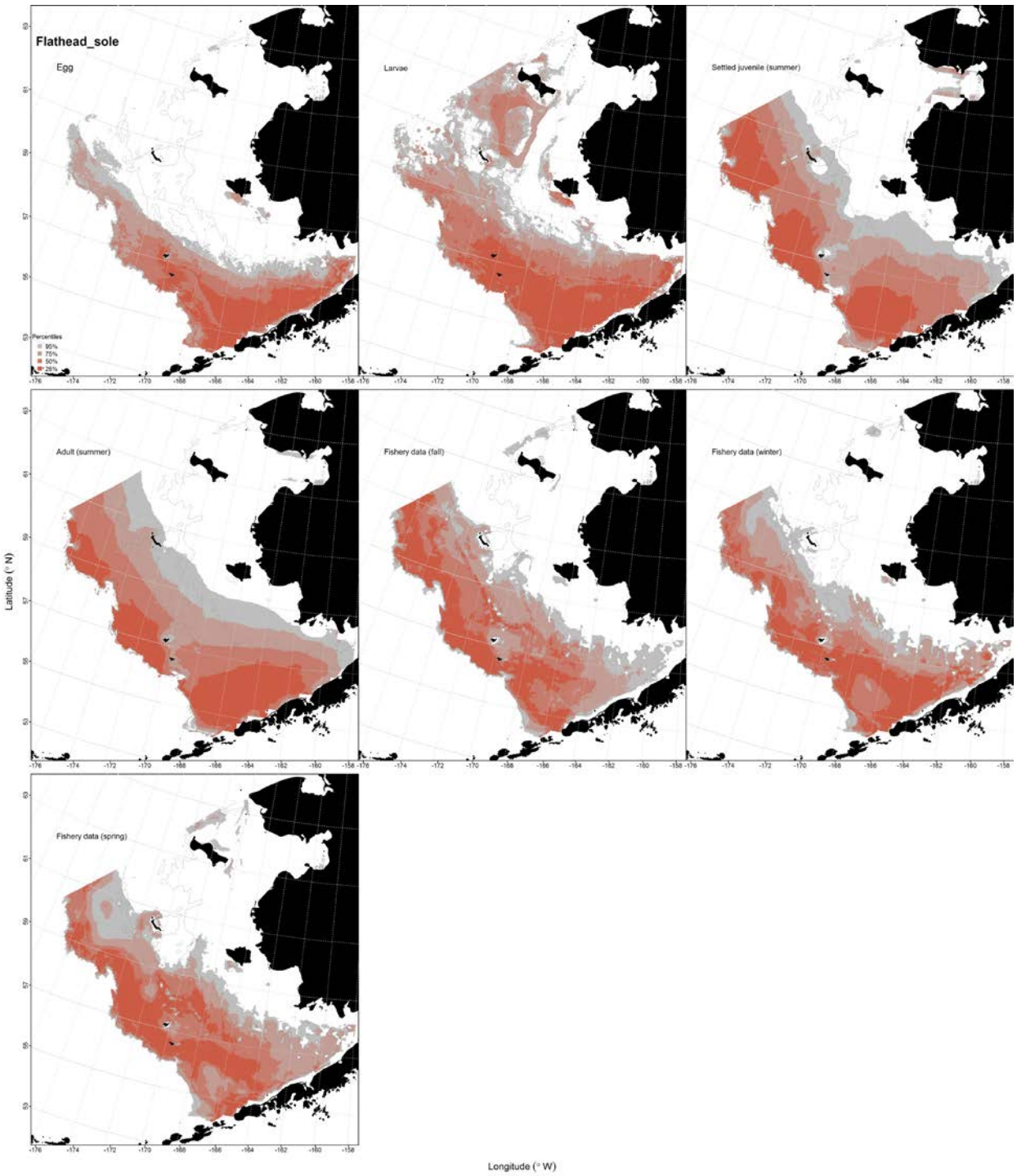

Figure 41. -- Essential habitat (EFH) predicted for flathead sole eggs and larvae (upper left and center panels) from EcoFOCI ichthyoplankton surveys (1991-2013), settled juveniles and adults from the RACE-GAP summer bottom trawl surveys (1982-2014; upper right and middle left panels), and predicted from their presence in commercial fishery catches (2003-2013) from fall and winter (middle center and right panels), and spring (bottom left panel) from the eastern Bering Sea.

Southern Rock Sole (*Lepidopsetta bilineata*)

Distribution of early life history stages of southern rock sole from EcoFOCI ichthyoplankton surveys of the eastern Bering Sea -- Southern rock sole larvae were caught on 1991 - 2013 EcoFOCI eastern Bering Sea ichthyoplankton surveys between May and September (Table 2) and were most common in the central and southern domains (Fig. 42). Archived rock sole larvae, originally generically identified as *Lepidopsetta* spp. from EcoFOCI surveys prior to 1996, were re-identified once southern and northern rock sole were formally recognized and separated by Orr and Matarese (2000). There were sufficient data to model EFH for southern rock sole larvae. The most important covariate predicting larval southern rock sole habitat was sea surface temperature (relative importance = 51.1%). The remaining covariates considered in the model (bottom current direction, bottom depth, slope, surface current velocity, ocean color, and current variability, comprised total relative importance of 23.6%. The AUC for the training data was 0.93 with 85% of cases correctly classified; AUC for the test data set was 0.83 and 83% of cases were correctly classified. The MaxEnt model predicts that suitable habitat for larval southern rock sole is found between 50 and 100 m depths from the Pribilof Islands southward to the northeast edge Unimak Pass and along the Alaska Peninsula into Bristol Bay.

Summertime distribution of late-juvenile and adult southern rock sole from RACE-GAP bottom trawl surveys of the eastern Bering Sea -- Southern rock sole are not common in RACE-GAP summer bottom trawls in the EBS and occur at less than 1% of stations sampled. When encountered, juveniles and adults occur primarily in the southern portion of the survey area close to the Alaska Peninsula (Fig. 43). Settled southern rock sole juveniles and adults did not occur frequently enough in summer bottom trawl surveys of the eastern Bering Sea to model their habitat distribution.

Essential fish habitat maps and conclusions for southern rock sole in the eastern Bering Sea -- Larval southern rock sole were collected in sufficient prevalence to model their essential habitat in the

EBS, but no other life stages were common enough to allow for distribution modeling. The core of essential larval southern rock sole habitat in the eastern Bering Sea is focused in the central and southern domains at depths ca. 100 m from just north of the Pribilof Islands to Unimak Pass and along the Alaska Peninsula into Bristol Bay (Fig. 44).

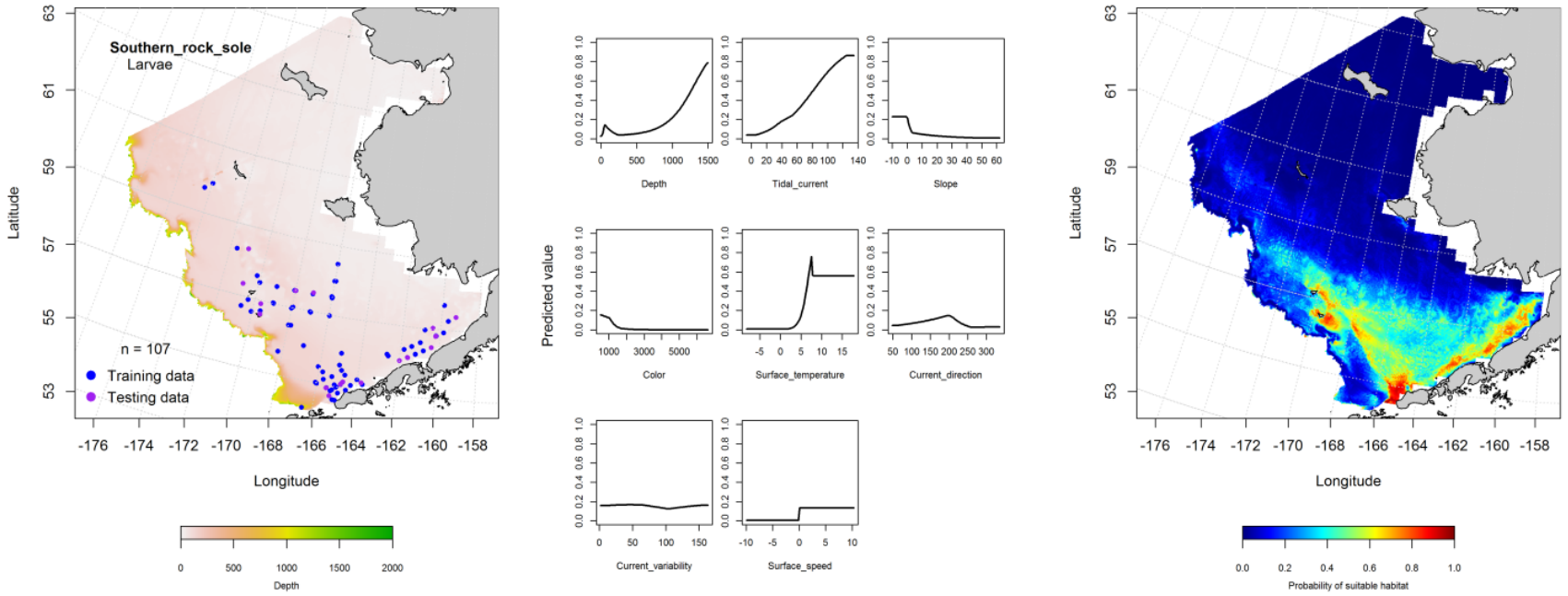

Figure 42. -- Presence of southern rock sole larvae in EcoFOCI ichthyoplankton surveys of the eastern Bering Sea (left panel) with training (blue dots) and testing (purple dots) data sets indicated alongside the maximum entropy model (MaxEnt) effects (center panel) and the MaxEnt spatial predictions of the probability of suitable larval southern rock sole habitat (right panel).

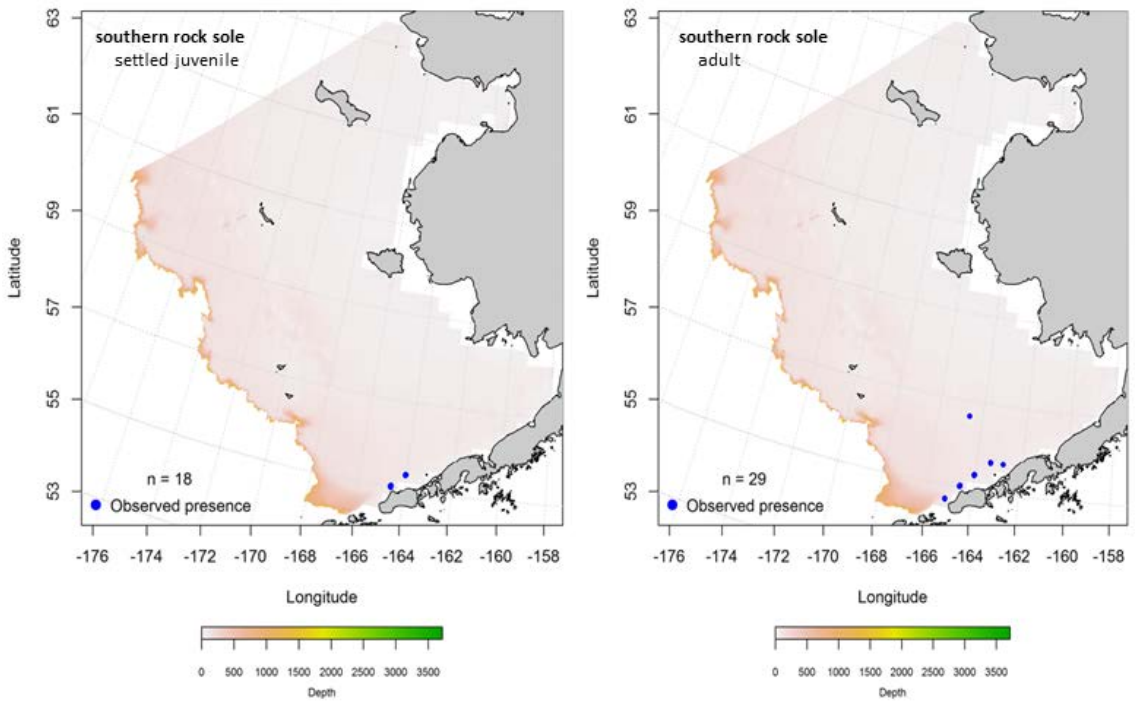

Figure 43. -- Presence of settled-juvenile (left) and adult (right) southern rock sole in catches from RACE-GAP summer bottom trawl surveys (1997-2014) from the eastern Bering Sea.

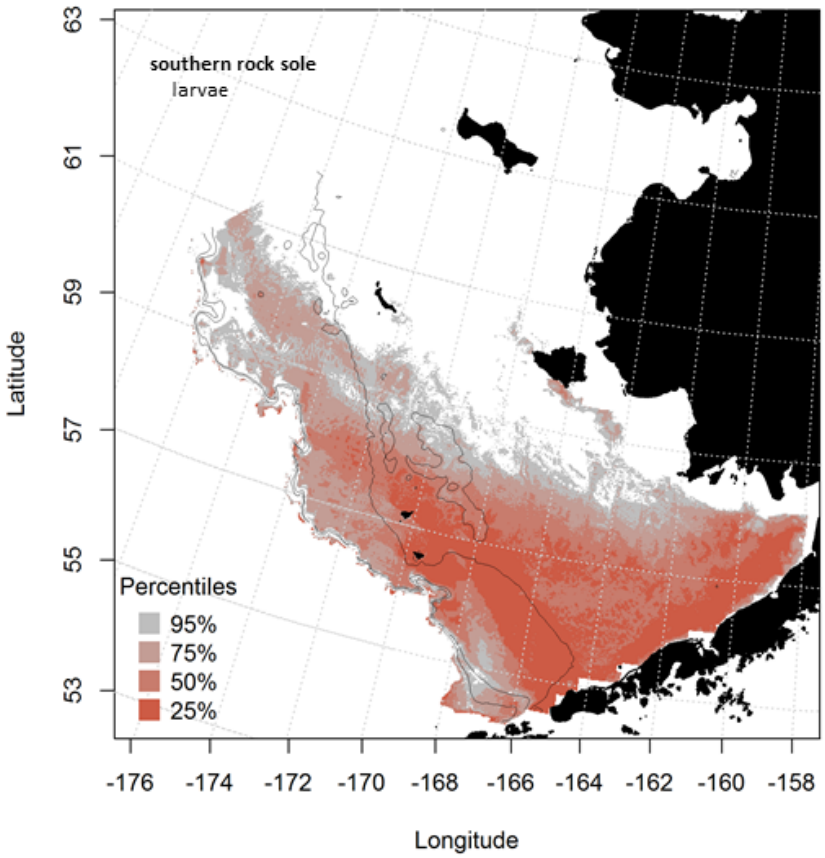

Figure 44. -- Essential habitat of larval southern rock sole predicted from EcoFOCI ichthyoplankton surveys of the eastern Bering Sea (1991-2013).

Northern Rock Sole (*Lepidopsetta polyxystra*)

Distribution of early life history stages of northern rock sole from EcoFOCI ichthyoplankton surveys of the eastern Bering Sea -- Northern rock sole larvae were collected on EcoFOCI ichthyoplankton between May and October 1991-2013 (Table 2; Fig. 45). Larval northern rock sole were primarily distributed across the southern and central domains on the middle and outer shelf of the EBS. Habitat covariates were fit to the larval northern rock sole presence data using MaxEnt modeling for the spring and summer months. The most important covariates describing northern rock sole distribution from these data were surface temperature and bottom depth (combined relative importance = 79.5%). Consequently, the general areas predicted to have the highest probability of suitable

habitat for northern rock sole larvae were located in the southern domain from Bristol Bay along the Alaska Peninsula and northward on the middle and outer shelf of the EBS to the Pribilofs. The model fit to the training data was outstanding (AUC = 0.93) correctly classifying 87% of predicted cases. The model was successfully validated using the test data with 85% of cases correctly classified and an excellent model fit (AUC = 0.85).

Pelagic juvenile northern rock sole were uncommon during EcoFOCI ichthyoplankton surveys (1991-2013) in the eastern Bering Sea (Fig. 46). They occurred on the middle shelf of the EBS in the southern domain and near St. Paul Island in the Pribilofs.

Summertime distribution of settled juvenile and adult northern rock sole from RACE-GAP bottom trawl surveys of the eastern Bering Sea -- Settled juvenile northern rock sole were common and widely distributed throughout the RACE-GAP summer bottom trawl survey area (Fig. 47). They occurred at around 65% of Bering Sea summer bottom trawl stations overall. The western extent of the juvenile distribution appears to be constrained by the 100 m isobath along the middle shelf. The most significant habitat covariates retained in the best-fitting abundance GAM were geographic location, sediment size, and bottom current speed. Their predicted abundance was high in the southern domain over the middle shelf, lower in the presence of finer sediments, and increased with increasing bottom current speed. The model explained 68.3% of the deviance in CPUE from the training data model fits to the training and test data were acceptable ($r^2 = 0.68$ for both).

The best-fitting abundance GAM for adult northern rock sole predicts that their distribution roughly corresponds to that of the settled juveniles, but with a geographic shift toward the north (Fig. 48). Similar to the GAM for settled juveniles, the most significant covariates retained in the adult abundance GAM were geographic location, sediment grain size, bottom temperature, and bottom depth; tidal and bottom currents also appear to play an important role in predicting their distribution. According to the GAM, predicted abundance of adult northern rock sole was highest in the northwest EBS over finer sediments where water temperatures were around 3°C. This model accounted for 73% of the deviance in

adult northern rock sole abundance estimated from RACE-GAP summer bottom trawl surveys ($r^2 = 0.73$). For model validation, the test data fit was good and matched the fit to the training data.

Seasonal distribution of northern rock sole in commercial fishery catches from the eastern Bering Sea -- There were seasonal differences to the presence of northern rock sole in commercial catches from the EBS (Fig. 49). In all seasons, northern rock sole catches were distributed over the middle and outer shelf of the EBS from the Alaska Peninsula northward to the U.S.-Russia Convention Line. In fall compared to winter, there appeared to be shift southward in the prevalence of northern rock sole catches. In springtime, there were more catches from the inner shelf outside of Kuskokwim Bay than in fall or winter. Bottom depth was the fixed habitat covariate with high relative importance in the MaxEnt models from all three seasons (31.2% in fall, 41.9% in winter, and 20.7% in spring). Bottom temperature, ocean productivity, and sediment grain size were the dynamic habitat covariates with high relative importance in the models. Ocean productivity and bottom temperature were important in the fall MaxEnt (combined relative importance = 51.7%), sediment grain size and ocean productivity were important in winter (50%), and bottom temperature and sediment grain size were important in spring (58.8%). Model fits to the training data were ranged from outstanding in spring (AUC = 0.88) to excellent in winter (AUC = 0.96) with the models correctly classifying 80-91% of predicted cases, respectively. Model validation was successful, AUC ranged from outstanding (0.80) to excellent (0.90) and correctly classified between 80 and 90% of predicted cases.

The Alaska rock sole fisheries, along with yellowfin sole, are the largest flatfish fisheries in the United States; most of this catch is sold in Asia. Northern and southern rock sole are difficult to distinguish and consequently are landed as a complex in the commercial fisheries of the BSAI. Evidence from RACE-GAP summer surveys and elsewhere indicates that southern rock sole are exceedingly rare in the EBS. Therefore, we have modeled only northern rock sole identified by trained fishery observers in commercial catches from the EBS.

Essential fish habitat maps and conclusions for northern rock sole from the EBS -- Predicted EFH of northern rock from EcoFOCI ichthyoplankton samples, RACE-GAP summer bottom trawl surveys, and commercial fishery VOE-CIA observer data varied by life stage and season (Fig. 50). The nearshore extent of larval northern rock sole EFH corresponded to the 50 m isobaths in the EBS. Summertime EFH was similar for settled juveniles and adults with core habitat (top 25%) predicted in the central and southern domains of the EBS constrained to the inner and middle shelf. Seasonal differences in EFH of northern rock sole predicted from presence data collected by commercial fishery observers were apparent, generally overlapped the EFH predicted from the EcoFOCI and RACE-GAP data, and were likely dependent upon seasonal fishing effort.

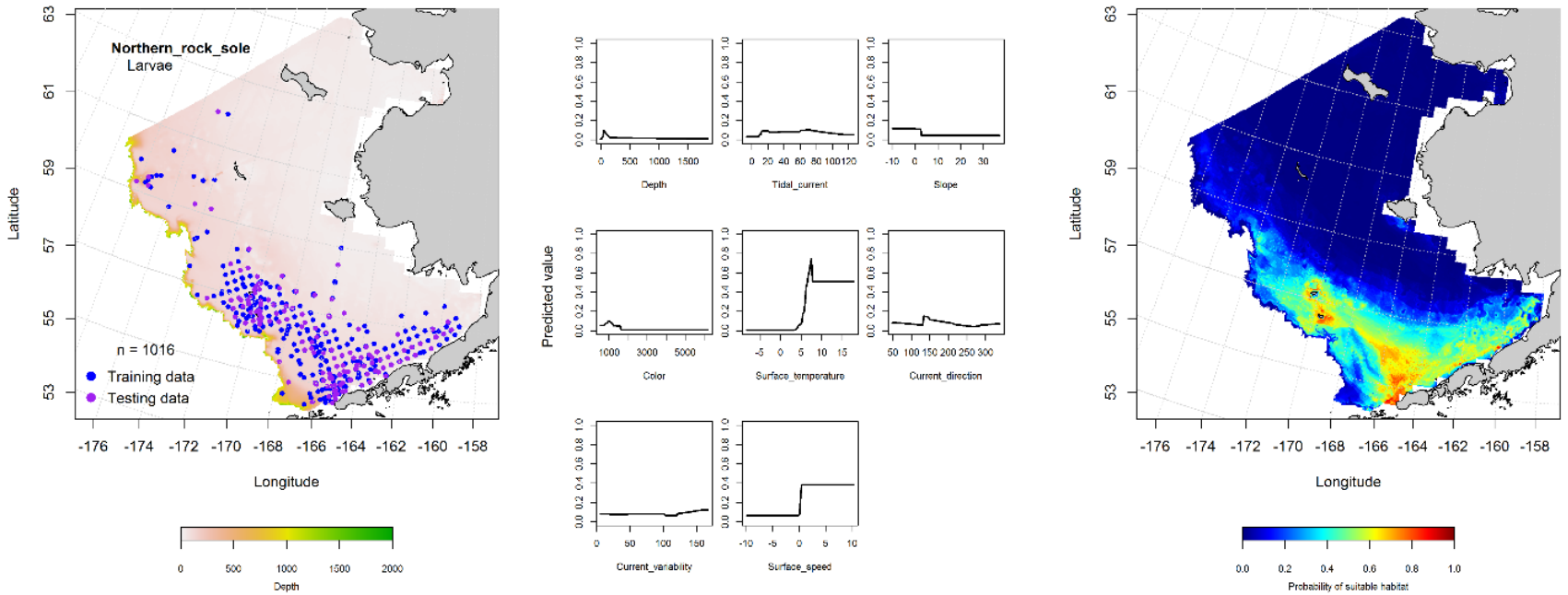

Figure 45. -- Presence of northern rock sole larvae in EcoFOCI ichthyoplankton surveys of the eastern Bering Sea (left panel) with training (blue dots) and testing (purple dots) data sets indicated alongside the maximum entropy model (MaxEnt) effects (center panel) and the MaxEnt spatial predictions of the probability of suitable larval northern rock sole habitat (right panel).

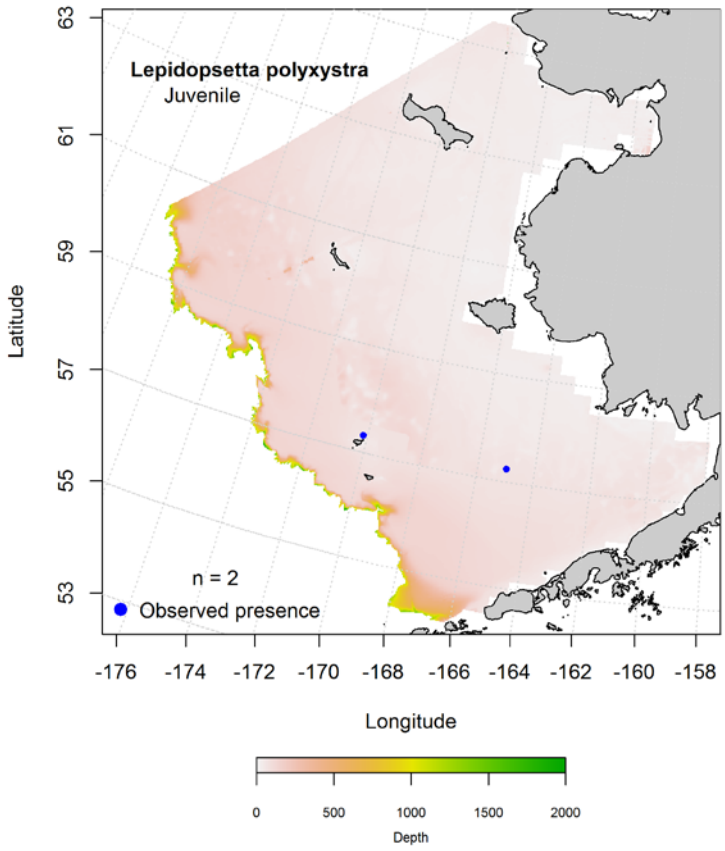

Figure 46. -- Presence of pelagic juvenile northern rock sole in EcoFOCI ichthyoplankton surveys of the eastern Bering Sea (1991-2013).

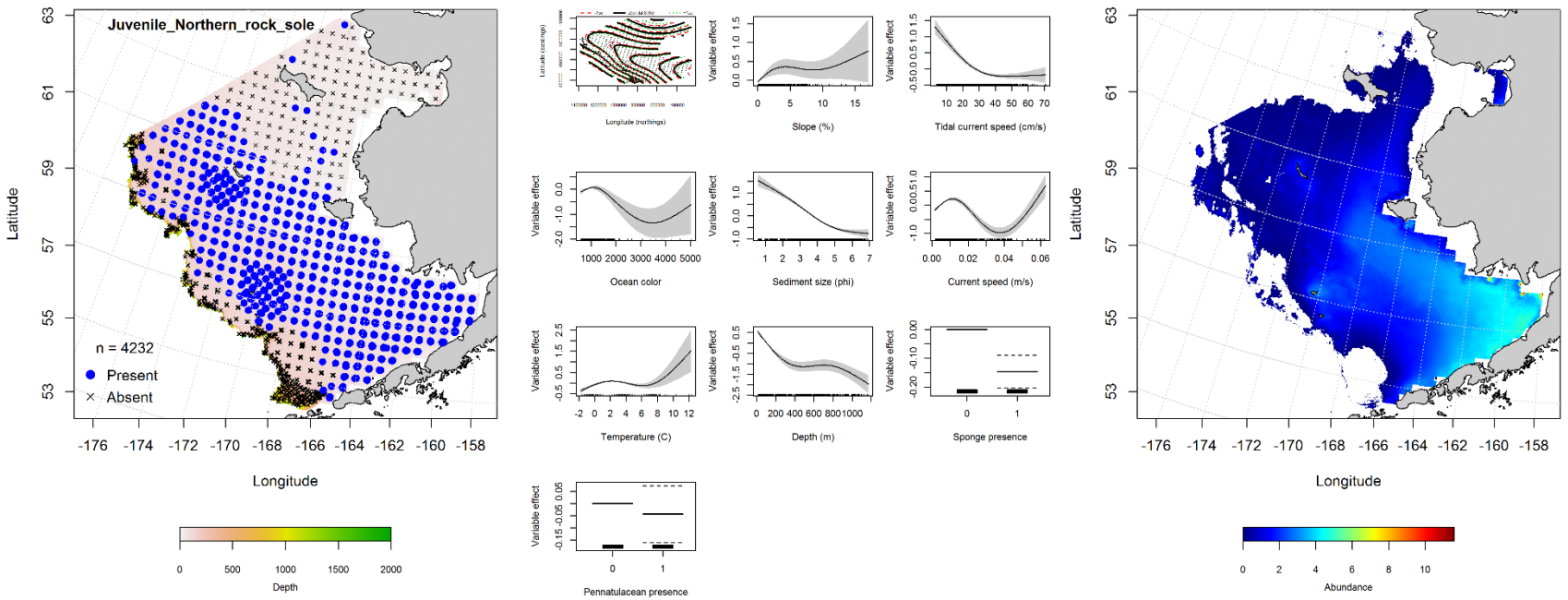

Figure 47. -- Distribution of settled juvenile northern rock sole in 1996-2014 RACE-GAP summer bottom trawl surveys (left panel) alongside effects of retained habitat covariates in the best-fitting generalized additive model (GAM; center panel) predicting spatial distribution of abundance (CPUE, right panel) across the eastern Bering Sea.

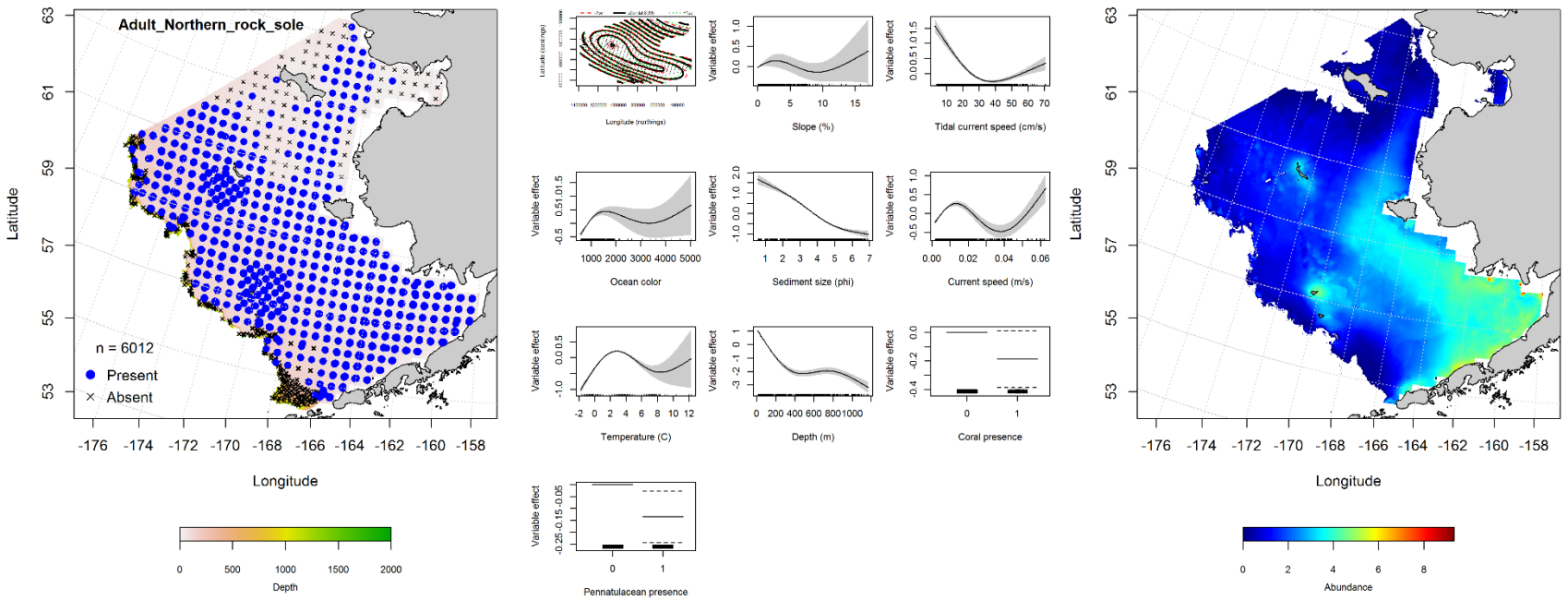

Figure 48. -- Distribution of adult northern rock sole in 1996-2014 RACE-GAP summer bottom trawl surveys (left panel) alongside effects of retained habitat covariates in the best-fitting generalized additive model (GAM; center panel) predicting spatial distribution of abundance (CPUE, right panel) across the eastern Bering Sea.

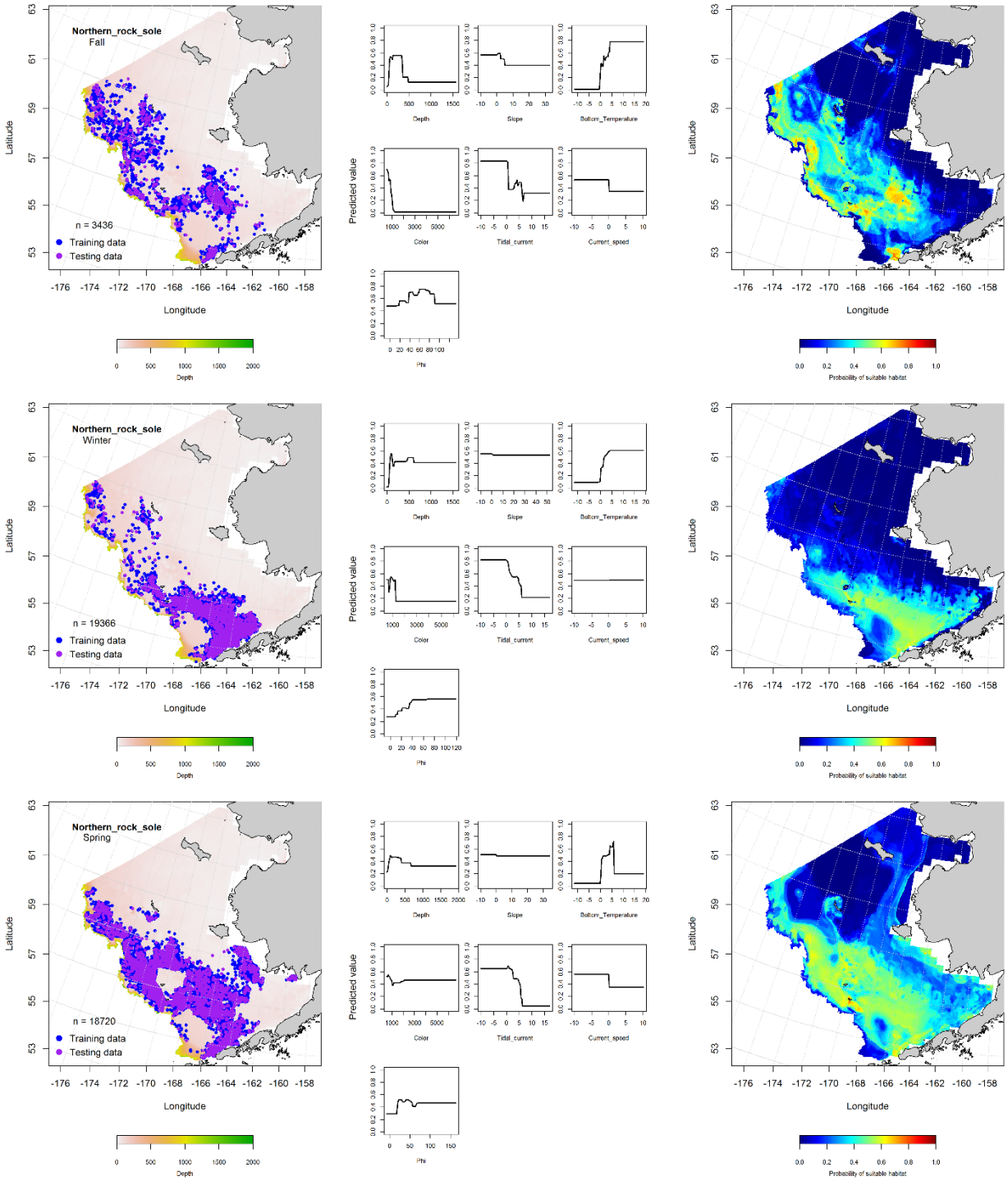

Figure 49. -- Locations of northern rock sole in fall (October-November; top row), winter (December-February; middle row), and spring (March-May; bottom row) commercial fisheries catches (2003-2013) from the eastern Bering Sea (left-hand column). Blue points were used to train the MaxEnt model (center column) predicting the probability of suitable habitat (right-hand column) and the purple points were used to validate the model.

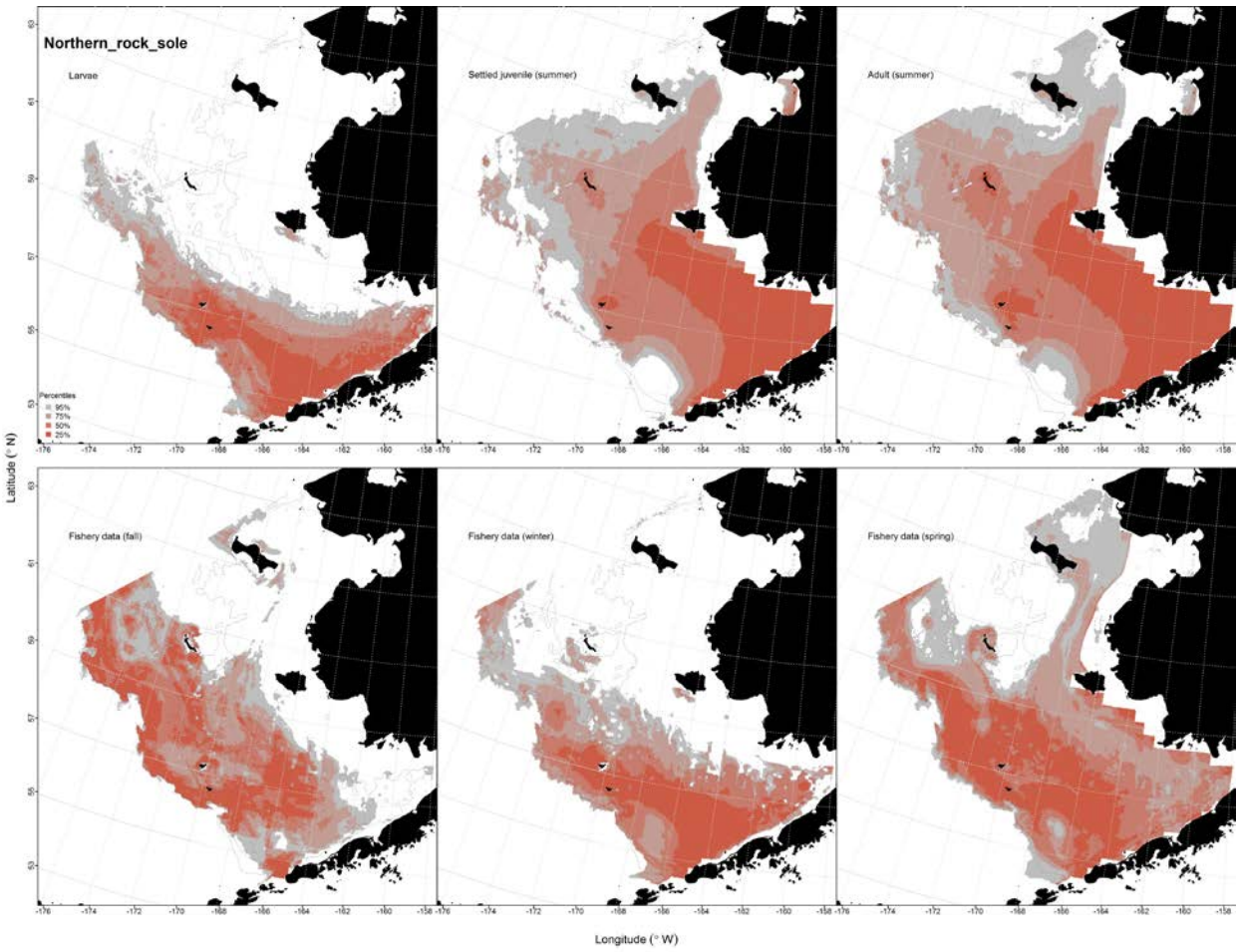

Figure 50. -- Essential fish habitat (EFH) predicted for larval northern rock sole (upper left panel) from EcoFOCI ichthyoplankton surveys (1992-2013), for settled juvenile (upper middle panel) and adult northern rock sole (upper right panel) modeled from RACE-GAP summertime bottom trawl surveys (1996-2014), and EFH predicted from presence in commercial fishery catches (2003-2013) from fall, winter, and spring in the eastern Bering Sea (bottom three panels).

Alaska Plaice (*Pleuronectes quadrituberculatus*)

Distribution of early life history stages of Alaska plaice in EcoFOCI ichthyoplankton surveys of the eastern Bering Sea -- Alaska plaice eggs were collected on EcoFOCI ichthyoplankton surveys in the EBS (1991-2013) between February and September (Table 2). Their eggs were distributed throughout the EBS and into the NBS, but were not collected from Norton Sound (Fig. 51). The most important covariates describing the probability of suitable Alaska plaice egg habitat were surface

temperature and bottom depth (combined relative importance = 54.5%). Model fits to the training data were outstanding (AUC = 0.87) and the model correctly classified 80% of predicted cases. Model validation was an acceptable fit to the test data (AUC = 0.76) and correctly classified 76% of cases

Alaska plaice larvae were present in EcoFOCI ichthyoplankton surveys (1991-2013) between May and September (Fig. 52). They were distributed from the Alaska Peninsula into the NBS across the inner, middle, and outer shelf of the eastern Bering Sea. The most important habitat covariates describing the distribution of suitable habitat in the EBS were surface temperature and bottom depth (combined relative importance = 27.2%). Overall, the covariate predictors used in this MaxEnt model comprised a total relative importance of only 39.5%. Despite that, the model fit to the training data was outstanding (AUC = 0.91) and correctly classified 82% of predicted cases. Model validation was also successful (AUC = 0.83) and correctly classified 83% of predicted cases.

Summertime distribution of adult Alaska plaice from RACE-GAP bottom trawl surveys of the eastern Bering Sea -- Adult Alaska plaice were distributed across the inner and middle shelf from Bristol Bay to the U.S.-Russia Convention Line; juvenile Alaska plaice were not reported from the RACE-GAP summertime bottom trawl surveys. The distribution of Alaska plaice in the EBS appears to be dependent upon the geographic extent of the Bering Sea cold pool (Lauth and Conner 2014). Alaska plaice are well-adapted to cold water temperatures and carry an antifreeze glycoprotein in their blood to prevent ice crystal formation (Knight et al. 1991). The best-fitting GAM describing adult Alaska plaice abundance explained 61.1% of the deviance in the CPUE data from the RACE-GAP summer bottom trawl surveys (Fig. 53). Geographical location, bottom depth, and sediment grain size were the habitat covariates with the greatest leverage in the model. Model effects predict highest Alaska plaice abundance in the central domain of the eastern Bering Sea over the middle shelf close to the 50 m isobath. Their predicted abundance increased in shallower depths over finer sediments. The GAM fits to the training and test data were acceptable (r^2 = 0.61 and = 0.63).

Seasonal distribution of Alaska plaice in commercial fishery catches from the eastern Bering Sea -- Alaska plaice were present in Bering Sea commercial fishery catches in the fall, winter, and spring (Fig. 54). The most important habitat covariate shared in common amongst the three seasonal models was sediment grain size (relative importance = 35.4% in fall, 35.7% in winter, and 43% in spring). In the fall, bottom temperature and bottom current were also important predictors of the probability of suitable Alaska plaice habitat; their combined relative importance in addition to that of sediment grain size was 46.8%. In winter, bottom depth and ocean productivity were important descriptors (combined relative importance = 56.4%) along with sediment grain size. The habitat covariates that were important in the springtime model in addition to sediment grain size were the same as those in fall; bottom temperature and current (combined relative importance = 36.3%). MaxEnt model fits were outstanding to the training data (AUC ranged from 0.91 to 0.98) and correctly classified from 85 to 94% of predicted cases. The fits to the test data in the model validation step ranged from excellent to outstanding (AUC =0.85- 0.91) and correctly classified 85 to 91% of cases.

Essential fish habitat maps and conclusions for Alaska plaice from the EBS -- Predicted EFH of Alaska plaice ELHS from EcoFOCI ichthyoplankton samples, RACE-GAP summer bottom trawl surveys, and commercial fishery VOE-CIA observer data varied by life stage and season (Fig. 55). The eastern boundary of the distribution of egg and larval Alaska plaice EFH roughly corresponds to the 50 m isobaths separating the middle and inner shelf of the eastern Bering Sea. The western extent of ELHS EFH is the western boundary of the survey area and extends from the Alaska Peninsula to the U.S.-Russia Convention Line. Core summertime EFH of Alaska plaice (top 25%) corresponds roughly to the historical extent of the cold pool in the EBS. Seasonal differences in EFH of Alaska plaice predicted from presence data collected by commercial fishery observers were apparent, generally overlapped the EFH predicted from the EcoFOCI and RACE-GAP data, but were more tightly constrained geographically, likely as the result of seasonal fishing activities.

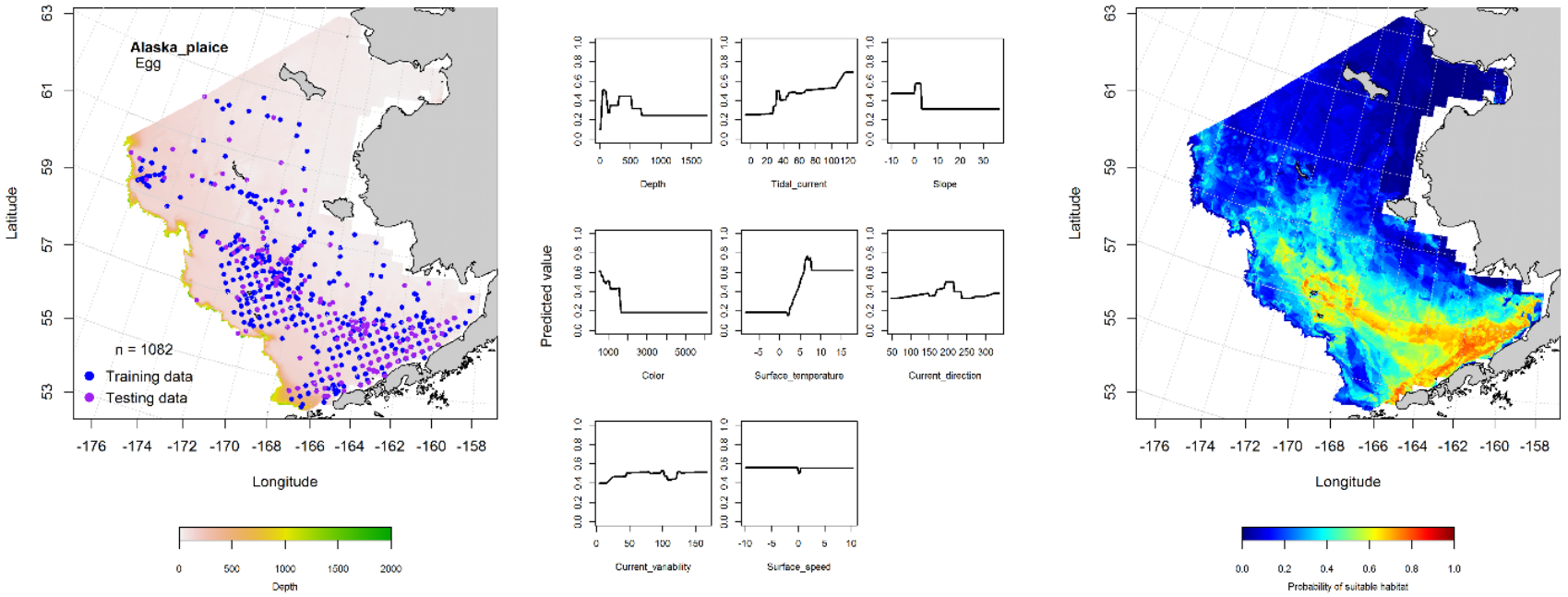

Figure 51. -- Presence of Alaska plaice eggs in EcoFOCI ichthyoplankton surveys of the eastern Bering Sea (left panel) with training (blue dots) and testing (purple dots) data sets indicated alongside the maximum entropy model (MaxEnt) effects (center panel) and the MaxEnt spatial predictions of the probability of suitable Alaska plaice egg habitat (right panel).

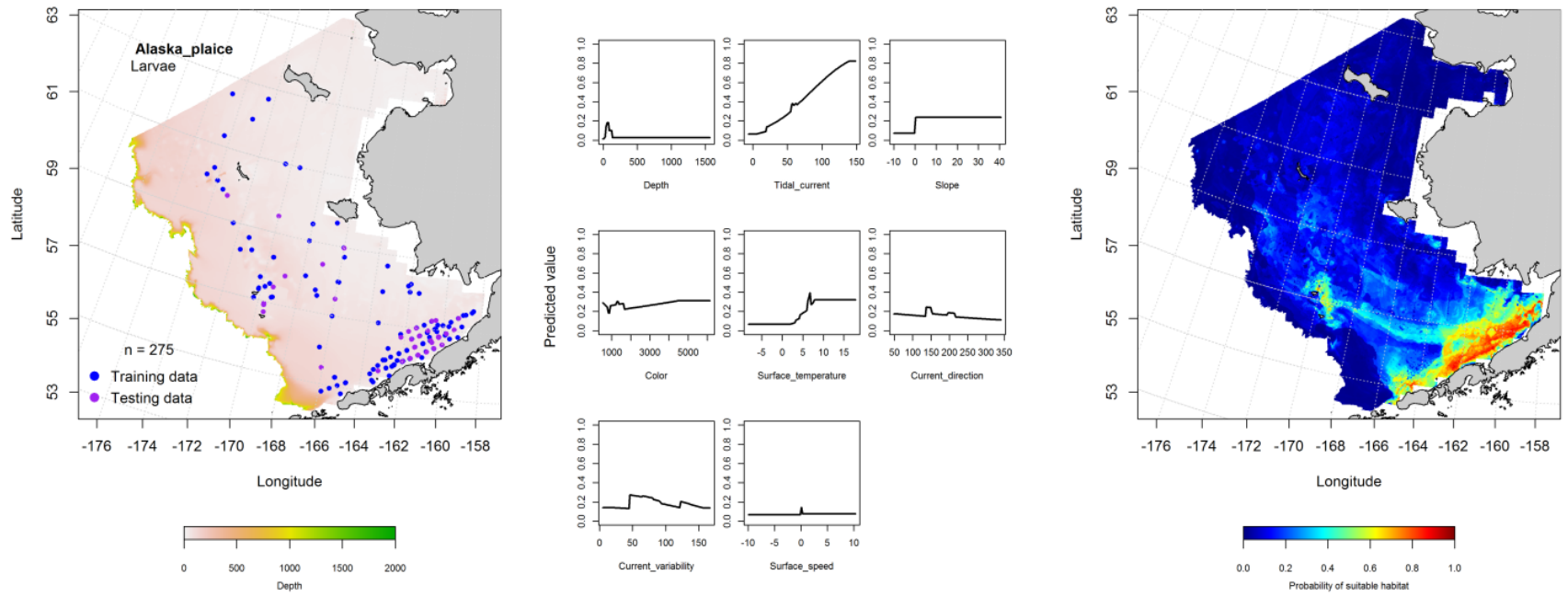

Figure 52. -- Presence of Alaska plaice larvae in EcoFOCI ichthyoplankton surveys of the eastern Bering Sea (left panel) with training (blue dots) and testing (purple dots) data sets indicated alongside the maximum entropy model (MaxEnt) effects (center panel) and the MaxEnt spatial predictions of the probability of suitable larval Alaska plaice habitat (right panel).

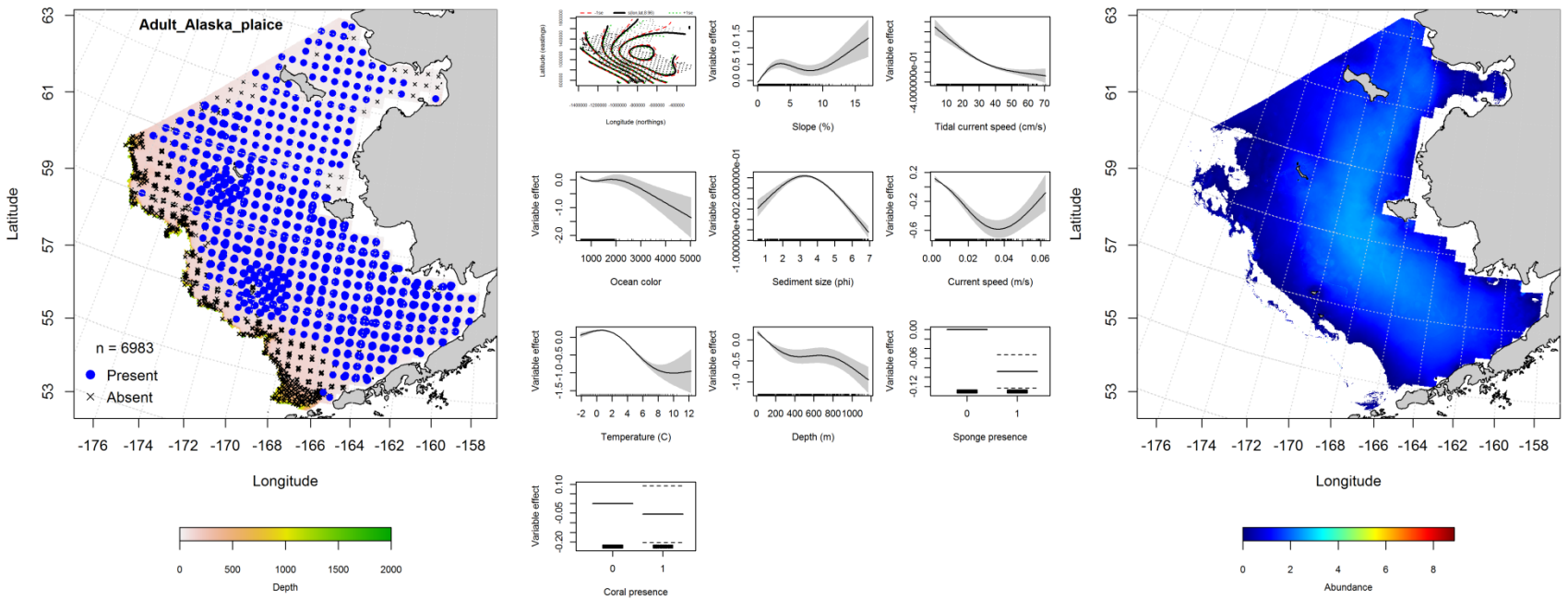

Figure 53. -- Presence of adult Alaska plaice in EcoFOCI ichthyoplankton surveys of the eastern Bering Sea (left panel) with training (blue dots) and testing (purple dots) data sets indicated alongside the maximum entropy model (MaxEnt) effects (center panel) and the MaxEnt spatial predictions of the probability of suitable adult Alaska plaice habitat (right panel).

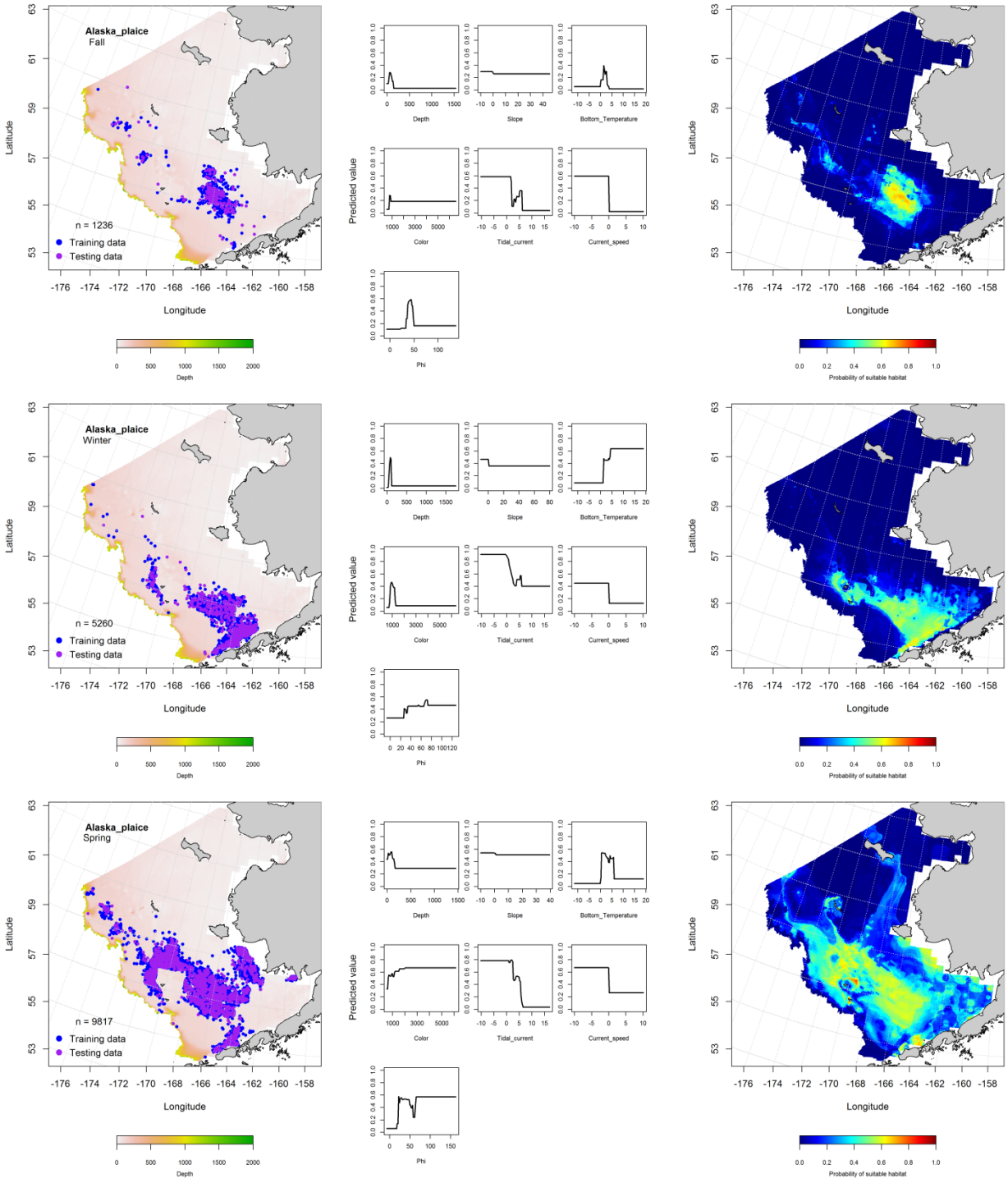

Figure 54. -- Locations of Alaska plaice in fall (October-November; top row), winter (December-February; middle row), and spring (March-May; bottom row) commercial fisheries catches (2003-2013) from the eastern Bering Sea (left-hand column). Blue points were used to train the MaxEnt model (center column) predicting the probability of suitable habitat (right-hand column) and the purple points were used to validate the model.

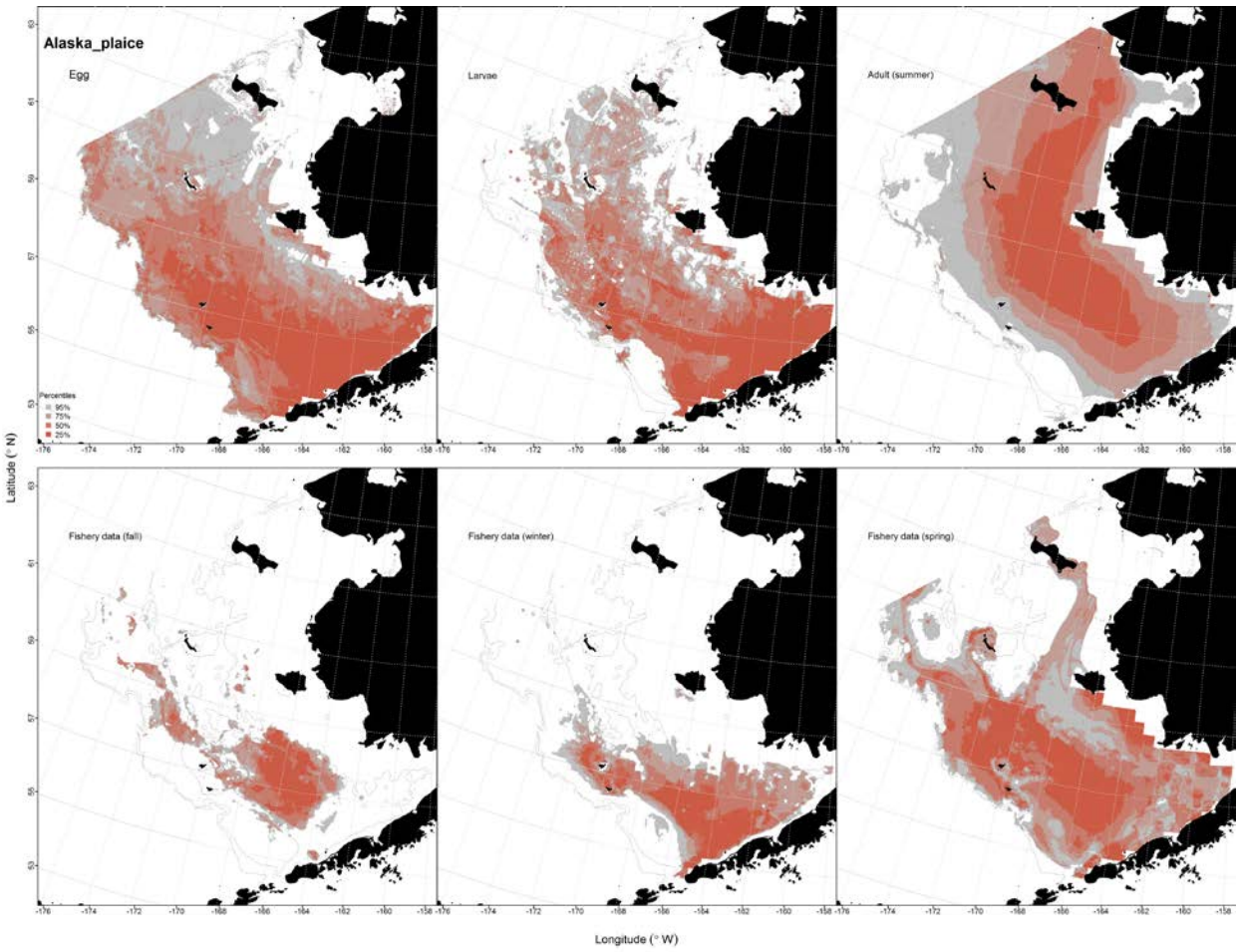

Figure 55. -- Essential fish habitat (EFH) predicted for settled juvenile (upper left panel) and adult Alaska plaice (upper right panel) from RACE-GAP summertime bottom trawl surveys (1982-2014) and predicted from presence in commercial fishery catches (2003-2013) from fall, winter, and spring in the eastern Bering Sea (bottom three panels).

Greenland Turbot (*Reinhardtius hippoglossoides*)

Distribution of early life history stages of Greenland turbot from EcoFOCI ichthyoplankton surveys of the eastern Bering Sea -- There were less than 50 occurrences of Greenland turbot eggs recorded in EcoFOCI ichthyoplankton samples in the southwestern portion of the EBS (Fig. 56). Eggs were between February and March (1991-2013) over the outer shelf (100 to 200 m) and slope (200 to 3,000 m) of the EBS and along the eastern end of the Aleutian Islands chain. These data were insufficient to parameterize a distribution model for Greenland turbot eggs.

Greenland turbot larvae were present in EcoFOCI ichthyoplankton samples (1991-2013) between February and September (Fig. 57). They appeared to be most prevalent over the outer shelf (100 to 200 m) and slope (200 to 3,000 m) of the EBS, but were collected from the NBS as well. The most important habitat covariates for predicting the probability of suitable larval Greenland turbot habitat were surface temperature and bottom depth which comprised a combined 81.3% of the relative importance of all predictors in the model. The area with the highest probability of providing suitable habitat was in the southwest portion of the EBS over the Bering Canyon. The model utilizing the training data was an outstanding fit (AUC = 0.94) and correctly classified (88%) of predicted cases. The MaxEnt model also fit the test data well during model validation (AUC = 0.86) and correctly predicted 86% of cases.

Pelagic juveniles of Greenland turbot were uncommon in EcoFOCI ichthyoplankton samples from the eastern Bering Sea (Fig. 58). Reported occurrences were near the Pribilof Islands and did not provide sufficient data for habitat modeling.

Summertime distribution of settled juvenile and adult Greenland turbot from RACE-GAP bottom trawl surveys of the eastern Bering Sea -- Settled juvenile Greenland turbot collected in RACE-GAP summer bottom trawl surveys from the eastern Bering Sea occur primarily over the middle and outer shelf (50 to 200 m) and continental slope (100 to 1,000 m; Fig. 59). Their distribution also extended into the NBS where they occurred in somewhat shallower depths near St. Lawrence Island. An hGAM was used to describe settled juvenile Greenland turbot distribution and abundance in the eastern Bering Sea. In the first stage of the hGAM, the best-fitting presence-absence GAM explained 46.2% of the variability in their distribution across the EBS. Bottom depth, geographic location, bottom temperature, and sediment grain size were the most important predictors amongst the 8 habitat covariates retained. The fit of this model was outstanding (AUC = 0.93) with 85% of presence-absence cases correctly predicted. The AUC for model validation using the test data also indicated an outstanding fit (0.94) with 86% of cases correctly classified. The presence GAM established the optimum threshold probability for presence (0.22) to inform the conditional abundance GAM in the second stage of the

hGAM. In the second stage of the hGAM, the abundance GAM accounted for just 24.8% of the variability in CPUE. The most important predictors of abundance were geographical location, bottom current speed, bottom temperature, and bottom depth. The greatest conditional abundance of settled juvenile Greenland turbot was predicted in the northwestern portion of the eastern Bering Sea shelf in waters deeper than 100 m.

An hGAM was also used to describe the distribution and abundance of adult Greenland turbot caught on RACE-GAP summer bottom trawl surveys in the EBS (Fig. 60). Adults were found primarily on the outer shelf, but were present on the middle shelf as well. The best-fitting presence-absence GAM explained 55.3% of the variability in their distribution across the eastern Bering Sea and was an outstanding fit to the training data (AUC = 0.96) which correctly classified 90% of predicted presence cases. The most significant predictors of adult Greenland turbot presence in these samples were bottom depth, geographic location, sediment grain size, and bottom temperature. Model validation using the test data was also successful (AUC = 0.95) and this data set correctly classified 89% of predicted cases. The best-fitting abundance GAM accounted for 34.5% of the variability in CPUE in the samples. The most significant habitat predictors of abundance were geographic location and bottom depth. Model fits for the abundance GAMs were marginal (training data $r^2 = 0.34$ and test data $r^2 = 0.39$). The optimum threshold for probability of presence established by the presence-absence GAM (0.15) was used to predict abundance where present from the best-fitting abundance GAM. The areas of greatest conditional abundance for adult Greenland turbot were along the continental shelf edge and upper slope of the eastern Bering Sea.

Seasonal distribution of Greenland turbot in commercial fishery catches from the eastern Bering Sea -- Greenland turbot were caught in Bering Sea commercial fisheries during the fall, winter, and spring (Fig. 61). Most of those catches came from the outer shelf and upper continental slope. In all three seasons, the most important habitat covariate predicting probability of suitable habitat was bottom depth (relative importance = 83.3% in fall, 88.5% in winter, and 83.0% in spring). MaxEnt model fits to

the training data were outstanding in all three seasons. The AUC ranged from 0.93 in fall to 0.97 in winter and rate of correctly classified cases of predicted presence ranged from 86-90% for those seasons. Model validation using the test data was successful in all three seasons. In fall, the validation fit was excellent (AUC = 0.83) and the MaxEnt correctly classified 83% of predicted cases of presence. In winter and spring, the fits to the test data were outstanding (AUC = 0.90 in both cases) and the models correctly classified 90% of predicted cases.

Essential fish habitat maps and conclusions for Greenland turbot (*Reinhardtius hippoglossoides*) from the eastern Bering Sea -- Predicted EFH for Greenland turbot ELHS from EcoFOCI ichthyoplankton samples, RACE-GAP summer bottom trawl surveys, and commercial fishery VOE-CIA observer data varied by life stage and season (Fig. 62). Core larval Greenland turbot EFH (the top 25% of predictions) was located primarily over the outer shelf and upper continental slope in the central and southern domains of the eastern Bering Sea. The EFH of settled juveniles tended to be farther north, but still over the outer shelf extending south from the U.S.-Russia Convention Line. Adult Greenland turbot EFH predicted from summer bottom trawls mostly conformed to the deeper waters of the upper continental slope. Apparent seasonal differences in the EFH of Greenland turbot predicted from presence data collected by commercial fishery observers may reflect more about fishing activity than about their distribution, but the results of these models basically confirmed the distribution of EFH predicted from our other, fishery-independent data sources.

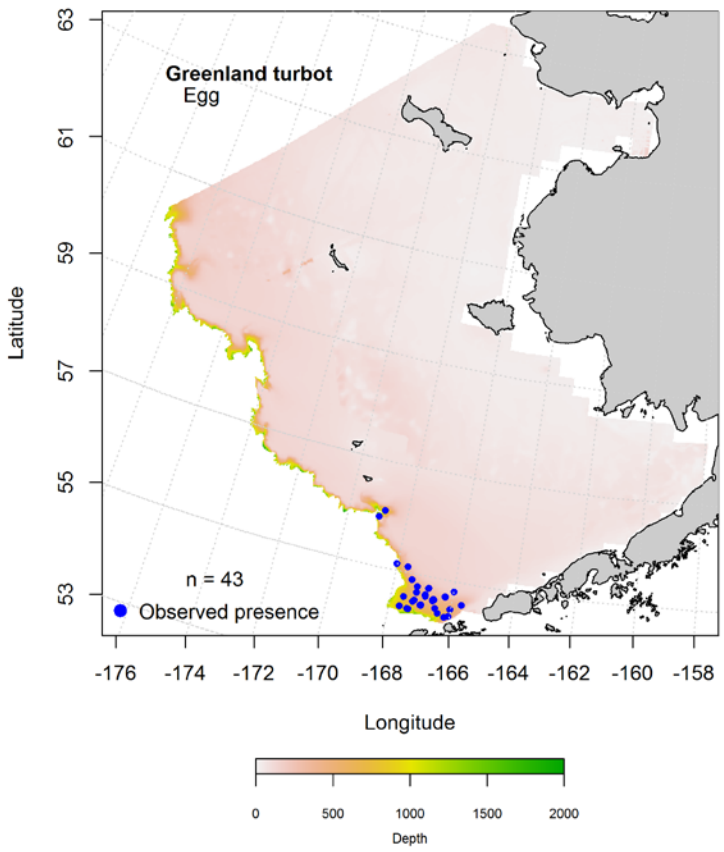

Figure 56. -- Presence of Greenland turbot eggs in EcoFOCI ichthyoplankton surveys of the eastern Bering Sea (1991-2013).

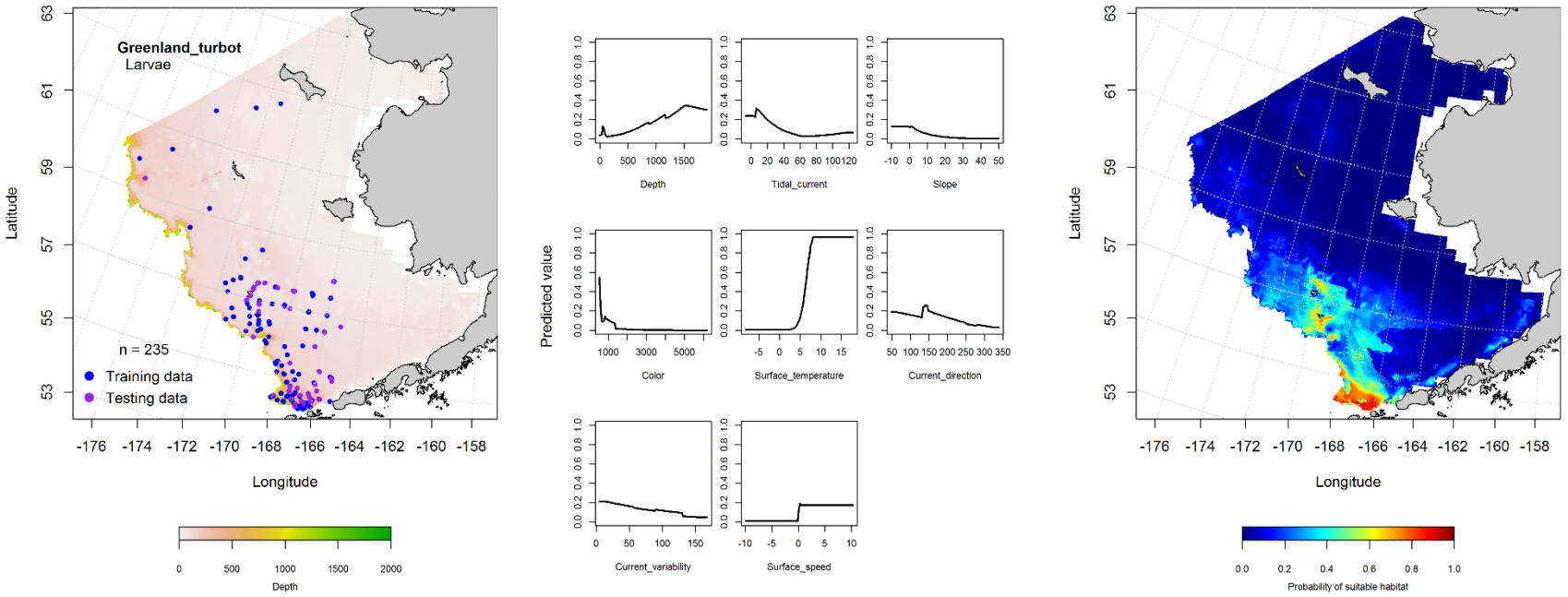

Figure 57. -- Presence of Greenland turbot larvae in EcoFOCI ichthyoplankton surveys of the eastern Bering Sea (left panel) with training (blue dots) and testing (purple dots) data sets indicated alongside the maximum entropy model (MaxEnt) effects (center panel) and the MaxEnt spatial predictions of the probability of suitable larval Greenland turbot habitat (right panel).

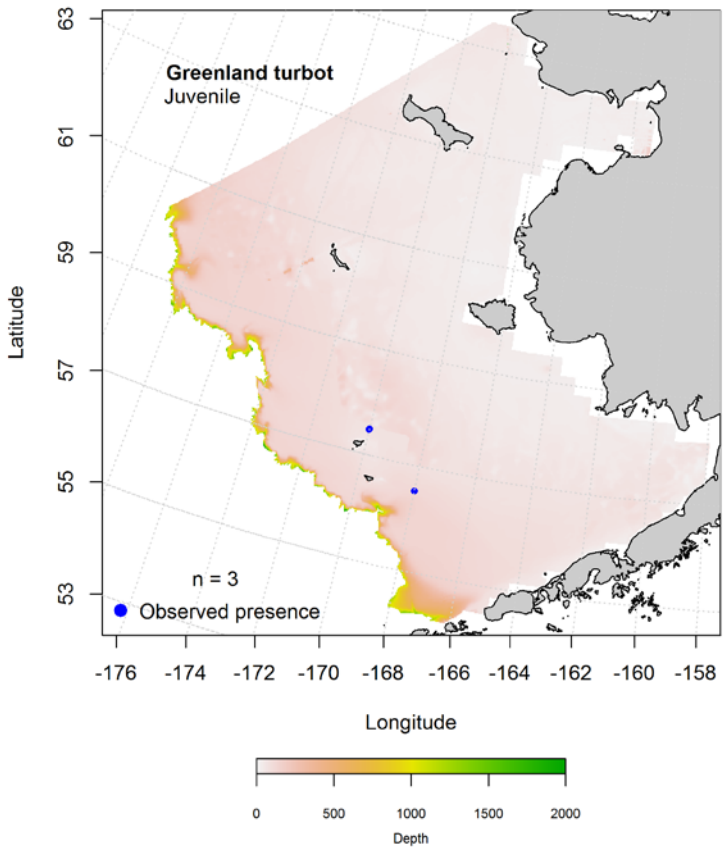

Figure 58. -- Presence of pelagic juvenile Greenland turbot in EcoFOCI ichthyoplankton surveys of the eastern Bering Sea (1991-2013).

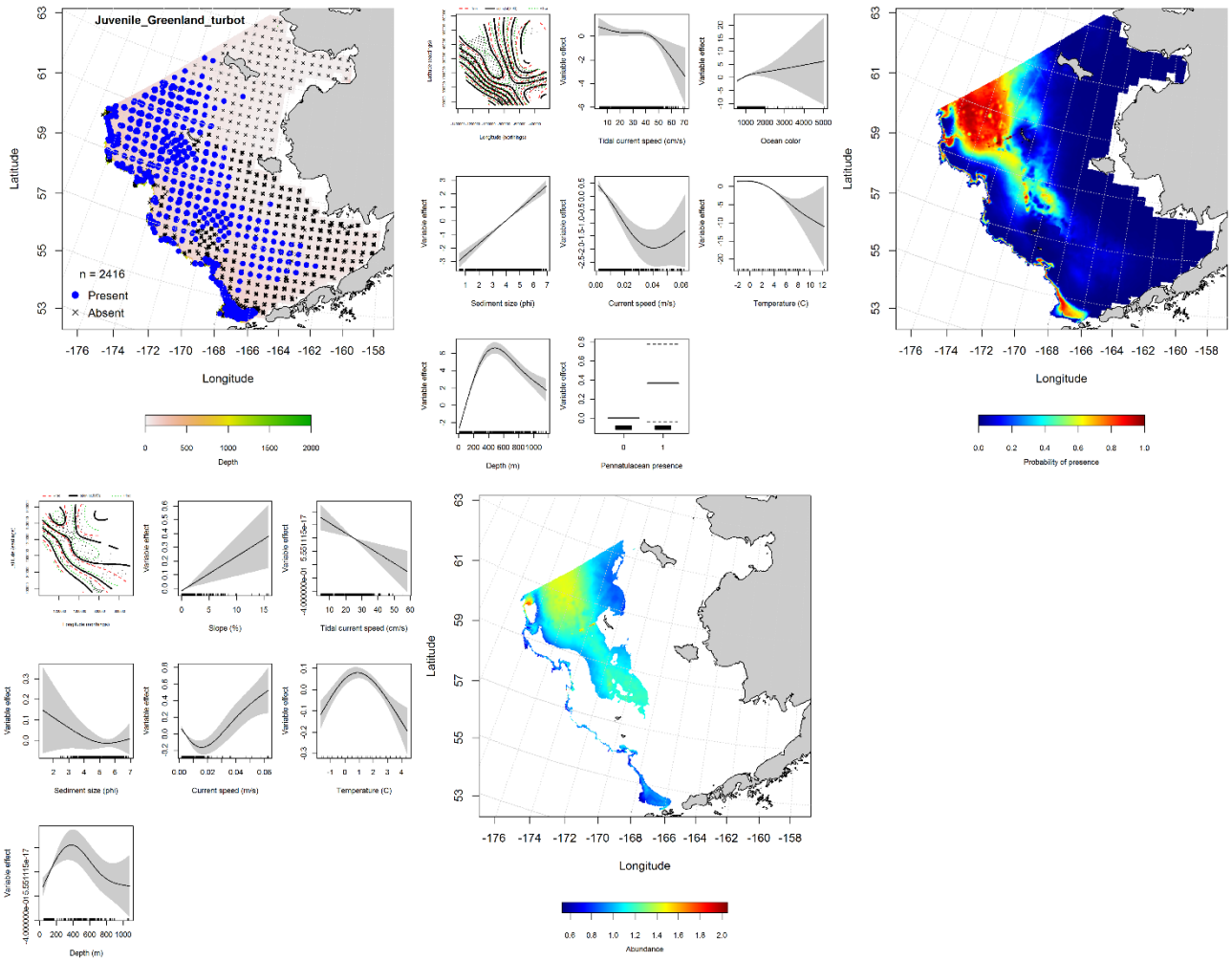

Figure 59. -- Distribution of settled juvenile Greenland turbot in 1982-2014 RACE-GAP summer bottom trawl surveys conducted in the eastern Bering Sea (upper left panel) and the effects of retained habitat covariates in the best-fitting generalized additive model (GAM) of presence-absence (upper center panel) spatially predicting the probability of their presence (upper right panel); the best-fitting abundance GAM (lower left panel) conditionally predicts settled juvenile Greenland turbot catch-per-unit-effort (CPUE) at sites where the optimum threshold for probability of presence was met or exceeded (lower center panel).

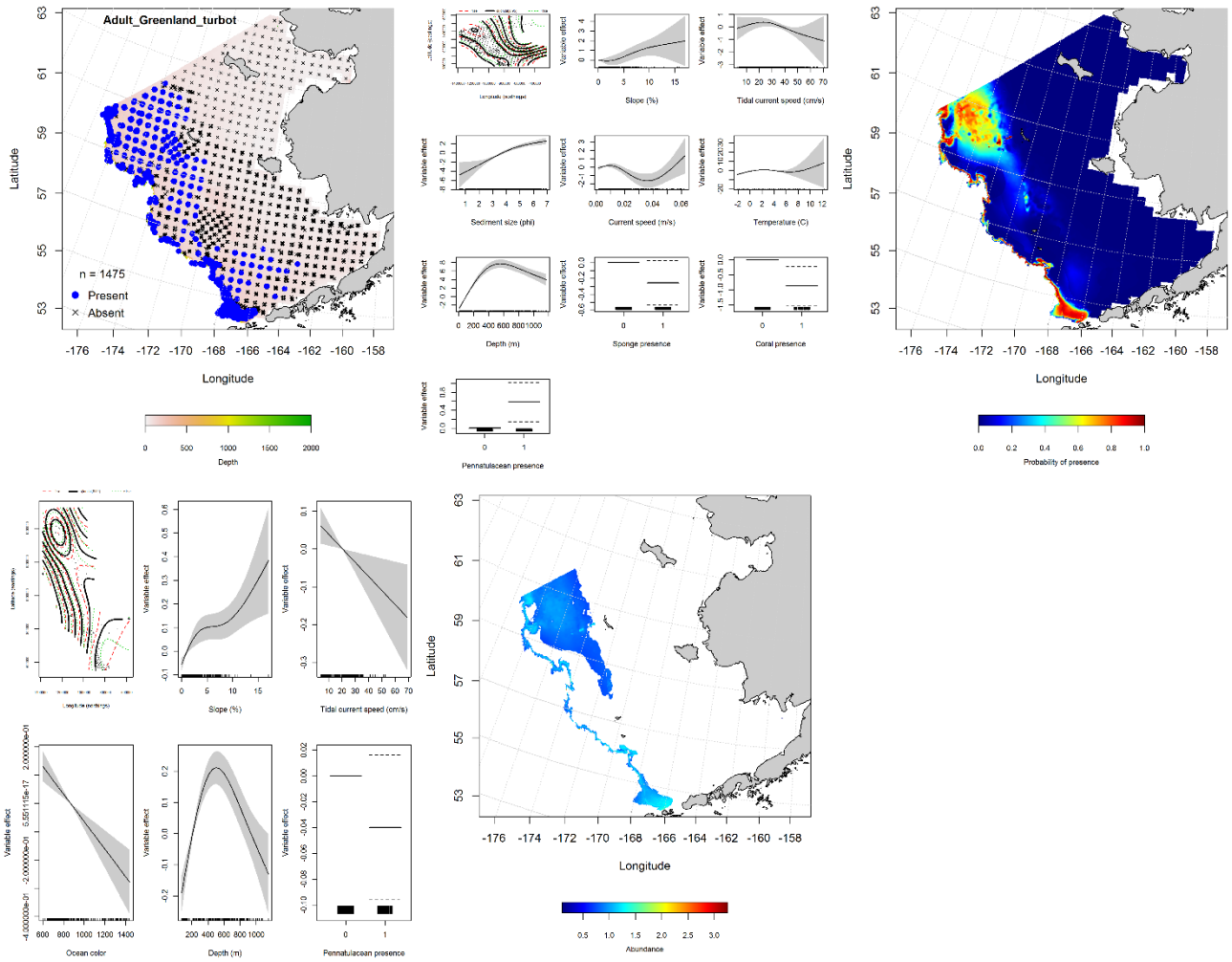

Figure 60. -- Distribution of adult Greenland turbot in 1982-2014 RACE-GAP summer bottom trawl surveys conducted in the eastern Bering Sea (upper left panel) and the effects of retained habitat covariates in the best-fitting generalized additive model (GAM) of presence-absence (upper center panel) spatially predicting the probability of their presence (upper right panel); the best-fitting abundance GAM (lower left panel) conditionally predicts adult Greenland turbot catch-per-unit-effort (CPUE) at sites where the optimum threshold for probability of presence was met or exceeded (lower center panel).

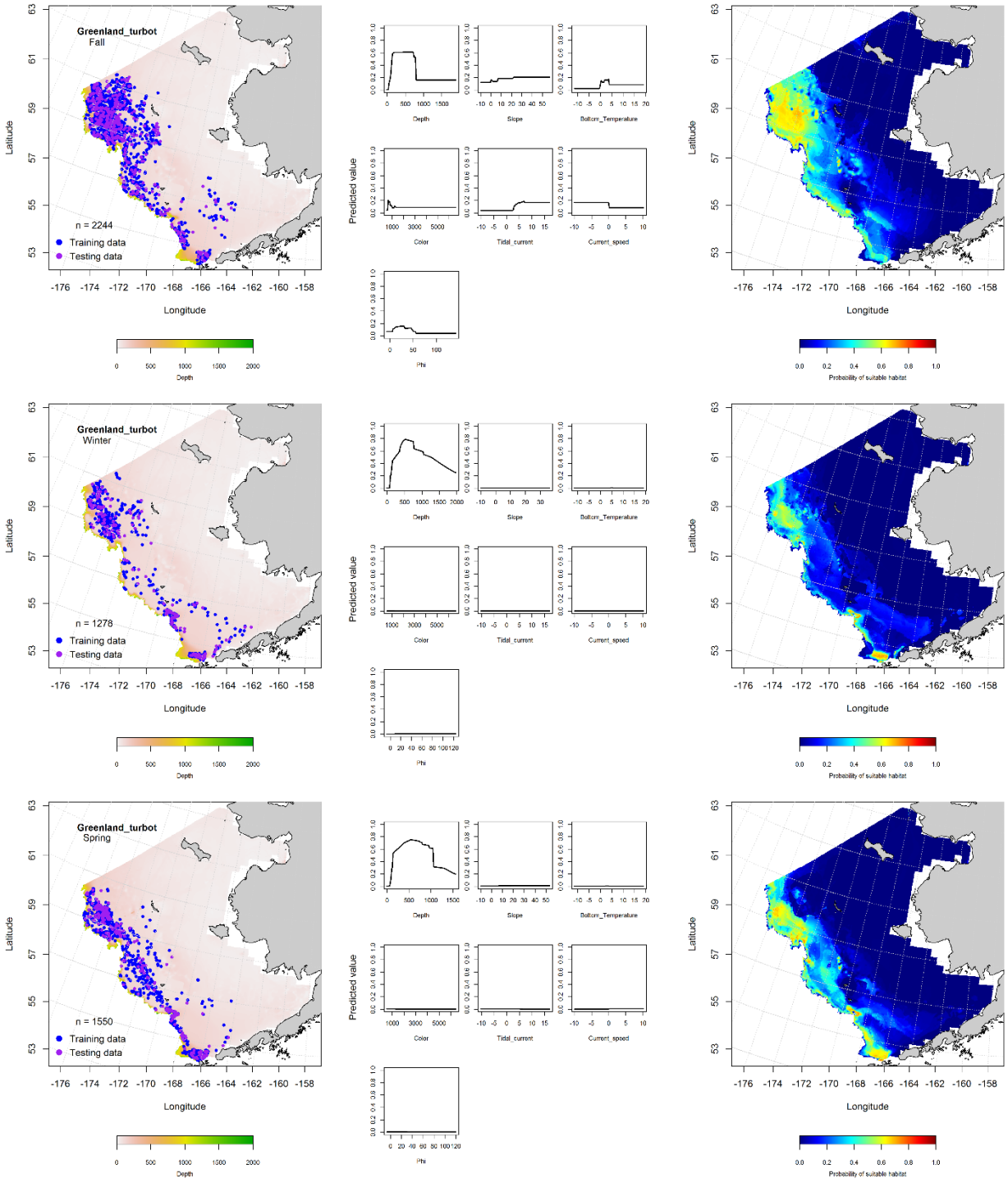

Figure 61. -- Locations of Greenland turbot in fall (October-November; top row), winter (December-February; middle row), and spring (March-May; bottom row) commercial fisheries catches (2003-2013) from the eastern Bering Sea (left-hand column). Blue points were used to train the MaxEnt model (center column) predicting the probability of suitable habitat (right-hand column) and the purple points were used to validate the model.

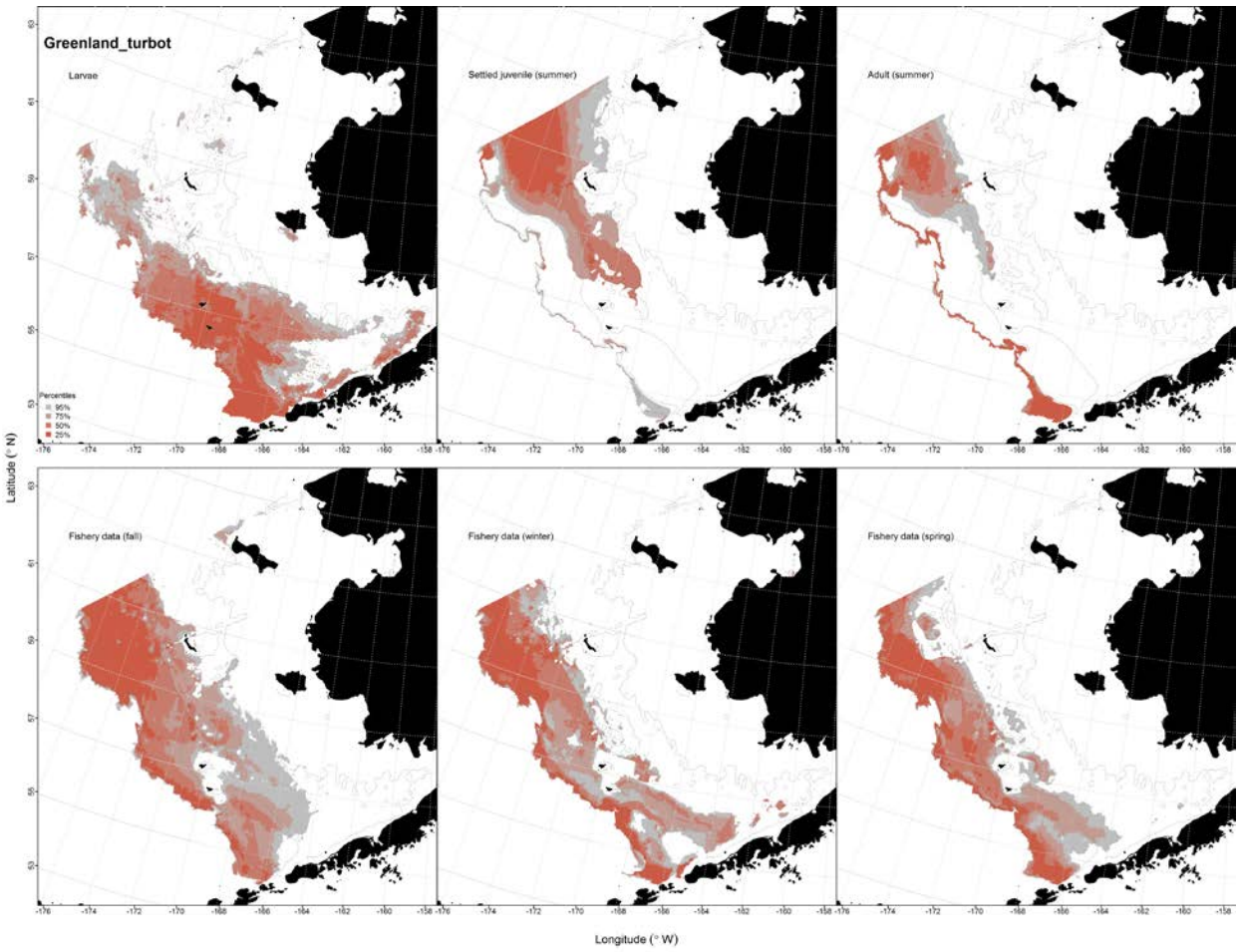

Figure 62. -- Essential fish habitat (EFH) predicted for Greenland turbot larvae (upper left panel) from EcoFOCI ichthyoplankton surveys, settled juveniles and adults (upper middle and right panels) from RACE-GAP summertime bottom trawl surveys (1982-2014), and predicted from presence in commercial fishery catches (2003-2013) from fall, winter, and spring in the eastern Bering Sea (bottom three panels).

Roundfishes

Walleye Pollock (*Gadus chalcogrammus*)

Distribution of early life history stages of walleye pollock (*Gadus chalcogrammus*) from EcoFOCI ichthyoplankton surveys of the eastern Bering Sea -- Eggs of walleye pollock were collected from the water column on EcoFOCI ichthyoplankton surveys between February and October

(Table 2, Fig. 63). Survey effort varied across years so that apparent differences in the distribution of pollock eggs incorporate changes in sampling effort, design, or gear type. MaxEnt modeling was used to predict the probability of suitable habitat from the walleye pollock egg presence data. The most influential habitat covariate predicting suitable habitat was surface temperature which had a relative importance to the model of 69.1%. Ocean productivity and bottom depth were the next most important covariates and comprised an additional 15.3% of the relative importance of covariates. The areas with highest probability for providing suitable egg habitat were located along the Alaska Peninsula, over the outer shelf in the southern portion of the EBS, and around the Pribilof Islands to the north. The MaxEnt fit to the training data was excellent (AUC = 0.88) and the model correctly classified 81% of predicted cases. Model validation was successful (AUC = 0.83). Predictions made from the test data correctly classified 83% of cases.

Walleye pollock larvae were present in EcoFOCI ichthyoplankton surveys between February and September (Table 2, Fig. 64). A MaxEnt model was used to predict the probability of suitable larval walleye pollock habitat in the EBS. The most influential habitat covariates in the model were surface temperature and ocean productivity (combined relative importance = 84.8%). Similar to the predictions for pollock egg habitat, the areas of highest probability for suitable larval pollock habitat occurred along the Alaska Peninsula above Unimak Pass and Unimak Island as well as around the Pribilof Islands to the north. The MaxEnt fit to the training data was outstanding (AUC = 0.90) and correctly classified 83% of predicted cases. Model validation with the test data had an excellent fit (AUC = 0.83) and correctly classified 83% of predicted cases.

Pelagic juvenile walleye pollock were distributed across the middle, inner and outer shelf of the EBS and were collected between May and October on EcoFOCI ichthyoplankton surveys (Fig. 65). The habitat covariates in the MaxEnt model that exercised the greatest influence on the prediction of the probability of suitable pelagic juvenile walleye pollock habitat were surface temperature and ocean productivity (combined relative importance = 62.2%). The areas holding the highest predicted

probabilities of suitable habitat were centered on the Pribilof Islands. The model fit to the training data was outstanding (AUC = 0.94) and the percent of cases correctly predicted was high (87%). Validation using the test data indicated an excellent model fit (AUC = 0.86) and a relatively high proportion of correctly classified cases (86%).

Summertime distribution of settled juvenile and adult walleye pollock (*Gadus chalcogrammus*) from RACE-GAP bottom trawl surveys of the eastern Bering Sea -- Settled juvenile walleye pollock collected in RACE-GAP summer bottom trawl surveys of the EBS were widely dispersed across the survey area (Fig. 66). Of the 10 habitat covariates retained in the best-fitting GAM, the most influential predictors were geographical location, sediment grain size, and bottom depth. Settled juvenile CPUE was predicted to be highest over the middle shelf in the central portion of the EBS with smaller sediment grain sizes and bottom depths shallower than 200 m. This GAM explained just 31.2% of the deviance in settled juvenile pollock CPUE. The fit to the training data was marginal ($r^2 = 0.31$) and model validation using the test data set had an equally marginal fit ($r^2 = 0.31$). The model predicted that settled juvenile walleye pollock abundance from RACE-GAP summer bottom trawl surveys was highest over the outer shelf between the Pribilof Islands and the U.S.-Russia Convention Line to the northwest. The relatively poor fit of this GAM to the settled juvenile CPUE data may be partially explained by their decreasing availability to the bottom trawl with decreasing fork length (Kotwicki et al. 2015).

Adult walleye pollock were also broadly distributed across the EBS in summer bottom trawl catches (Fig. 67). The most influential habitat covariates retained in the best-fitting GAM were geographic location, bottom temperature, and bottom depth. Adult pollock CPUE was highest over the middle shelf between the Pribilof Islands and the U.S.-Russia Convention Line in waters around 2.5°C and shallower than 200 m. The best-fitting model explained just 45.9% of the variability in the adult pollock CPUE data and was a marginal fit to the training data ($r^2 = 0.46$); the fit to the test data in model validation was also marginal ($r^2 = 0.47$).

Seasonal distribution of walleye pollock (*Gadus chalcogrammus*) in commercial fishery catches from the eastern Bering Sea -- Walleye pollock were reported from commercial catches in the EBS throughout the fall, winter, and spring (Fig. 68). Catches were constrained to the middle and outer shelf, but extended from the Alaska Peninsula to the U.S.-Russia Convention Line. MaxEnt modeling predicted that the highest likelihood of suitable walleye pollock habitat occurred over the outer shelf in patches extending along the western edge of the EBS shelf. Bottom depth and bottom temperature were the most important variables for predicting suitable habitat from commercial catches; their combined influence was high in all three seasons (relative importance = 91.8% in fall, 90% in winter, and 78.1% in spring). Model fits to the training data ranged from excellent (AUC = 0.88 in fall) to outstanding (AUC = 0.93 in winter) and the models correctly classified a high percentage of predicted cases (79-85%). The model validation step was successful (AUC ranged from 0.78 to 0.84) with 78 to 84% of predicted cases classified correctly using the test data.

Essential habitat maps and conclusions for walleye pollock (*Gadus chalcogrammus*) from the eastern Bering Sea -- Walleye pollock EFH is distributed across much of the EBS (Fig. 69). Essential ELHS habitat extends from the inner shelf in Bristol Bay to the western boundary of the survey area and north to the U.S.-Russia Convention Line. The core of ELHS EFH (the top 25% of suitable habitat) is primarily located on the middle and outer shelf of the southern and central western portions of the EBS. Settled juvenile and adult EFH from summer surveys covers nearly all of the RACE-GAP bottom trawl study area with core EFH for both life stages located primarily over the middle and outer shelf. Settled juvenile EFH extends slightly farther inshore than that of adults. Seasonal differences in the presence of pollock reported by observers in commercial fishery catches were apparent in descriptions of EFH based on these data, but in all seasons reported the core EFH from the fisheries generally confirmed the distribution of EFH described from the RACE-GAP summer bottom trawl survey data.

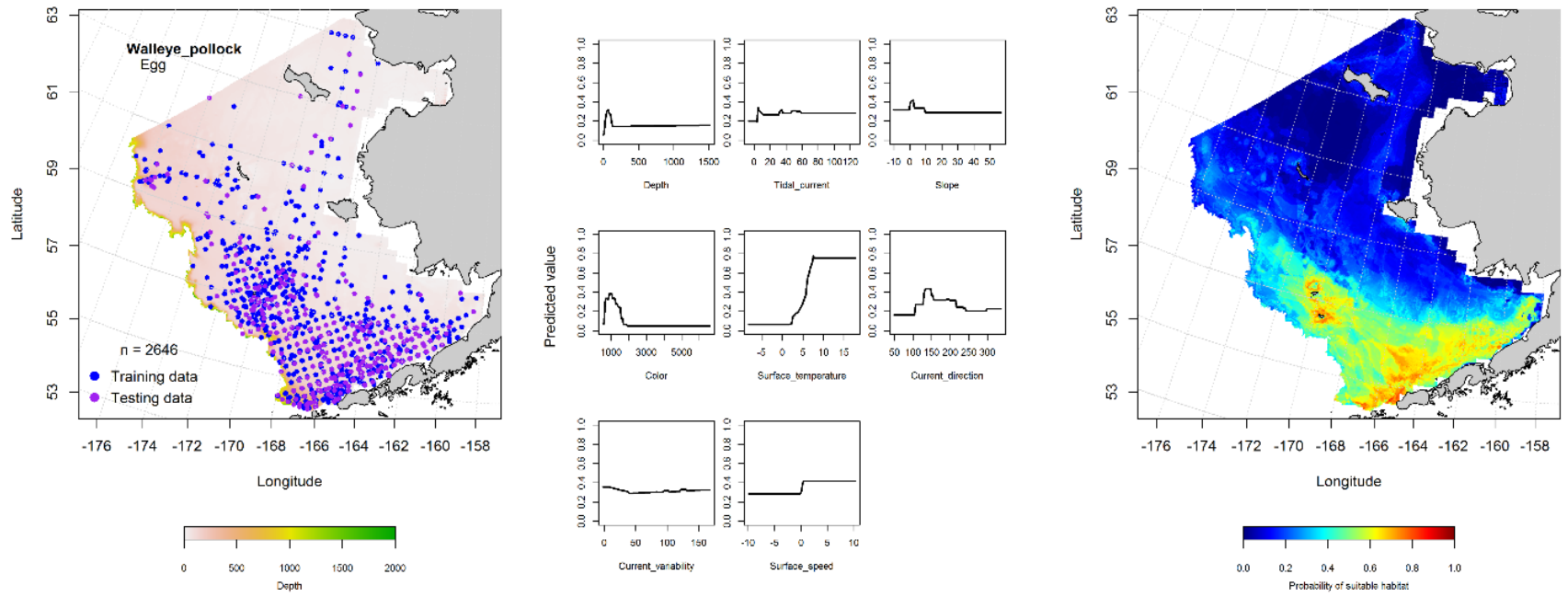

Figure 63. -- Presence of walleye pollock eggs in EcoFOCI ichthyoplankton surveys of the eastern Bering Sea (left panel) with training (blue dots) and testing (purple dots) data sets indicated alongside the maximum entropy model (MaxEnt) effects (center panel) and the MaxEnt spatial predictions of the probability of suitable walleye pollock egg habitat (right panel).

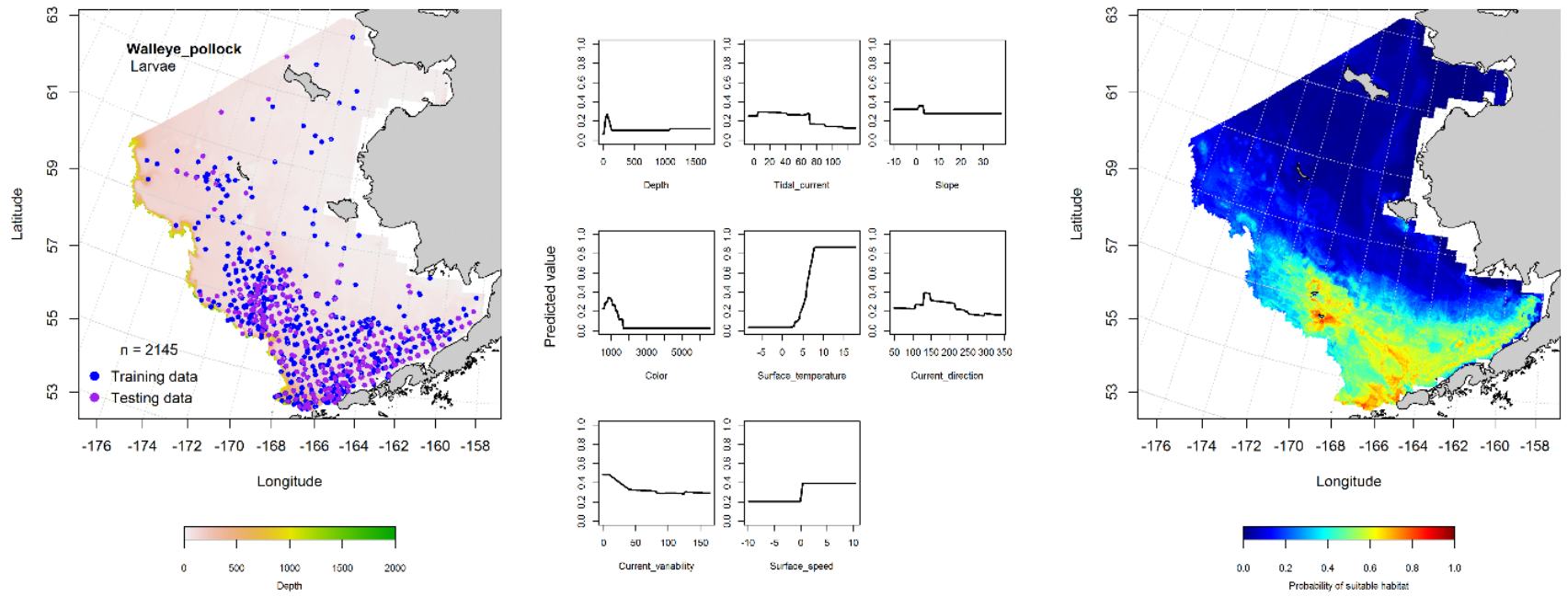

Figure 64. -- Presence of walleye pollock larvae in EcoFOCI ichthyoplankton surveys of the eastern Bering Sea (left panel) with training (blue dots) and testing (purple dots) data sets indicated alongside the maximum entropy model (MaxEnt) effects (center panel) and the MaxEnt spatial predictions of the probability of suitable larval walleye pollock habitat (right panel).

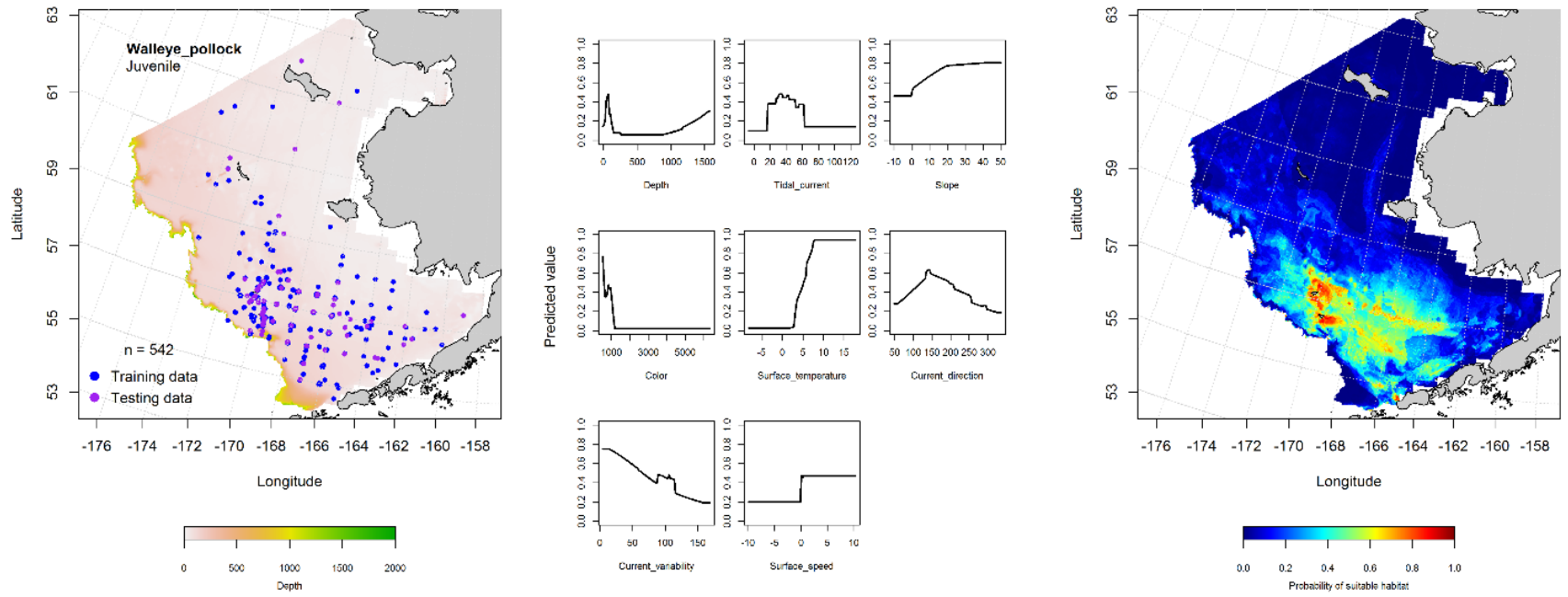

Figure 65. -- Presence of pelagic juvenile walleye pollock in EcoFOCI ichthyoplankton surveys of the eastern Bering Sea (left panel) with training (blue dots) and testing (purple dots) data sets indicated alongside the maximum entropy model (MaxEnt) effects (center panel) and the MaxEnt spatial predictions of the probability of suitable pelagic juvenile walleye pollock habitat (right panel).

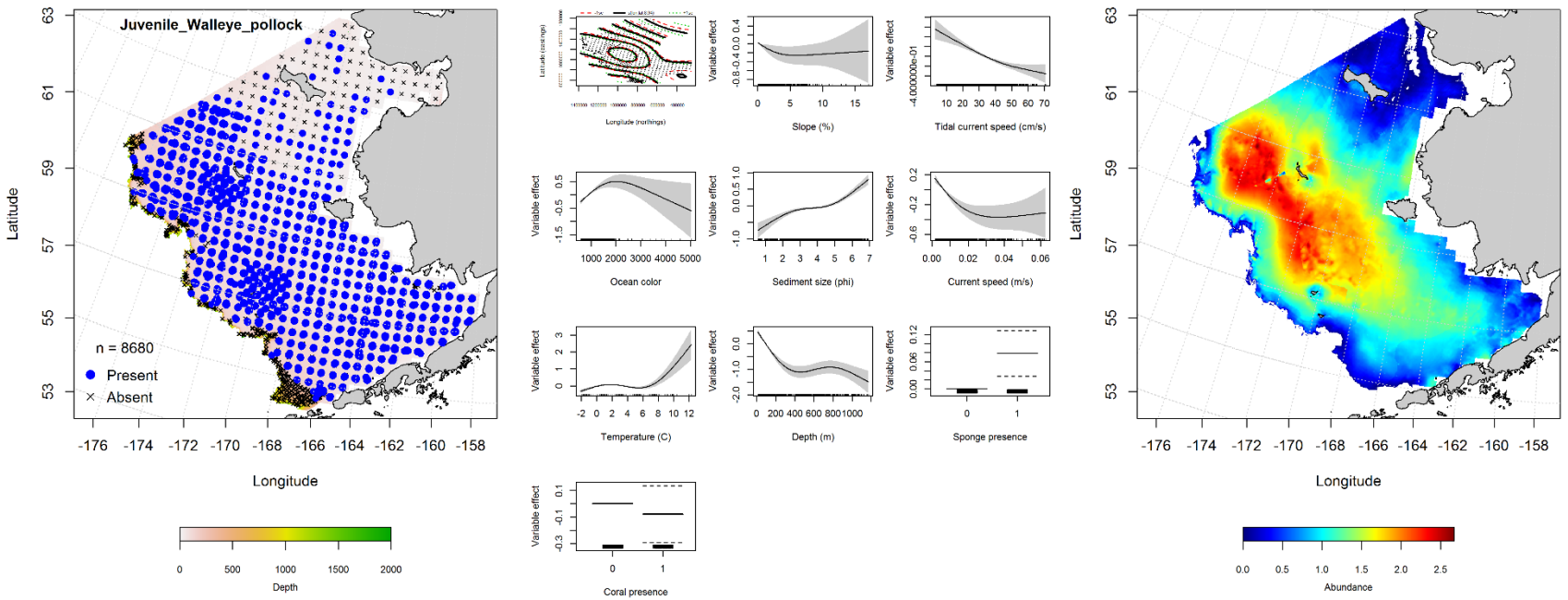

Figure 66. -- Distribution of settled juvenile walleye pollock in 1982-2014 RACE-GAP summer bottom trawl surveys (left panel) alongside effects of retained habitat covariates in the best-fitting generalized additive model (GAM; center panel) predicting spatial distribution of abundance (CPUE, right panel) across the eastern Bering Sea.

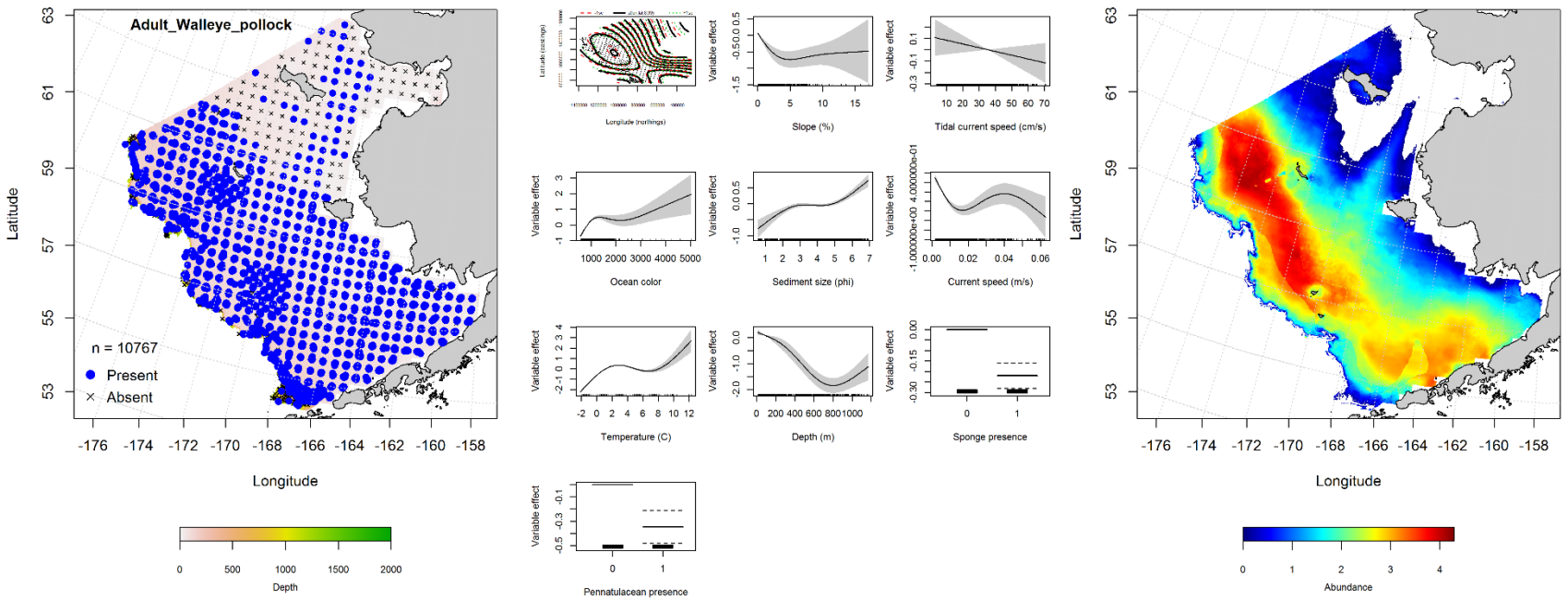

Figure 67. -- Distribution of adult walleye pollock in 1982-2014 RACE-GAP summer bottom trawl surveys (left panel) alongside effects of retained habitat covariates in the best-fitting generalized additive model (GAM; center panel) predicting spatial distribution of abundance (CPUE, right panel) across the eastern Bering Sea.

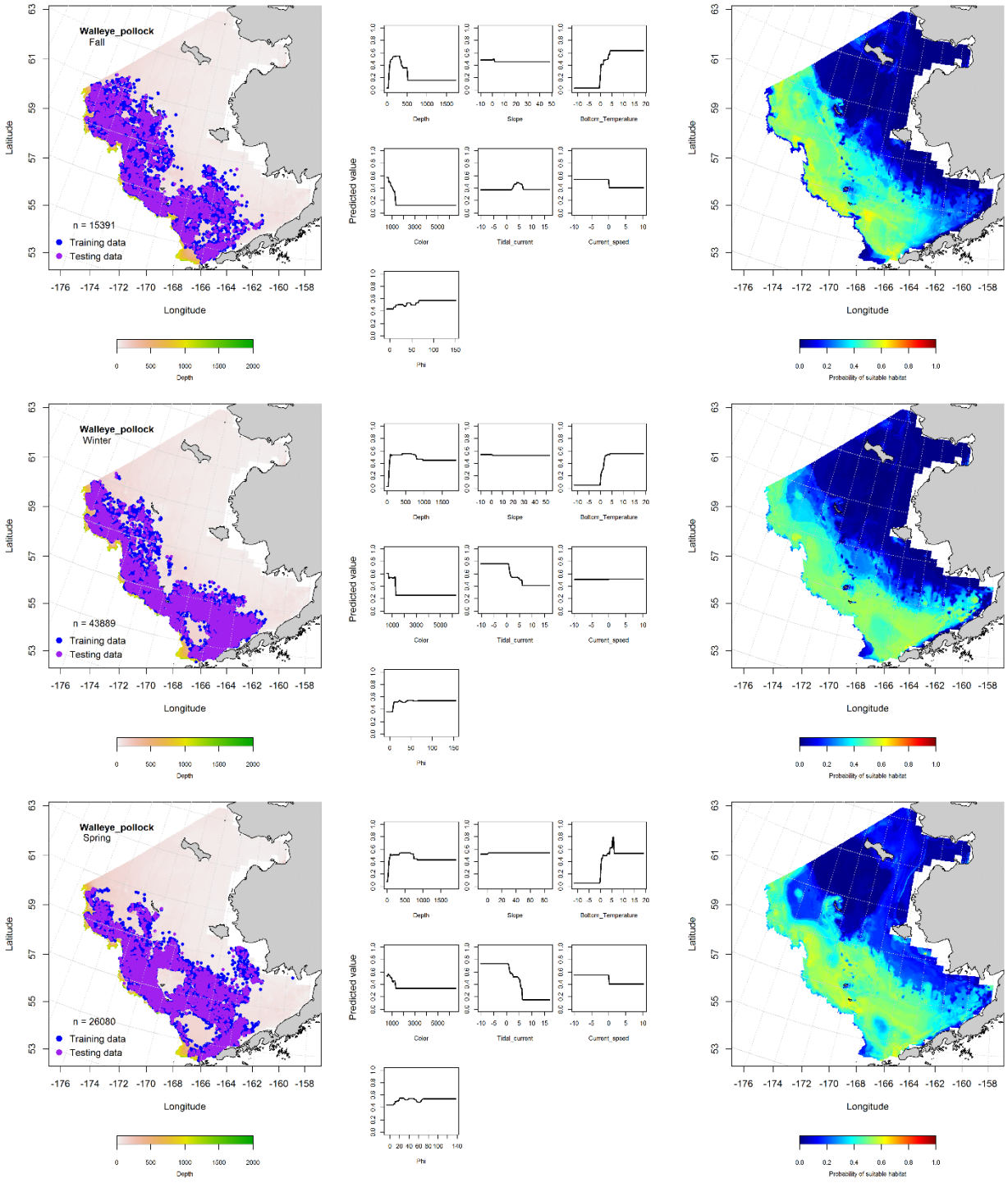

Figure 68. -- Locations of walleye pollock in fall (October-November; top row), winter (December-February; middle row), and spring (March-May; bottom row) commercial fisheries catches (2003-2013) from the eastern Bering Sea (left-hand column). Blue points were used to train the MaxEnt model (center column) predicting the probability of suitable habitat (right-hand column) and the purple points were used to validate the model.

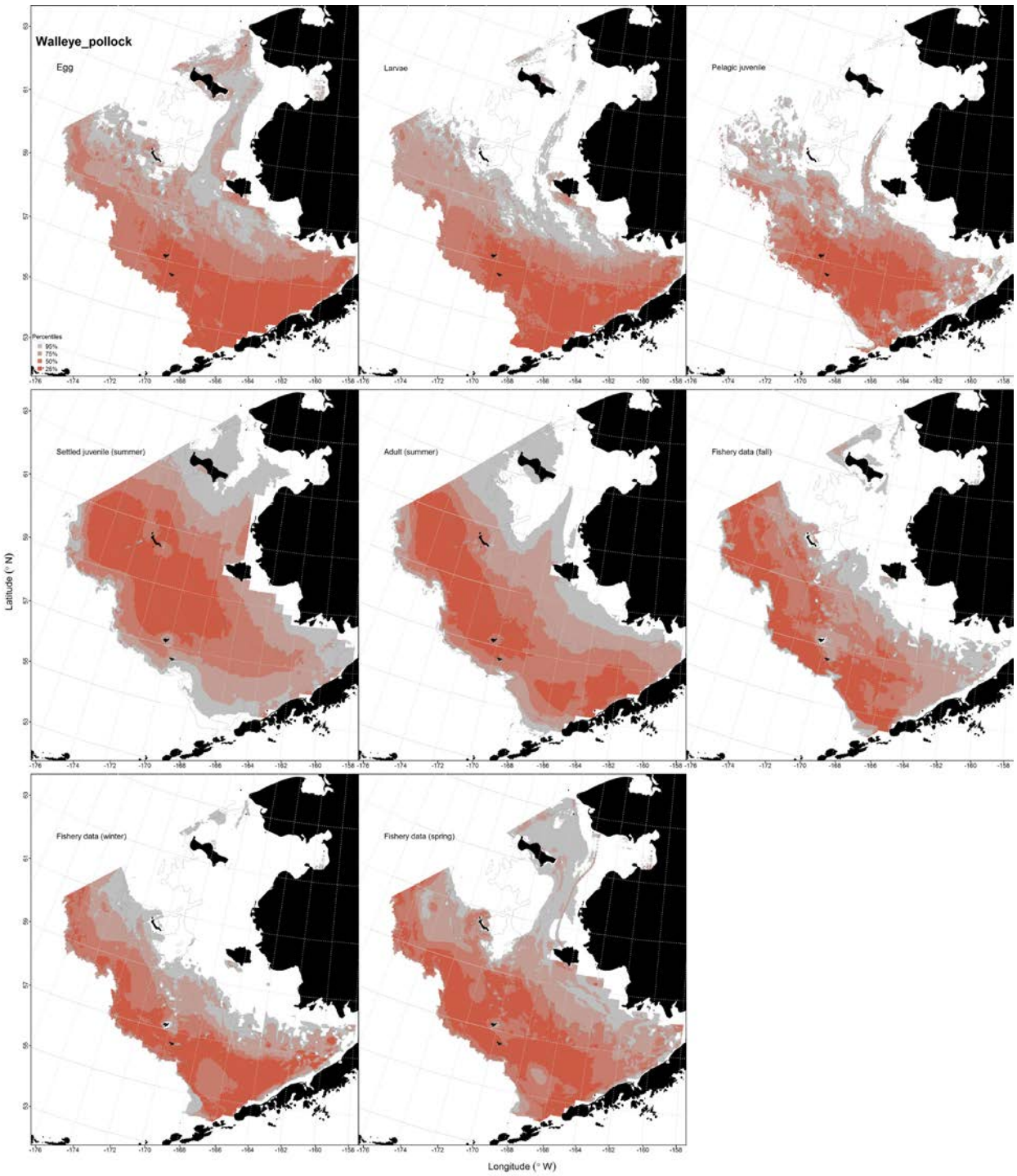

Figure 69. -- Essential fish habitat (EFH) predicted for walleye pollock eggs, larvae, and pelagic juveniles (upper row of panels) from EcoFOCI ichthyoplankton surveys (1991-2013), settled juveniles and adults (left and center panel of middle row) from RACE-GAP summertime bottom trawl surveys (1982-2014), and predicted from presence in commercial fishery catches (2003-2013) from fall (center row left panel), winter, and spring (bottom two panels) in the eastern Bering Sea.

Pacific Cod (*Gadus macrocephalus*)

Seasonal distribution of egg, larval, and pelagic juvenile stages of Pacific cod (*Gadus macrocephalus*) from EcoFOCI ichthyoplankton surveys of the eastern Bering Sea -- Pacific cod are demersal broadcast spawners and their eggs were encountered between April and July in EcoFOCI ichthyoplankton surveys of the EBS (Table 2; Fig. 70). Pacific cod eggs were uncommon in the ichthyoplankton samples which did not target these demersal life stages; cod eggs are demersal and adhesive. Prevalence of Pacific cod eggs was not sufficient to undertake distribution modeling for this life stage.

Pacific cod larvae were collected on EcoFOCI ichthyoplankton surveys between February and October (Table 2; Fig. 71). Larvae were primarily encountered in the southwestern portion of the study area over the middle and outer shelf as well as on the middle shelf around the Pribilof Islands. The most important covariate in the MaxEnt model used to predict probability of suitable habitat from larval Pacific cod presence in ichthyoplankton samples was surface temperature (relative importance = 69.8%). The predicted probability of suitable habitat increased over the 5-10°C surface temperature range. The model fit to the training data was outstanding (AUC = 0.95) and it correctly classified 89% of predicted cases. Model validation was successful (AUC = 0.87) and 87% of cases were of correctly classified using the test data.

Pelagic juvenile Pacific cod were encountered on EcoFOCI ichthyoplankton surveys between July and September (Table 2; Fig. 72). This life stage was collected primarily from the southwestern portion of the EBS over the middle and outer shelf. The most important habitat covariates for predicting suitable pelagic juvenile Pacific cod habitat from the MaxEnt model were surface temperature and ocean productivity (combined relative importance = 69.3%). The areas with the highest probabilities to provide suitable habitat for this life stage were distributed between the northern edge of the Bering Canyon and St. Paul Island in the Pribilofs. The model fit to the training data was outstanding (AUC = 0.97) and the

percent of cases correctly predicted was also high (91%). Validation using the test data produced an excellent model fit (AUC = 0.85) and a high proportion of correctly classified cases (85%).

Summertime distribution of settled juvenile and adult Pacific cod (*Gadus macrocephalus*) from RACE-GAP bottom trawl surveys of the eastern Bering Sea -- Settled juvenile Pacific cod collected in RACE-GAP summer bottom trawl surveys of the EBS were broadly distributed across the survey area (Fig. 73). Occurrence of settled juvenile Pacific cod was less common in the NBS and there were no records of this life stage occurring in Norton Sound samples. The most significant habitat covariates remaining in the best-fitting GAM were geographic location and sediment grain size; bottom depth, bottom temperature, and tidal current were also important. The GAM explained 39.5% of the deviance in settled juvenile Pacific cod CPUE in the EBS. Model effects favored the northwest portion of the survey area over decreasing sediment grain size and tidal current at shallower depths and bottom temperatures around 2°C. The fit to the training data was marginal ($r^2 = 0.40$) and model validation using the test data set had a similar fit ($r^2 = 0.39$).

Adult Pacific cod were distributed across the RACE-GAP summer bottom trawl survey area similarly to settled juveniles (Fig. 74). The best-fitting GAM retained 10 significant predictors of species distribution, the most significant of which were bottom temperature, geographic location, and bottom depth. Model effects were greatest in the northwest portion of the survey area at shallower bottom depths and bottom temperatures around 2°C. The GAM explained just 35.2% of the variability in the adult Pacific cod CPUE data and was a marginal fit to the training and test data ($r^2 = 0.35$).

Seasonal distribution of Pacific cod (*Gadus macrocephalus*) in commercial fishery catches from the eastern Bering Sea -- The distribution of Pacific cod in commercial catches from the EBS varied across the fall, winter, and spring seasons (Fig. 75). Their distribution in commercial catches was more geographically constrained during wintertime than in fall or spring. MaxEnt modeling from presence-only records identified that the most important terms determining Pacific cod distribution in commercial catch data were bottom depth and bottom temperature in all seasons. The combined relative

importance of these two terms in the suite of habitat covariates parameterizing the MaxEnt model ranged from 77.1% in springtime to 89.8% in winter. The MaxEnt model fits to the training data ranged from excellent in the fall (AUC = 0.87 and 79% of cases correctly predicted) to outstanding in the winter (AUC = 0.93 and 86% of cases correctly predicted). Model validation was generally successful; AUC ranged from 0.78 in fall to 0.85 in winter and the model with test data correctly classified 78% of predicted cases in fall and 85% in winter.

Essential fish habitat maps and conclusions for Pacific cod (*Gadus macrocephalus*) in the eastern Bering Sea -- Species distribution modeling of ELHS and later life stages of Pacific cod in the EBS was translated into maps of EFH (Fig. 76). Larvae and pelagic juveniles of Pacific cod were geographically constrained to the middle and outer shelf with EFH for the larval forms extending along the outer shelf northward to the U.S.-Russia Convention Line. Core habitat for these ELHS (top 25% of model predictions) was generally constrained to the outer shelf in the southern portion of the EBS and to the area around the Pribilof Islands. The EFH of Pacific cod settled juveniles and adults in summertime extended over the majority of the RACE-GAP EBS study area. Core habitat for settled juveniles was restricted to the middle shelf in the central and southern portions of the region while, for adults, core habitat had a disjunct distribution with patches in Bristol Bay and on the middle and outer shelf around the Pribilofs and northward. Pacific cod EFH predicted from commercial fishery catches varied little seasonally and core habitat was consistently predicted on the middle and outer shelf from the Alaska Peninsula to the U.S.-Russia Convention Line.

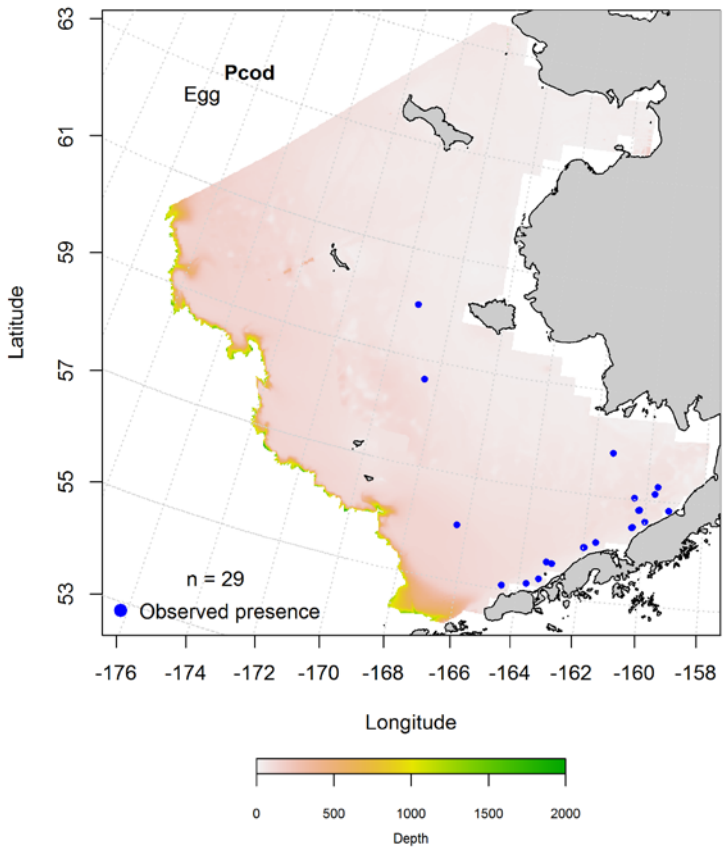

Figure 70. -- Presence of Pacific cod eggs in EcoFOCI ichthyoplankton surveys of the eastern Bering Sea (1991-2013).

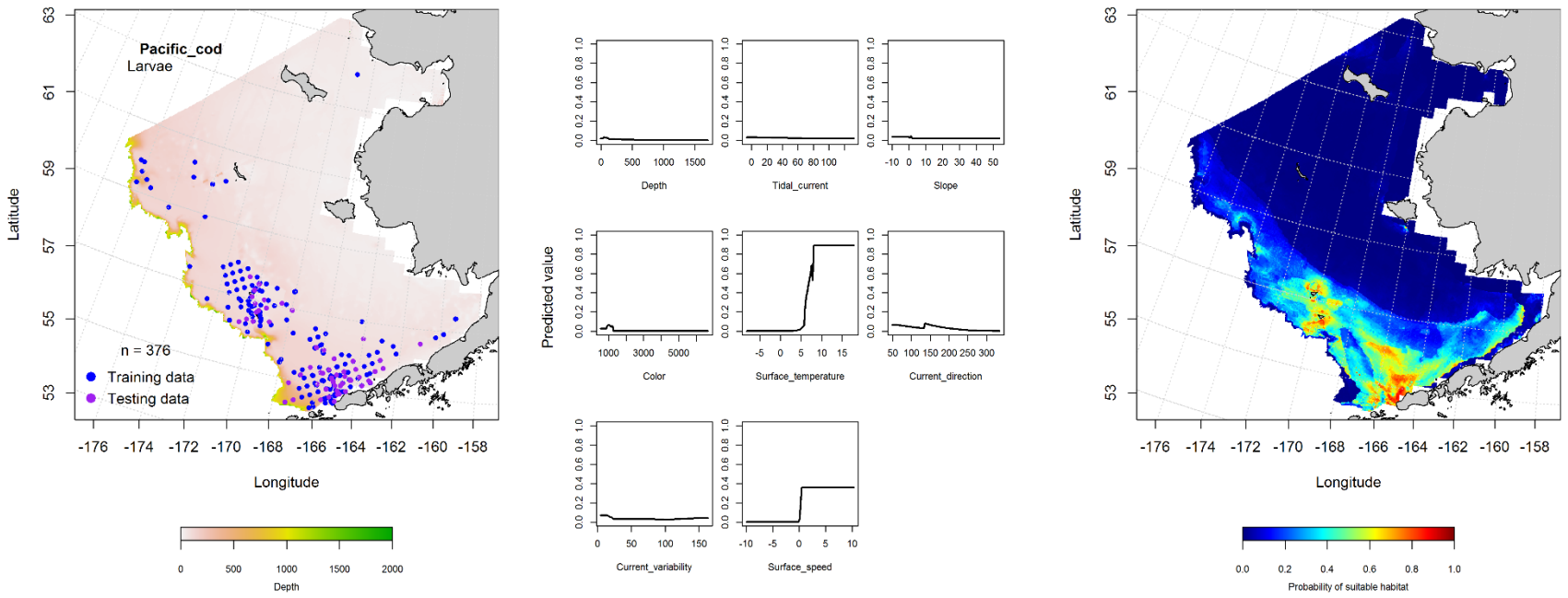

Figure 71. -- Presence of Pacific cod larvae in EcoFOCI (1991-2014) ichthyoplankton surveys of the eastern Bering Sea (left panel) with training (blue dots) and testing (purple dots) data sets indicated alongside the maximum entropy model (MaxEnt) effects (center panel) and the MaxEnt spatial predictions of the probability of suitable larval Pacific cod habitat (right panel).

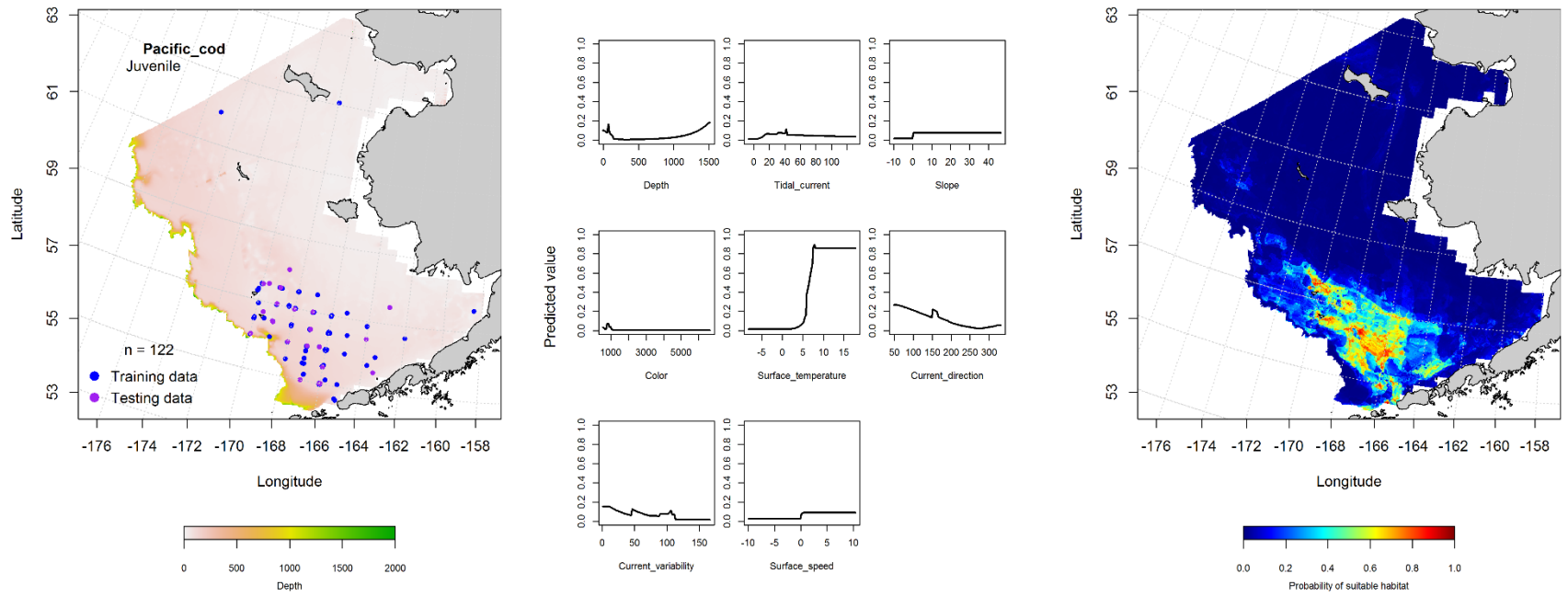

Figure 72. -- Presence of Pacific cod pelagic juveniles in EcoFOCI (1991-2014) ichthyoplankton surveys of the eastern Bering Sea (left panel) with training (blue dots) and testing (purple dots) data sets indicated alongside the maximum entropy model (MaxEnt) effects (center panel) and the MaxEnt spatial predictions of the probability of suitable pelagic juvenile Pacific cod habitat (right panel).

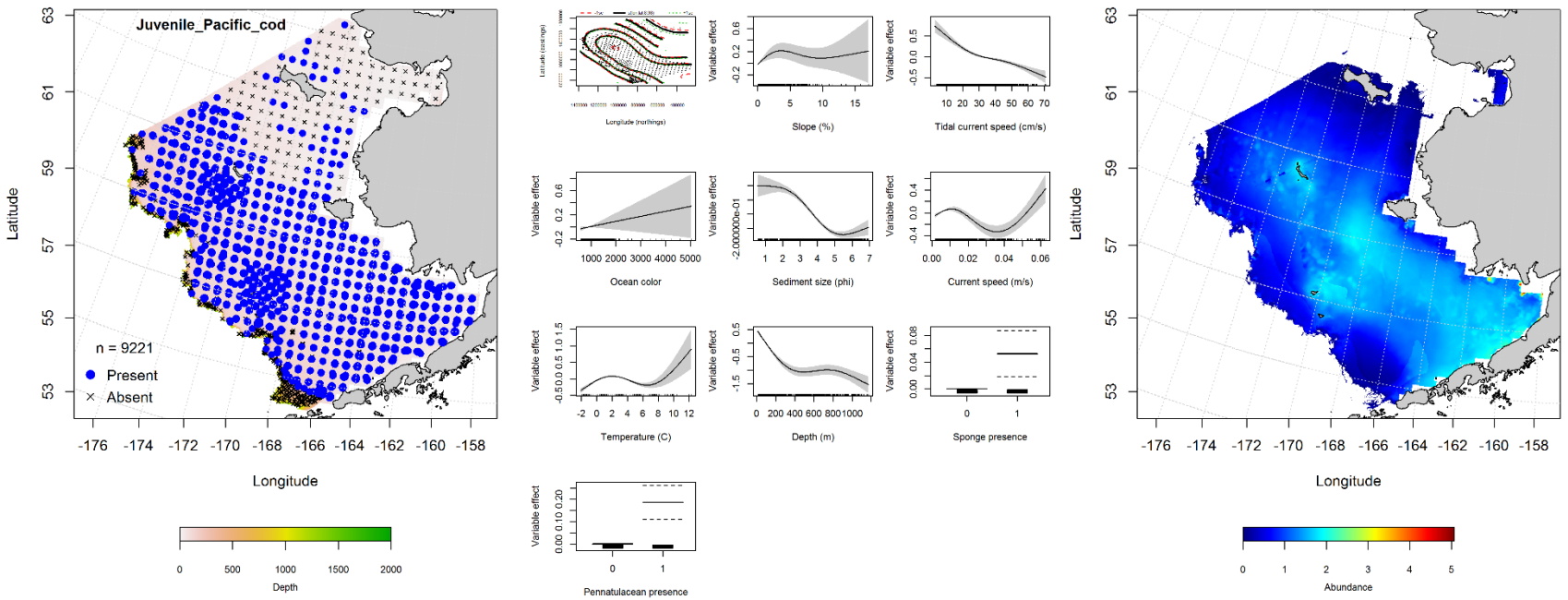

Figure 73. -- Distribution of settled juvenile Pacific cod in 1982-2014 RACE-GAP summer bottom trawl surveys (left panel) alongside effects of retained habitat covariates in the best-fitting generalized additive model (GAM; center panel) predicting spatial distribution of abundance (CPUE, right panel) across the eastern Bering Sea.

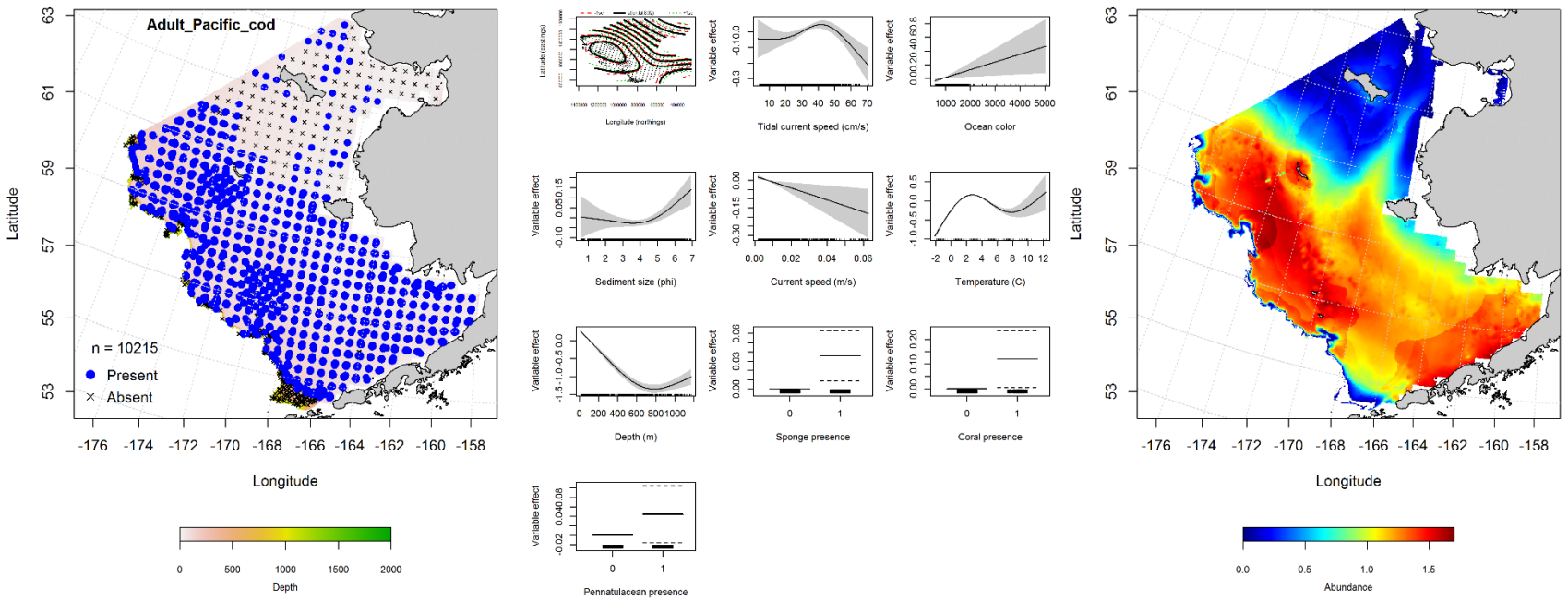

Figure 74. -- Distribution of adult Pacific cod in 1982-2014 RACE-GAP summer bottom trawl surveys (left panel) alongside effects of retained habitat covariates in the best-fitting generalized additive model (GAM; center panel) predicting spatial distribution of abundance (CPUE, right panel) across the eastern Bering Sea.

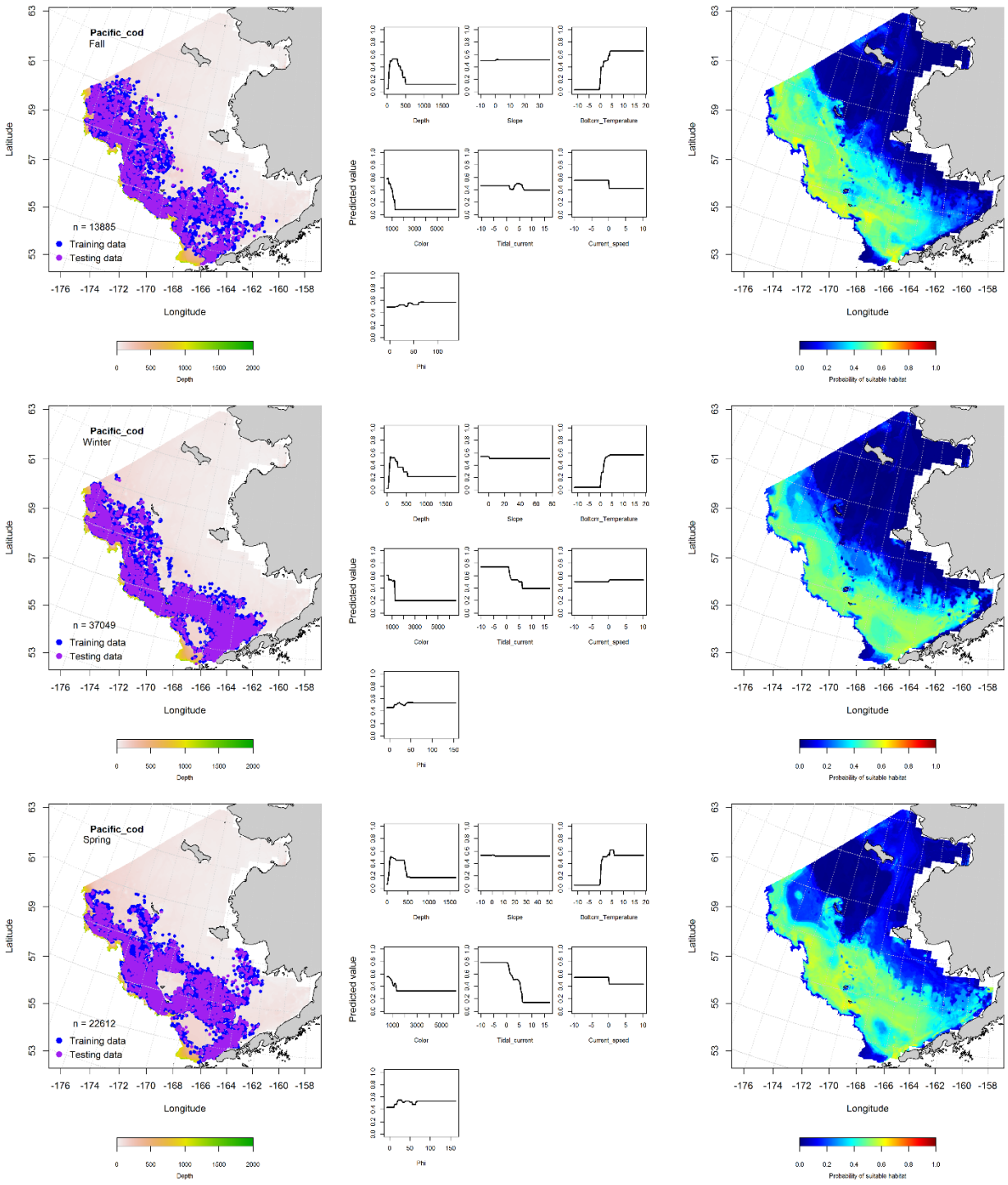

Figure 75. -- Locations of Pacific cod in fall (October-November; top row), winter (December-February; middle row), and spring (March-May; bottom row) commercial fisheries catches (2003-2013) from the eastern Bering Sea (left-hand column). Blue points were used to train the MaxEnt model (center column) predicting the probability of suitable habitat (right-hand column) and the purple points were used to validate the model.

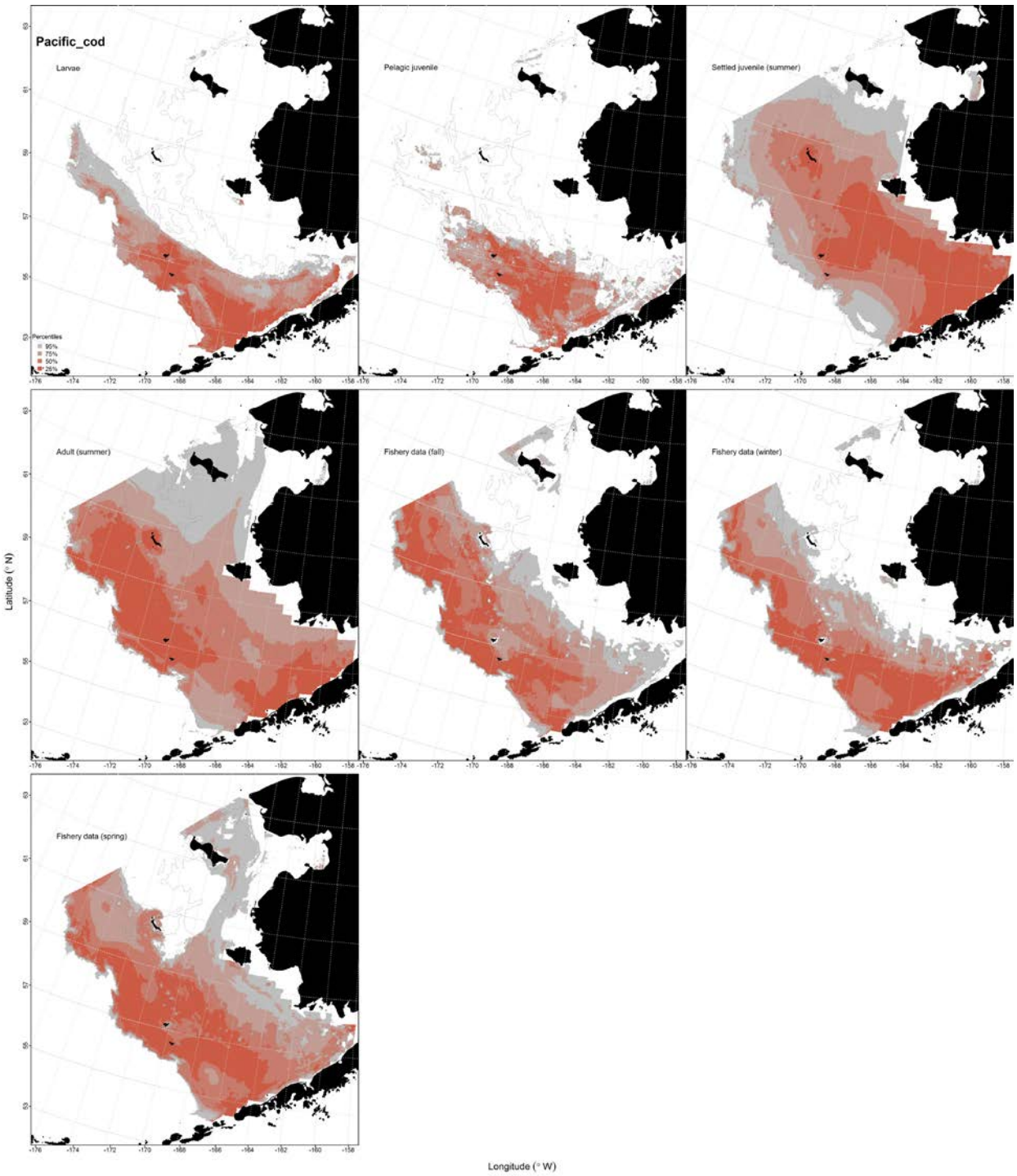

Figure 76. -- Essential fish habitat (EFH) predicted for larvae and pelagic juvenile Pacific cod (upper left and middle panels) from EcoFOCI (1991-2013) ichthyoplankton surveys, settled juveniles and adults (upper right and center left panels) from RACE-GAP summertime bottom trawl surveys (1982-2014), and predicted from presence in commercial fishery catches (2003-2013) from fall, winter, and spring (center middle and left panels and bottom panel, respectively) in the eastern Bering Sea.

Sablefish (*Anoplopoma fimbria*)

Distribution of early life history stages of sablefish (*Anoplopoma fimbria*) from EcoFOCI ichthyoplankton surveys of the eastern Bering Sea -- Sablefish eggs were uncommon in EcoFOCI ichthyoplankton samples from the EBS, but were present in the water column between February and May (Table 2; Fig. 77). Most occurrences of sablefish eggs were over the Bering Canyon in the southwestern corner of the EBS study area. Sablefish eggs were not collected in sufficient prevalence to model distribution of this life stage.

Sablefish larvae were uncommon in EcoFOCI ichthyoplankton samples in the EBS and were collected between February and August (Table 2; Fig. 78). Most occurrences of larval sablefish were observed over the Bering Canyon in the southwestern corner of the EBS study area. This sablefish ELHS was not encountered in sufficient prevalence to warrant modeling its distribution.

Pelagic juvenile sablefish were rare in EcoFOCI ichthyoplankton samples from the EBS, but occurred between July and September when observed (Table 2; Fig. 79). The few occurrences of pelagic juvenile sablefish were all observed near the Pribilof Islands. This level of prevalence was not sufficient to model pelagic juvenile sablefish distribution in the EBS.

Summertime distribution of settled juvenile and adult sablefish (*Anoplopoma fimbria*) from RACE-GAP bottom trawl surveys of the eastern Bering Sea -- Settled juvenile sablefish were collected on RACE-GAP summer bottom trawl surveys of the EBS (Fig. 80). There were less than 50 stations where this life stage occurred in summer bottom trawls and this was insufficient to model their distribution. They were primarily distributed in the southern portion of the study area, but occurred at a few stations in the western central region of the EBS around Pribilof Canyon and the Pribilof Islands.

Adult sablefish collected in RACE-GAP summer bottom trawl surveys of the EBS primarily occurred over the outer shelf (100 to 200 m) and upper continental shelf and slope (> 200 m; Fig. 81). A MaxEnt model was used to predict the probability of suitable adult sablefish habitat from their presence in

summer bottom trawl catches from the EBS. Bottom depth and temperature were the most important habitat covariates in the model accounting for 97.4% combined relative importance amongst all predictor terms. The greatest effect on the model prediction was observed over depths ranging from 500 to 1,000 m and at bottom temperatures around 4° C. The outer shelf and upper Bering Sea slope waters had the greatest probability for encountering suitable summertime adult sablefish habitat with the highest probability areas found in the southern part of the EBS near the Bering Canyon. The MaxEnt model was an outstanding fit to the training (AUC = 0.99) and the test data used for validation (AUC = 0.95). In both of the training and test cases, the models correctly classified 95% of the predicted cases.

Seasonal distribution of sablefish (*Anoplopoma fimbria*) in commercial fishery catches from the eastern Bering Sea -- The distribution of sablefish in commercial catches from the EBS did not vary greatly across the fall, winter, and spring fishing seasons (Fig. 82). They were primarily encountered along the east-west axis of the Bering Canyon into Bristol Bay and along the outer shelf northward. MaxEnt modeling from presence-only records identified the most important covariates describing the probability of suitable habitat for this species. In general, bottom depth and bottom temperature were the most important predictors of the probability of suitable sablefish habitat from commercial catches. Relative importance amongst all predictors ranged from 74.6% (bottom depth and temperature combined) in winter to 89.7% in spring. Model fits to the training data were outstanding (AUC = 0.98-0.99) and model validation using the test data was successful (AUC = 0.92-0.96). Models utilizing either data set correctly classified 92 to 96% of predicted cases.

Essential fish habitat maps and conclusions for sablefish (*Anoplopoma fimbria*) in the eastern Bering Sea -- Species distribution modeling of adult sablefish from RACE-GAP summer bottom trawl surveys and presumed adults from observations of commercial fishery catches in the EBS was translated into maps of EFH (Fig. 83). The distributions of EFH from these data sources largely overlapped. Core habitat (the top 25% of predictions) based on either source was primarily predicted in

waters 100 m and deeper from the Bering Canyon in the southwestern region of the EBS along the outer shelf and upper continental slope northward to the U.S.-Russia Convention Line.

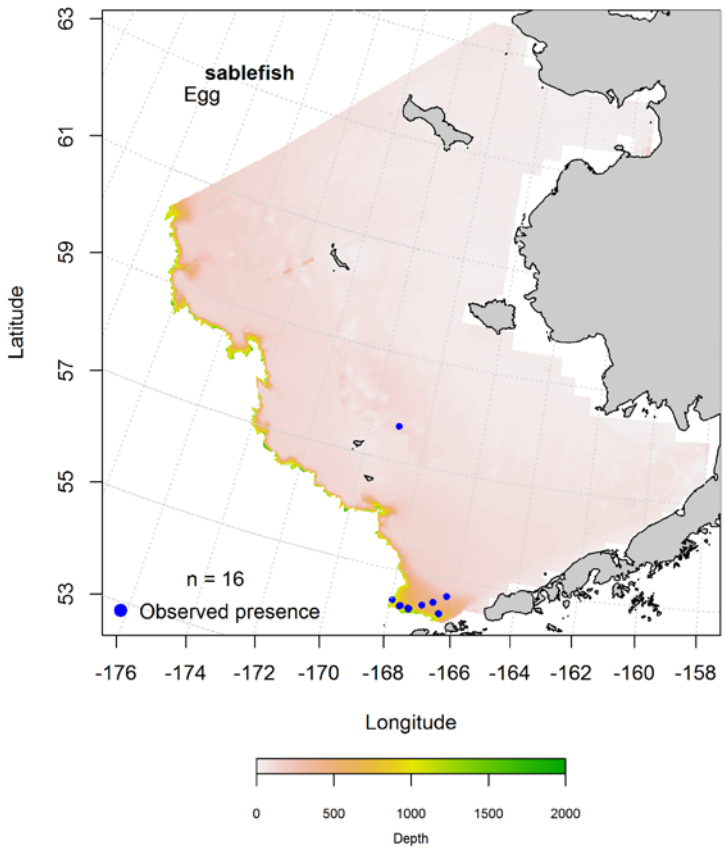

Figure 77. -- Presence of sablefish eggs in EcoFOCI ichthyoplankton surveys of the eastern Bering Sea (1991-2013).

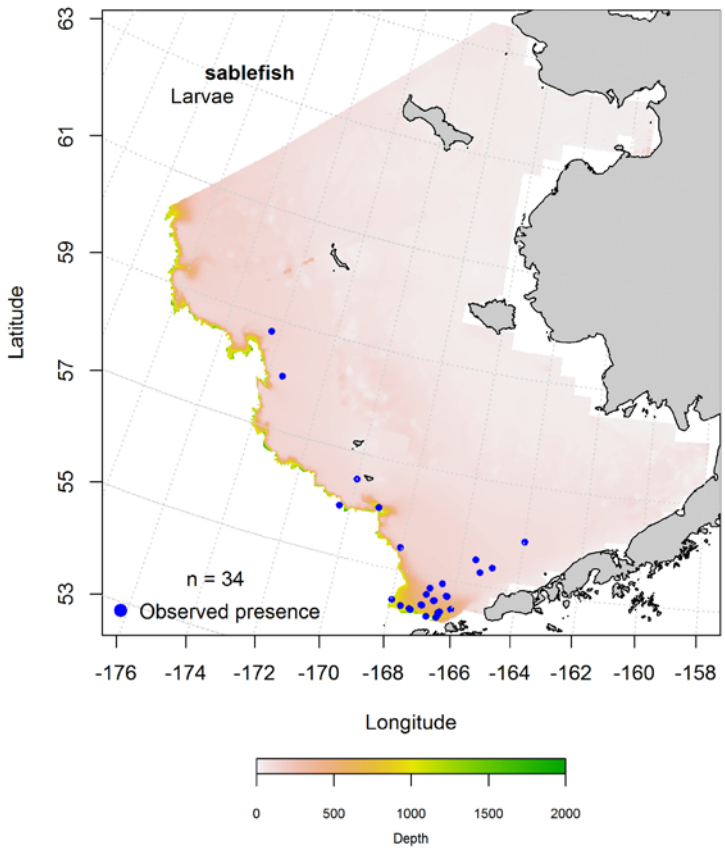

Figure 78. -- Presence of sablefish larvae in EcoFOCI ichthyoplankton surveys of the eastern Bering Sea (1991-2013).

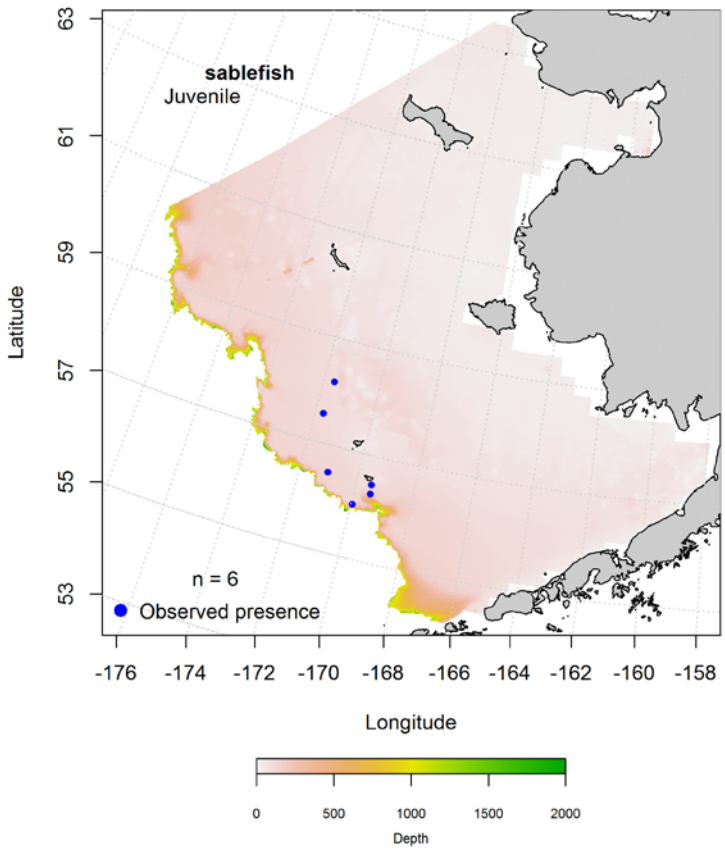

Figure 79. -- Presence of pelagic juvenile sablefish in EcoFOCI ichthyoplankton surveys of the eastern Bering Sea (1991-2013).

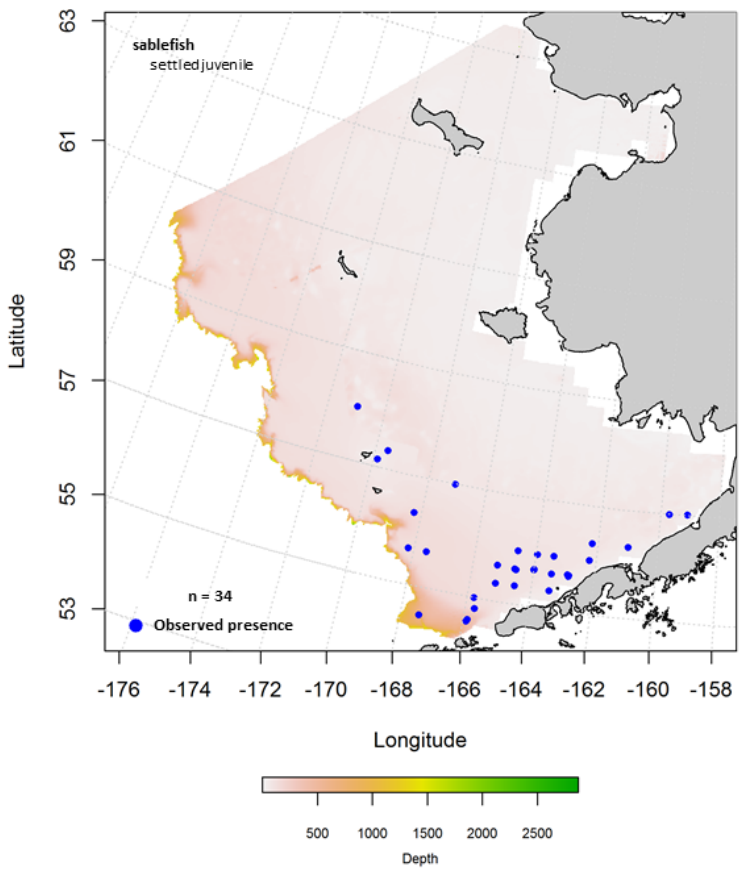

Figure 80. -- Presence of settled juvenile sablefish in RACE-GAP summer bottom trawl surveys (n = 34) of the eastern Bering Sea (1982-2014).

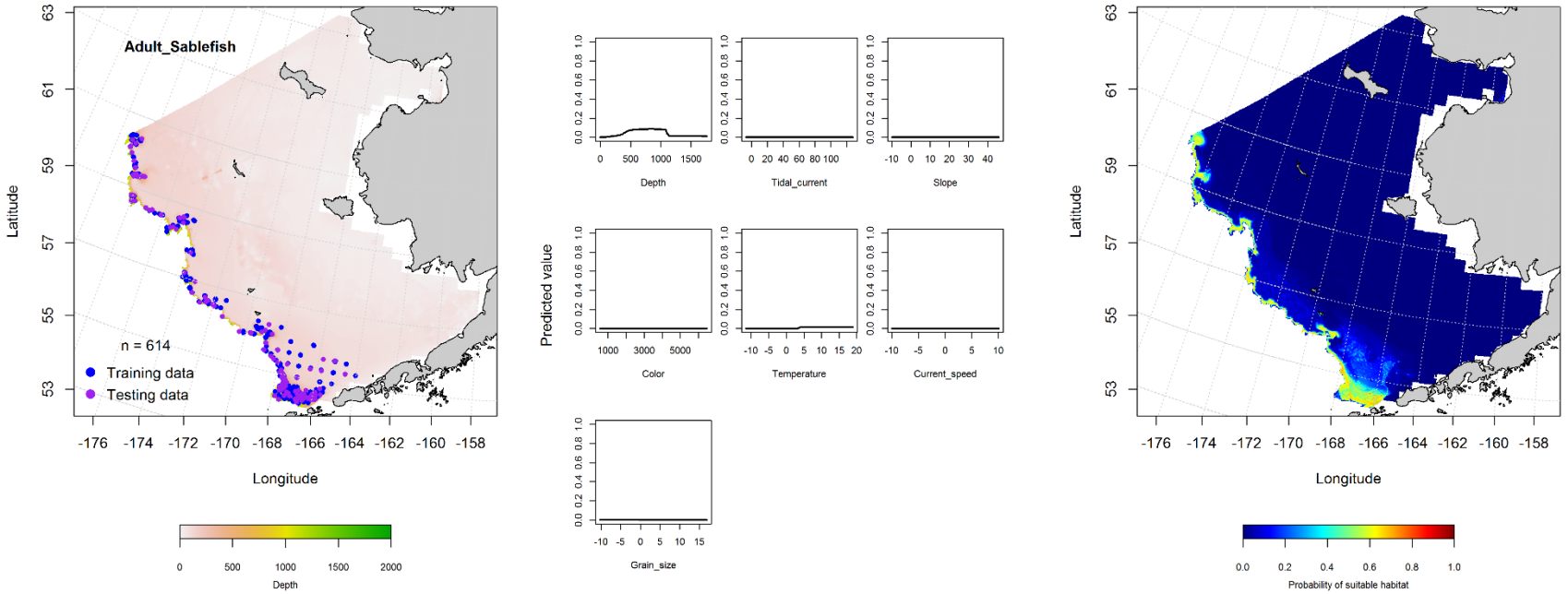

Figure 81. -- Presence of adult sablefish in RACE-GAP summer bottom trawl surveys (1982-2014) of the eastern Bering Sea (left panel) with training (blue dots) and testing (purple dots) data sets indicated alongside the maximum entropy model (MaxEnt) effects (center panel) and the MaxEnt spatial predictions of the probability of suitable adult sablefish habitat (right panel).

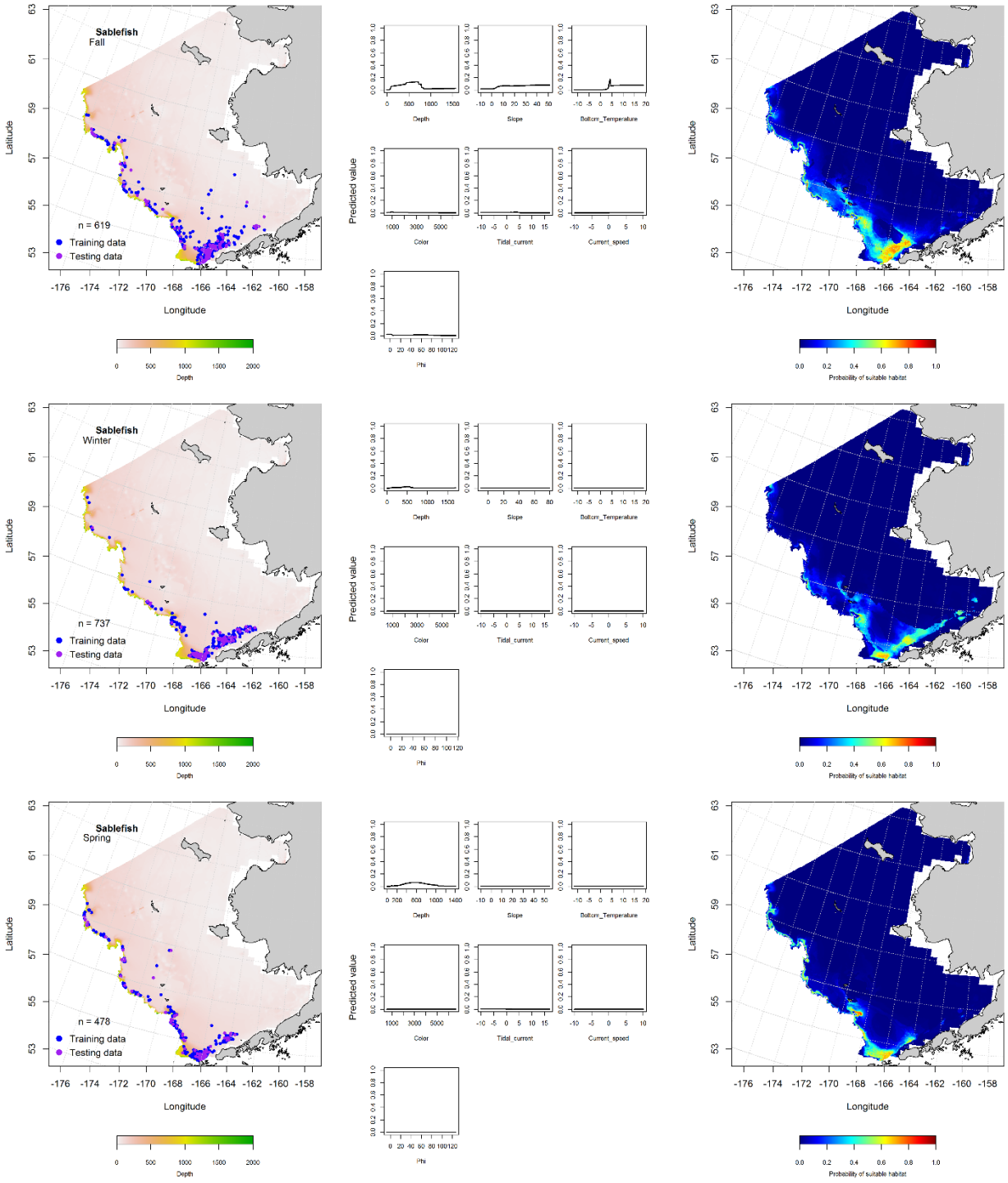

Figure 82. -- Locations of sablefish in fall (October-November; top row), winter (December-February; middle row), and spring (March-May; bottom row) commercial fisheries catches (2003-2013) from the eastern Bering Sea (left-hand column). Blue points were used to train the MaxEnt model (center column) predicting the probability of suitable habitat (right-hand column) and the purple points were used to validate the model.

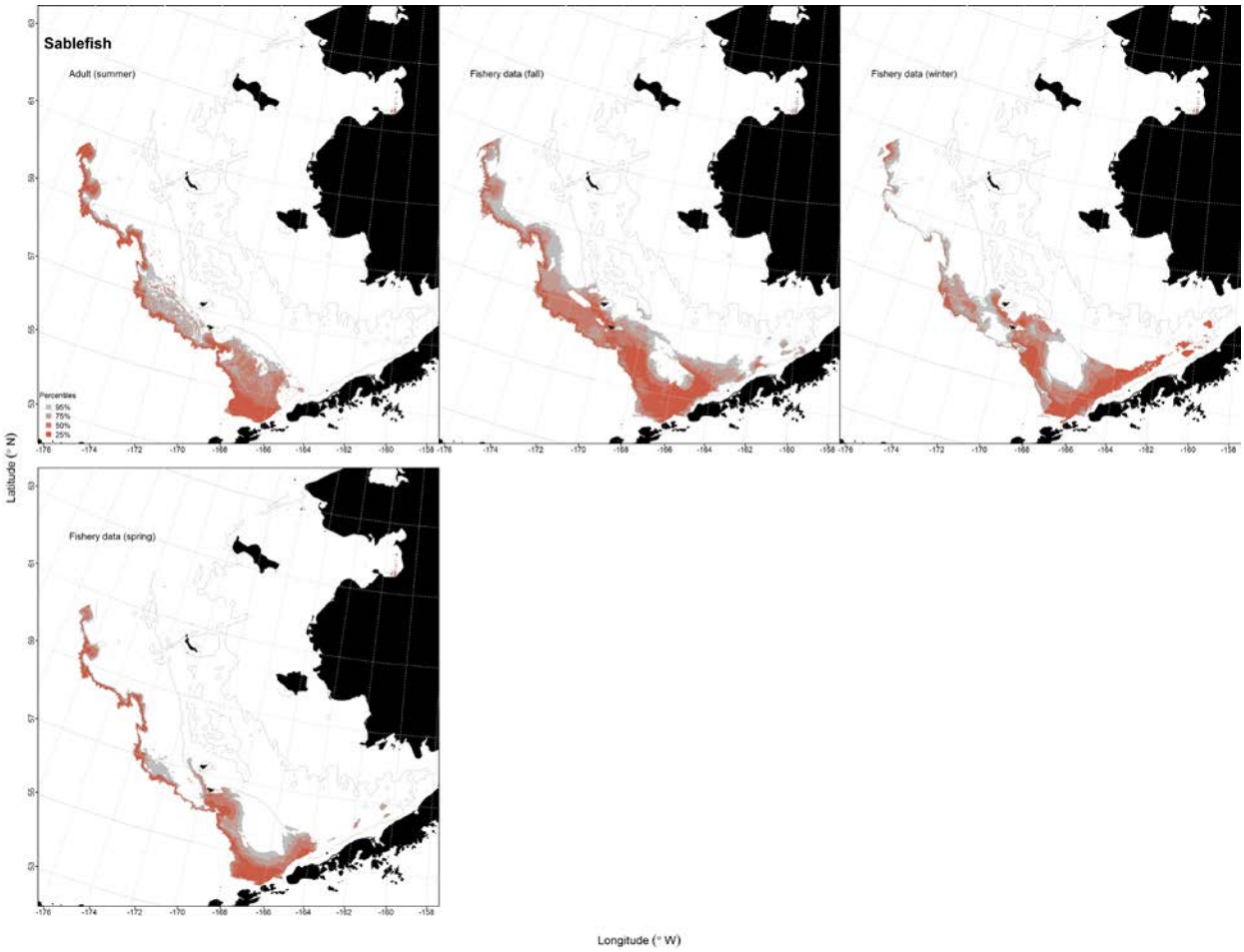

Figure 83. -- Essential fish habitat (EFH) predicted for adult sablefish (upper left) from RACE-GAP summertime bottom trawl surveys (1982-2014) and predicted from presence in commercial fishery catches (2003-2013) from fall, winter (upper middle and right panels), and spring (bottom panel) in the eastern Bering Sea.

Atka Mackerel (*Pleurogrammus monopterygius*)

Distribution of Atka mackerel early life history stages in EcoFOCI ichthyoplankton surveys of the eastern Bering Sea -- Atka mackerel larvae were collected during EcoFOCI ichthyoplankton surveys between February and September (1991-2013) primarily over the middle and outer shelf of the southwestern portion of the EBS (Table 2; Fig. 84). MaxEnt modeling of larval Atka mackerel presence was used to predict the probability of suitable habitat for this life stage. The most important habitat covariates probability of suitable habitat were surface temperature and bottom depth comprising a

combined relative importance of 92.1% of all predictor variables in the model. Predicted probabilities were highest when surface temperature was ca. 8°C. The model fit to the training data was outstanding (AUC = 0.97) and correctly classified 93% of presence-absence cases predicted. Model validation with the test data was successful (AUC = 0.88), correctly classifying 88% of predicted cases. No Atka mackerel eggs or pelagic juveniles were reported from EcoFOCI ichthyoplankton surveys of the EBS.

Summertime distribution of settled juvenile and adult Atka mackerel from RACE-GAP bottom trawl surveys of the eastern Bering Sea -- Atka mackerel were uncommon in catches from RACE-GAP summer bottom trawl surveys of the EBS (Fig. 85). Although they were present in bottom trawl surveys in most years between 1982 and 2014 they typically occurred at less than 3% of the stations sampled in any given year. Due to their relative rarity in bottom trawl catches (n = 59), adult Atka mackerel distribution was predicted from a MaxEnt model. The most important covariates predicting the probability of suitable adult Atka mackerel habitat were bottom depth and bottom temperature. Combined, they comprised 82.6% of the relative importance of all predictor terms in the model and resulted in the highest predicted probabilities at ca. 100 m water depths with bottom temperatures above 4°C. The model fit to the training data was outstanding (AUC = 0.90) and correctly classified 83% of predicted cases. Model validation using the test data was moderately successful (AUC = 0.79) with 79% of cases predicted correctly. No settled juvenile Atka mackerel were collected in EBS summer bottom trawls.

Seasonal distribution of Atka mackerel in commercial fishery catches from the eastern Bering Sea -- The distribution of Atka mackerel in commercial catches from the EBS varied by season, possibly reflecting changes in the focus of fishing activities (Fig. 86). There were more catches in the northern Bering Sea in the fall than in winter and spring when most observations were occurring along the Alaska Peninsula. MaxEnt modeling identified that bottom temperature and bottom depth were the most important predictors of the probability of suitable Atka mackerel habitat based on their presence in commercial catches. Their relative importance amongst all predictors ranged from 51.9% (bottom

temperature and bottom depth combined) in winter to 68.2% in spring. Model fits to the training data were outstanding (AUC= 0.98-0.99) and model validation using the test data was successful (AUC = 0.86-0.96). Models using training or test data correctly classified 86 to 96% of predicted cases.

Essential fish habitat maps and conclusions for Atka mackerel (*Pleurogrammus monopterygius*) in the eastern Bering Sea -- Species distribution modeling of Atka mackerel from the EBS was translated into maps of EFH (Fig. 87). Larval distribution appeared to be more constrained than that predicted from RACE-GAP summer bottom trawls or from observations of commercial fishery catches. Where larvae were constrained to the southern and central western portions of the EBS, Atka mackerel distributions from all other sources extended from Bristol Bay and the Alaska Peninsula to the U.S.-Russia Convention Line in the north. Core Atka mackerel habitat (top 25% of predictions) was generally found in waters greater than 100 m deep for the life stages modeled.

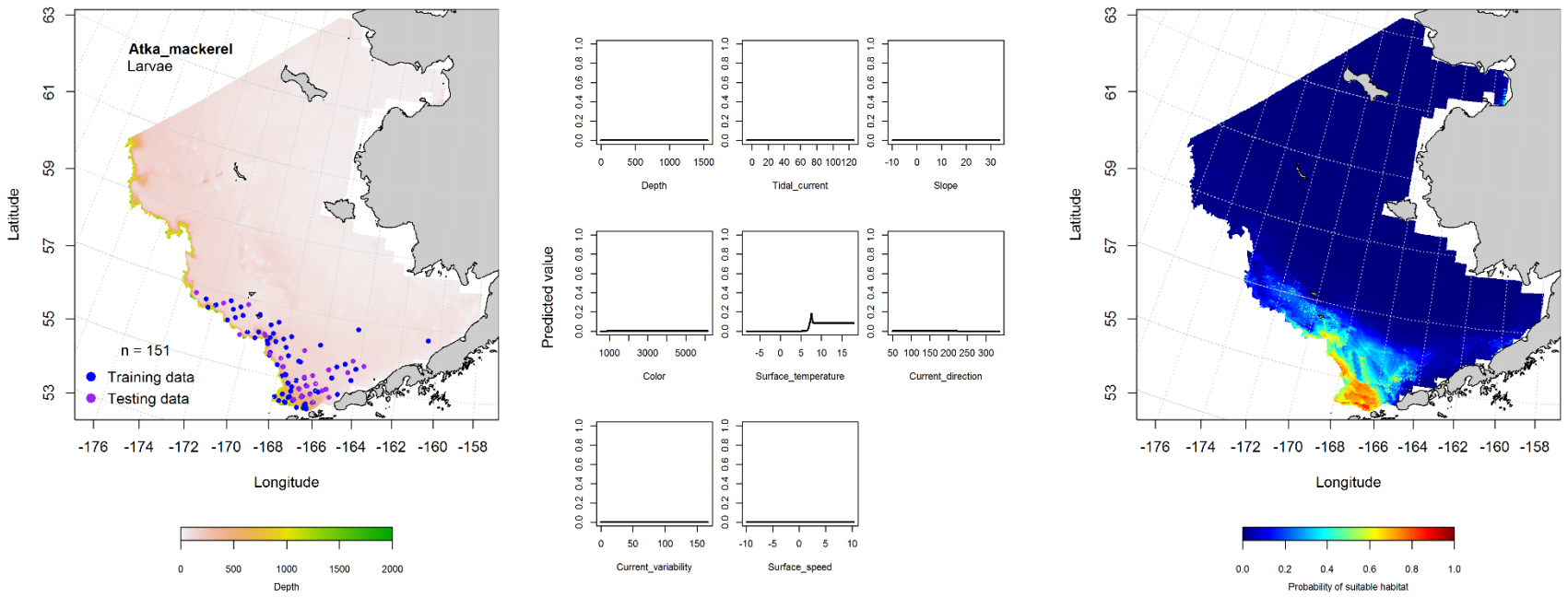

Figure 84. -- Presence of Atka mackerel larvae in EcoFOCI ichthyoplankton surveys of the eastern Bering Sea (left panel) with training (blue dots) and testing (purple dots) data sets indicated alongside the maximum entropy model (MaxEnt) effects (center panel) and the MaxEnt spatial predictions of the probability of suitable larval Atka mackerel habitat (right panel).

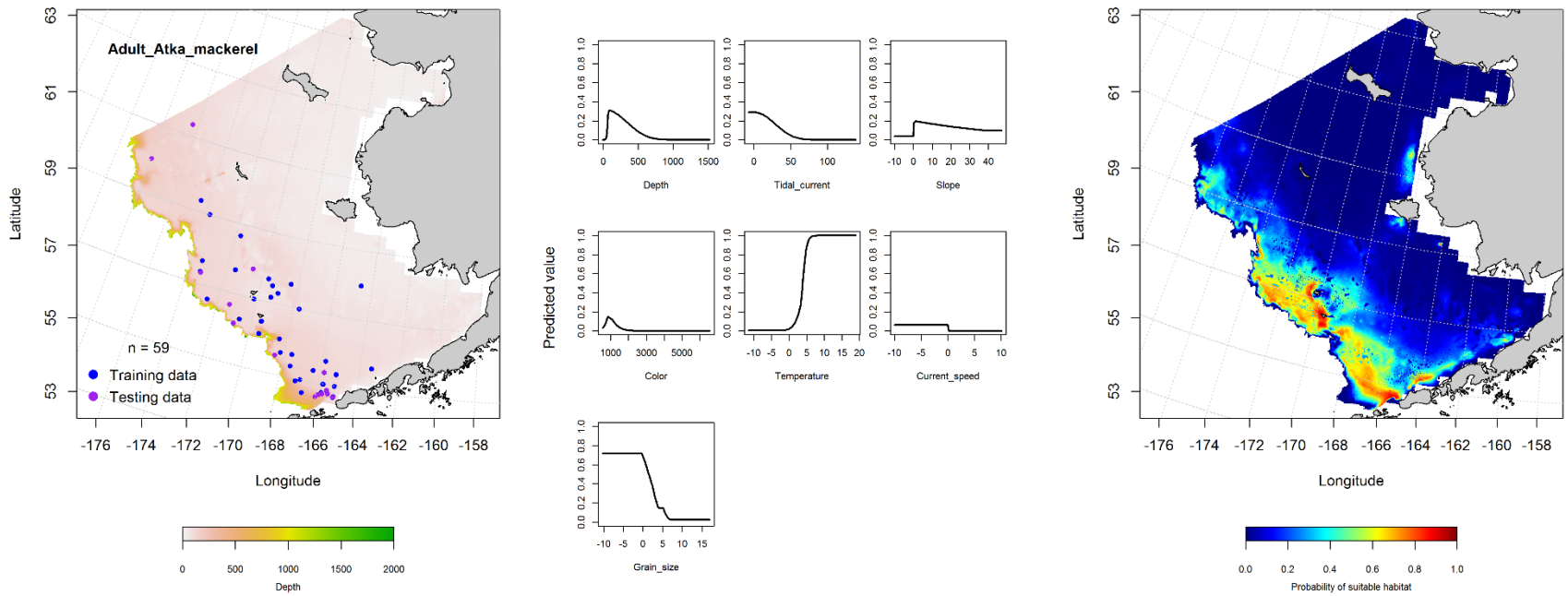

Figure 85. -- Presence of adult Atka mackerel in RACE-GAP summer bottom trawl surveys (1982-2014) of the eastern Bering Sea (left panel) with training (blue dots) and testing (purple dots) data sets indicated alongside the maximum entropy model (MaxEnt) effects (center panel) and the MaxEnt spatial predictions of the probability of suitable adult Atka mackerel habitat (right panel).

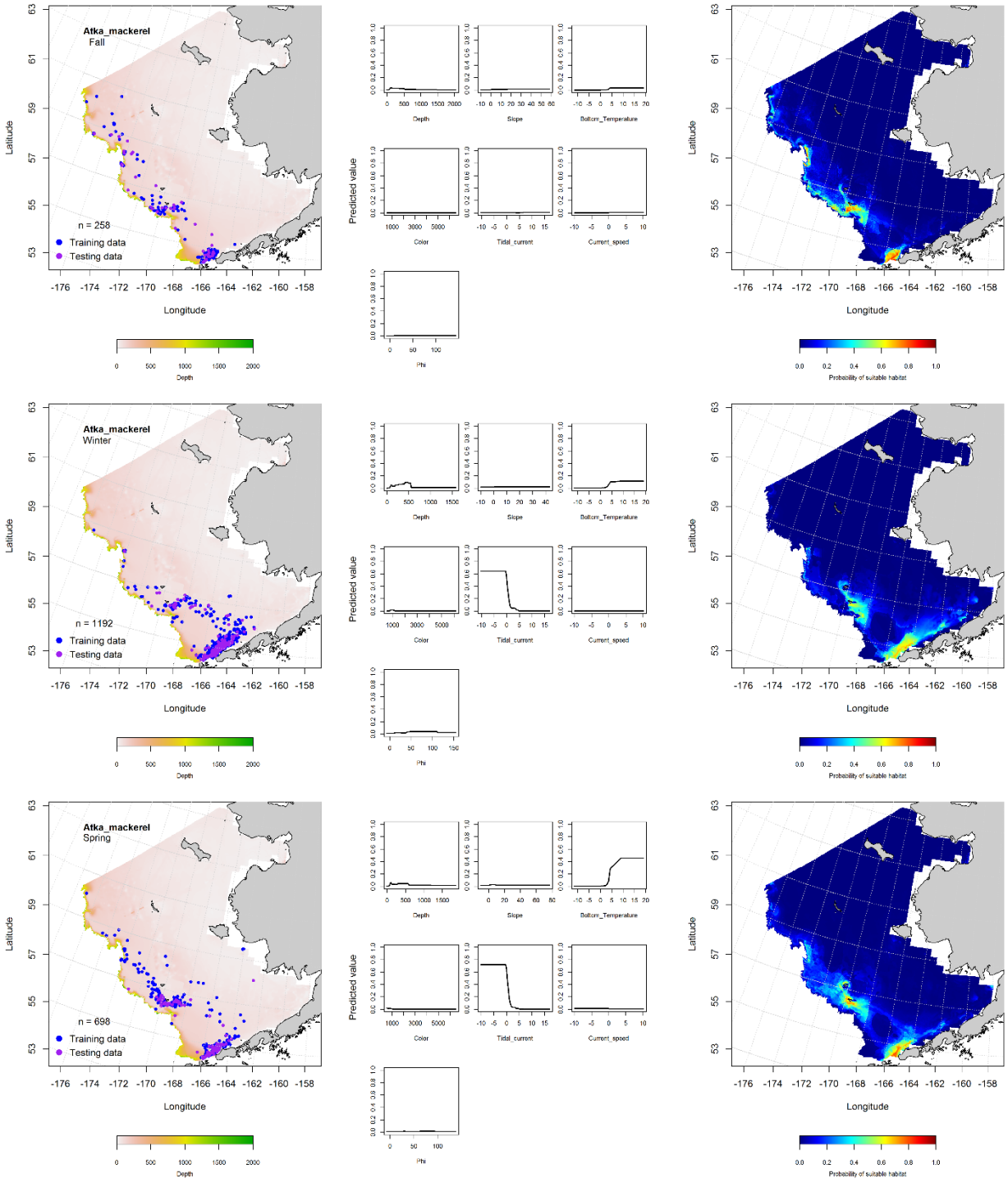

Figure 86. -- Locations of Atka mackerel in fall (October-November; top row), winter (December-February; middle row), and spring (March-May; bottom row) commercial fisheries catches (2003-2013) from the eastern Bering Sea (left-hand column). Blue points were used to train the MaxEnt model (center column) predicting the probability of suitable habitat (right-hand column) and the purple points were used to validate the model.

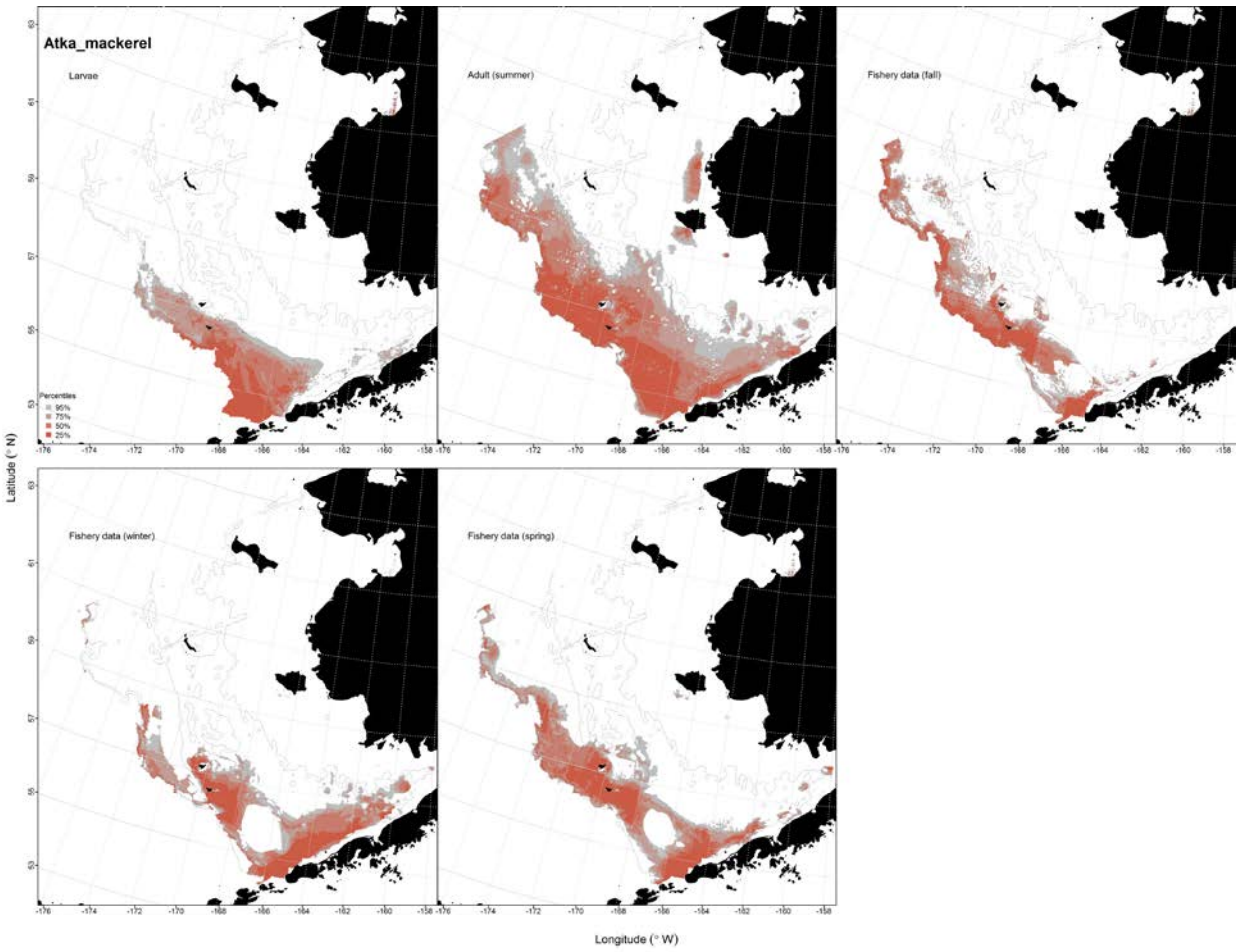

Figure 87. -- Essential fish habitat (EFH) predicted for Atka mackerel larvae (upper left panel) from EcoFOCI ichthyoplankton surveys (1991-2013), adults (upper middle panel) from RACE-GAP summertime bottom trawl surveys (1982-2014), and predicted from presence in commercial fishery catches (2003-2013) from fall (upper right panel), winter, and spring (bottom two panels) in the eastern Bering Sea.

Yellow Irish Lord (*Hemilepidotus jordani*)

Distribution of early life history stages of yellow Irish lord from EcoFOCI ichthyoplankton surveys of the eastern Bering Sea -- Larval yellow Irish lords were not common but were present in EcoFOCI ichthyoplankton surveys (1991-2013) between January and September (Table 2; Fig. 88). They were primarily distributed on the outer shelf in the southwest corner of the EBS study area over the

Bering Canyon. Yellow Irish lord larvae were not prevalent in EcoFOCI ichthyoplankton samples (n = 25) and consequently did not qualify for distribution modeling.

Pelagic juvenile yellow Irish lords were present in EcoFOCI ichthyoplankton surveys from EBS (1991-2013) between April and July (Table 2; Fig. 89). They occurred on the middle and outer shelf in the central and southern portions of the study area. Pelagic juvenile yellow Irish lords did not occur in EcoFOCI ichthyoplankton surveys in sufficient prevalence (n = 25) to support distribution modeling.

Summertime distribution of settled juvenile and adult yellow Irish lords from RACE-GAP bottom trawl surveys of the eastern Bering Sea -- Settled juvenile yellow Irish lords caught on RACE-GAP summer bottom trawl surveys were distributed over the inner, middle, and outer shelf of the EBS from the Alaska Peninsula and Bristol Bay to the northern Bering Sea (Fig. 90). A MaxEnt model was used to predict the probability of suitable habitat from their presence in bottom trawl catches. The model identified that bottom depth and bottom temperature were the most important predictors of suitable habitat and had a combined relative importance of 56.0%. Model effects were greatest in shallower waters (< 100 m) and increased with increasing temperature above 0°C. The next most important predictors were ocean productivity, tidal maxima, and sediment grain size accounting for an additional 39.2% of the relative importance of predictors in the model. The model was an outstanding fit to the training data (AUC = 0.91) and correctly classified 81% of predicted cases. In the validation step, the MaxEnt model fit to the test data was better than chance (AUC = 0.69) and correctly classified 69% of cases.

Adult yellow Irish lord were collected in RACE-GAP summer bottom trawls across the inner, middle, and outer shelf of the EBS from the Alaska Peninsula and Bristol Bay to the U.S.-Russia Convention Line in the north (Fig. 91). An hGAM was used to describe the distribution of adult yellow Irish lords from the summer bottom trawl survey data. The seven habitat covariates retained in the best-fitting GAM for adult yellow Irish lord presence-absence explained just 22.3% of the deviance in their distribution across the survey area. Geographic location and bottom depth were the most significant variables for predicting their distribution in this model and the highest probabilities of presence were

predicted around St. Paul Island. Despite the relatively low amount of deviance explained by the model, this GAM was an excellent fit to the training data (AUC = 0.86) and the AUC for the test data in the model validation step also indicated an excellent model fit (0.84). The training data model correctly classified slightly fewer predicted cases than did the test data in the validation step (77% vs. 78%). Abundance of adult yellow Irish lords was predicted at locations where their presence was predicted; the threshold probability of occurrence of 0.07 was established in the presence-absence GAM above. This conditional abundance GAM explained 56.2% of the deviance in their CPUE at these sites. The most significant habitat predictors retained in the conditional abundance GAM were geographic location, bottom current speed, and bottom depth. Adult yellow Irish lord abundance increased to the west where bottom depths were around 75 m and in areas of increased bottom current speeds. The GAM predicted the highest conditional abundances north and east of St. George Island. The GAM fit to the training data was acceptable ($r^2 = 0.56$), but was poor in the model validation step with the test data set ($r^2 = 0.18$).

Seasonal distribution of yellow Irish lord in commercial fishery catches from the eastern Bering Sea -- Yellow Irish lord presence in commercial fishery catches varied across the fishing seasons modeled (Fig. 92). MaxEnt modeling of the presence-only data provided from observations of yellow Irish lords in commercial catches was used to predict probability of suitable habitat for this species. The most important covariates predicting yellow Irish lord habitat in all three seasons were bottom depth, bottom temperature, and ocean productivity. These three predictors comprised 82.2% of the relative importance among variables in the model in fall, 79.3% in winter, and 85.7% in springtime. Model fits to the training data were outstanding with AUC ranging from 0.96 to 0.98 and the proportion of cases correctly predicted ranging from 89 to 94%. Model validation using the test data was successful (AUC = 0.85-0.90) correctly predicting 85 to 90% of cases.

Essential fish habitat maps and conclusions for adult yellow Irish lord (*Hemilepidotus jordani*) in the eastern Bering Sea -- Species distribution modeling of yellow Irish lords from the EBS was translated into maps of EFH (Fig. 93). Settled juvenile yellow Irish lord EFH was the most extensive

among the maps generated for this species and ranged across the inner, middle and outer shelf of the EBS from the Alaska Peninsula and Bristol Bay to the U.S.-Russia Convention Line in the north. Adult EFH from the summer bottom trawl surveys was similar to that predicted from the commercial catches and core habitat (the top 25% of predictions) was largely found on the middle and outer shelf.

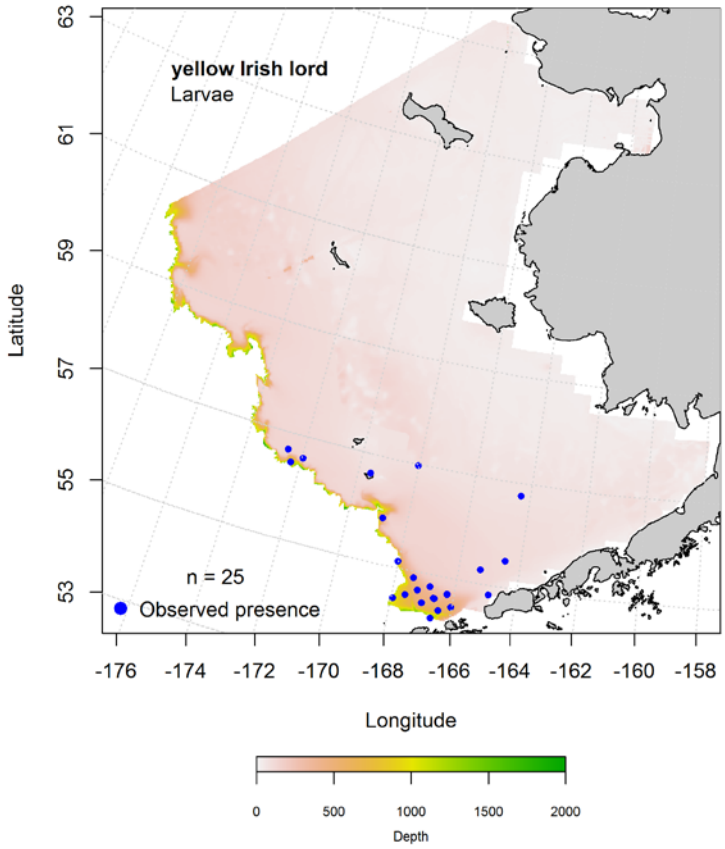

Figure 88. -- Presence of yellow Irish lord larvae in EcoFOCI ichthyoplankton surveys of the eastern Bering Sea (1991-2013).

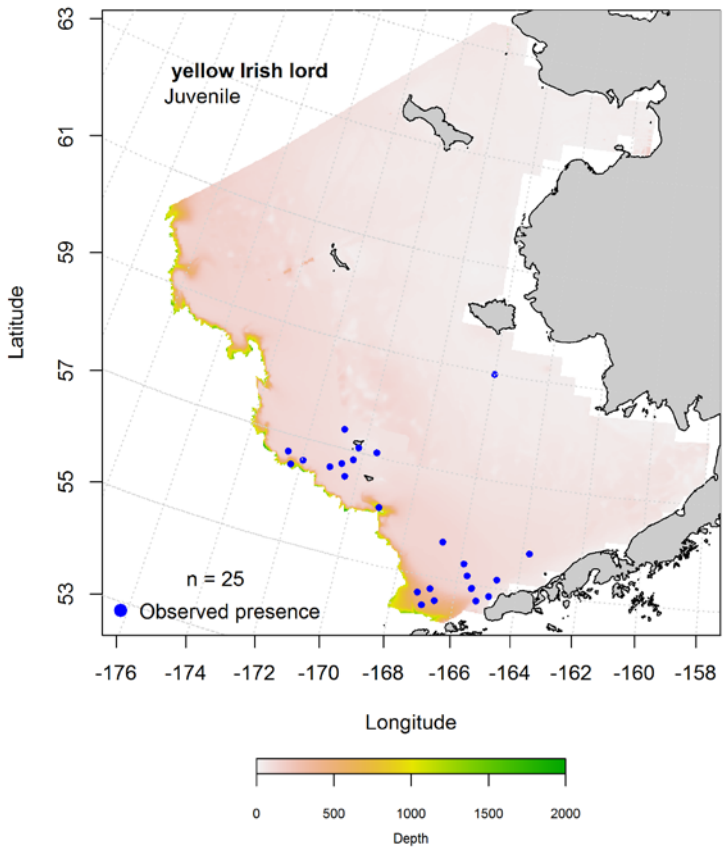

Figure 89. -- Presence of pelagic juvenile yellow Irish lord in EcoFOCI ichthyoplankton surveys of the eastern Bering Sea (1991-2013).

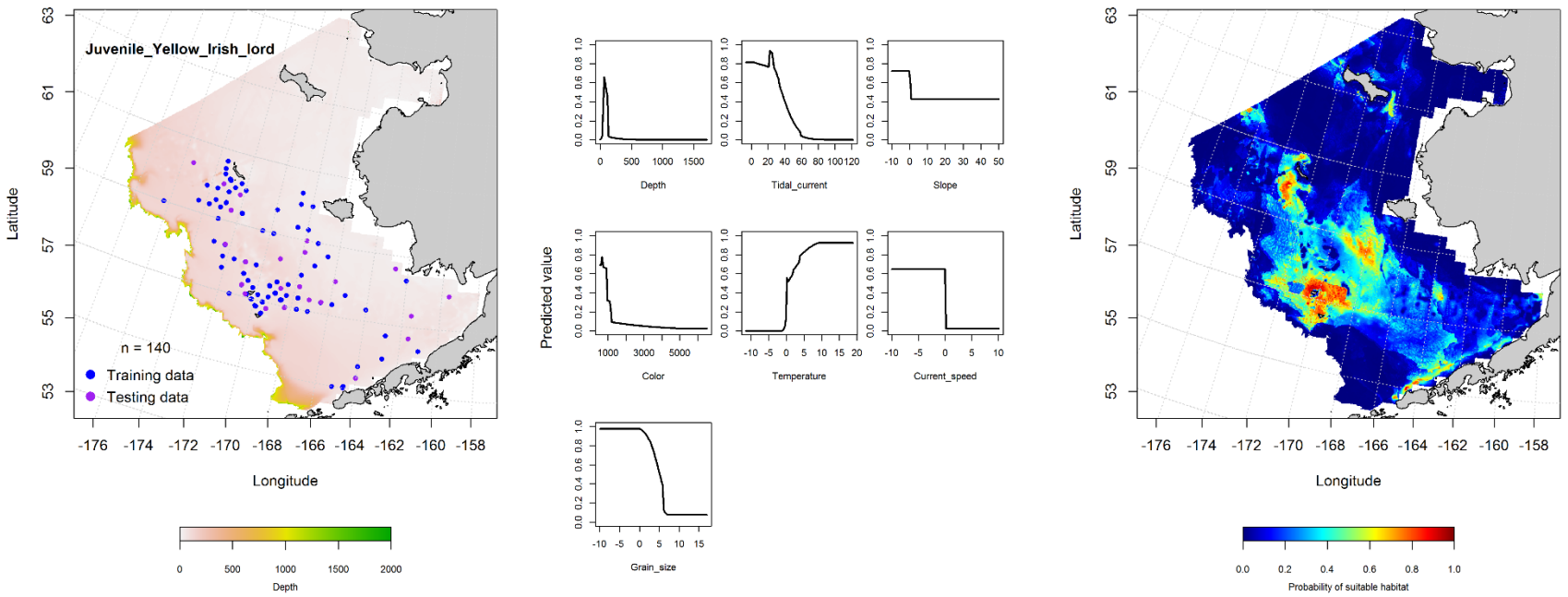

Figure 90. -- Presence of settled juvenile yellow Irish lord in RACE-GAP summer bottom trawl surveys (1982-2014) of the eastern Bering Sea (left panel) with training (blue dots) and testing (purple dots) data sets indicated alongside the maximum entropy model (MaxEnt) effects (center panel) and the MaxEnt spatial predictions of the probability of suitable juvenile yellow Irish lord habitat (right panel).

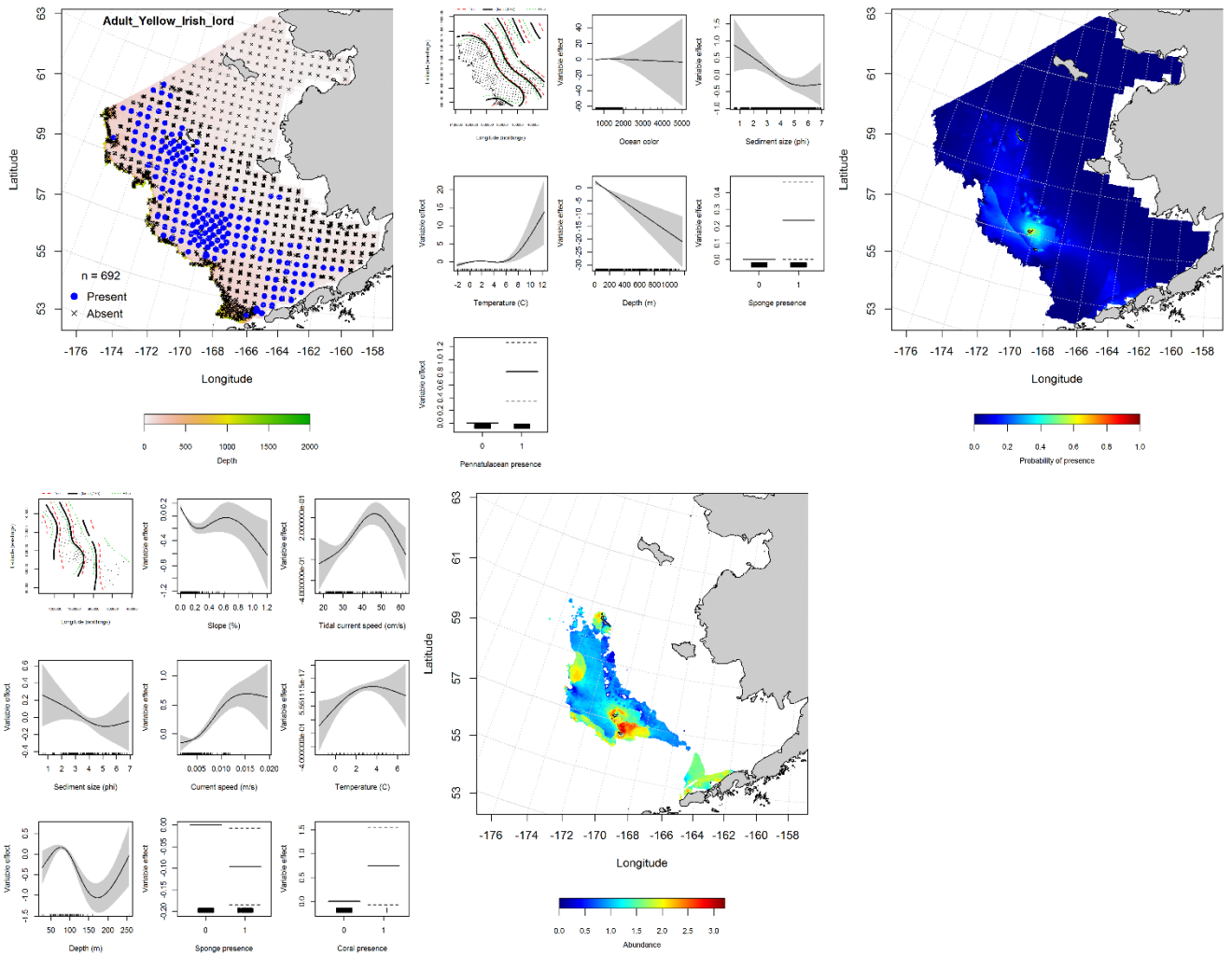

Figure 91. -- Distribution of adult yellow Irish lord in 1982-2014 RACE-GAP summer bottom trawl surveys conducted in the eastern Bering Sea (upper left panel) and the effects of retained habitat covariates in the best-fitting generalized additive model (GAM) of presence-absence (upper center panel) spatially predicting the probability of their presence (upper right panel); the best-fitting abundance GAM (lower left panel) conditionally predicts adult yellow Irish lord catch-per-unit-effort (CPUE) at sites where the optimum threshold for probability of presence was met or exceeded (lower center panel).

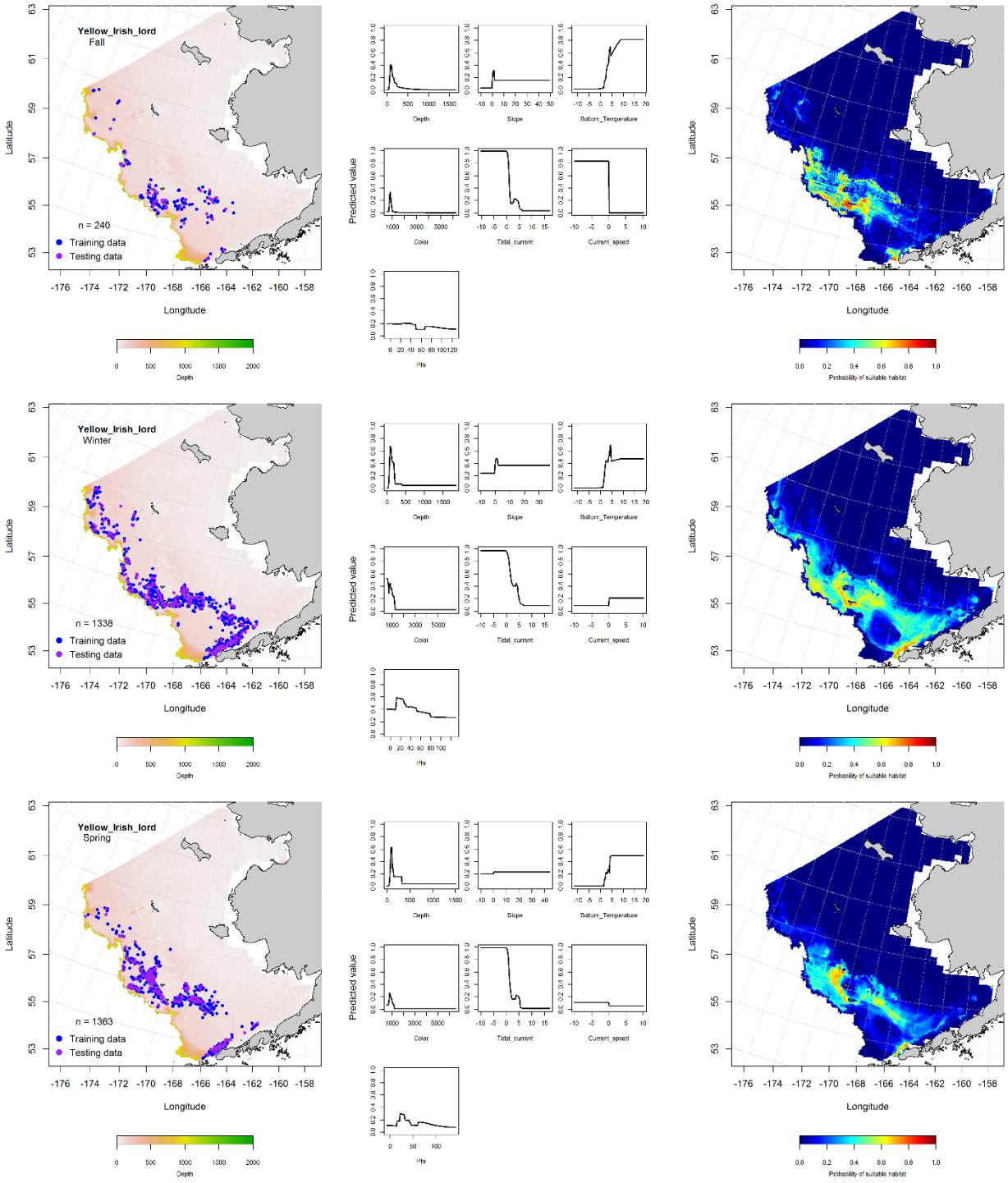

Figure 92. -- Locations of yellow Irish lord in fall (October-November; top row), winter (December-February; middle row), and spring (March-May; bottom row) commercial fisheries catches (2003-2013) from the eastern Bering Sea (left-hand column). Blue points were used to train the MaxEnt model (center column) predicting the probability of suitable habitat (right-hand column) and the purple points were used to validate the model.

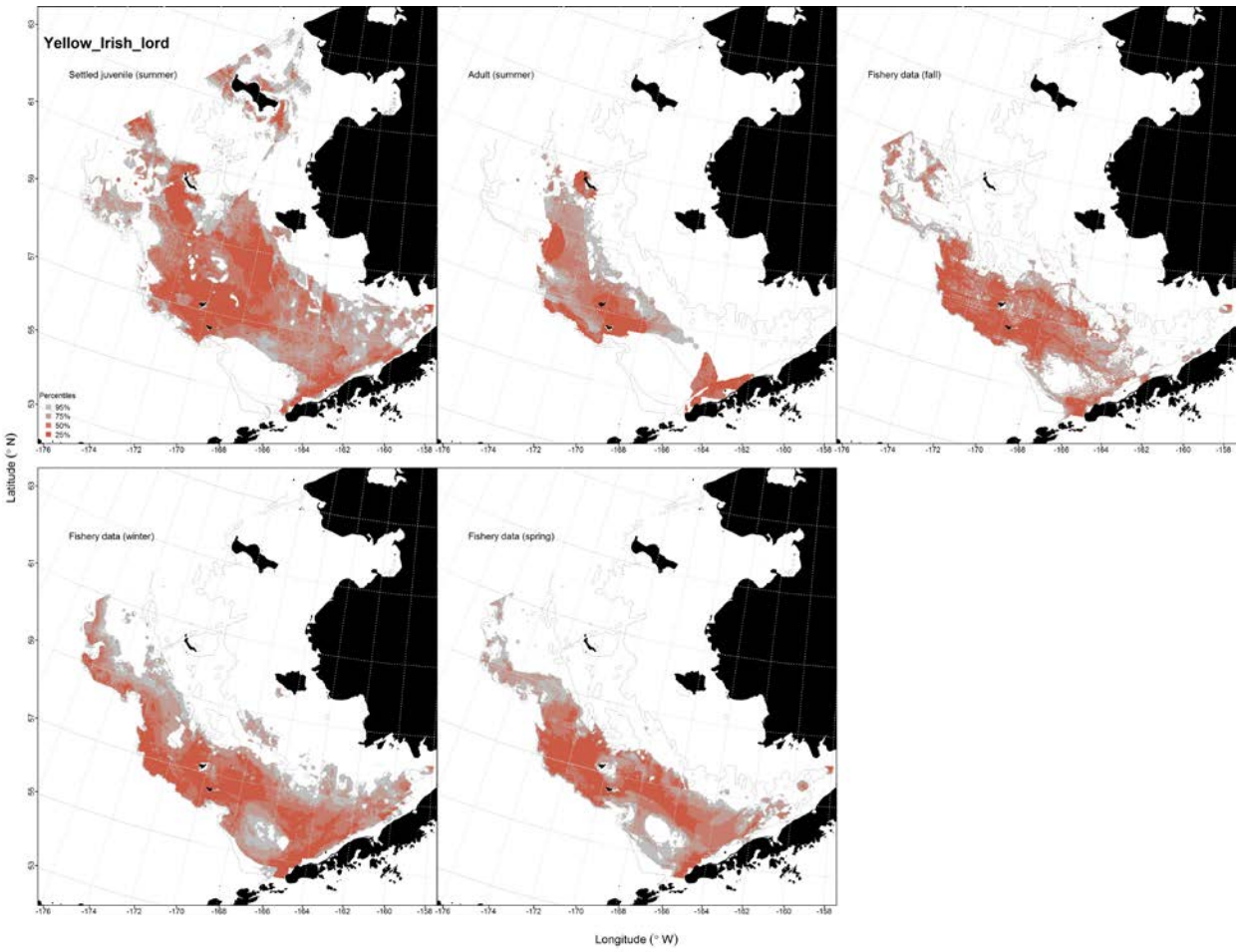

Figure 93. -- Essential fish habitat (EFH) predicted for settled juvenile and adult yellow Irish lord (upper left and middle panels) from RACE-GAP summertime bottom trawl surveys (1982-2014) and predicted from presence in commercial fishery catches (2003-2013) from fall (upper right panel), winter, and spring (bottom two panels) in the eastern Bering Sea.

Great Sculpin (*Myoxocephalus polyacanthocephalus*)

Distribution of early life history stages of great sculpin from EcoFOCI ichthyoplankton surveys of the eastern Bering Sea -- There was one occurrence of larval great sculpin on an EcoFOCI ichthyoplankton survey of the EBS in July (Table 2; Fig. 94). No pelagic juvenile great sculpin were reported from the ECODAAT database. Prevalence of larvae was too low to support distribution modeling for this species.

Summertime distribution of settled juvenile and adult great sculpin from RACE-GAP bottom trawl surveys of the eastern Bering Sea -- Settled juvenile great sculpin occurred in RACE-GAP bottom trawls across the inner, middle, and outer shelf of the EBS as well as in the northern Bering Sea around St. Lawrence Island (Fig. 95). An hGAM was used to describe the distribution of settled juvenile great sculpin from the summer bottom trawl survey data. The six habitat covariates retained in the best-fitting presence-absence GAM explained just 27.5% of the deviance in their distribution across the survey area. Geographic location and bottom temperature were the most significant variables for predicting their distribution in this model and the highest probabilities of presence were predicted in Bristol Bay and in the northern Bering Sea northwest of St. Matthew Island at temperatures ca. 2°C. Although the model explained just over a quarter of the deviance in the data, this GAM was an excellent fit to the training data set (AUC = 0.84) and to the test data in the validation step (0.81). The training data model correctly classified slightly more predicted cases than did the test data (76% vs. 75%). Abundance of settled juvenile great sculpin was predicted at locations where the threshold probability of occurrence (0.38) established in the presence-absence GAM above was met or exceeded. This conditional abundance GAM explained only 10% of the deviance in their CPUE at these sites and the model fits were universally poor to both the training ($r^2 = 0.10$) and test data sets ($r^2 = 0.03$). Consequently, there was very low confidence in the predictions of settled juvenile great sculpin distribution.

Adult great sculpin occurred in RACE-GAP summer bottom trawls across the inner, middle, and outer shelf of the EBS from the Alaska Peninsula and Bristol Bay northward into the northern Bering Sea (Fig. 96). We used an hGAM to describe the distribution of adult great sculpin from the summer bottom trawl survey data. The seven habitat covariates retained in the best-fitting presence-absence GAM explained just 30% of the deviance in their distribution across the survey area. Geographic location and bottom temperature were the most significant variables for predicting their distribution with the highest probabilities of presence predicted in Bristol Bay, around St. Paul Island in the Pribilofs, and northwest of St. Matthew Island at temperatures ca. 2°C. Although the model explained just over a third of the deviance in the data, this GAM was an excellent fit to the training data set (AUC = 0.86) and to the test data in the validation step (0.83). The training data model correctly classified more predicted cases than did the test data (78% vs. 75%). Abundance of adult great sculpin was predicted at locations where the threshold probability of occurrence (0.26) established in the presence-absence GAM above was met or exceeded. This conditional abundance GAM explained only 13.6% of the deviance in their CPUE at these sites and the model fits were universally poor to both the training ($r^2 = 0.14$) and test data sets ($r^2 = 0.03$). Consequently, there was very low confidence in the predictions of adult great sculpin distribution from these data.

Seasonal distribution of great sculpin in commercial fishery catches from the eastern Bering Sea -- Great sculpin were observed in commercial fishery catches during the fall, winter, and spring fishing seasons (Fig. 97). MaxEnt modeling of the presence-only great sculpin observations was used to predict the probability of suitable habitat for this species. The most important covariates shared across all three seasons were bottom depth and bottom temperature with combined relative importance ranging from 48.7% in fall to 73.6% in spring. In fall, an additional 37.5% of the relative importance of habitat covariates was attributable to ocean productivity and sediment grain size. Model fits to the training data were outstanding with AUC ranging from 0.92 to 0.95 and the proportion of cases correctly predicted

ranging from 82% to 87%. Model validation using the test data was successful (AUC = 0.82-0.84) correctly predicting 82% to 84% of cases.

Essential fish habitat maps and conclusions for great sculpin (*Myoxocephalus polyacanthocephalus*) in the eastern Bering Sea -- Species distribution modeling of great sculpin from the EBS was translated into maps of EFH (Fig. 98). Settled juvenile and adult great sculpin EFH based summer bottom trawl catches was contiguous and centered in Bristol Bay and around St. Matthew Island. The EFH maps based on their presence in commercial catches was continuous and extended from the Alaska Peninsula and Bristol Bay to the U.S.-Russia Convention Line in the north. Most of their core habitat (top 25% of predictions) was found in waters deeper than 50 m on the middle and outer shelf of the EBS.

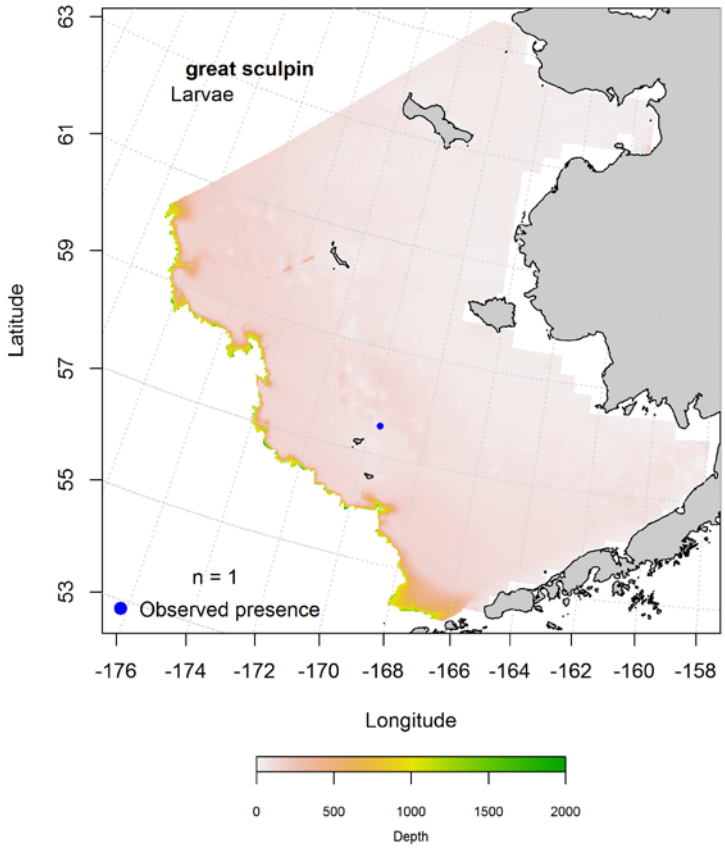

Figure 94. -- Presence of great sculpin larvae in EcoFOCI ichthyoplankton surveys of the eastern Bering Sea (1991-2013).

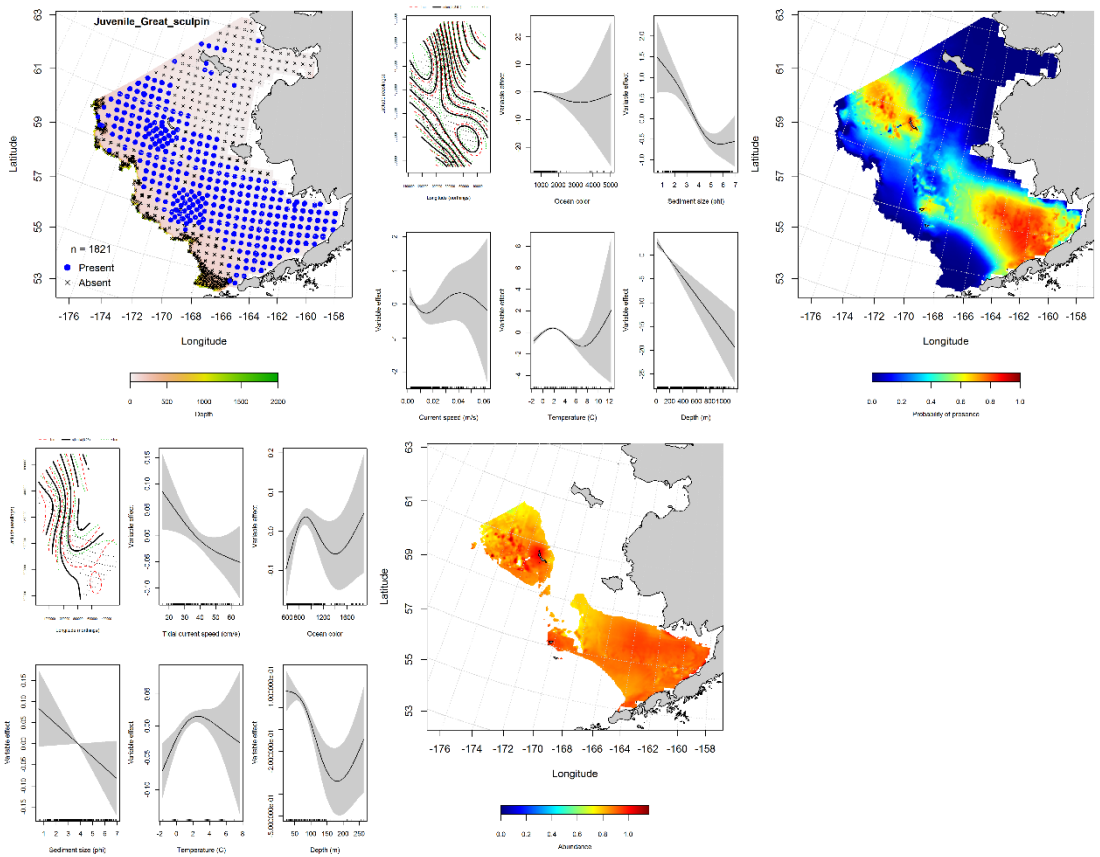

Figure 95. -- Distribution of settled juvenile great sculpin in 1982-2014 RACE-GAP summer bottom trawl surveys conducted in the eastern Bering Sea (upper left panel) and the effects of retained habitat covariates in the best-fitting generalized additive model (GAM) of presence-absence (upper center panel) spatially predicting the probability of their presence (upper right panel); the best-fitting abundance GAM (lower left panel) conditionally predicts settled juvenile great sculpin catch-per-unit-effort (CPUE) at sites where the optimum threshold for probability of presence was met or exceeded (lower center panel).

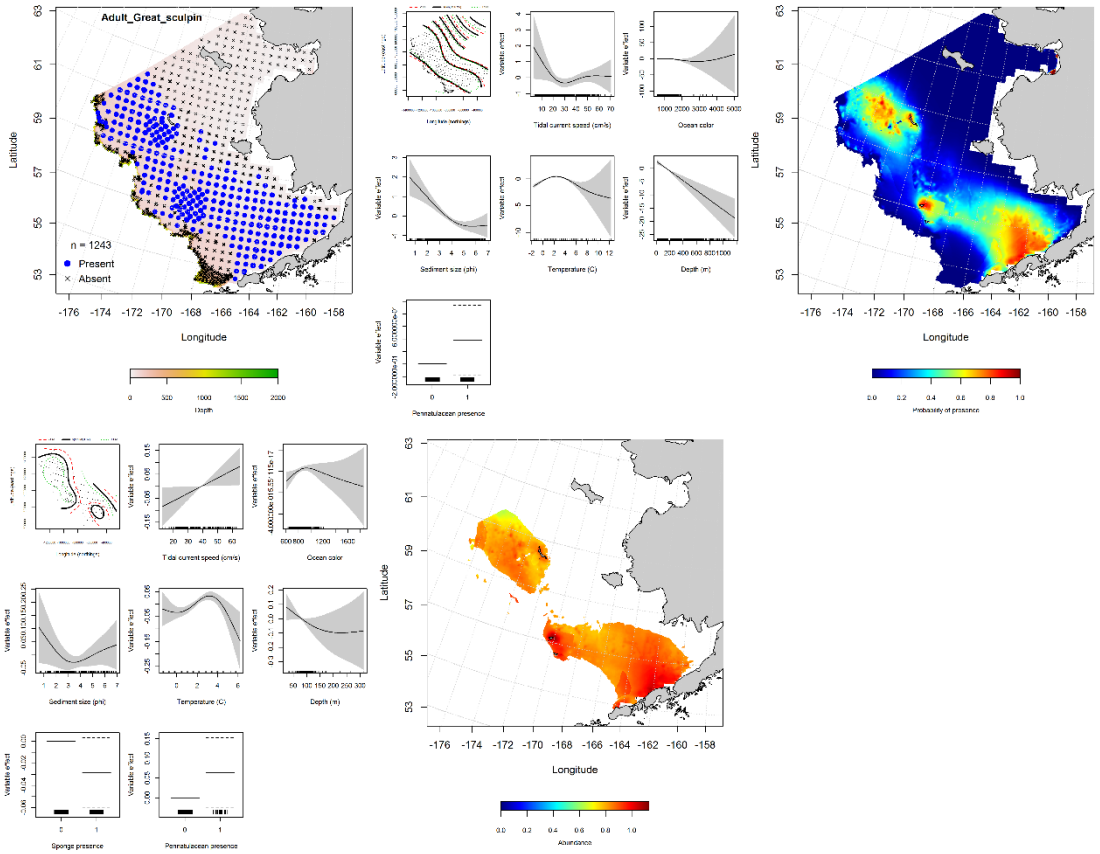

Figure 96. -- Distribution of adult great sculpin in 1982-2014 RACE-GAP summer bottom trawl surveys conducted in the eastern Bering Sea (upper left panel) and the effects of retained habitat covariates in the best-fitting generalized additive model (GAM) of presence-absence (upper center panel) spatially predicting the probability of their presence (upper right panel); the best-fitting abundance GAM (lower left panel) conditionally predicts adult great sculpin catch-per-unit-effort (CPUE) at sites where the optimum threshold for probability of presence was met or exceeded (lower center panel).

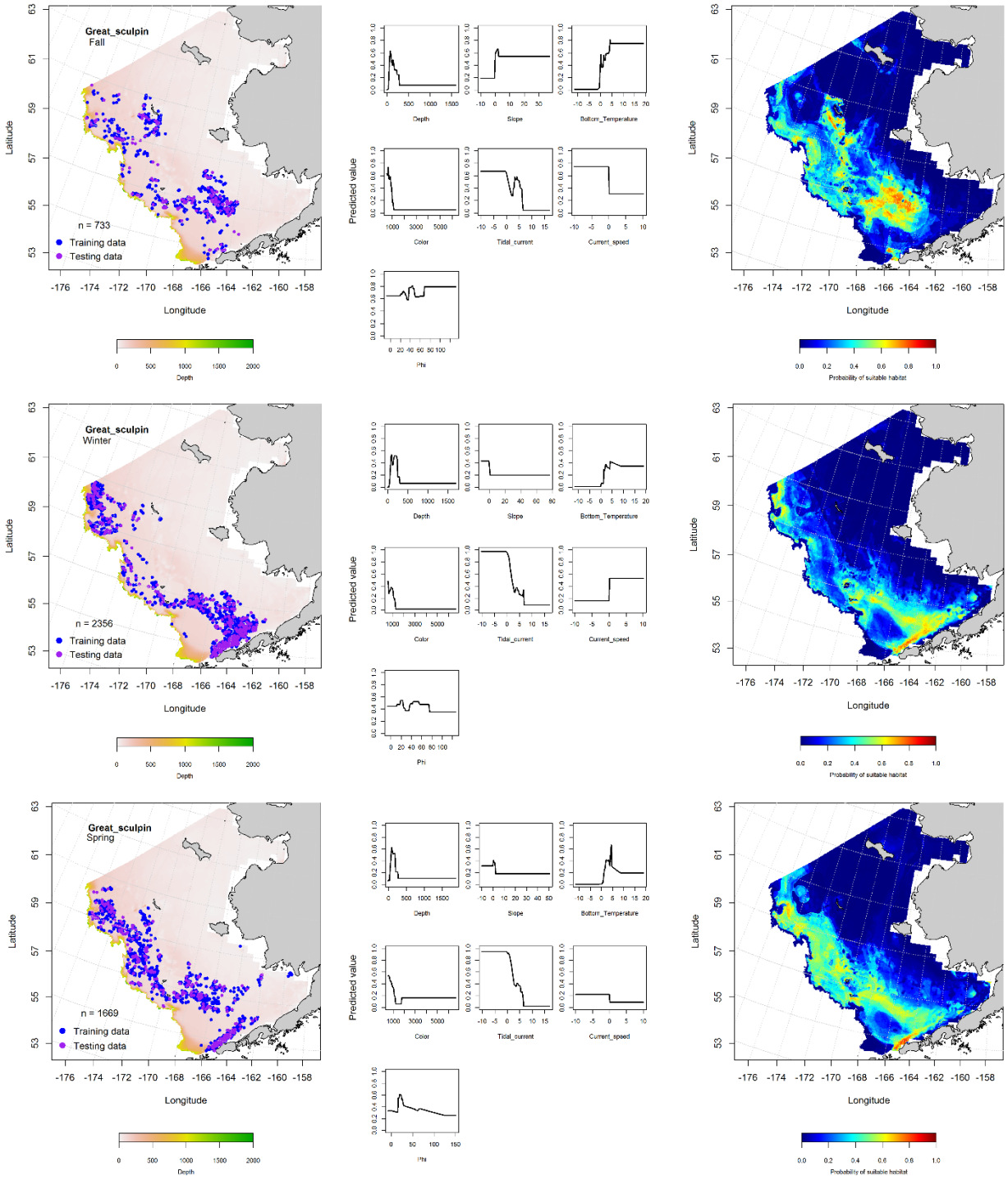

Figure 97. -- Locations of great sculpin in fall (October-November; top row), winter (December-February; middle row), and spring (March-May; bottom row) commercial fisheries catches (2003-2013) from the eastern Bering Sea (left-hand column). Blue points were used to train the MaxEnt model (center column) predicting the probability of suitable habitat (right-hand column) and the purple points were used to validate the model.

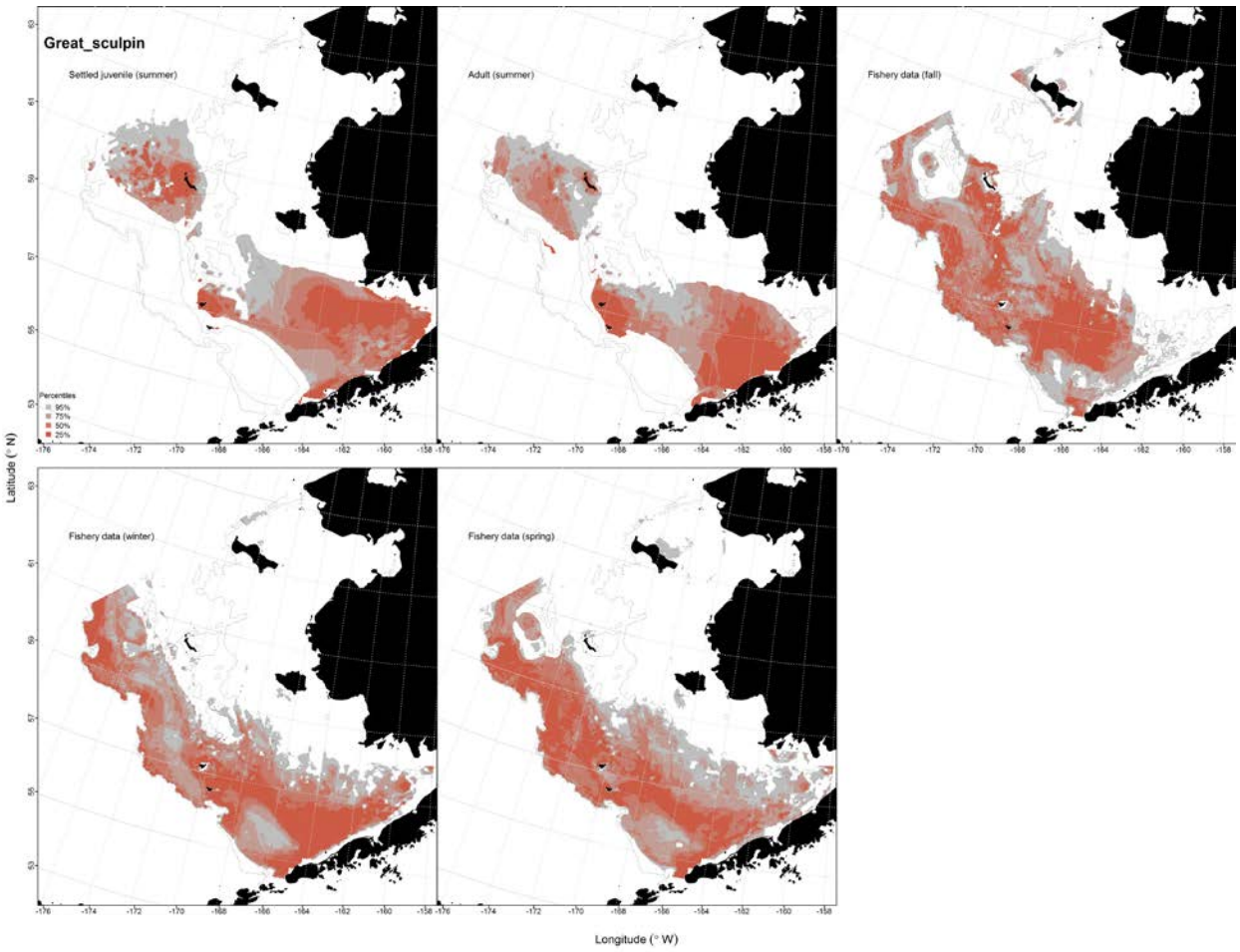

Figure 98. -- Essential fish habitat (EFH) predicted for settled juvenile and adult great sculpin (upper left and middle panels) from RACE-GAP summertime bottom trawl surveys (1982-2014) and predicted from presence in commercial fishery catches (2003-2013) from fall (upper right panel), winter, and spring (bottom two panels) in the eastern Bering Sea.

Bigmouth Sculpin (*Hemitripterus bolini*)

Distribution of early life history stages of bigmouth sculpin from EcoFOCI ichthyoplankton surveys of the eastern Bering Sea -- Bigmouth sculpins have demersal eggs and pelagic larvae. There was one record of larval bigmouth sculpin from a May EcoFOCI ichthyoplankton survey (1991-2013) of the EBS (Table 2; Fig. 99); no pelagic juveniles were reported. There were not sufficient data to model the distribution of the ELHS of this species.

Summertime distribution of settled juvenile and adult bigmouth sculpin from RACE-GAP bottom trawl surveys of the eastern Bering Sea -- Settled juvenile bigmouth sculpin were collected from the middle and outer shelf of the EBS during RACE-GAP summer bottom trawl surveys (1982-2014) between the Alaska Peninsula and the U.S.-Russia Convention Line (Fig. 100). A MaxEnt model was used to predict the probability of suitable habitat from the presence of settled juvenile bigmouth sculpin these trawl catches. Bottom depth, tidal maxima, and bottom temperature were the habitat covariates with the highest leverage amongst predictor variables in the model. Combined they accounted for 95% of the relative importance among predictor terms. The model indicated that occurrence of settled juvenile bigmouth sculpin was more likely in water depths between 150 and 650 m over a range of moderate tidal maxima where water temperatures were greater than 1°C. High probability suitable habitat for this life stage was predicted in patches on the middle shelf north of the Pribilof Islands and along the upper slope edge of the outer shelf. The MaxEnt model was an outstanding fit to the training data (AUC = 0.94) and correctly classified 86% of predicted cases. In the model validation step, the MaxEnt model fit was acceptable (AUC = 0.79), correctly classifying 79% of cases predicted from the test data.

Adult bigmouth sculpin were distributed over the outer and middle shelf in RACE-GAP summer bottom trawl surveys of the EBS (Fig. 101). An hGAM was used to model their distribution in the region. The most significant habitat covariates retained in the best-fitting presence-absence GAM were geographic location and bottom depth. The probability of bigmouth sculpin presence was highest at depths ca. 500 m along the upper slope edge of the outer shelf across the southeast to northwest extent of the survey area. This GAM explained just under a third of the deviance in their distribution data (29.3%) and the fit was excellent (AUC = 0.87) correctly predicting 79% of predicted cases. Model validation was successful (AUC = 0.86) and predictions from the test data correctly classified 79% of cases. Abundance of adult bigmouth sculpin was predicted at locations where the threshold probability of occurrence (0.16) established in the presence-absence GAM above was met or exceeded. This conditional abundance GAM

explained only 20.7% of the deviance in their CPUE at these sites and the model fits were universally poor to both the training ($r^2 = 0.21$) and test data sets ($r^2 = 0.07$). Consequently, there was very low confidence in the predictions of adult bigmouth sculpin distribution from these data.

Seasonal distribution of bigmouth sculpin in the eastern Bering Sea -- Bigmouth sculpin were present in commercial fishery catches from the middle and outer shelf of the EBS during the fall, winter, and spring fishing seasons (Fig. 102). MaxEnt modeling of bigmouth sculpin presence in these catches was used to predict the probability of suitable habitat for this species. The most important covariates shared across all three seasons, in order of importance, were bottom depth, bottom temperature, and ocean productivity with combined relative importance ranging from 88.7% in spring to 97.3% in fall. The highest predicted probabilities were associated with depths ca. 100 m, increasing bottom temperatures above 0°C, and ocean productivity $\leq$ 1,000 $g \cdot C \cdot m^{-2} \cdot day^{-1}$. Model fits to the training data were outstanding with AUC ranging from 0.92 to 0.94 and the proportion of cases correctly predicted ranging from 82% to 85%. Model validation using the test data was successful (AUC = 0.84-0.88), correctly predicting 82% to 85% of cases.

Essential fish habitat maps and conclusions for bigmouth sculpin (*Hemitripterus bolini*) in the eastern Bering Sea -- Species distribution modeling of bigmouth sculpin from the EBS was translated into maps of EFH (Fig. 103). Settled juvenile EFH predicted from summer bottom trawl catches extended further inshore across the middle shelf than did EFH for adults while core habitat for both life stages (top 25% of predicted values) was largely restricted to the outer shelf and depths greater than 100 m. The EFH maps based on presence in commercial catches were most similar to that seen for settled juveniles and may have included both life stages in composite. These latter maps also reflect the distribution of fishing activity during the fall, winter, and spring months but generally reinforced the distribution of EFH predicted from the RACE-GAP summer bottom trawl surveys.

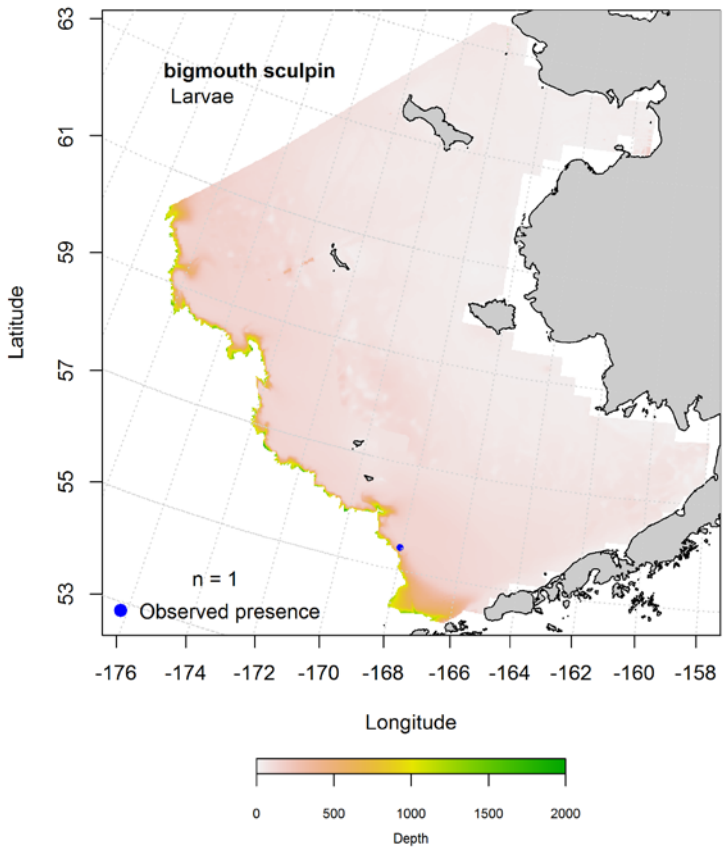

Figure 99. -- Presence of bigmouth sculpin larvae in EcoFOCI ichthyoplankton surveys of the eastern Bering Sea (1991-2013).

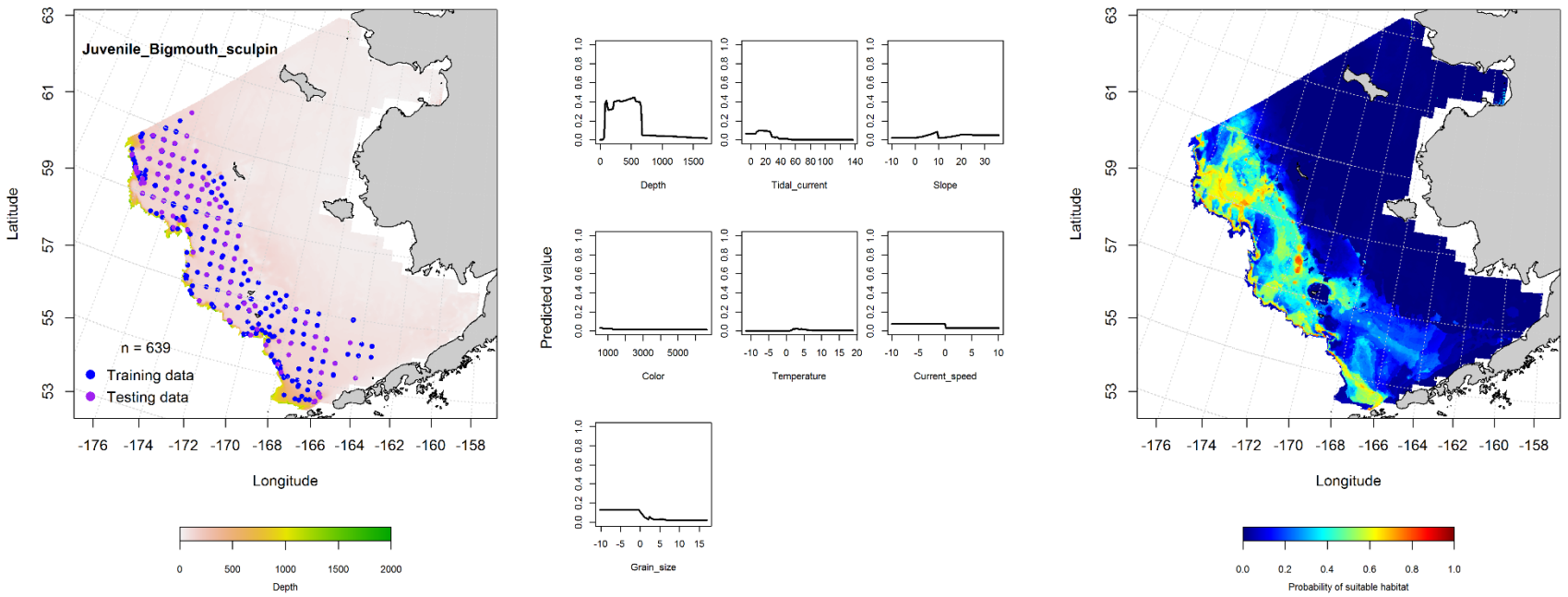

Figure 100. -- Presence of settled juvenile bigmouth sculpin in RACE-GAP summer bottom trawl surveys (1982-2014) of the eastern Bering Sea (left panel) with training (blue dots) and testing (purple dots) data sets indicated alongside the maximum entropy model (MaxEnt) effects (center panel) and the MaxEnt spatial predictions of the probability of suitable settled juvenile bigmouth sculpin habitat (right panel).

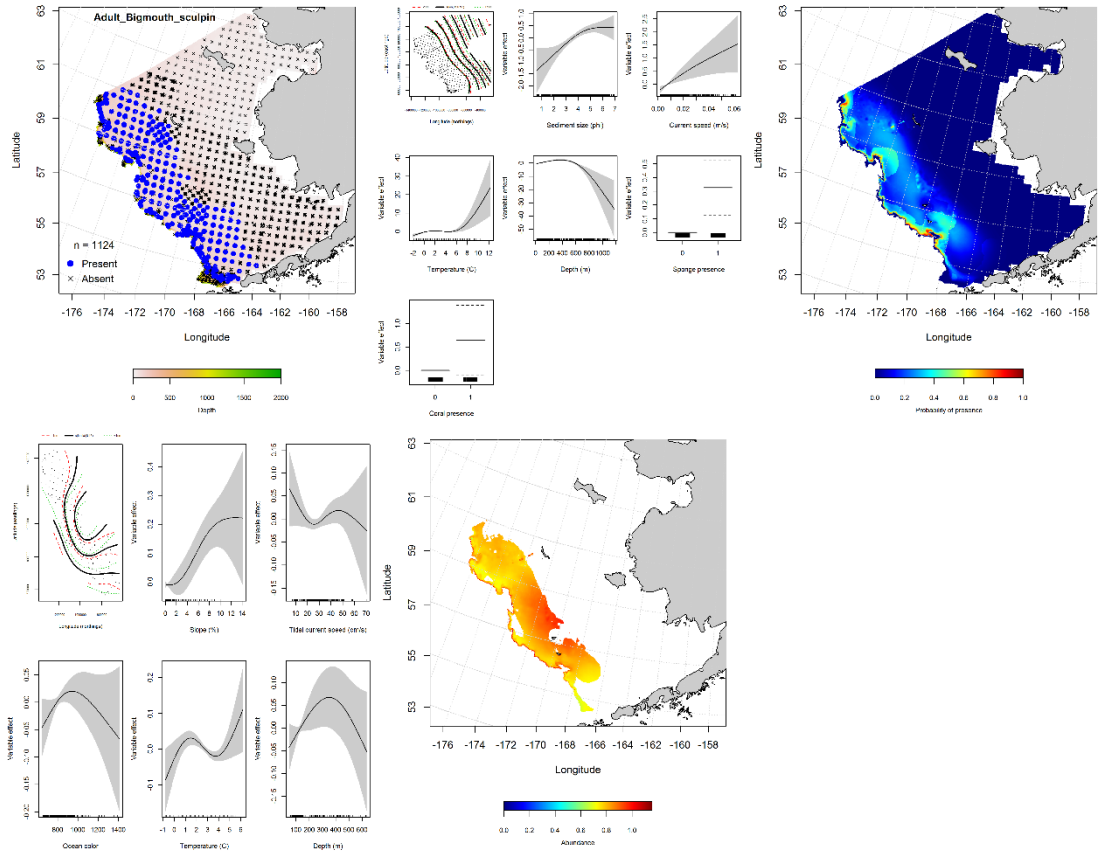

Figure 101. -- Distribution of adult bigmouth sculpin in 1982-2014 RACE-GAP summer bottom trawl surveys conducted in the eastern Bering Sea (upper left panel) and the effects of retained habitat covariates in the best-fitting generalized additive model (GAM) of presence-absence (upper center panel) spatially predicting the probability of their presence (upper right panel); the best-fitting abundance GAM (lower left panel) conditionally predicts adult bigmouth sculpin catch-per-unit-effort (CPUE) at sites where the optimum threshold for probability of presence was met or exceeded (lower center panel).

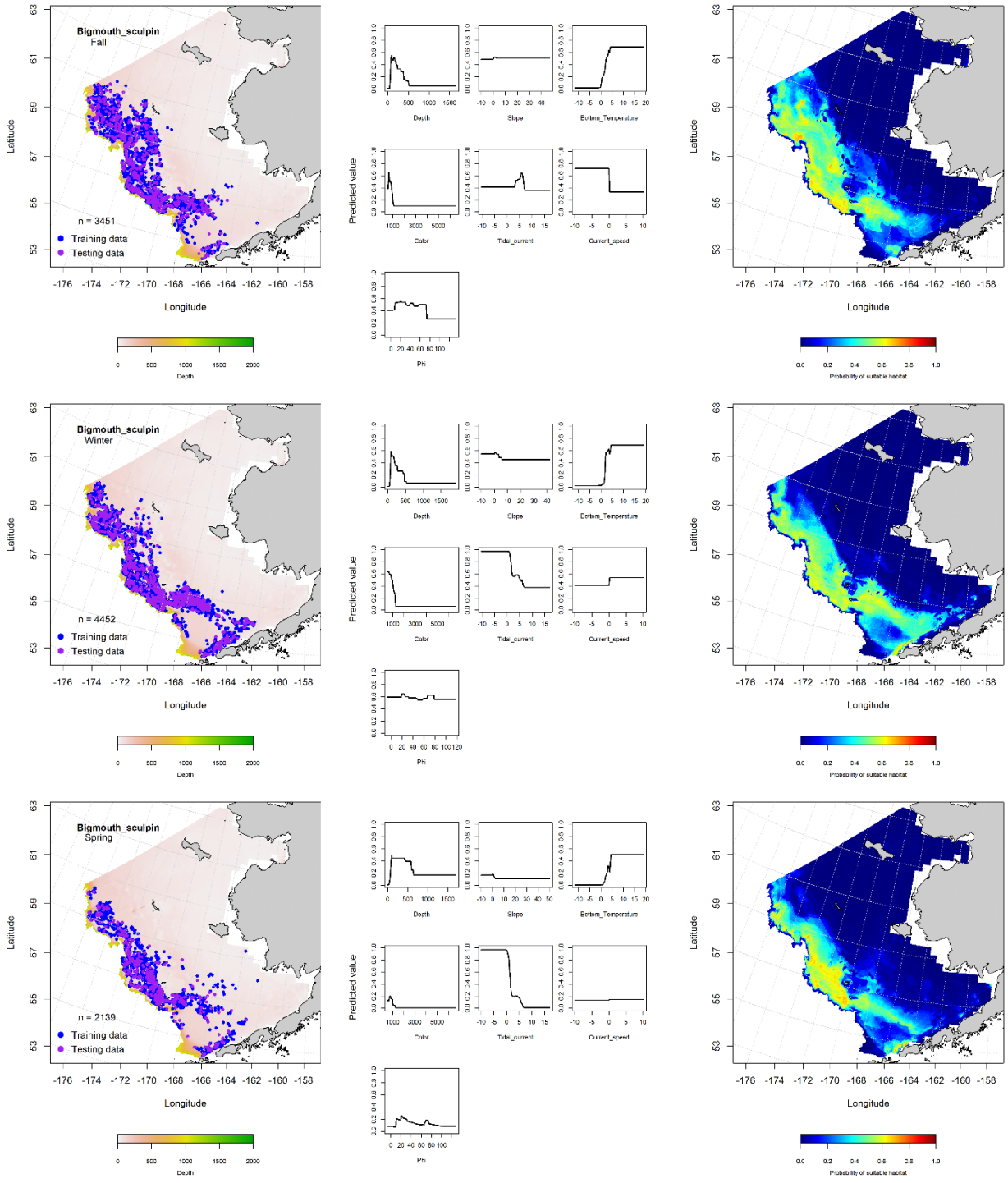

Figure 102. -- Locations of bigmouth sculpin in fall (October-November; top row), winter (December-February; middle row), and spring (March-May; bottom row) commercial fisheries catches (2003-2013) from the eastern Bering Sea (left-hand column). Blue points were used to train the MaxEnt model (center column) predicting the probability of suitable habitat (right-hand column) and the purple points were used to validate the model.

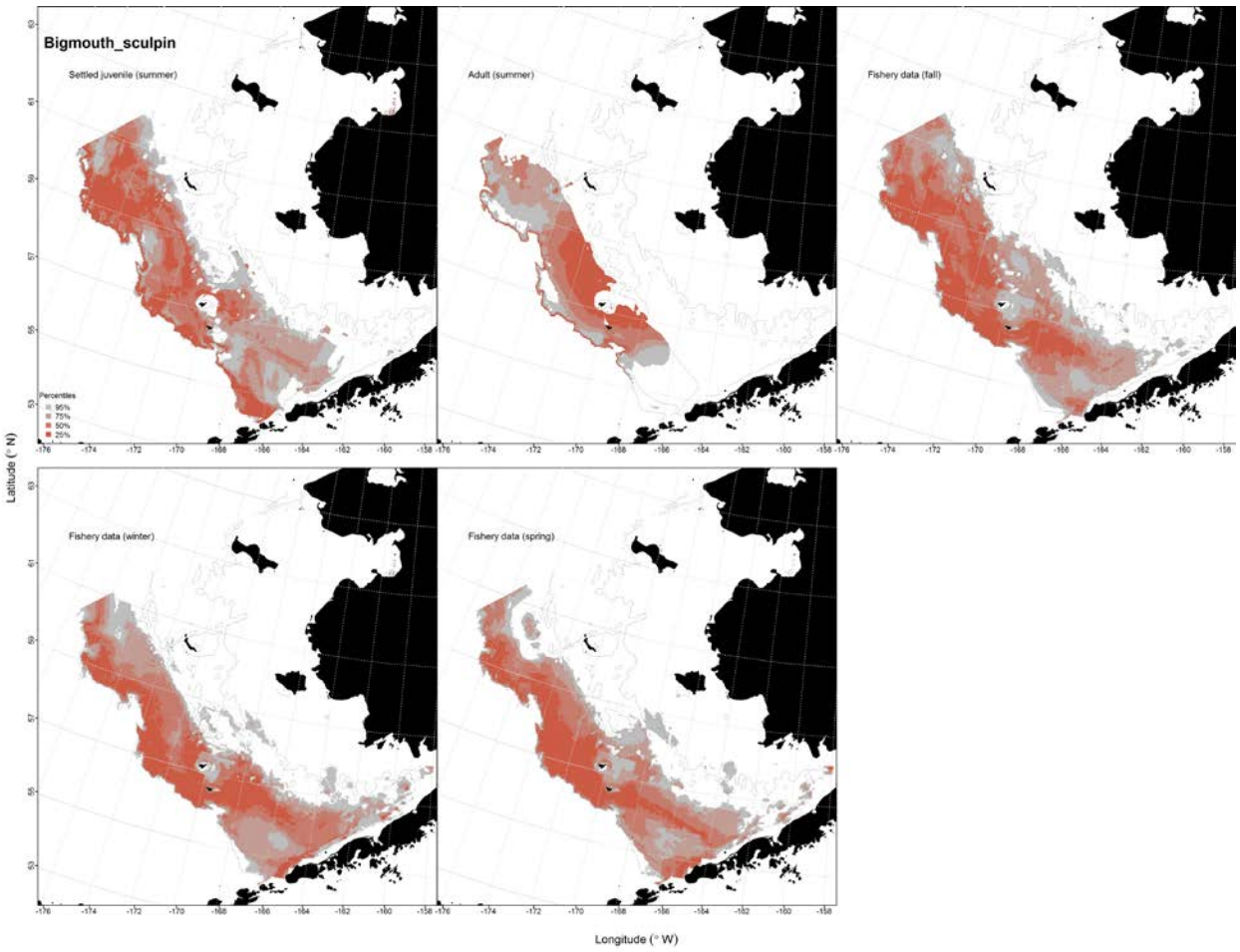

Figure 103. -- Essential fish habitat (EFH) predicted for settled juvenile and adult bigmouth sculpin (upper left and middle panels) from RACE-GAP summertime bottom trawl surveys (1982-2014) and predicted from presence in commercial fishery catches (2003-2013) from fall (upper right panel), winter, and spring (bottom two panels) in the eastern Bering Sea.

Rockfishes (*Sebastes* spp.)

Rockfishes (*Sebastes* spp.) are ovoviparous with internal fertilization. Their larvae and early juveniles cannot be readily distinguished from other species in the genus using visible external characters alone. Rockfish ELHS collected in the EcoFOCI ichthyoplankton samples used here were visually identified. Therefore, we combined rockfish early life stages at the genus for distribution modeling.

Distribution of early life history stages of *Sebastes* spp. in the eastern Bering Sea -- Larval rockfishes were distributed across much of the EBS and collected during most months of the year

(February through September) on EcoFOCI ichthyoplankton surveys (1991-2014) of the region (Table 2; Fig. 104). A MaxEnt model was used to predict the probability of suitable larval *Sebastes* spp. habitat in the study area. Surface temperature was the most important habitat covariate predicting the probability of suitable larval rockfish habitat and accounted for 83.8% of the relative importance of the predictor terms in the model. The model effect was greatest when surface temperature was around 7°C. The MaxEnt fit to the training data set was outstanding (AUC = 0.95) and correctly classified 89% of predicted cases. Model validation was successful (AUC = 0.86) and correctly predicted 86% of cases from the test data.

Pelagic juvenile *Sebastes* spp. occurred at 30 stations in September (Table 2) during EcoFOCI ichthyoplankton surveys (1991-2014) of the EBS (Fig. 105). Most of these occurrences were in the vicinity of the Pribilof Islands. The prevalence of pelagic juveniles *Sebastes* spp. was less than 50 stations and this genus and life stage did not qualify for species distribution modeling.

Essential fish habitat maps and conclusions for larval *Sebastes* spp. in the eastern Bering Sea -- The results of the MaxEnt model were translated into a map of EFH for larval *Sebastes* spp. (Fig. 106). The extent of EFH for this life stage and genus goes from Bristol Bay and along the Alaska Peninsula northward on the middle and outer shelf to the U.S.-Russia Convention Line. Core habitat (top 25% of predictions) is mostly centered over the outer shelf in the central and southern portions of the EBS.

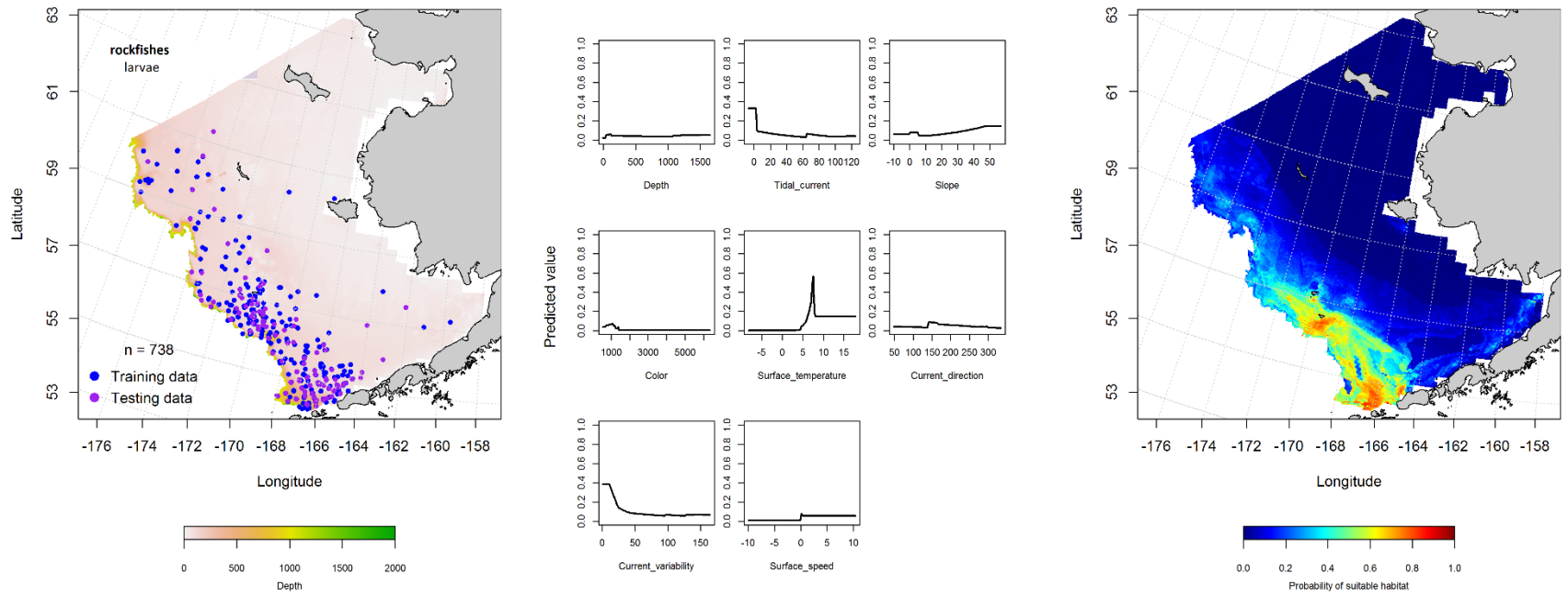

Figure 104. -- Presence of *Sebastes* spp. larvae in EcoFOCI ichthyoplankton surveys of the eastern Bering Sea (left panel) with training (blue dots) and testing (purple dots) data sets indicated alongside the maximum entropy model (MaxEnt) effects (center panel) and the MaxEnt spatial predictions of the probability of suitable larval *Sebastes* spp. habitat (right panel).

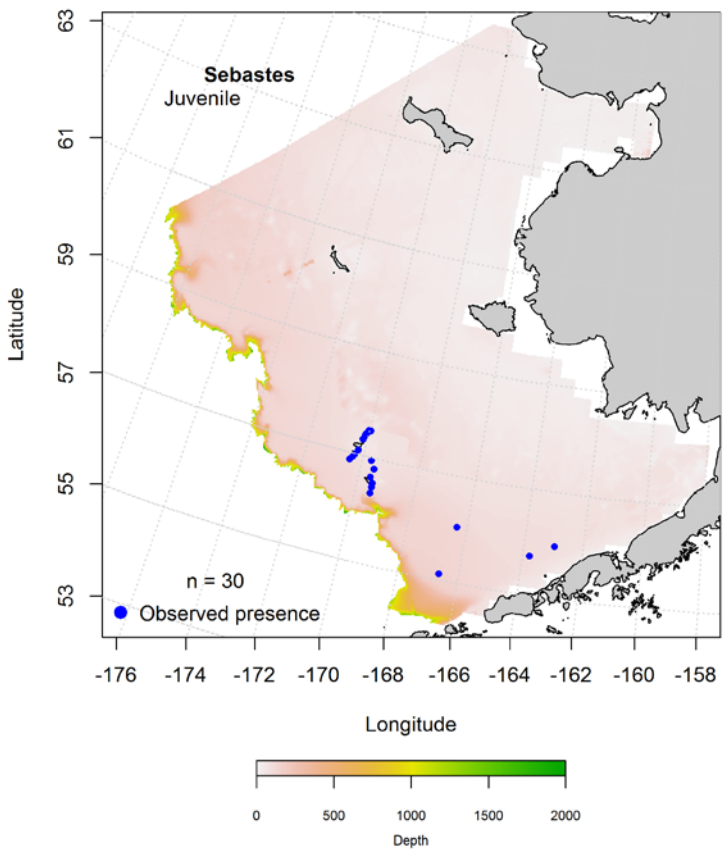

Figure 105. -- Presence of *Sebastes* spp. pelagic juveniles in EcoFOCI ichthyoplankton surveys of the eastern Bering Sea (1991-2013).

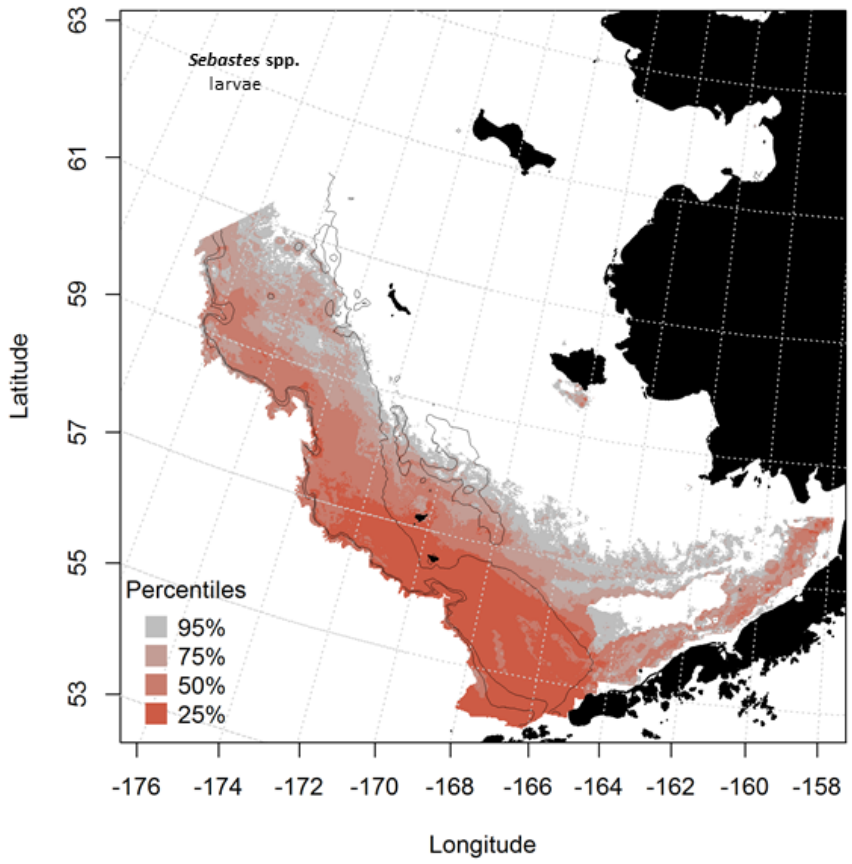

Figure 106. -- Essential habitat of larval *Sebastes* spp. predicted from EcoFOCI ichthyoplankton surveys of the eastern Bering Sea (1991-2013).

Rougheye Rockfish (*Sebastes aleutianus*)

Beginning in 2006, rougheye rockfish (*Sebastes aleutianus*) was consistently identified from RACE-GAP summer bottom trawl survey catches. Subsequently, Orr and Hawkins (2008) formally re-described rougheye rockfish (Jordan and Evermann, 1898). Although rougheye and blackspotted rockfish (*S. melanostictus*) have been consistently separated on EBS bottom trawl surveys since 2006, commercial catches of these two species continue to be landed under the rougheye/blackspotted rockfish category.

Summertime distribution of settled juvenile and adult rougheye rockfish from RACE-GAP bottom trawl surveys of the eastern Bering Sea -- Settled juvenile rougheye rockfish primarily occurred on the outer shelf in the southwest portion of the EBS on RACE-GAP summer bottom trawl

surveys (2006-2014; Fig. 107). They were not common in survey trawls occurring at ca. 1% of trawling stations in recent years. Most of those occurrences were recorded from shelf edge and slope waters greater than 200 m in depth and they were sufficiently prevalent to support MaxEnt modeling. The most important habitat covariates describing their distribution in the EBS were bottom depth and ocean productivity comprising a combined relative importance of 84.6%. Probability of suitable habitat predicted by the MaxEnt was highest at depths ca. 300 m and nominally at sites where ocean productivity was ca. 1,000 $g \cdot C \cdot m^{-2} \cdot day^{-1}$. The area predicted to have the highest probability for suitable settled juvenile rougheye rockfish habitat was on the outer shelf between Pribilof Canyon and Unimak Pass. The model fit to the training data was outstanding (AUC = 0.99) and it correctly classified 93% of predicted cases. Model validation was successful (AUC = 0.93) and 95% of predicted cases were correctly classified based on the test data.

Adult rougheye rockfish were also present in RACE-GAP summer bottom trawl catches (2006-2014) from the EBS (Fig. 108) and were less common than the settled juveniles. They occurred in similar areas on the outer shelf in deeper waters. However, they were collected at just 26 stations and were not sufficiently prevalent to warrant species distribution modeling for this life stage.

Seasonal distribution of the rougheye/blackspotted rockfish complex in commercial fishery catches from the eastern Bering Sea -- As indicated above, rougheye rockfish are managed by the NPFMC as the other half of a complex with blackspotted rockfish because they are difficult to separate in the field. Since they are not separated in commercial catches from Alaska, fishery observers do not separate them when they are processing the catches. Therefore, for VOE-CIA data, we will summarize the presence-only data for the rougheye/blackspotted landing category

Representatives of the rougheye/blackspotted rockfish complex were present in commercial fishery catches primarily from the outer shelf of the EBS during the fall, winter, and spring fishing seasons (Fig. 109). MaxEnt modeling of their presence in these catches was used to predict the probability of suitable habitat for this complex. Bottom depth was the most important habitat covariate shared across

all three seasons and ranged in relative importance 41.3% in fall to 74.8% in spring. Peak model effects due to bottom depth varied by season with the probability of suitable habitat predicted to be deeper during winter (ca. 500-600 m) compared with fall and spring (ca. 200-400 m). In fall, bottom temperature and local slope comprised an additional combined 43% of the relative importance of predictor terms in that model. Model fits to the training data were outstanding (AUC = 0.99 in all three seasons) and the proportion of cases correctly predicted ranged from 94% to 96%. Model validation using the test data was successful (AUC = 0.90-0.98) correctly predicting 90 to 98% of cases.

Essential fish habitat maps and conclusions for rougheye rockfish in RACE-GAP summer bottom trawls surveys and for rougheye/blackpotted rockfish complex observed in commercial fishery catches from the eastern Bering Sea -- Distribution modeling of rougheye rockfish from summer bottom trawl surveys and of rougheye/blackspotted rockfish complex from commercial fisheries catches was translated into maps of EFH (Fig. 110). For both the complex and the species, EFH was constrained to the outer shelf of the EBS. Core habitat (top 25% of predictions) was typically in waters greater than 500 m along the shelf edge and upper continental slope. There was little difference in the extent or location of EFH predicted from the two disparate data sources.

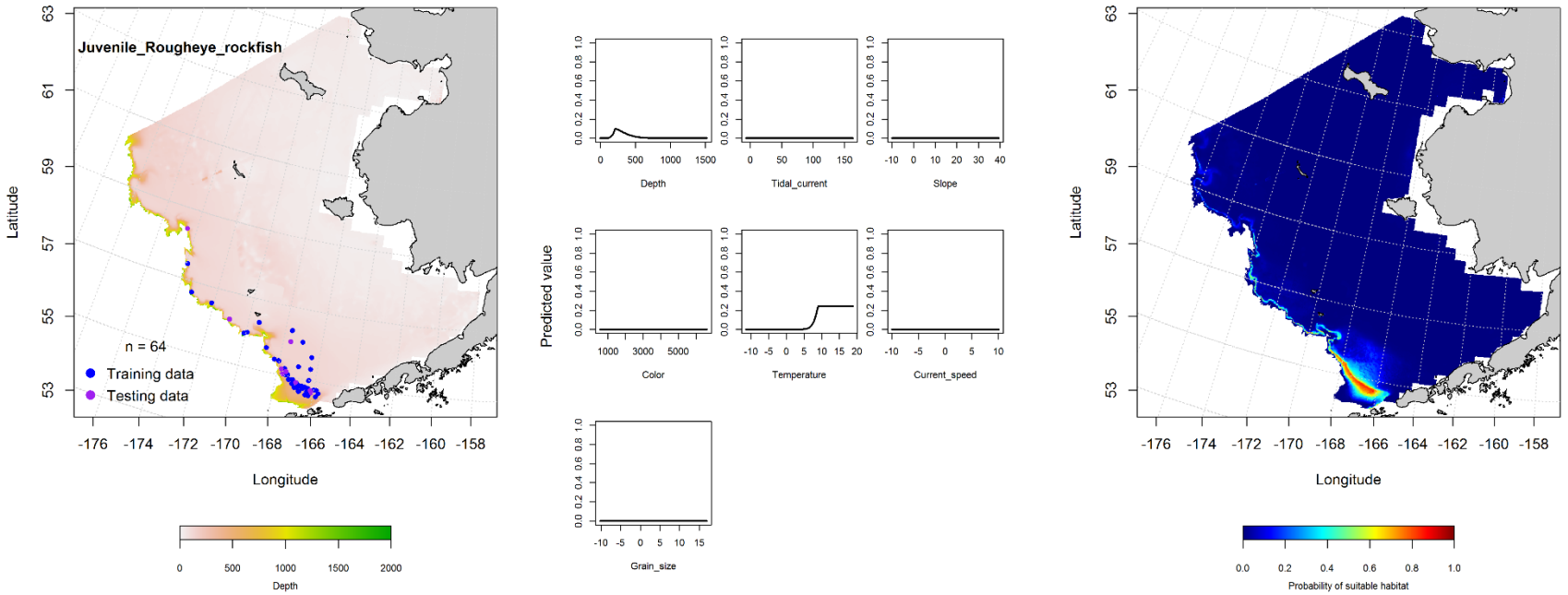

Figure 107. -- Presence of settled juvenile rougheye rockfish in RACE-GAP summer bottom trawl surveys (2007-2014) of the eastern Bering Sea (left panel) with training (blue dots) and testing (purple dots) data sets indicated alongside the maximum entropy model (MaxEnt) effects (center panel) and the MaxEnt spatial predictions of the probability of suitable settled juvenile rougheye rockfish habitat (right panel).

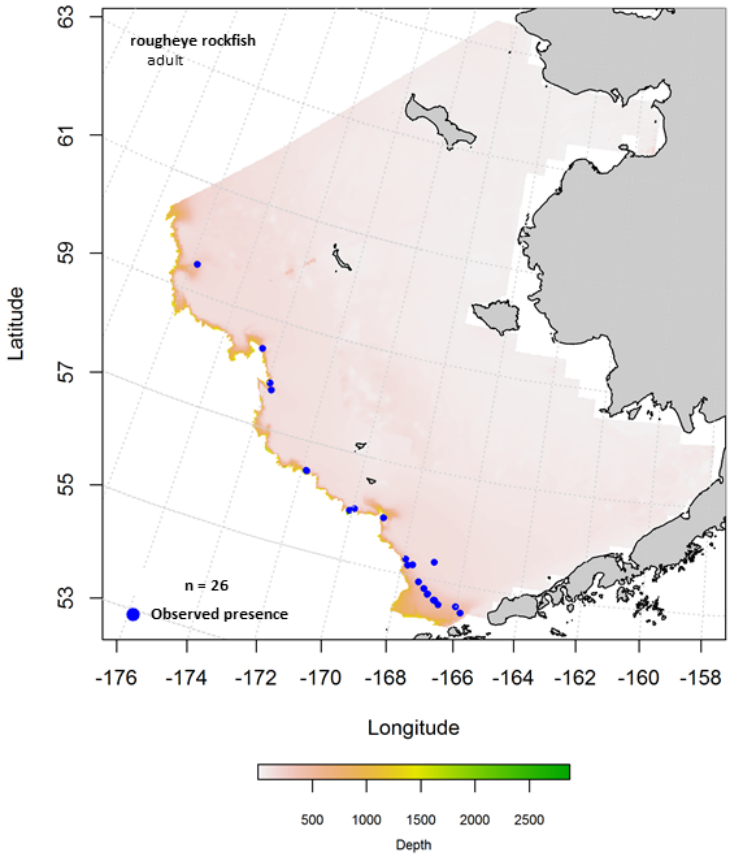

Figure 108. -- Presence of adult rougheye rockfish in RACE-GAP summer bottom trawl surveys of the eastern Bering Sea (2006-2014).

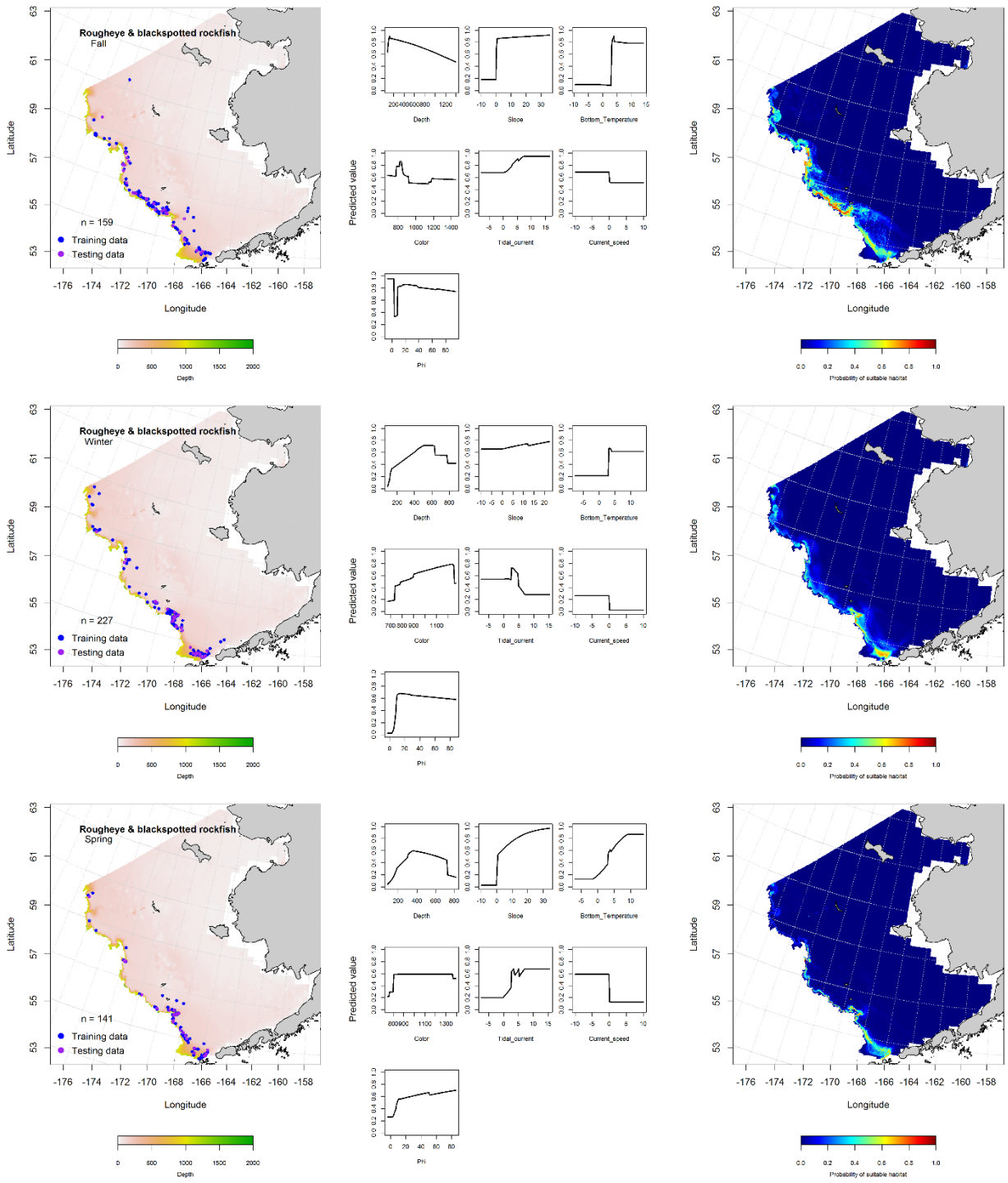

Figure 109. -- Locations of rougheye/blackspotted rockfish complex catches in fall (October-November; top row), winter (December-February; middle row), and spring (March-May; bottom row) commercial fisheries catches (2003-2013) from the eastern Bering Sea (left-hand column). Blue points were used to train the MaxEnt model (center column) predicting the probability of suitable habitat (right-hand column) and the purple points were used to validate the model.

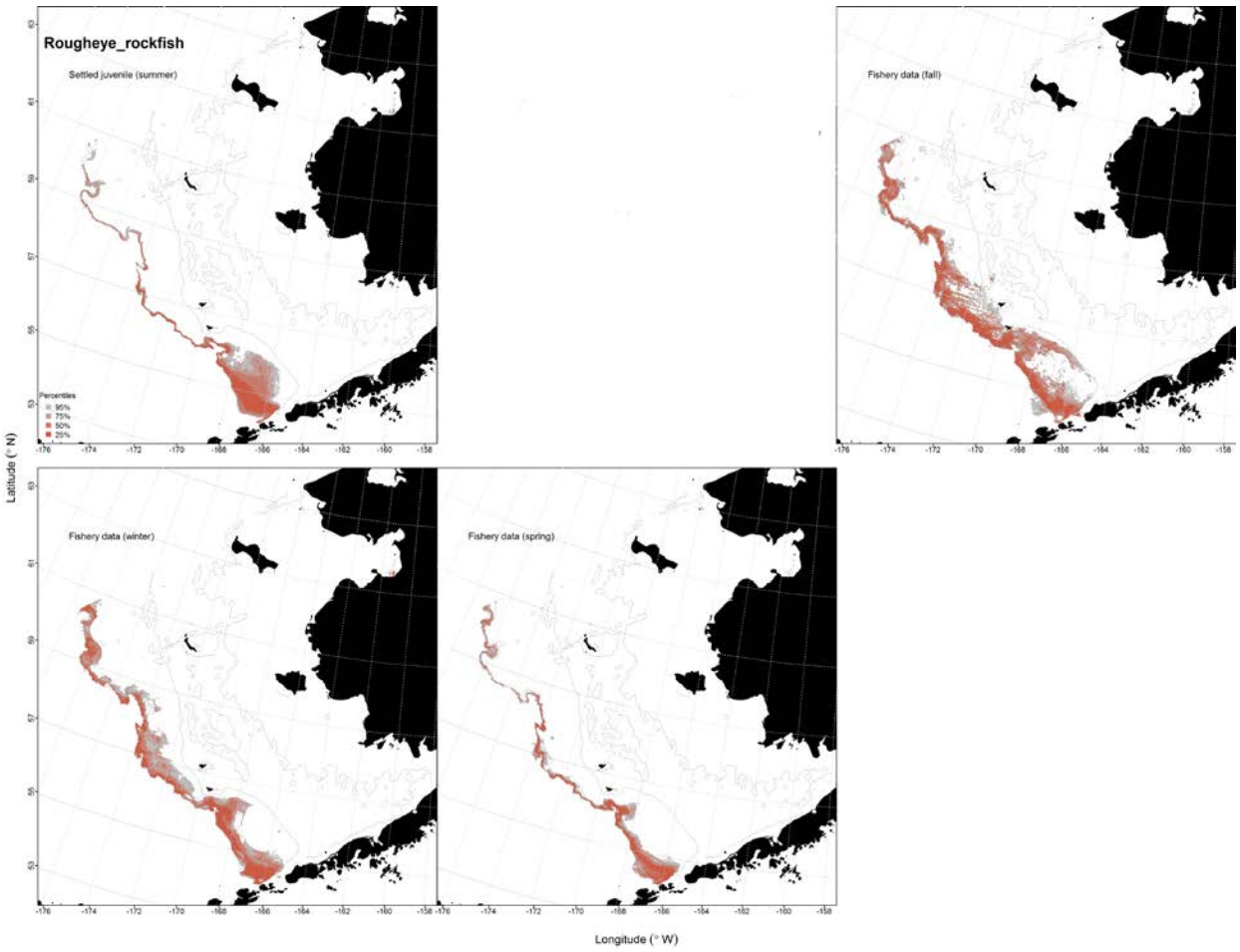

Figure 110. -- Essential fish habitat (EFH) predicted for settled juvenile rougheye rockfish (upper left panel) from RACE-GAP summertime bottom trawl surveys (2007-2014) and for rougheye/blackspotted rockfish complex observed in commercial fishery catches (2003-2013) from fall (upper right panel), winter, and spring (bottom two panels) in the eastern Bering Sea.

Pacific Ocean Perch (*Sebastes alutus*)

Summertime distribution of settled juvenile and adult Pacific ocean perch from RACE-GAP bottom trawl surveys of the eastern Bering Sea -- Catches of settled juvenile Pacific ocean perch on RACE-GAP bottom trawl surveys (1982-2014) of the EBS show that this species is primarily distributed over the outer shelf and along the slope edge from Bering Canyon in the south to the U.S.-Russia Convention Line in the north (Fig. 111). Although they were not common on summer bottom

trawl surveys (n = 125), they were sufficiently prevalent to parameterize a MaxEnt model to predict the probability of suitable habitat for this life stage in the study area. The most important habitat covariates describing their potential distribution were bottom depth and bottom temperature together comprising 88.4% of the relative importance of the contributions of model predictor terms. Probability of suitable settled juvenile Pacific ocean perch habitat was highest in depths ca. 200 m and temperatures ≥ 5°C. The areas predicted to have the highest probability of suitable habitat were typically associated with the heads of submarine canyons along the shelf edge. The MaxEnt fit to the training data was outstanding (AUC = 1) and the model correctly classified 97% of predicted cases. Model validation with the test data set also demonstrated an outstanding fit (AUC = 0.96) and correctly classified 96% of predicted cases.

Adult Pacific ocean perch in RACE-GAP summer bottom trawl surveys (1982-2014) were distributed similarly to settled juveniles along the outer shelf and upper slope edge (Fig. 112) and were slightly more prevalent; they were present at ca. 9% of trawled stations. A MaxEnt model was selected to predict probability of suitable habitat in the EBS for this life stage. The most important habitat covariates describing the potential habitat for adult Pacific ocean perch were bottom depth and bottom temperature which comprised a combined 96.3% of the relative importance of predictor terms. Probability of suitable habitat increased for this life stage at depths between 250 and 500 m and where bottom temperatures ≥ 4°C. The MaxEnt model was an outstanding fit to the training data (AUC = 0.98) and correctly classified 95% of predicted cases. Model validation was successful (AUC = 0.95) and 95% of cases predicted from the test data set were correctly classified.

Seasonal distribution of Pacific ocean perch in commercial fishery catches from the eastern Bering Sea -- Pacific ocean perch were present in commercial fishery catches primarily from the outer shelf of the EBS from the Alaska Peninsula north to the U.S.-Russia Convention Line during the fall, winter, and spring (Fig. 113). MaxEnt modeling of their presence in these catches was used to predict the probability of suitable habitat for this species. Bottom depth was the most important habitat covariate predicting their potential habitat in all three seasons with relative importance ranging from 52.9% in fall

to 75.5% in winter. During fall, the peak model effect occurred at depths between 100 and 400 m, but peak effects were deeper in winter and spring (ca. 500 m). Model fits to the training data were outstanding (AUC = 0.98-0.99) and the proportion of cases correctly predicted ranged from 93 to 96%. Model validation using the test data was successful (AUC = 0.89-0.96) correctly predicting 89 to 93% of cases.

Essential fish habitat maps and conclusions for Pacific ocean perch in the eastern Bering Sea -- Species distribution modeling of Pacific ocean perch from the EBS was translated into maps of EFH (Fig. 114). Predicted EFH for settled juveniles and adults from summer bottom trawl catches as well as EFH predicted from Pacific ocean perch present in commercial fisheries catches extended over the outer shelf from the Alaska Peninsula to the U.S.-Russia Convention Line in the north. The majority of EFH was deeper than 100 m. Most of the core habitat (the top 25% of predictions) was centered around 200 m and deeper. Even though the EFH maps based on Pacific ocean perch presence in commercial fisheries catches were largely dependent upon targeted fishing activities, there remains a great deal of congruence between them and the EFH maps generated from the annual RACE-GAP summer bottom trawl surveys.

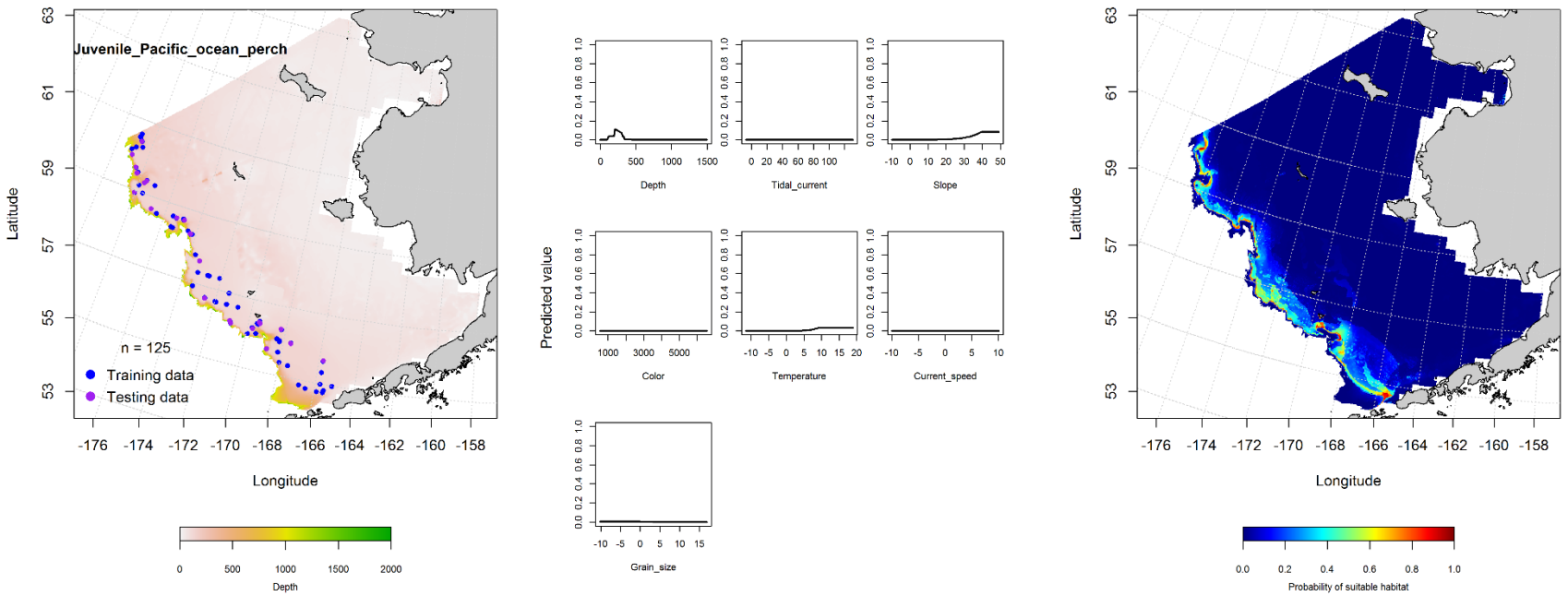

Figure 111. -- Presence of settled juvenile Pacific ocean perch in RACE-GAP summer bottom trawl surveys (1982-2014) of the eastern Bering Sea (left panel) with training (blue dots) and testing (purple dots) data sets indicated alongside the maximum entropy model (MaxEnt) effects (center panel) and the MaxEnt spatial predictions of the probability of suitable settled juvenile Pacific ocean perch habitat (right panel).

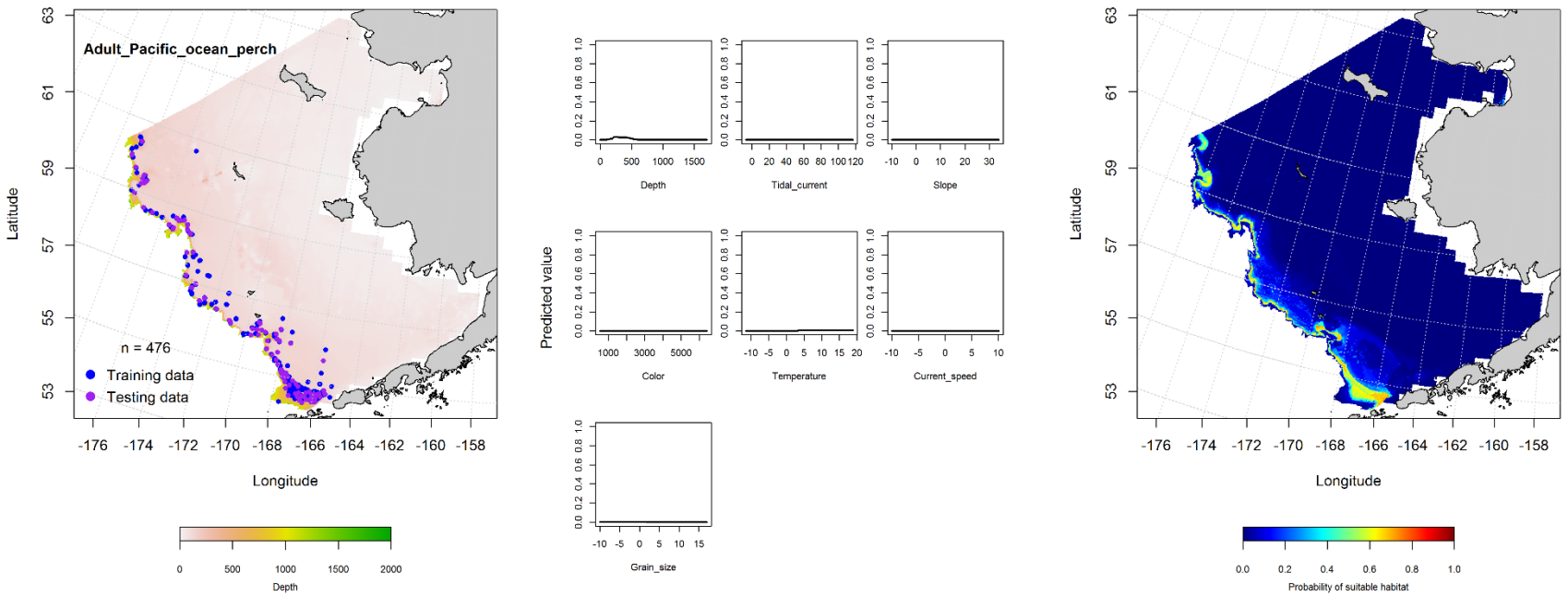

Figure 112. -- Presence of adult Pacific ocean perch in RACE-GAP summer bottom trawl surveys (1982-2014) of the eastern Bering Sea (left panel) with training (blue dots) and testing (purple dots) data sets indicated alongside the maximum entropy model (MaxEnt) effects (center panel) and the MaxEnt spatial predictions of the probability of suitable adult Pacific ocean perch habitat (right panel).

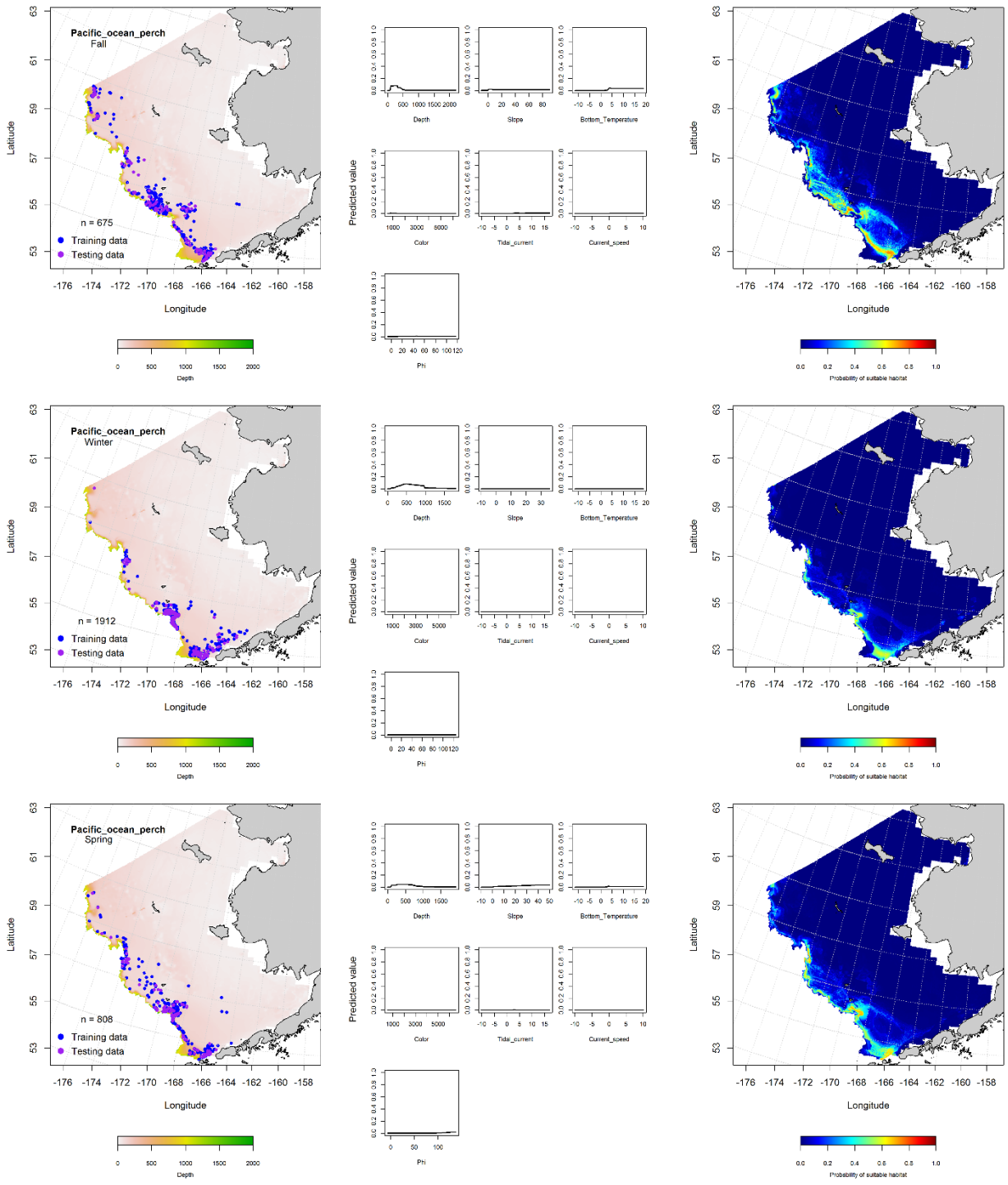

Figure 113. -- Locations of Pacific ocean perch in fall (October-November; top row), winter (December-February; middle row), and spring (March-May; bottom row) commercial fisheries catches (2003-2013) from the eastern Bering Sea (left-hand column). Blue points were used to train the MaxEnt model (center column) predicting the probability of suitable habitat (right-hand column) and the purple points were used to validate the model.

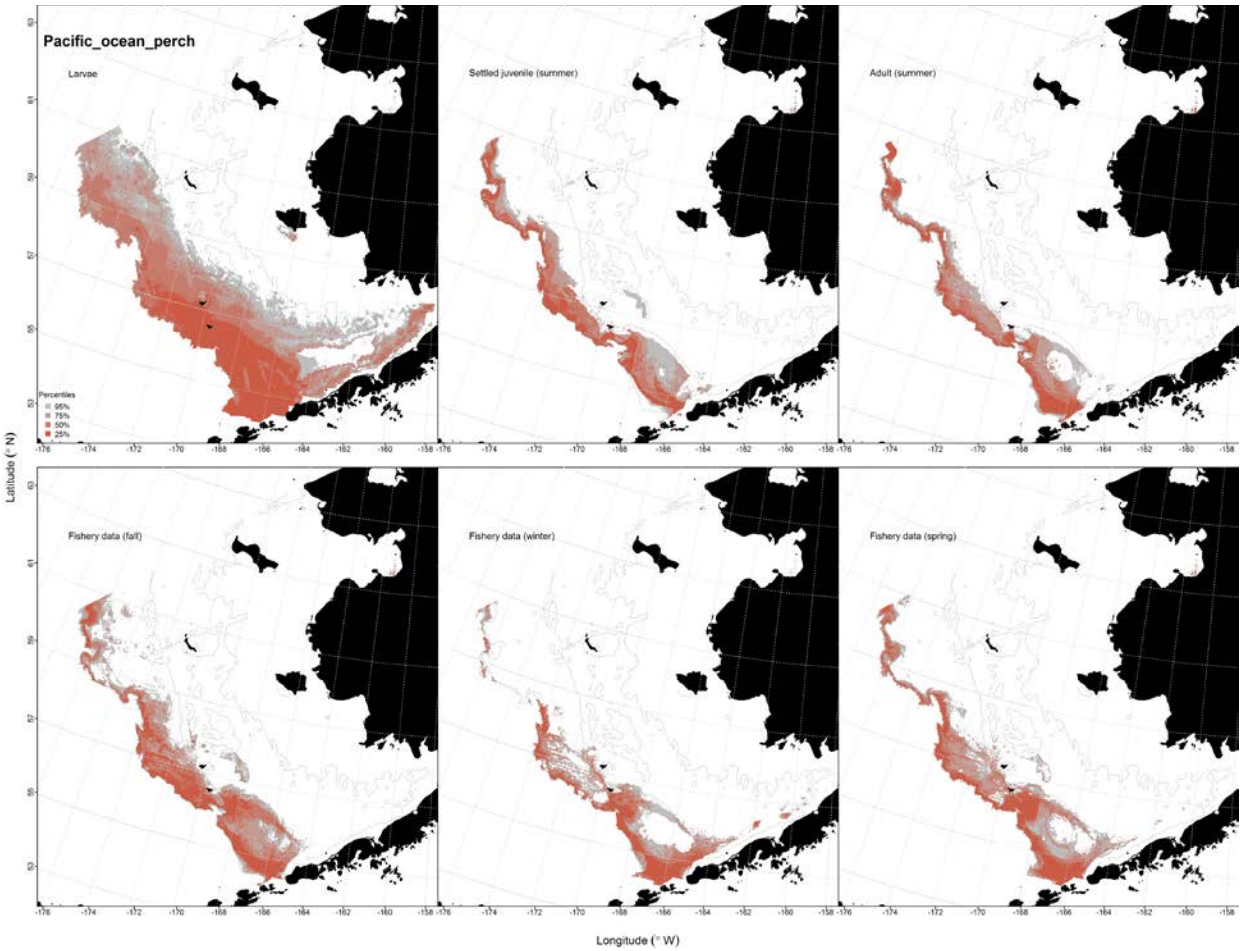

Figure 114. -- Essential fish habitat (EFH) predicted for settled juvenile and adult Pacific ocean perch (upper left and middle panels) from RACE-GAP summertime bottom trawl surveys (1982-2014) and predicted from presence in commercial fishery catches (2003-2013) from fall (upper right panel), winter, and spring (bottom two panels) in the eastern Bering Sea.

Shortraker Rockfish (*Sebastes borealis*)

Summertime distribution of settled juvenile and adult shortraker rockfish from RACE-GAP bottom trawl surveys of the eastern Bering Sea -- Catches of settled juvenile shortraker rockfish have only been reported from the RACE-GAP bottom trawl survey of the EBS slope focusing on the upper continental slope and shelf edge (Fig. 115). MaxEnt modeling of their distribution from presence only records indicated that the most important habitat covariates determining the probability of suitable habitat for this life stage were bottom depth and local slope comprising a combined relative importance of

98.9% for these two predictor terms. Model effects were highest in 400-500 m depths over moderate slope roughly corresponding to the shelf break in these areas. The MaxEnt fit to the training data was outstanding (AUC = 1) and the model correctly classified 98% of predicted cases. Model validation was successful (AUC = 1) correctly classifying 100% of the cases predicted from the test data.

The distribution of adult shortraker rockfish on the EBS slope surveys mirrored that of the settled juveniles (Fig. 115). The MaxEnt model predicting probability of suitable adult shortraker habitat identified that, like in the settled juvenile model, the most important habitat covariates were bottom depth and local slope. They were primarily distributed along the upper slope edge and outer shelf from the Bering Canyon in the southern domain to Navarin Canyon in the northern domain. Bottom depth and bottom slope were the highest leverage habitat covariates among the predictors in the model. Combined they accounted for 99.3% of the relative importance among predictor terms. The MaxEnt model was an outstanding fit to the training data (AUC = 0.99) and model validation was successful (AUC = 0.98). Predictions from this model with either the training or test data sets correctly classified 98% of the cases.

A MaxEnt model was selected to predict suitable habitat from the presence of adult shortraker rockfish observed in RACE-GAP summer bottom trawl surveys of the eastern Bering Sea Slope (Fig. 116). They were primarily distributed along the upper slope edge and outer shelf from south to north across the survey area. Bottom depth and local slope were the most important habitat covariates in the model comprising a combined 89.7% of the relative importance of predictor terms. The MaxEnt model was an outstanding fit to the training data (AUC = 0.99) and correctly classified 97% of predicted cases. Model validation was successful (AUC = 0.95) and 95% of cases predicted from the test data set were correctly classified.

Seasonal distribution of shortraker rockfish in commercial fishery catches from the eastern Bering Sea -- Shortraker rockfish were present in commercial fishery catches from the outer shelf and slope edge of the EBS from the Alaska Peninsula north to the U.S.-Russia Convention Line during the fall, winter, and spring (Fig. 117). MaxEnt modeling of their presence in these catches was used to predict

the probability of suitable habitat for this species. Bottom depth was the most important habitat covariate predicting their potential habitat in all three seasons with relative importance ranging from 37.5% in fall to 82.6% in winter. During fall, bottom temperature and local slope comprised an additional 45.4% of the relative importance of predictor terms. Peak model effects due to depth varied between seasons, but generally fell between 200 and 600 m, and in fall, the probability of suitable shortraker habitat predicted from commercial catch observations increased with increasing local slope and bottom temperature. Model fits to the training data were outstanding (AUC = 0.99 in all three seasons) and the proportion of cases correctly predicted ranged from 96 to 97%. Model validation using the test data was successful (AUC = 0.92-0.98) correctly predicting 92 to 98% of cases.

Essential fish habitat maps and conclusions for shortraker rockfish in the eastern Bering Sea -- Species distribution modeling of shortraker rockfish from the EBS was translated into maps of EFH (Fig. 118). Predicted EFH for settled juveniles and adults from summer bottom trawl catches as well as EFH predicted from shortraker rockfish present in commercial fisheries catches extended over the outer shelf and shelf edge from the Alaska Peninsula to the U.S.-Russia Convention Line in the north. The majority of EFH was deeper than 200 m and core habitat (the top 25% of predictions) was deeper and centered below 400 m. Although the EFH maps based on shortraker rockfish presence in commercial fisheries catches were likely dependent upon targeted fishing activities, there was a great deal of similarity between them and the EFH maps generated from the annual RACE-GAP summer bottom trawl surveys.

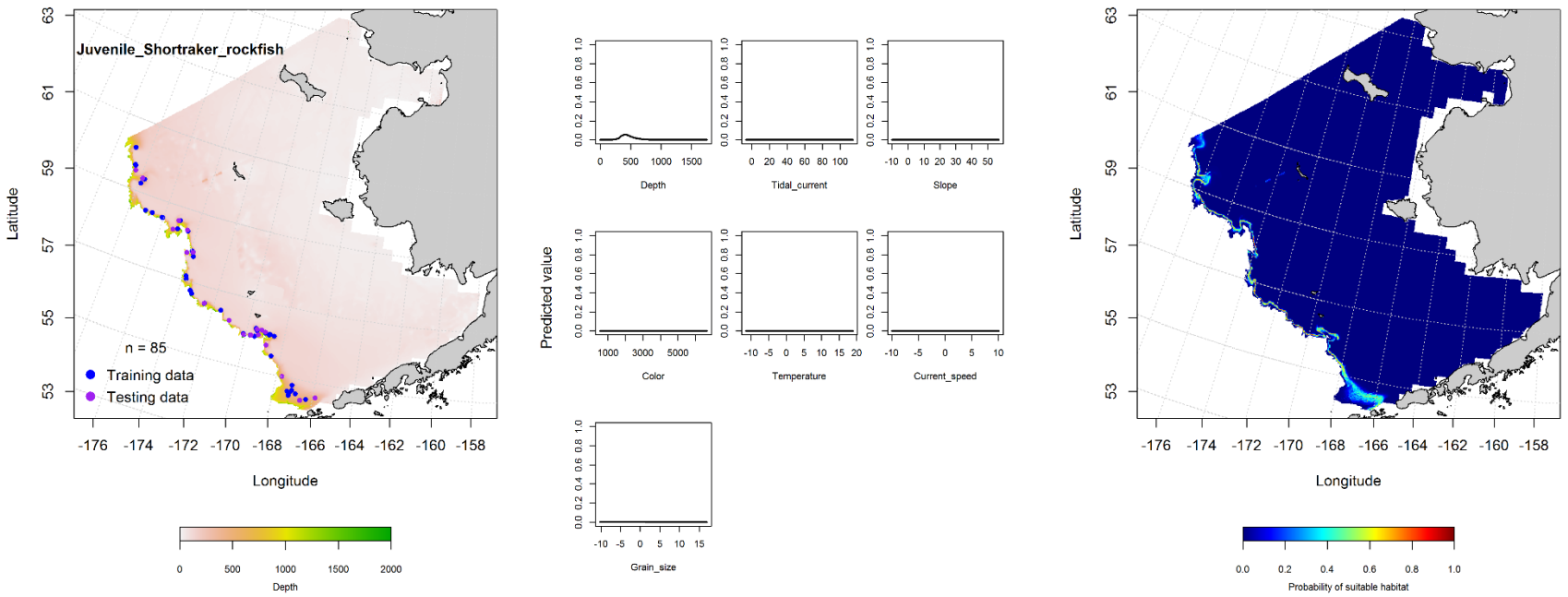

Figure 115. -- Presence of settled juvenile shortraker rockfish in RACE-GAP summer bottom trawl surveys (1982-2014) of the eastern Bering Sea (left panel) with training (blue dots) and testing (purple dots) data sets indicated alongside the maximum entropy model (MaxEnt) effects (center panel) and the MaxEnt spatial predictions of the probability of suitable settled juvenile shortraker rockfish habitat (right panel).

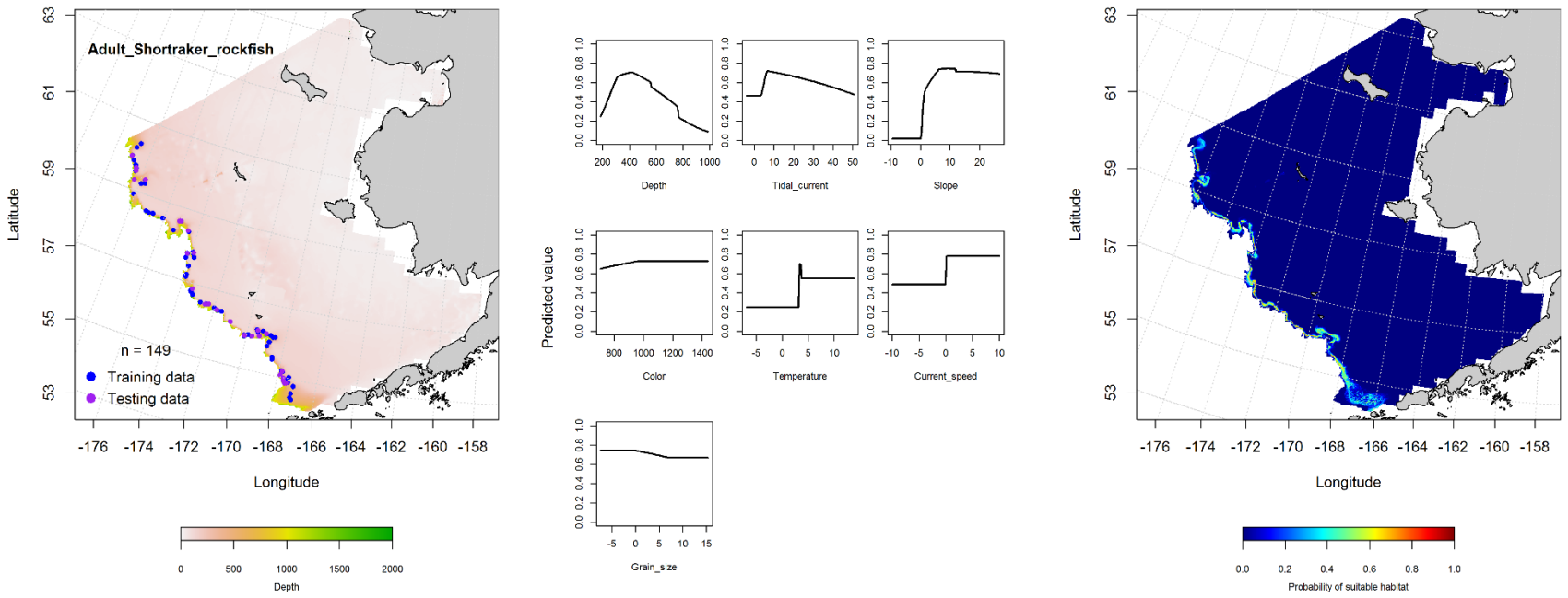

Figure 116. -- Presence of adult shortraker rockfish in RACE-GAP summer bottom trawl surveys (1982-2014) of the eastern Bering Sea (left panel) with training (blue dots) and testing (purple dots) data sets indicated alongside the maximum entropy model (MaxEnt) effects (center panel) and the MaxEnt spatial predictions of the probability of suitable adult shortraker rockfish habitat (right panel).

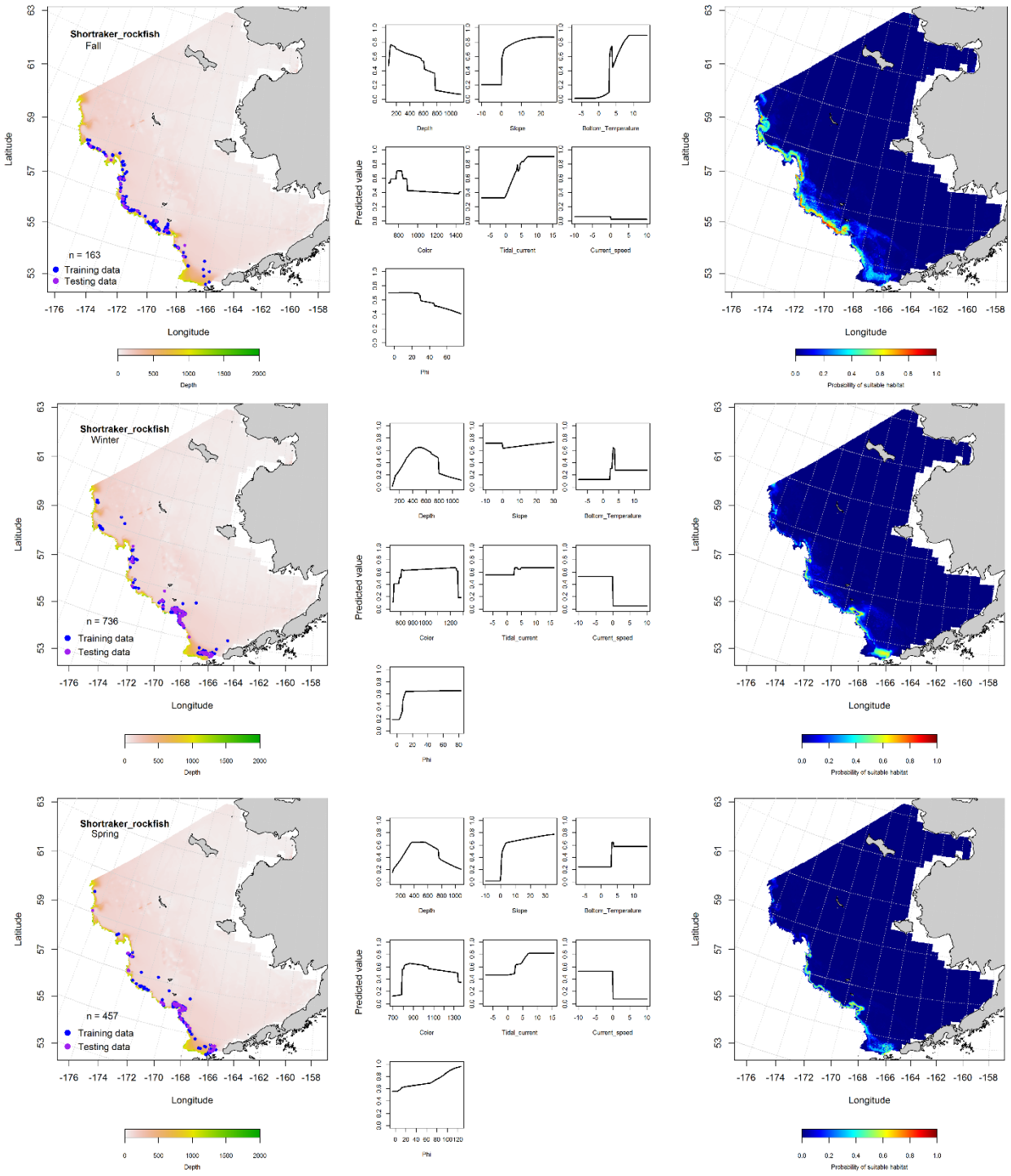

Figure 117. -- Locations of shortraker rockfish in fall (October-November; top row), winter (December-February; middle row), and spring (March-May; bottom row) commercial fisheries catches (2003-2013) from the eastern Bering Sea (left-hand column). Blue points were used to train the MaxEnt model (center column) predicting the probability of suitable habitat (right-hand column) and the purple points were used to validate the model.

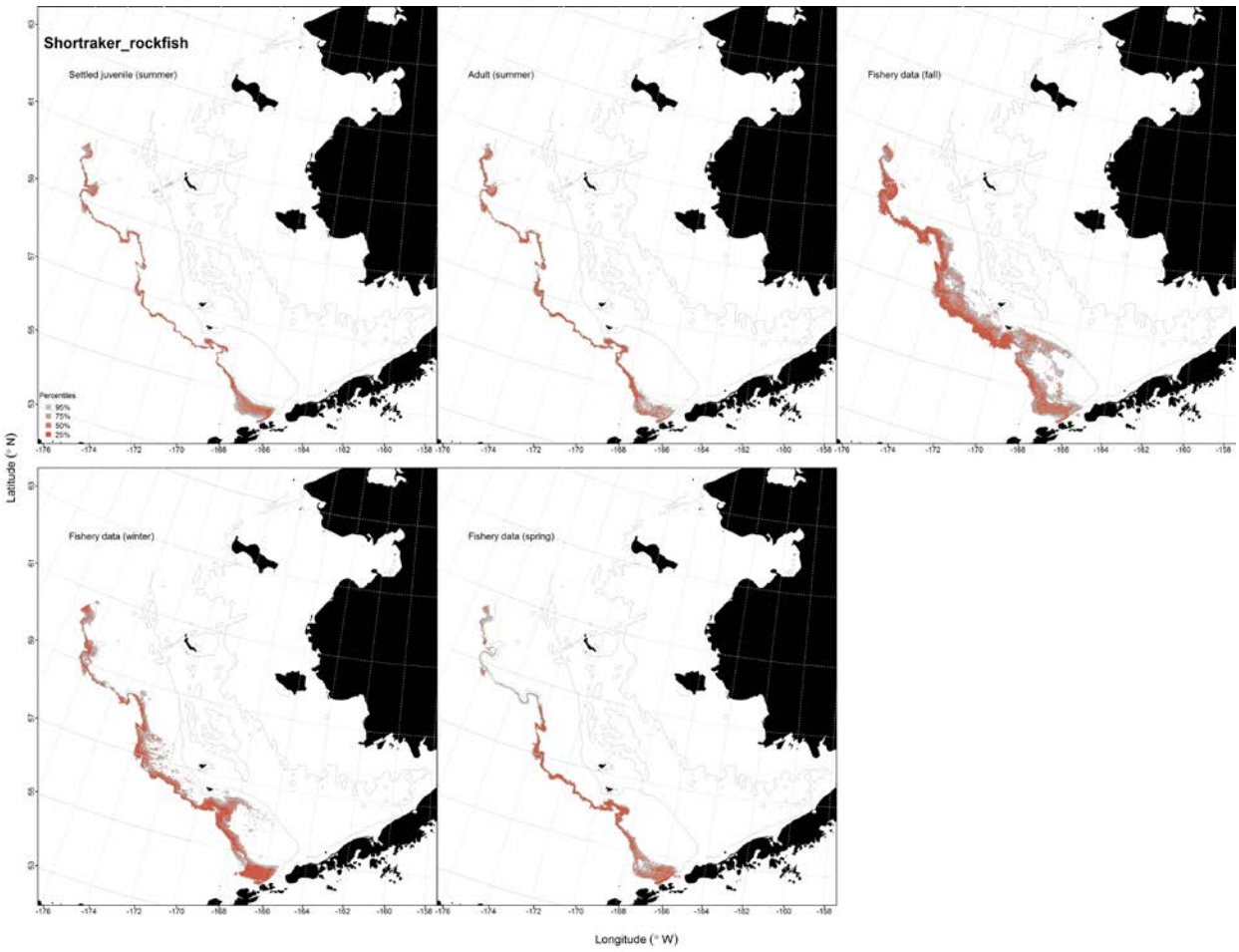

Figure 118. -- Essential fish habitat (EFH) predicted for settled juvenile and adult shortraker rockfish (upper left and middle panels) from RACE-GAP summertime bottom trawl surveys (1982-2014) and predicted from presence in commercial fishery catches (2003-2013) from fall (upper right panel), winter, and spring (bottom two panels) in the eastern Bering Sea.

Blackspotted Rockfish (*Sebastes melanostictus*)

Summertime distribution of settled juvenile and adult blackspotted rockfish from RACE-GAP bottom trawl surveys of the eastern Bering Sea -- Settled juvenile blackspotted rockfish in RACE-GAP summer bottom trawl surveys of the EBS (2006-2014) were primarily collected from the outer shelf in the southern portion of the study area (Fig. 119). There were less than 50 stations where they were collected. Consequently, there were two few instances of their presence in the samples to allow for species distribution modeling for this life stage.

Adult blackspotted rockfish were not common on RACE-GAP summer bottom trawl surveys of the EBS (2006-2014), but were sufficiently prevalent to model their distribution (Fig. 120). MaxEnt modeling of presence only data for adult blackspotted rockfish identified that the most important habitat covariates describing their distribution were local slope and bottom depth comprising a combined total of 96.4% of the relative importance of predictor terms in the model. Predictions of probability of suitable habitat for this life stage increased over moderate local slope values at depths ≥ 400 m. The model fit was outstanding to the training data (AUC = 1) and it correctly classified 97% of predicted cases. Model validation was successful (AUC = 0.93) and 93% of cases predicted from the test data were correctly classified.

Seasonal distribution of blackspotted rockfish in commercial fishery catches from the eastern Bering Sea -- Rougheye and blackspotted rockfishes are not separated in commercial catches from Alaska. The two species are combined in landings and managed together as a complex. Results of distribution models for the rougheye/blackspotted complex landed from commercial fisheries in the EBS were reported in the rougheye rockfish section above.

Essential fish habitat maps and conclusions for blackspotted rockfish in the eastern Bering Sea -- Species distribution modeling of blackspotted rockfish from the EBS was translated into maps of EFH (Fig. 121). Predicted EFH for settled juveniles and adults from summer bottom trawl catches extended over the outer shelf and shelf edge from the Alaska Peninsula to the U.S.-Russia Convention Line in the north. Core habitat (the top 25% of predictions) was concentrated below 400 m.

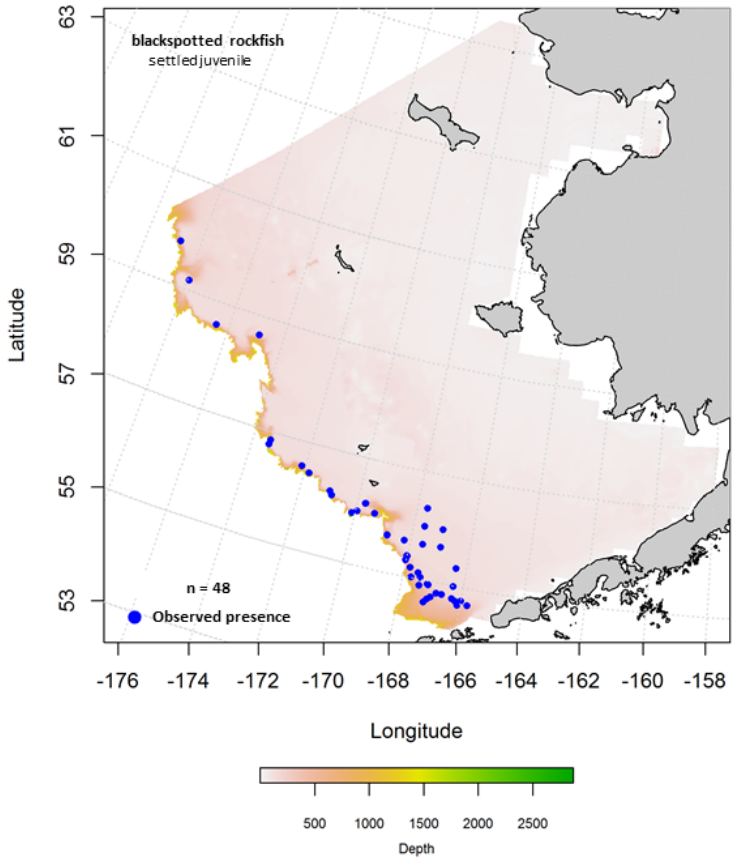

Figure 119. -- Presence of settled juvenile blackspotted rockfish in RACE-GAP summer bottom trawl surveys (2007-2014) of the eastern Bering Sea (left panel) with training (blue dots) and testing (purple dots) data sets indicated alongside the maximum entropy model (MaxEnt) effects (center panel) and the MaxEnt spatial predictions of the probability of suitable settled juvenile blackspotted rockfish habitat (right panel).

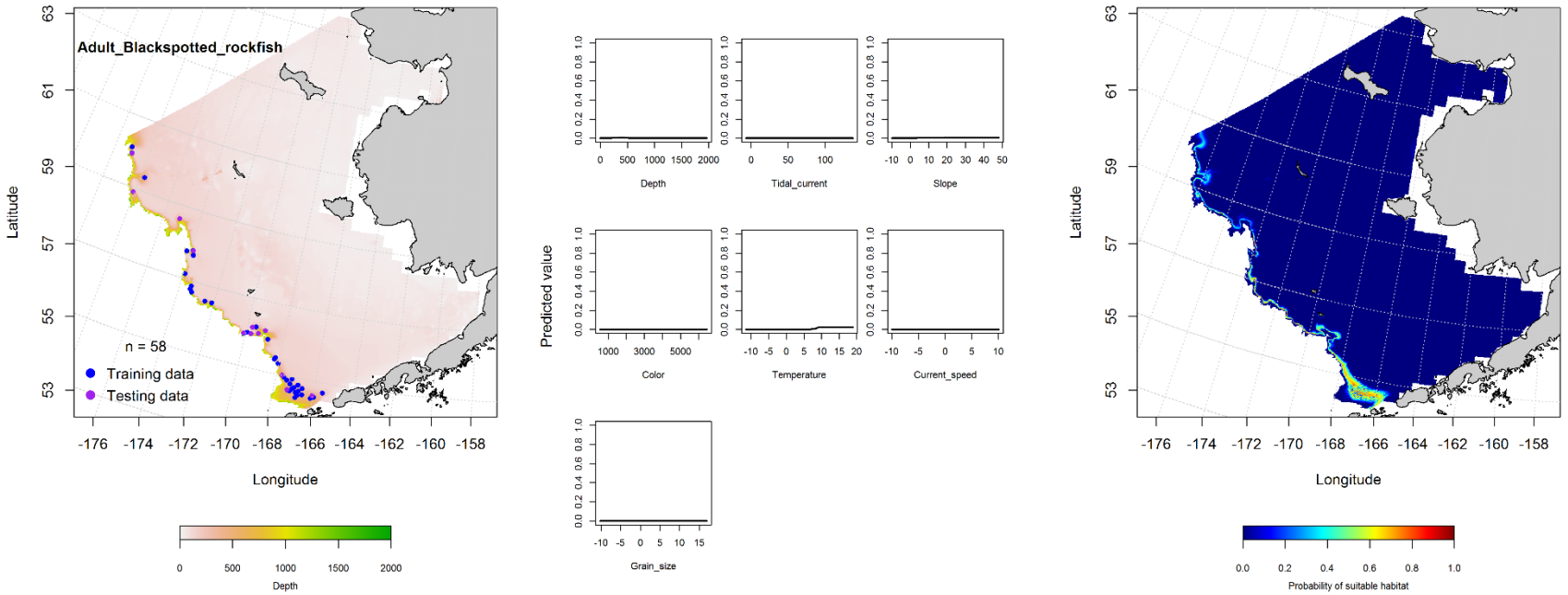

Figure 120. -- Presence of settled adult blackspotted rockfish in RACE-GAP summer bottom trawl surveys (2007-2014) of the eastern Bering Sea (left panel) with training (blue dots) and testing (purple dots) data sets indicated alongside the maximum entropy model (MaxEnt) effects (center panel) and the MaxEnt spatial predictions of the probability of suitable settled adult blackspotted rockfish habitat (right panel).

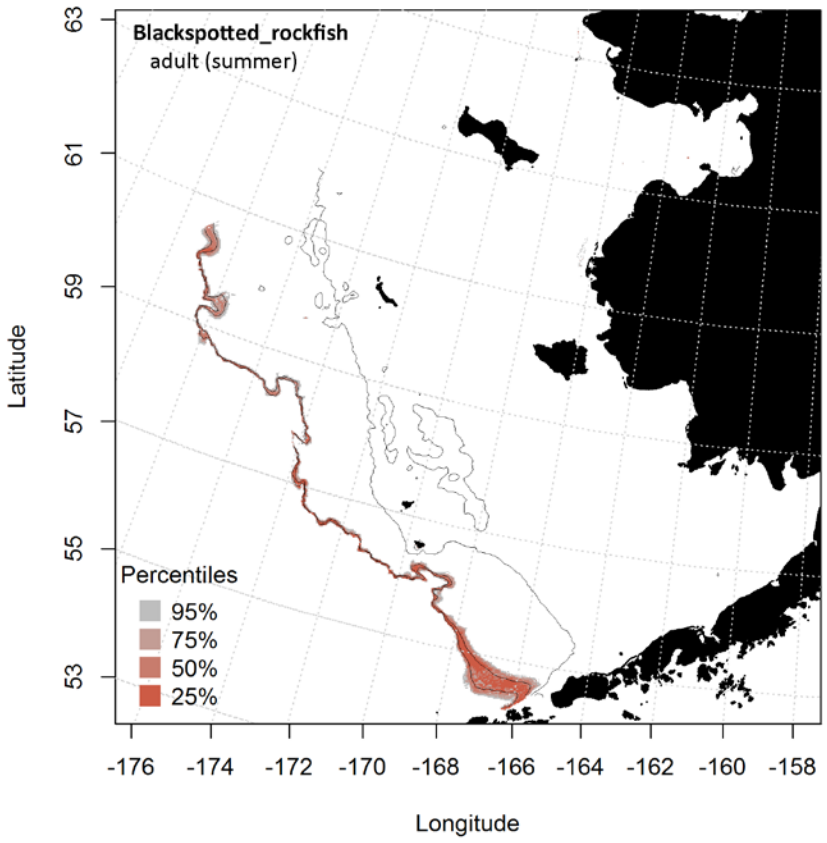

Figure 121. -- Essential fish habitat (EFH) predicted for settled juvenile and adult blackspotted rockfish from RACE-GAP summertime bottom trawl surveys (2007-2014) of the eastern Bering Sea.

Northern Rockfish (*Sebastes polyspinis*)

Summertime distribution of adult northern rockfish from RACE-GAP bottom trawl surveys of the eastern Bering Sea -- Adult northern rockfish were collected on summer RACE-GAP bottom trawl surveys of the EBS (1982-2014) primarily in the central and southern portions of the survey area (Fig. 122). They were sufficiently prevalent to model their distribution using a MaxEnt model and presence-only data. The most important habitat covariates in the model were bottom depth and bottom temperature comprising a combined relative importance of 79.7%. The probability of suitable habitat was predicted to be highest for adult northern rockfish at depths ca. 150-250 m and bottom temperatures

≥ 5°C. The model fit to the training data was outstanding (AUC = 0.98) and it correctly classified 92% of predicted cases. Model validation was successful (AUC = 0.85) correctly classifying 85% of predicted cases.

Seasonal distribution of northern rockfish in commercial fishery catches from the eastern Bering Sea -- Northern rockfish were observed in commercial fishery catches from the middle and outer shelf in fall, winter, and spring (Fig. 123). MaxEnt models used to predict the probability of suitable habitat for this species determined that bottom depth and bottom temperature were the most important habitat covariates predicting their potential habitat in all three seasons. The combined relative importance of these two predictors ranged from 68.1% in spring to 79.1% in fall and the probability of potential habitat was highest ca. 100 m and 4°C. Model fits to the training data were outstanding (AUC = 0.98-0.99) and the proportion of cases correctly classified was high (92-95%). Model validation using the test data was successful (AUC = 0.91-0.92) correctly classifying 91 to 92% of cases.

Essential fish habitat maps and conclusions for northern rockfish from the eastern Bering Sea -- Species distribution modeling results for northern rockfish from the EBS were translated into EFH maps (Fig. 124). For northern rockfish adults from summer bottom trawl catches as well as for presumed adults from commercial fisheries catches, EFH was primarily found on the western side of the middle shelf and along the outer shelf from the Alaska Peninsula to the northern Bering Sea. Core habitat (top 25% of predictions) was mainly constrained to depths greater than 200 m on the outer shelf. There was a great deal of spatial overlap between EFH predicted from RACE-GAP summer bottom trawl surveys and that predicted from commercial fishery catches in all seasons despite the assumed dependence of the latter on targeted fishing activities.

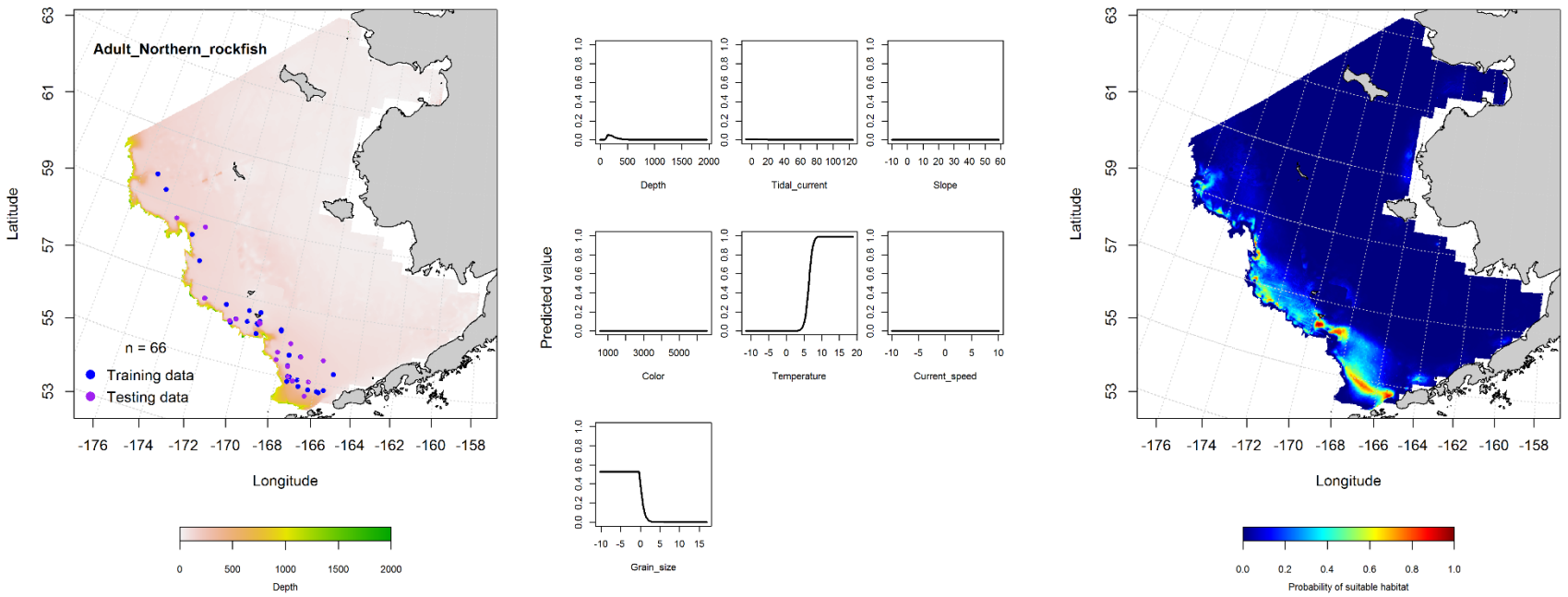

Figure 122. -- Presence of settled adult northern rockfish in RACE-GAP summer bottom trawl surveys (1982-2014) of the eastern Bering Sea (left panel) with training (blue dots) and testing (purple dots) data sets indicated alongside the maximum entropy model (MaxEnt) effects (center panel) and the MaxEnt spatial predictions of the probability of suitable settled adult northern rockfish habitat (right panel).

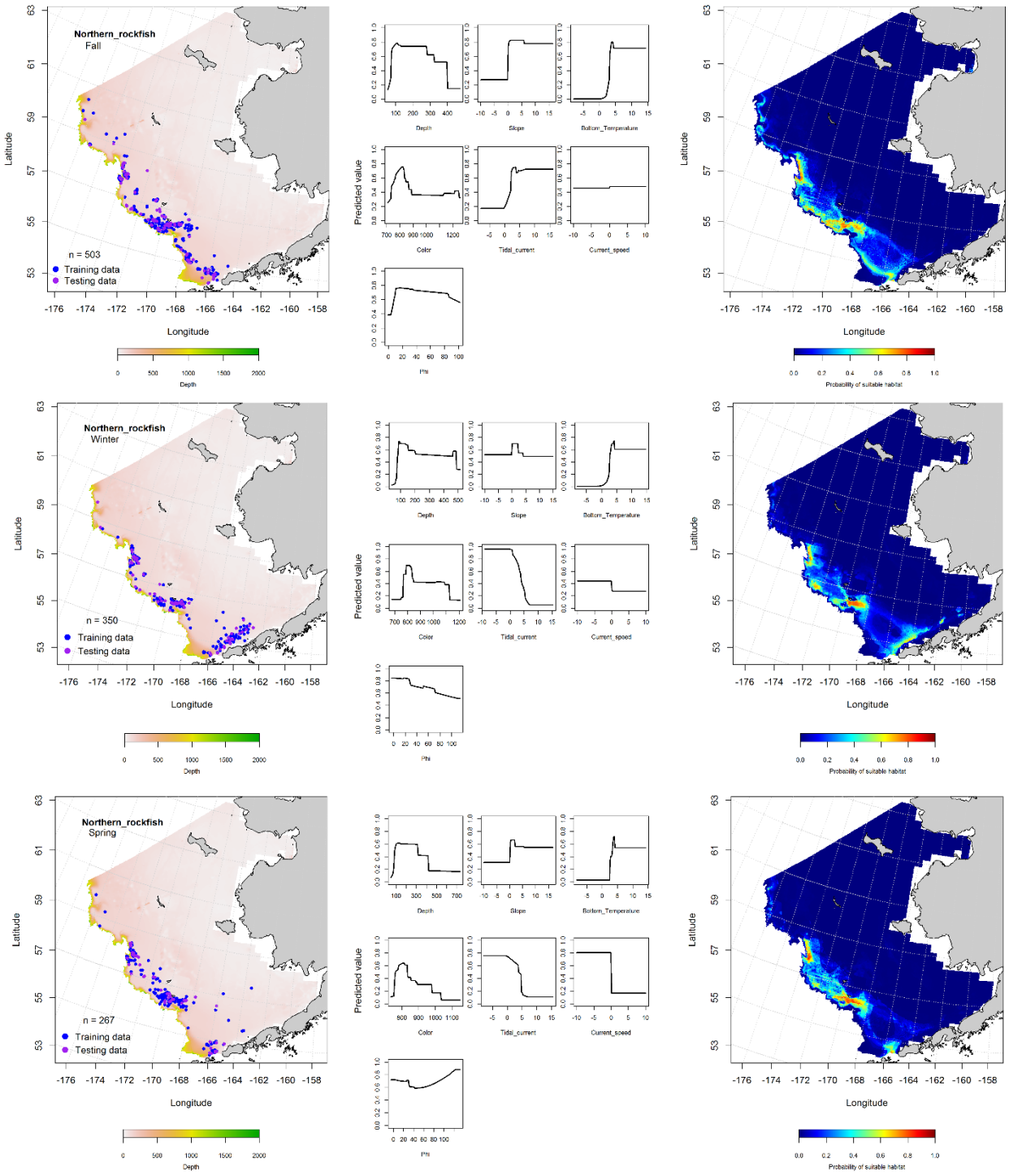

Figure 123. -- Locations of northern rockfish in fall (October-November; top row), winter (December-February; middle row), and spring (March-May; bottom row) commercial fisheries catches (2003-2013) from the eastern Bering Sea (left-hand column). Blue points were used to train the MaxEnt model (center column) predicting the probability of suitable habitat (right-hand column) and the purple points were used to validate the model.

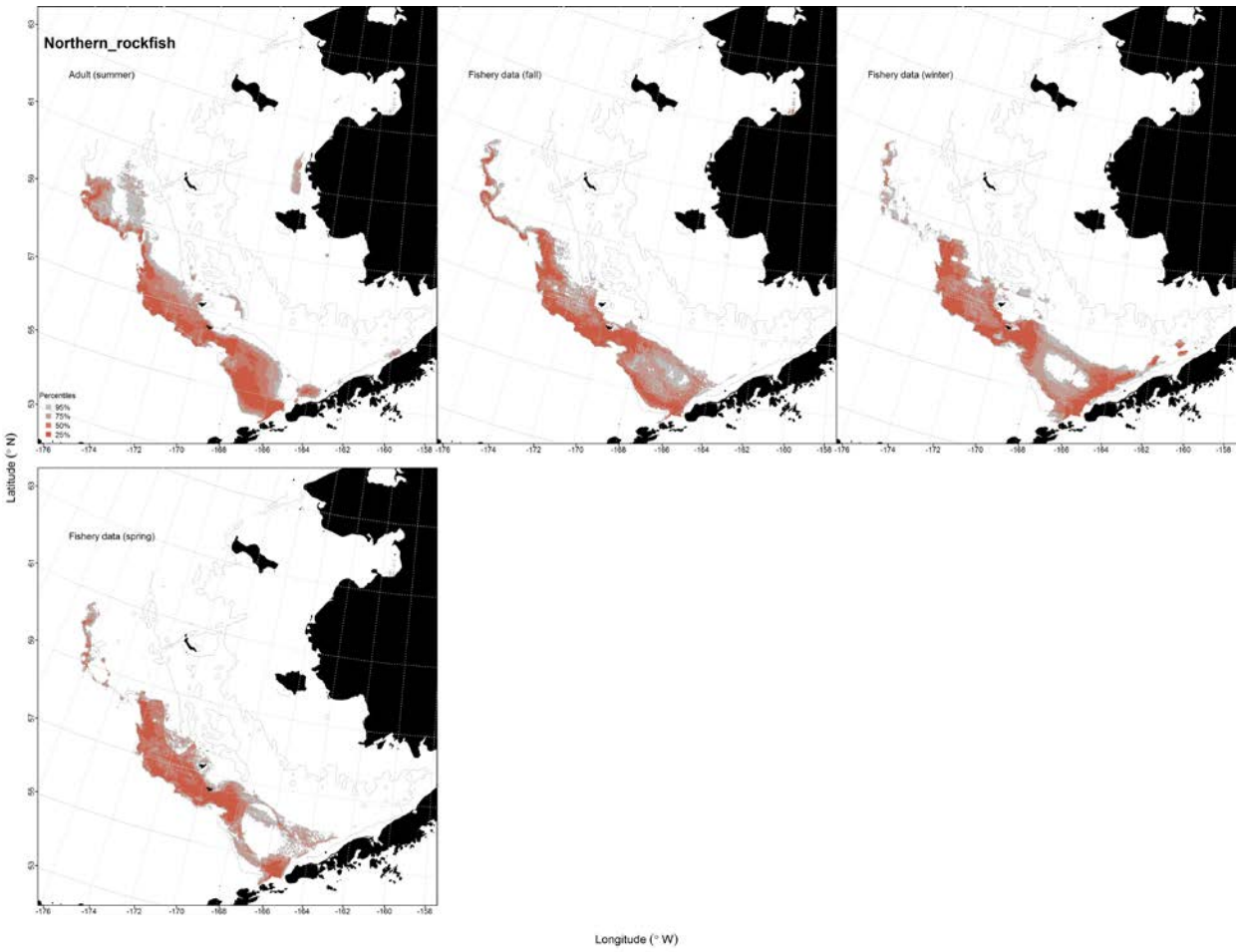

Figure 124. -- Essential fish habitat (EFH) predicted for adult northern rockfish (upper left panel) from RACE-GAP summertime bottom trawl surveys (1982-2014) and predicted from presence in commercial fishery catches (2003-2013) from fall, winter (upper middle and right panels), and spring in the eastern Bering Sea (bottom panel).

Dusky Rockfish (*Sebastes variabilis*)

Summertime distribution of settled juvenile and adult dusky rockfish from RACE-GAP bottom trawl surveys of the eastern Bering Sea -- Adult dusky rockfish were present in RACE-GAP summer bottom trawl surveys (1996-2014) from the EBS (Fig. 125); no settled juveniles of this species were reported from these catches. Adults were not common in bottom trawl catches and historically have occurred in less than 1% of survey stations on average annually. When they were encountered, they were primarily caught along on the middle and outer shelf in the central and southern portion of the survey

area. There were less than 50 occurrences of adult dusky rockfish in the RACE-GAP summer bottom trawl survey samples which was insufficient to parameterize a distribution model for this species.

Seasonal distribution of the dusky rockfish in commercial fishery catches from the eastern Bering Sea -- Dusky rockfish were observed in commercial fishery catches primarily from the outer shelf in fall, winter, and spring (Fig. 126). During winter, dusky rockfish were more prevalent to the east of the Bering Canyon than in fall or spring. MaxEnt models used to predict the probability of suitable habitat for this species determined that bottom depth and bottom temperature were the most important habitat covariates predicting their potential habitat in all three seasons. The combined relative importance of these two predictors ranged from 64.6% in spring to 76.8% in fall and the probability of potential habitat was highest ca. 150 m and greater than 3°C. Model fits to the training data were outstanding (AUC = 0.97-0.98) and the proportion of cases correctly classified was high (89-92%). Model validation using the test data was successful (AUC = 0.86-0.92) correctly classifying 86 to 92% of cases.

Essential fish habitat maps and conclusions for dusky rockfish in the eastern Bering Sea -- Species distribution modeling results for dusky rockfish from their presence in commercial fisheries of the EBS were translated into EFH maps (Fig. 127). Dusky rockfish EFH was primarily found on the western side of the middle shelf and along the outer shelf from the Alaska Peninsula to the northern Bering Sea. Core habitat (top 25% of predictions) was mainly found at depths between 100 and 200 m on the outer shelf. An exception was a large proportion of the core winter habitat was found between 50 and 100 m on the middle shelf in Bristol Bay.

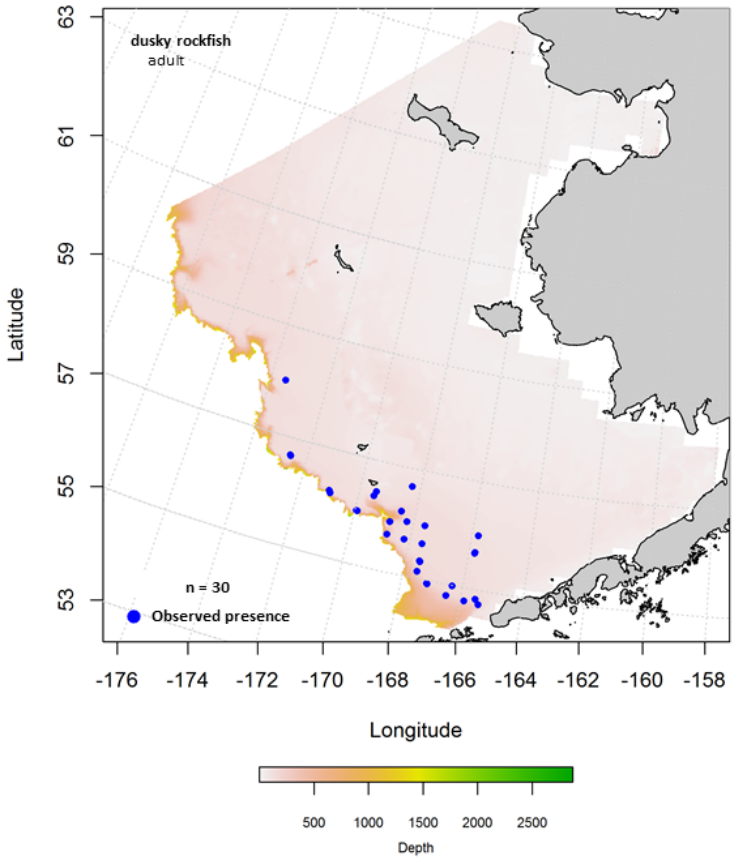

Figure 125. -- Presence of adult dusky rockfish in RACE-GAP summer bottom trawl survey catches from the eastern Bering Sea (1996-2014).

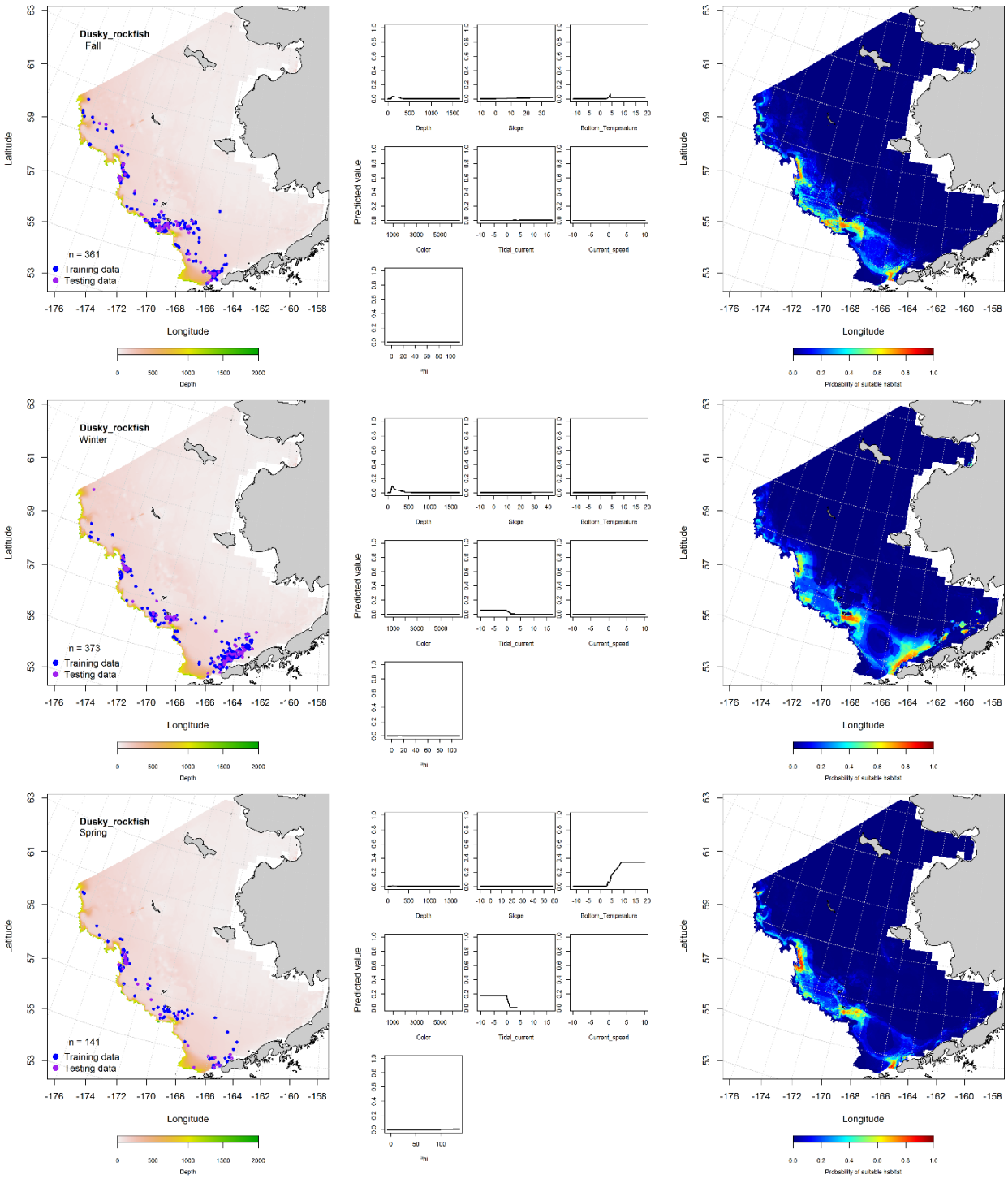

Figure 126. -- Locations of dusky rockfish in fall (October-November; top row), winter (December-February; middle row), and spring (March-May; bottom row) commercial fisheries catches (2003-2013) from the eastern Bering Sea (left-hand column). Blue points were used to train the MaxEnt model (center column) predicting the probability of suitable habitat (right-hand column) and the purple points were used to validate the model.

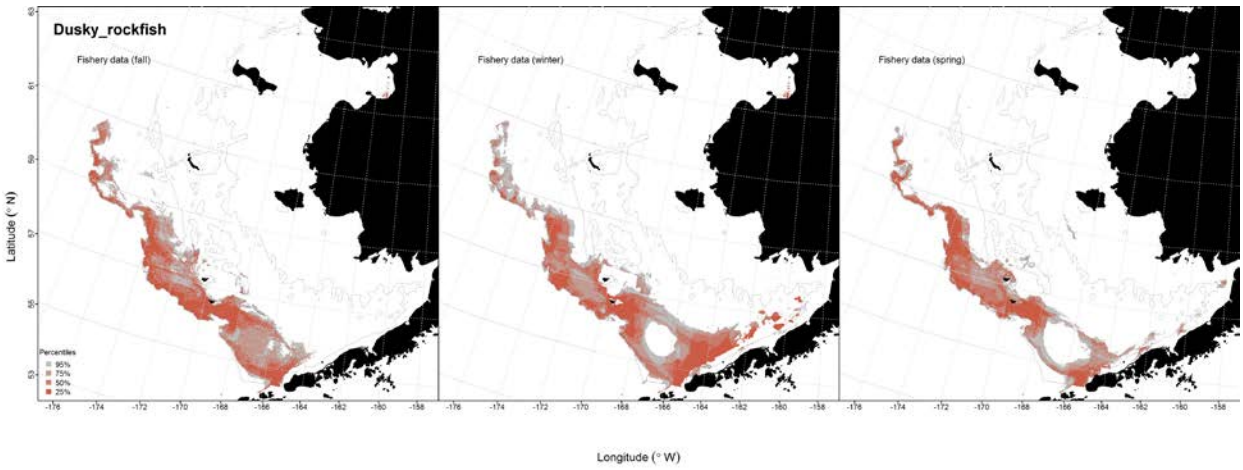

Figure 127. -- Essential fish habitat (EFH) for dusky rockfish predicted from presence in commercial fishery catches (2003-2013) in fall, winter, and spring in the eastern Bering Sea.

Thornyheads (*Sebastolobus* spp.)

Thornyheads (*Sebastolobus* spp.) are represented by three species in the EBS: broadfin (*Sebastolobus macrochir*), shortspine (*S. alascanus*), and longspine (*S. altivelis*) thornyheads (Mecklenburg et al. 2002). Historically, eggs and larvae from this genus collected on EcoFOCI ichthyoplankton surveys in the EBS have been identified only to the genus *Sebastolobus*. Shortspine thornyhead are the only species of *Sebastolobus* (settled juveniles and adults) reported from RACE-GAP summer bottom trawl surveys in the EBS and all of these came from the EBS Slope survey. This is also the primary thornyhead species reported in commercial fishery catches by fishery observers.

Distribution of early life history stages of *Sebastolobus* spp. in the eastern Bering Sea -- Eggs of *Sebastolobus* spp. were uncommon on EcoFOCI ichthyoplankton surveys (1991-2013) of the EBS (Fig. 128). When present, they were collected between June and August (Table 2). Occurrences were recorded from the inner, middle, and outer shelf of the central and southern portions of the survey area. Thornyhead eggs did not occur with sufficient frequency to parameterize a distribution model for this life stage.

Larval thornyheads were collected rarely on EcoFOCI ichthyoplankton surveys of the eastern Bering Sea (Fig. 129). The two occurrences of this life stage were recorded on the outer shelf north of the Pribilof Islands. No juvenile thornyheads were reported on EcoFOCI ichthyoplankton surveys. Thornyhead larvae were not sufficiently prevalent to parameterize a distribution model for this life stage.

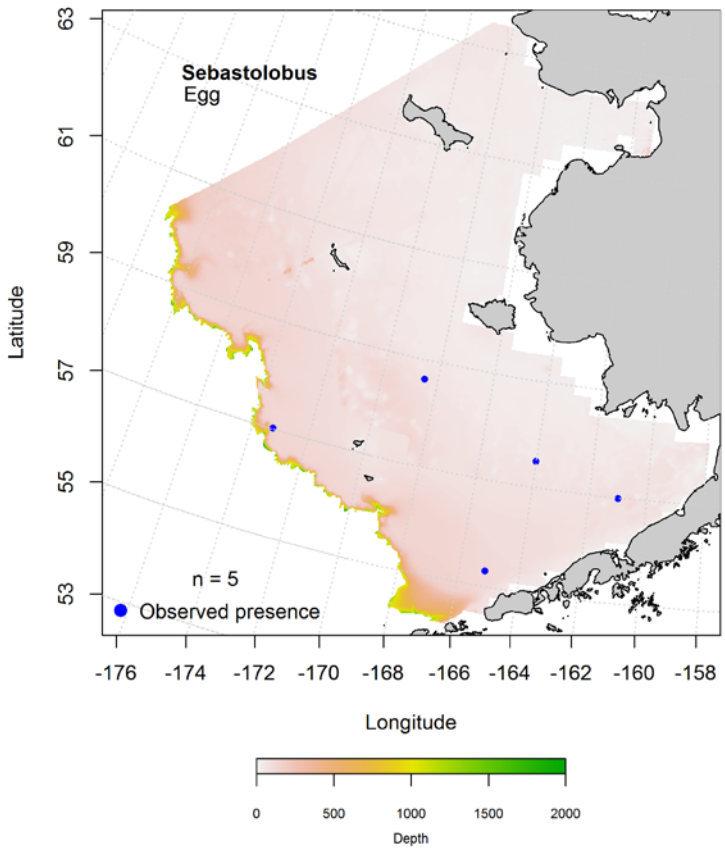

Figure 128. -- Presence of *Sebastolobus* spp. eggs in EcoFOCI ichthyoplankton surveys of the eastern Bering Sea (1991-2013).

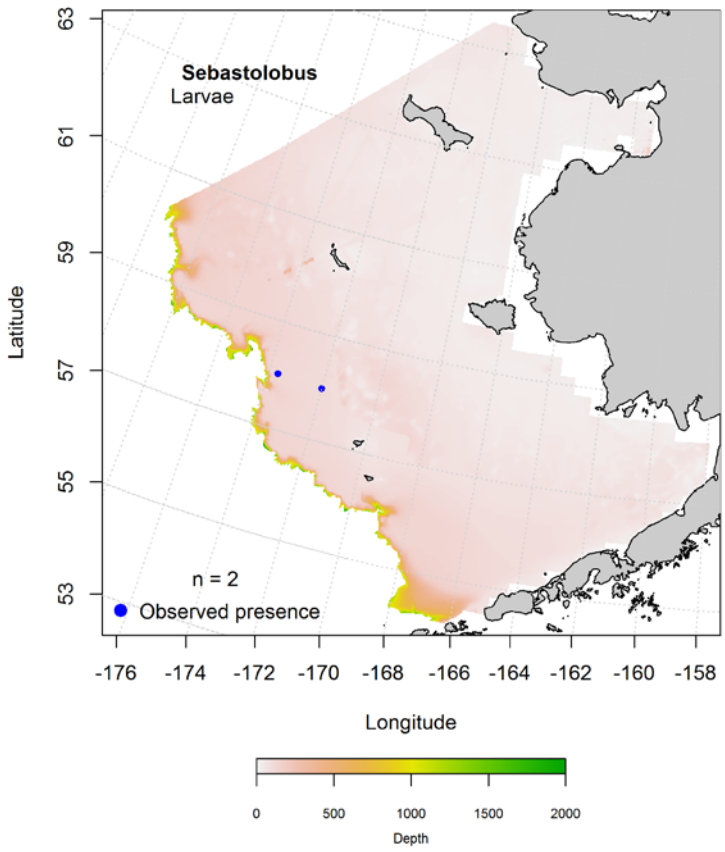

Figure 129. -- Presence of *Sebastolobus* spp. larvae in EcoFOCI ichthyoplankton surveys of the eastern Bering Sea (1991-2013).

Shortspine Thornyhead (*Sebastolobus alascanus*)

Summertime distribution of settled juvenile and adult shortspine thornyhead from RACE-GAP bottom trawl surveys of the eastern Bering Sea -- Settled juvenile shortspine thornyhead were present in RACE-GAP summer bottom trawl surveys of the EBS (1982-2014; Fig. 130). A MaxEnt model was used to predict the probability of suitable habitat for this life stage. The most important habitat covariate describing their potential habitat was bottom depth (relative importance = 90.8%). The model effect was maximized at a depth ca. 450 m. The area predicted to have the highest probability of suitable settled juvenile shortspine thornyhead habitat was on the outer shelf in the southern portion of the survey area. The MaxEnt model fit to the training data was outstanding (AUC = 0.99) and correctly classified

97% of predicted cases. The model fit to the test data in the validation step was also outstanding (AUC = 0.97) and correctly classified 97% of predicted cases.

Adult shortspine thornyhead were relatively prevalent at the shelf break and on the upper continental slope of the EBS in summertime RACE-GAP bottom trawl surveys (1982-2014; Fig. 131). Using a MaxEnt model to predict the probability of suitable habitat for this life stage identified that the most important habitat covariate describing its distribution was bottom depth (relative importance = 97.6%). The highest predicted probabilities for suitable habitat were associated with depths ca. 500 m for adult shortspine thornyhead. The model fit to the training data was outstanding (AUC = 0.99) and correctly classified 96% of predicted cases. Model validation using the test data set was successful (AUC = 0.96) and correctly classified 96% of predicted cases.

Seasonal distribution of the shortspine thornyhead in commercial fishery catches from the eastern Bering Sea -- Shortspine thornyheads were observed in commercial fishery catches on the outer shelf of the EBS in fall, winter, and spring (Fig. 132). MaxEnt models used to predict the probability of suitable habitat for this species determined that bottom depth was the most important covariate predicting their potential habitat in all three seasons. The relative importance of the bottom depth predictor term ranged from 73.7% in fall to 92.5% in spring and the probability of potential habitat was highest between approximately 400-800 m. Model fits to the training data were outstanding (AUC = 1 in all three seasons) and the proportion of cases correctly classified was high (97-99%). Model validation was successful (AUC = 0.95-0.98) and predictions based on the test data were correctly classified for 95 to 98% of cases.

Essential fish habitat maps and conclusions for shortspine thornyhead in the eastern Bering Sea -- Species distribution modeling results for shortspine thornyheads from catches in the EBS were translated into EFH maps (Fig. 133). Their EFH was primarily mapped onto the outer shelf in waters deeper than 200 m. Core habitat (top 25% of predictions) was typically deeper still in waters greater than 300 m deep. The EFH predicted from the RACE-GAP summer bottom trawl surveys for settled

juveniles and adults shared almost complete spatial overlap with the EFH predicted from shortspine thornyhead presence in commercial fishery catches.

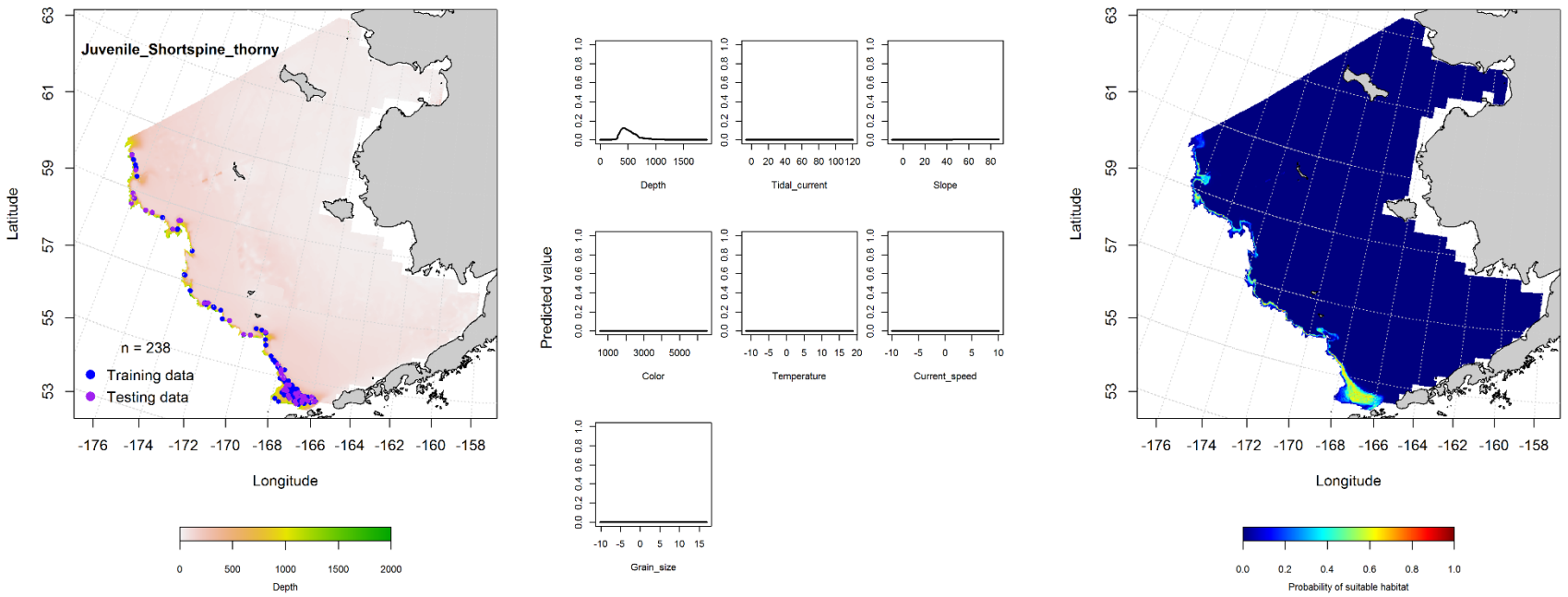

Figure 130. -- Presence of settled juvenile shortspine thornyhead in RACE-GAP summer bottom trawl surveys (1982-2014) of the eastern Bering Sea (left panel) with training (blue dots) and testing (purple dots) data sets indicated alongside the maximum entropy model (MaxEnt) effects (center panel) and the MaxEnt spatial predictions of the probability of suitable settled juvenile shortspine thornyhead habitat (right panel).

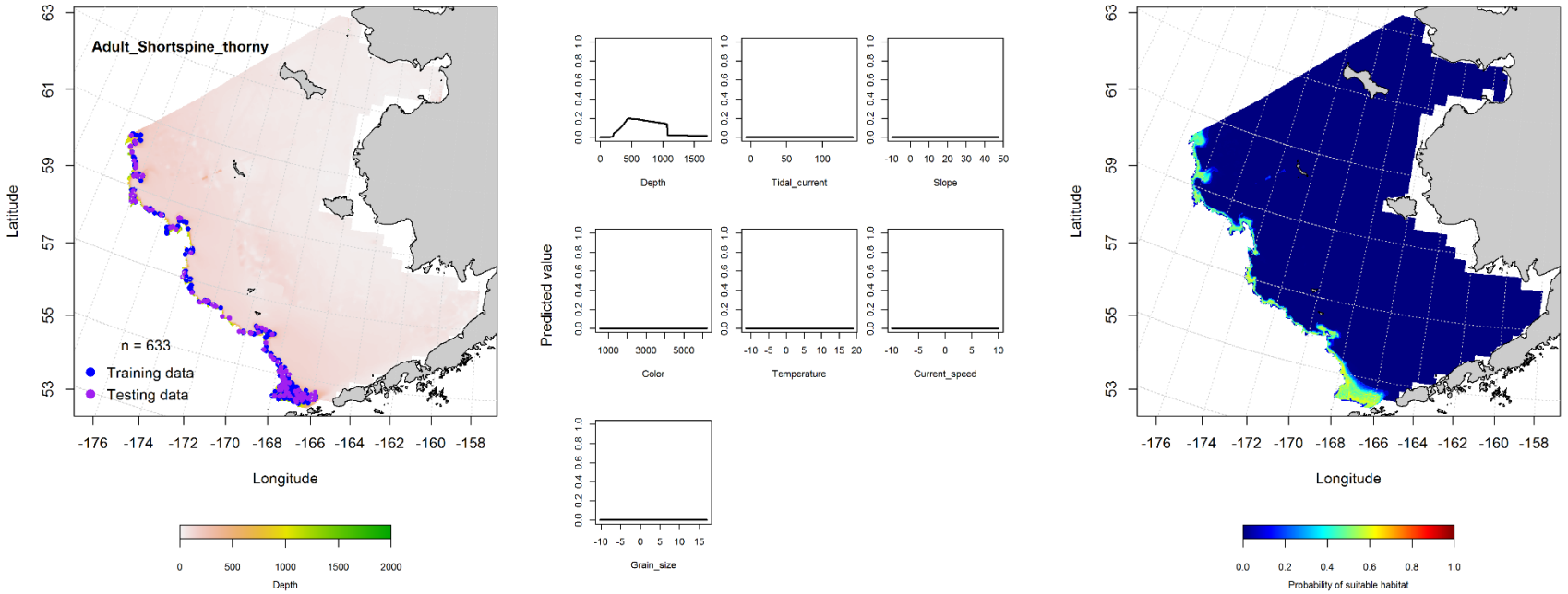

Figure 131. -- Presence of adult shortspine thornyhead in RACE-GAP summer bottom trawl surveys (1982-2014) of the eastern Bering Sea (left panel) with training (blue dots) and testing (purple dots) data sets indicated alongside the maximum entropy model (MaxEnt) effects (center panel) and the MaxEnt spatial predictions of the probability of suitable adult shortspine thornyhead habitat (right panel).

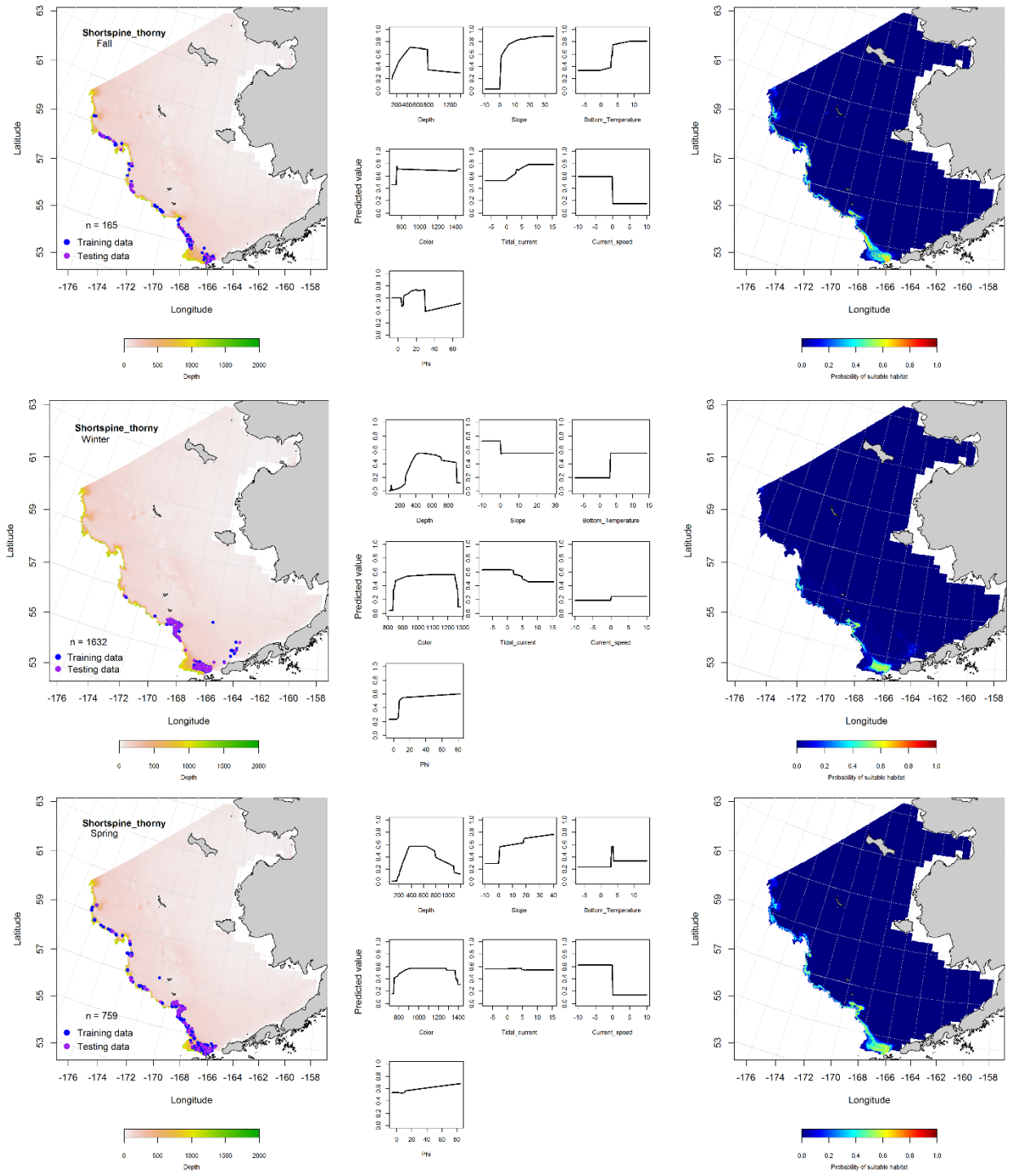

Figure 132. -- Locations of shortspine thornyhead in fall (October-November; top row), winter (December-February; middle row), and spring (March-May; bottom row) commercial fisheries catches (2003-2013) from the eastern Bering Sea (left-hand column). Blue points were used to train the MaxEnt model (center column) predicting the probability of suitable habitat (right-hand column) and the purple points were used to validate the model.

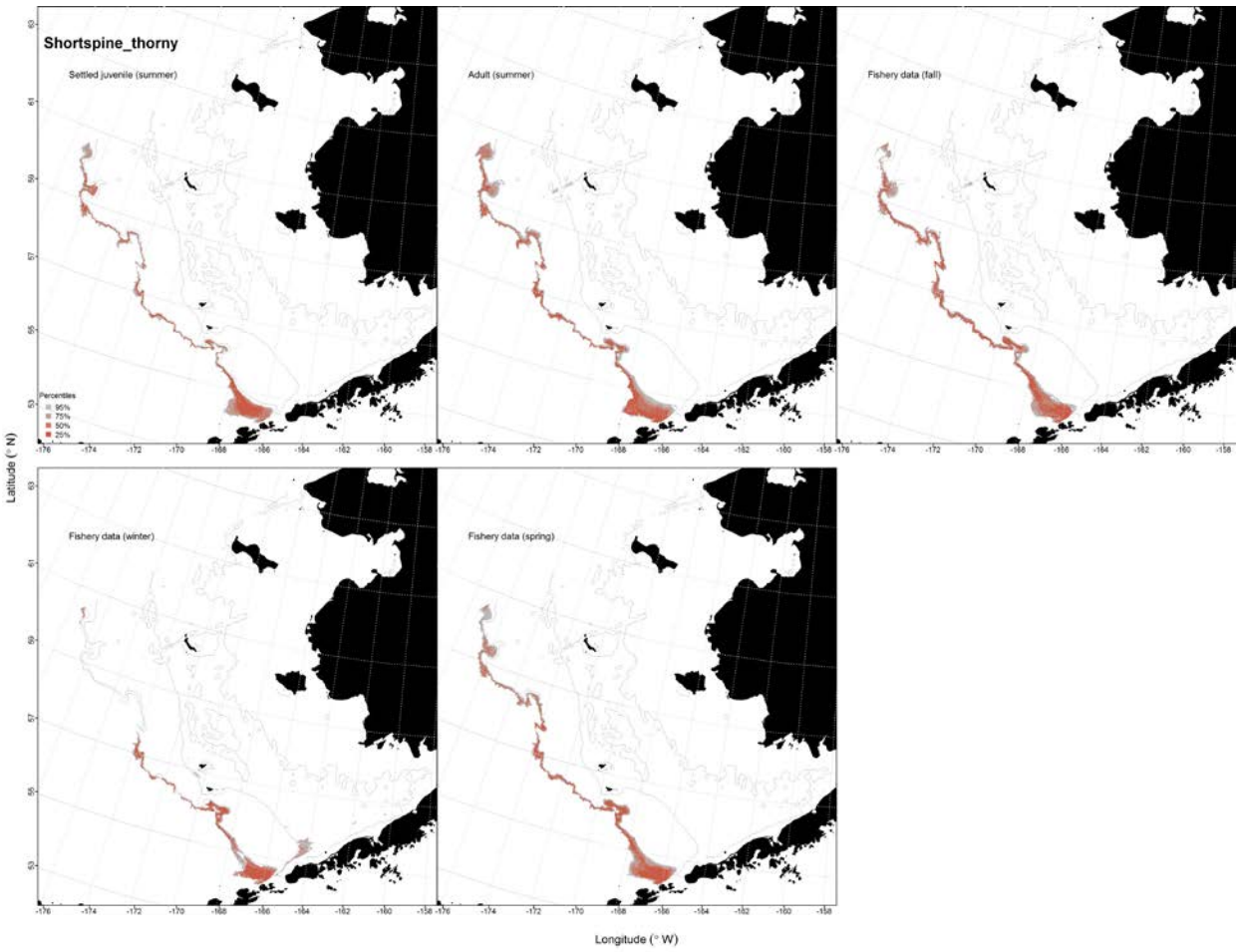

Figure 133. -- Essential fish habitat (EFH) predicted for settled juvenile (upper left panel) and adult shortspine thornyhead (upper right panel) from RACE-GAP summertime bottom trawl surveys (1982-2014) and predicted from presence in commercial fishery catches (2003-2013) from fall (upper right panel), winter, and spring (bottom two panels) in the eastern Bering Sea.

Skates

The early life history of skates determined which life stages were available to our data collection methods. Skates lay demersal eggs that hatch fully-formed, benthically-oriented juveniles. Thus, there was no expectation to encounter skates on EcoFOCI ichthyoplankton surveys. Juvenile and adult skates were available to the RACE summer bottom trawl survey and results for these life stages are reported below. Most species of skates that occur in the EBS are represented in the commercial catches from the region. The data summaries provided by AKRO in the VOE-CIA database grouped some species in a general skate category while reporting others by species. We were able to model species distribution for

Alaska and Aleutian skates from these data, but Bering skate were not reported separately and so their distribution was not modeled from the commercial fishery observer data.

Aleutian Skate (*Bathyraja aleutica*)

Summertime distribution of juvenile and adult Aleutian skate from RACE-GAP bottom trawl surveys of the eastern Bering Sea -- Juvenile Aleutian skates were primarily distributed across the outer shelf of the EBS in RACE-GAP summer bottom trawl surveys (1999-2014) from the Alaska Peninsula to the U.S.-Russia Convention Line in the north (Fig. 134). An hGAM was used to model their distribution. The most significant habitat covariates retained in the best-fitting presence-absence GAM were bottom depth, geographic location, and sediment grain size. The probability of juvenile Aleutian skate presence increased with increasing depth and decreasing sediment grain size in the western portion of the survey area. This GAM explained 70.5% of the deviance in their distribution data. The model fit to the training data and to the test data in the validation step was outstanding (AUC = 0.98 in both cases). The training data model correctly classified slightly more predicted cases than did the test data (95 vs. 94%). Abundance of juvenile Aleutian skate was predicted at locations where the threshold probability of occurrence (0.14) established in the presence-absence GAM above was met or exceeded. The most important covariates describing the habitat for juvenile Aleutian skates based on their conditional abundance were bottom depth and geographic position where predicted CPUE increased with increasing depth in the western portion of the survey area (i.e., the outer shelf of the EBS). This conditional abundance GAM explained 40.8% of the deviance in their CPUE at these sites and the model fit was marginal ($r^2 = 0.41$). The model fit to the test data in the validation step was less ($r^2 = 0.30$).

Adult Aleutian skates were distributed across the outer shelf of the EBS in RACE-GAP summer bottom trawl survey catches (1999-2014) between the Alaska Peninsula and the U.S.-Russia Convention Line in the north (Fig. 135). A MaxEnt model identified that adult Aleutian skate distribution was

primarily determined by bottom depth (relative importance = 81.7%) over the outer shelf of the EBS with a peak in the predicted probability of suitable habitat ca. 250 m depth. The MaxEnt model was an outstanding fit to the training data (AUC = 0.98) and correctly classified 96% of predicted cases. In the model validation step, the fit was outstanding as well (AUC = 0.97) correctly classifying 97% of cases predicted from the test data.

Seasonal distribution of Aleutian skate in commercial fishery catches from the eastern Bering Sea -- Aleutian skates were observed in commercial fishery catches primarily from the middle and outer shelf of the EBS in fall, winter, and spring (Fig. 136). MaxEnt models used to predict the probability of suitable habitat for this species determined that bottom depth and bottom temperature were the most important covariates predicting their potential habitat in all three seasons. The combined relative importance of the two predictor terms ranged from 84.3% in fall to 73.2% in spring and the probability of potential habitat was highest in waters deeper than 200 m where the bottom temperature was ca. 5°C. Model fits to the training data were outstanding (AUC = 0.92-0.95) and the proportion of cases correctly classified was moderately high (84-89%). Model validation was successful (AUC = 0.86 for all three seasons) and predictions based on the test data were correctly classified for 86% of cases.

Essential fish habitat maps and conclusions for Aleutian skate (*Bathyraja aleutica*) in the eastern Bering Sea -- Species distribution modeling results for Aleutian skates from RACE-GAP summer bottom trawl surveys and catches in commercial fisheries were translated into EFH maps (Fig. 137). Summertime distribution of predicted EFH was primarily constrained to the outer shelf of the EBS. The EFH distribution based on commercial fishery catches incorporated the outer shelf, but extended inshore onto the middle and inner shelf as well. Much of the core habitat (top 25% of predictions) was predicted to be in deeper waters (≥ 200 m) although there were some shallower exceptions from the commercial fishery data predictions.

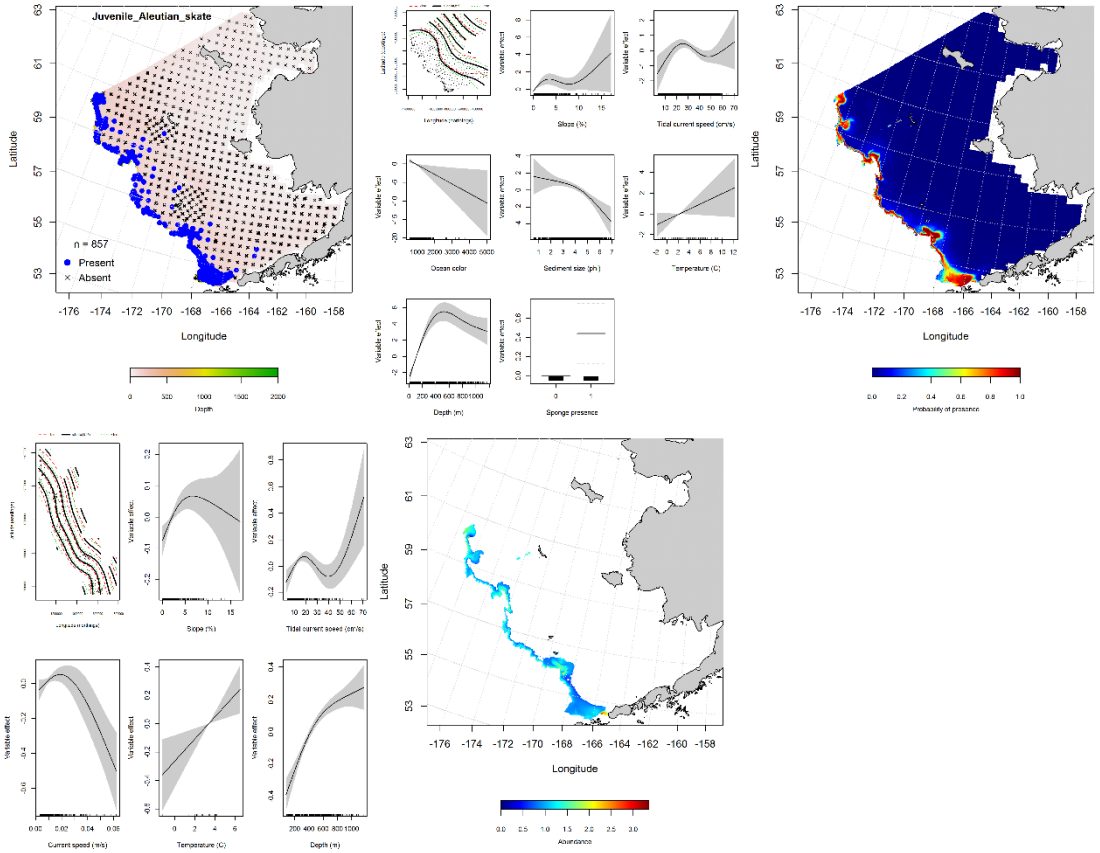

Figure 134. -- Distribution of juvenile Aleutian skates in 1999-2014 RACE-GAP summer bottom trawl surveys conducted in the eastern Bering Sea (upper left panel) and the effects of retained habitat covariates in the best-fitting generalized additive model (GAM) of presence-absence (upper center panel) spatially predicting the probability of their presence (upper right panel); the best-fitting abundance GAM (lower left panel) conditionally predicts juvenile Aleutian skate catch-per-unit-effort (CPUE) at sites where the optimum threshold for probability of presence was met or exceeded (lower center panel).

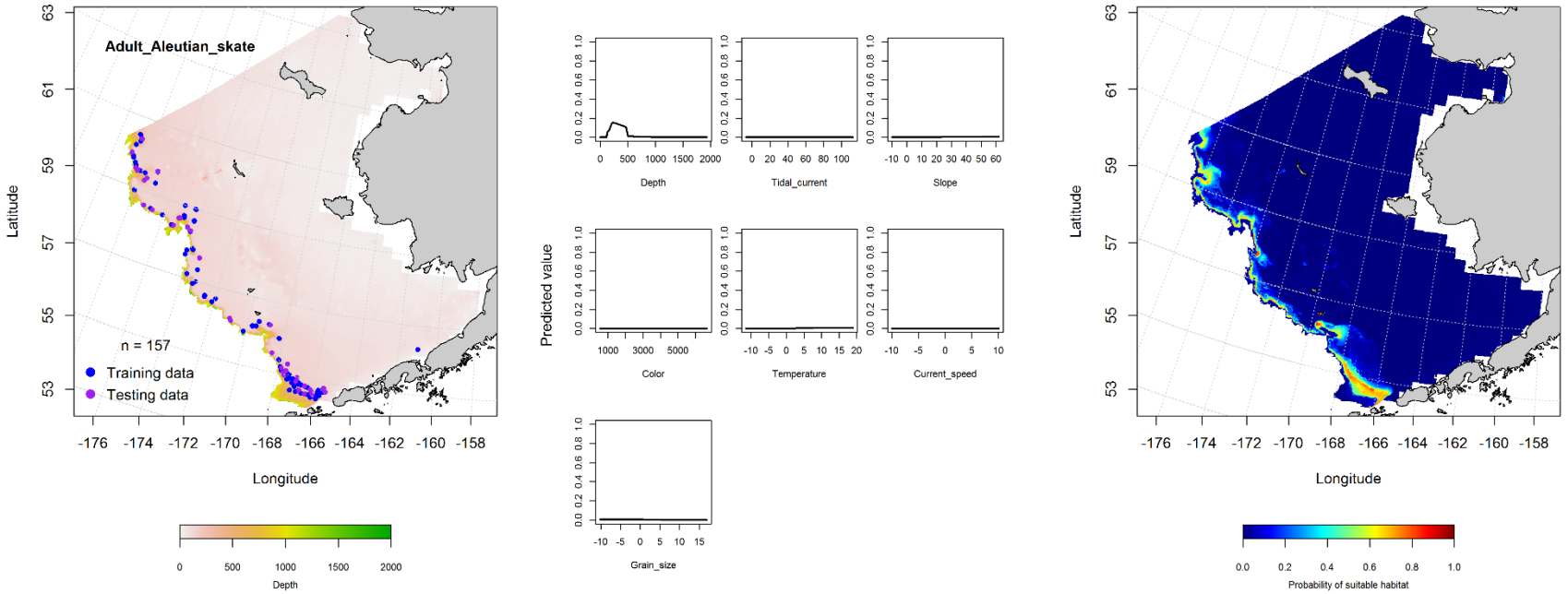

Figure 135. -- Presence of adult Aleutian skates in RACE-GAP summer bottom trawl surveys (1999-2014) of the eastern Bering Sea (left panel) with training (blue dots) and testing (purple dots) data sets indicated alongside the maximum entropy model (MaxEnt) effects (center panel) and the MaxEnt spatial predictions of the probability of suitable adult Aleutian skate habitat (right panel).

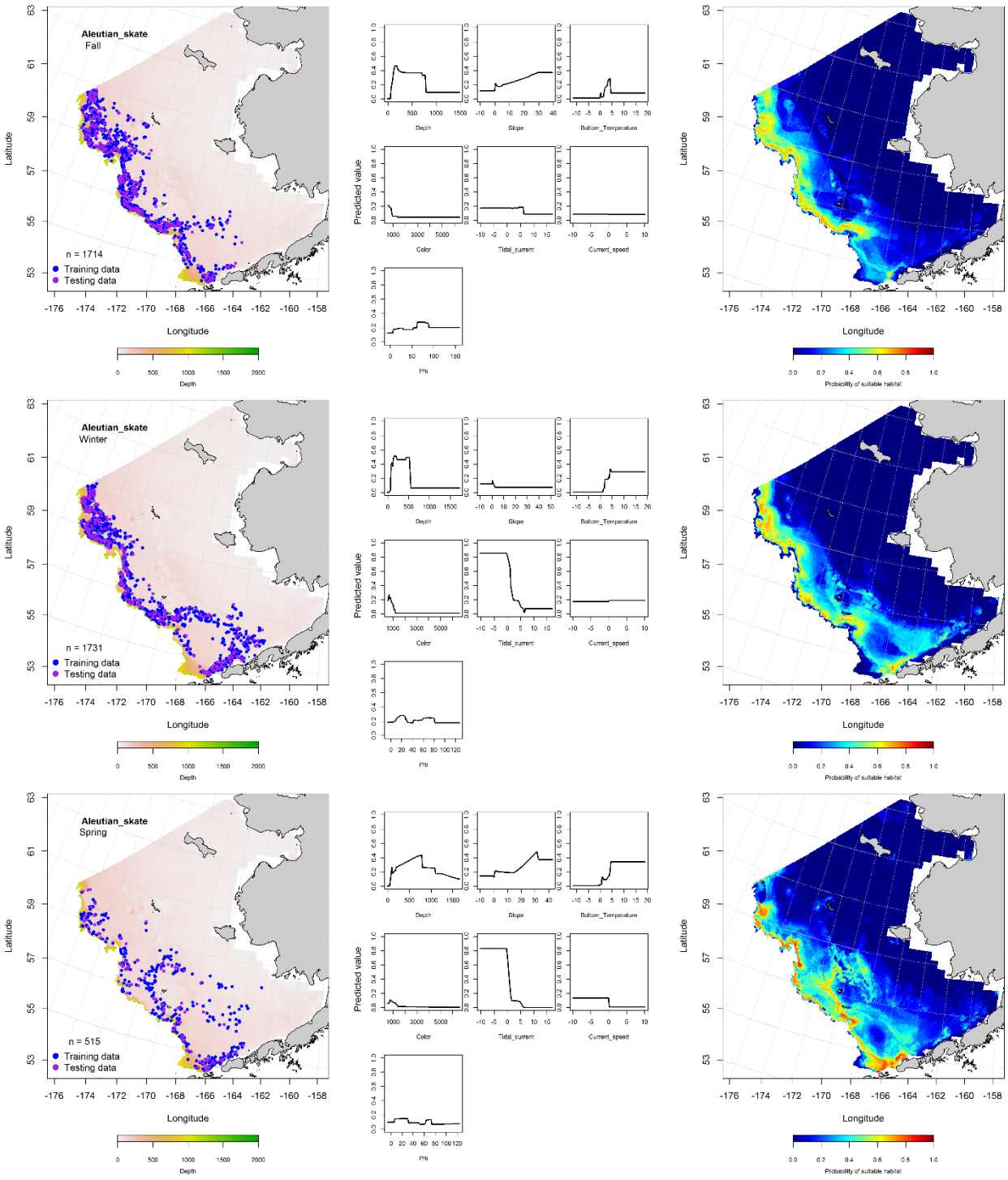

Figure 136. -- Locations of Aleutian skate in fall (October-November; top row), winter (December-February; middle row), and spring (March-May; bottom row) commercial fisheries catches (2003-2013) from the eastern Bering Sea (left-hand column). Blue points were used to train the MaxEnt model (center column) predicting the probability of suitable habitat (right-hand column) and the purple points were used to validate the model.

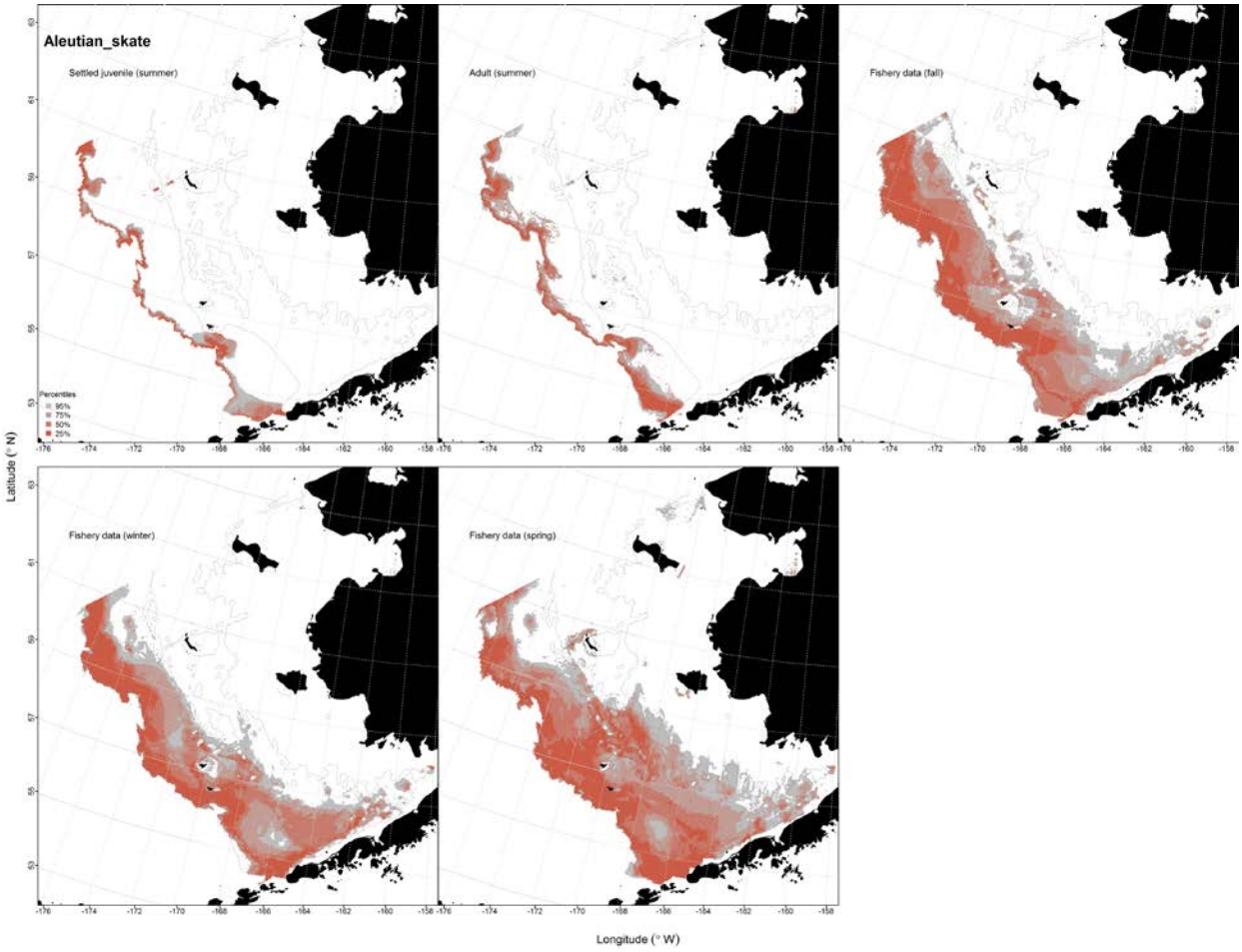

Figure 137. -- Essential fish habitat (EFH) predicted for juvenile and adult Aleutian skate (upper left and middle panels) from RACE-GAP summertime bottom trawl surveys (1999-2014) and predicted from presence in commercial fishery catches (2003-2013) from fall (upper right panel), winter, and spring (bottom two panels) in the eastern Bering Sea.

Bering Skate (*Bathyraja interrupta*)

Summertime distribution of juvenile and adult Bering skate from RACE-GAP bottom trawl surveys of the eastern Bering Sea -- Juvenile Bering skates were distributed across the middle and outer shelf of the EBS in RACE-GAP summer bottom trawl surveys (1999-2014) from the Alaska Peninsula to the U.S.-Russia Convention Line (Fig. 138). An hGAM was used to identify and model the habitat covariates describing their distribution in the EBS. The most significant habitat covariates retained in the best-fitting presence-absence GAM were bottom depth and geographic location. The probability of

juvenile Bering skate presence was highest in the western portion of the survey area at depths around 300 m. This GAM explained 46.3% of the deviance in their distribution data, was an outstanding model fit to the training data (AUC = 0.93), and correctly classified 86% of predicted cases. Model validation was successful (AUC = 0.93) and also correctly classified 86% of predicted presence-absence cases. Abundance of juvenile Bering skate was predicted at locations where the threshold probability of occurrence (0.22) established in the presence-absence GAM above was met or exceeded. The most important covariates describing the habitat for juvenile Bering skates based on their conditional abundance remained bottom depth and geographic position and predicted CPUE increased with increasing depth (up to ca. 300 m) in the central western portion of the survey area. This conditional abundance GAM explained 32.2% of the deviance in their CPUE at these sites ($r^2 = 0.32$). The model fit to the test data in the validation step was slightly less ($r^2 = 0.27$).

Adult Bering skate in RACE-GAP summer bottom trawl surveys (1999-2014) share a similar distribution to settled juveniles but with greater prevalence on the middle shelf of the EBS (Fig. 139). An hGAM identified the habitat covariates describing adult Bering skate distribution in the EBS. The most significant habitat covariates retained in the best-fitting presence-absence GAM were geographic location, bottom depth, and sediment size. The probability of their presence was highest in the western portion of the survey area over coarser sediments and decreased with increasing depth greater than 300 m. This GAM explained 38.6% of the deviance in their distribution data, was an outstanding model fit to the training data (AUC = 0.90), and correctly classified 83% of predicted cases. Model validation was successful (AUC = 0.90) and also correctly classified 83% of predicted presence-absence cases. Abundance of adult Bering skate was predicted at locations where the threshold probability of occurrence (0.23) established in the presence-absence GAM above was met or exceeded. The most important habitat covariates describing distribution of adult Bering skates based on their conditional abundance were ocean productivity, geographic location, and tidal current maxima. Predicted CPUE was highest in the southern portion of the survey area where maximum tidal current speeds were lower and ocean productivity was

moderate. This conditional abundance GAM explained just 13.8% of the deviance in their CPUE at these sites ($r^2 = 0.14$). The model fit to the test data in the validation step was similar to that of the training set ($r^2 = 0.15$).

Essential fish habitat maps and conclusions for Bering skate (*Bathyraja interrupta*) in the eastern Bering Sea -- Results of the species distribution modeling for Bering skates from RACE-GAP summer bottom trawl surveys were transformed into EFH maps (Fig. 140). Summertime distribution of predicted EFH was constrained to the outer shelf of the EBS and generally to waters deeper than 200 m. Much of the core habitat (top 25% of predictions) was predicted to be in deeper waters (≥ 300 m). No commercial fisheries observations of Bering skate were reported in the VOE-CIA data provided by the AKRO.

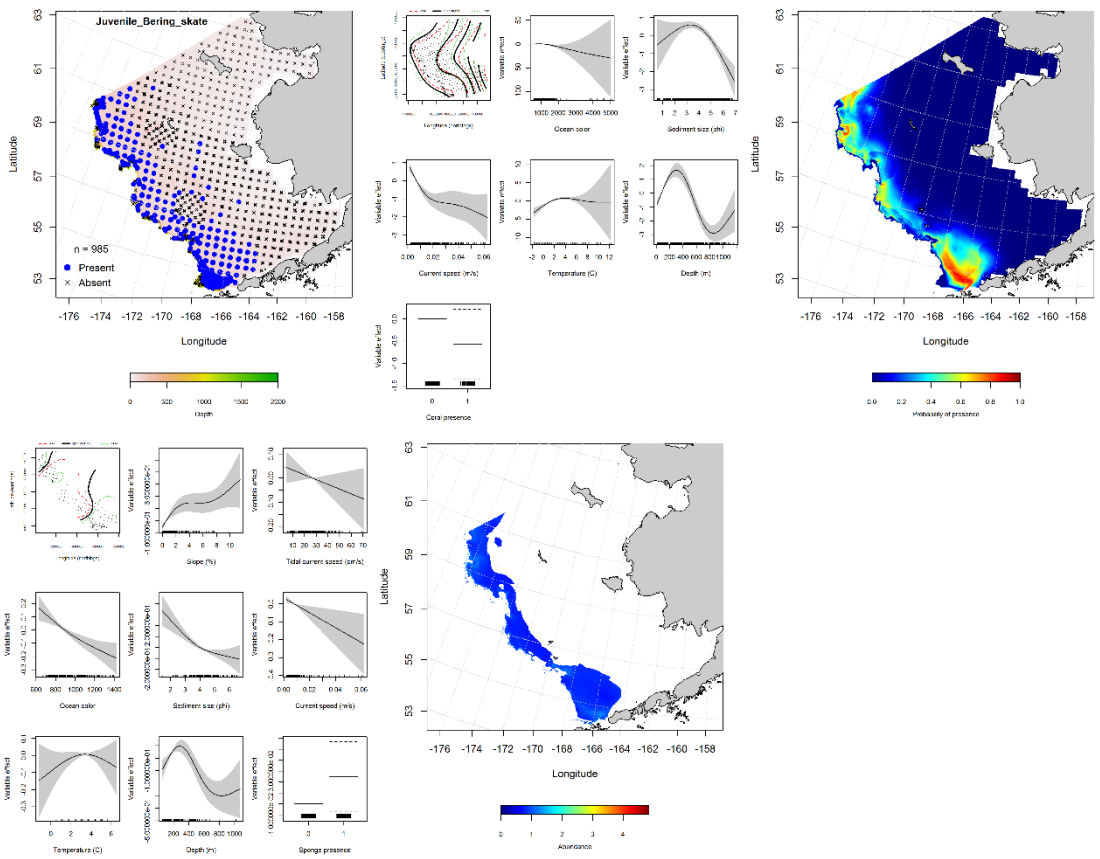

Figure 138. -- Distribution of juvenile Bering skate in 1999-2014 RACE-GAP summer bottom trawl surveys conducted in the eastern Bering Sea (upper left panel) and the effects of retained habitat covariates in the best-fitting generalized additive model (GAM) of presence-absence (upper center panel) spatially predicting the probability of their presence (upper right panel); the best-fitting abundance GAM (lower left panel) conditionally predicts juvenile Bering skate catch-per-unit-effort (CPUE) at sites where the optimum threshold for probability of presence was met or exceeded (lower center panel).

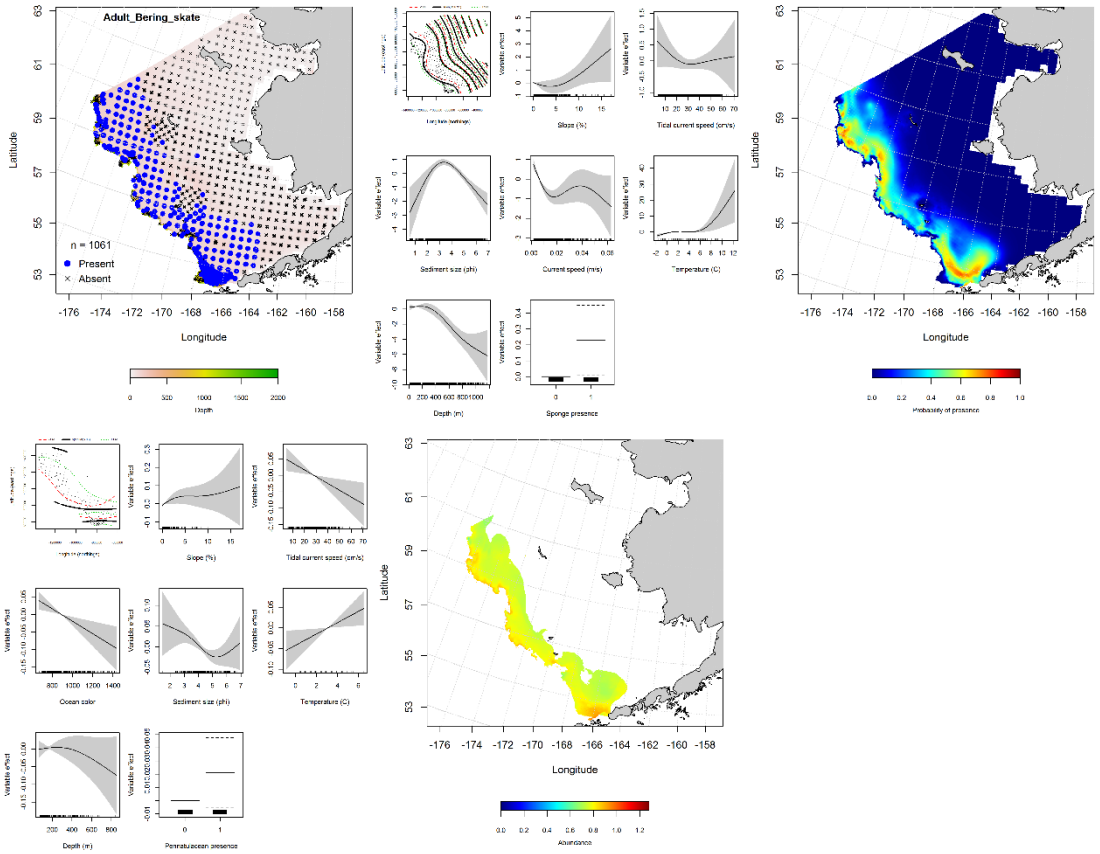

Figure 139. -- Distribution of adult Bering skate in 1999-2014 RACE-GAP summer bottom trawl surveys conducted in the eastern Bering Sea (upper left panel) and the effects of retained habitat covariates in the best-fitting generalized additive model (GAM) of presence-absence (upper center panel) spatially predicting the probability of their presence (upper right panel); the best-fitting abundance GAM (lower left panel) conditionally predicts adult Bering skate catch-per-unit-effort (CPUE) at sites where the optimum threshold for probability of presence was met or exceeded (lower center panel).

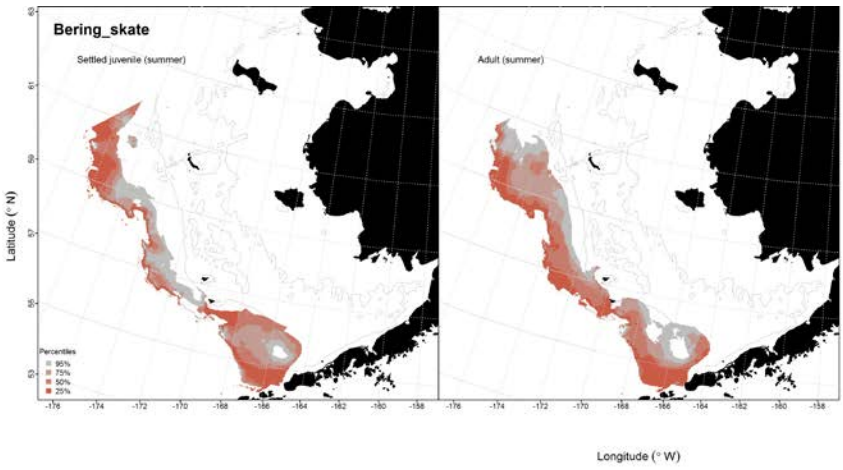

Figure 140. -- Essential fish habitat (EFH) predicted for juvenile and adult Bering skate from RACE-GAP summertime bottom trawl surveys (1999-2014) in the eastern Bering Sea.

Alaska Skate (*Bathyraja parmifera*)

Summertime distribution of juvenile and adult Alaska skate from RACE-GAP bottom trawl surveys of the eastern Bering Sea -- Juvenile Alaska skates occurred from the inner shelf on to the outer shelf (< 600 m) in RACE-GAP summer bottom trawl surveys of the EBS (1999-2014) from Bristol Bay and the Alaska Peninsula into the northern Bering Sea (Fig. 141). Distribution of juvenile Alaska skates in the EBS was modeled using a standard GAM of abundance data from the bottom trawl survey. The most significant habitat covariates retained in the best-fitting GAM were geographic location, bottom temperature, and bottom depth. Model effects were highest in the central region of the EBS, increased with increasing temperature, and decreased with increasing bottom depth. This model using the training data set explained 45.1% of the deviance in their CPUE data ($r^2 = 0.45$). The model fit to the test data was higher ($r^2 = 0.50$).

Adult Alaska skate distribution in RACE-GAP summer bottom trawl surveys of the EBS (1999-2014) mirrored that of the settled juveniles with an additional incursion into Norton Sound

(Fig. 142). Using an hGAM, the distribution of adult Alaska skate in the EBS was modeled from habitat covariates. The most significant predictors retained in the best-fitting presence-absence GAM were geographical location and bottom temperature and the complete model explained 20.8% of the deviance in their distribution. The probability of adult Alaska skate presence increased to the west of the survey area over increasing bottom temperatures. This GAM, using the training data set, had an acceptable fit (AUC = 0.77) and correctly classified 70% of predicted presence-absence case. Model validation using the test data had similar fit (AUC = 0.76) and predictive success; correctly classifying 70% of cases. Abundance of adult Alaska skate was predicted at locations where the threshold probability of occurrence (0.56) established in the presence-absence GAM above was met or exceeded. The most important habitat covariates describing their distribution from their conditional abundance remained geographic location and bottom temperature. Predicted CPUE was highest in the northwestern portion of the survey area and over increasing bottom temperatures. This conditional abundance GAM explained just 21.1% of the deviance in their CPUE at these sites ($r^2 = 0.21$). The model fit to the test data in the validation step was less ($r^2 = 0.12$).

Seasonal distribution of Alaska skate in commercial fishery catches from the eastern Bering Sea -- Alaska skates were observed in fall, winter, and spring commercial fishery catches primarily on the middle and outer shelf of the EBS (Fig. 143). MaxEnt models used to predict the probability of suitable habitat for this species determined that bottom depth and bottom temperature were consistently among the most important covariates predicting their potential habitat in all three seasons. The combined relative importance of the two predictor terms ranged from 79.3% in spring to 90.8% in winter and the probability of potential habitat was highest in waters ca. 200 m where the bottom temperature was ca. 5°C. Model fits to the training data ranged from excellent to outstanding (AUC = 0.86-0.93) and the proportion of cases correctly classified was moderately high (79-85%). Model validation was successful (AUC = 0.79-0.85) and predictions based on the test data correctly classified for 79 to 85% of predicted cases.

Essential fish habitat maps and conclusions for Alaska skate (*Bathyraja parmifera*) in the eastern Bering Sea – Results of the species distribution modeling for Alaska skates from RACE-GAP summer bottom trawl surveys were transformed into EFH maps (Fig. 144). Predicted summertime distribution of juvenile Alaska Skate EFH extended from the inner to the outer shelf of the EBS covering the majority of the survey area. Predicted EFH for adults extended from the inner to outer shelf in the central portion of the study area, but in the northern and southern portions was constrained to the middle and outer shelf. Much of the core habitat (top 25% of predictions) for adults (presumed in the case of EFH predicted from commercial catches) was predicted to be in waters deeper than 200 m.

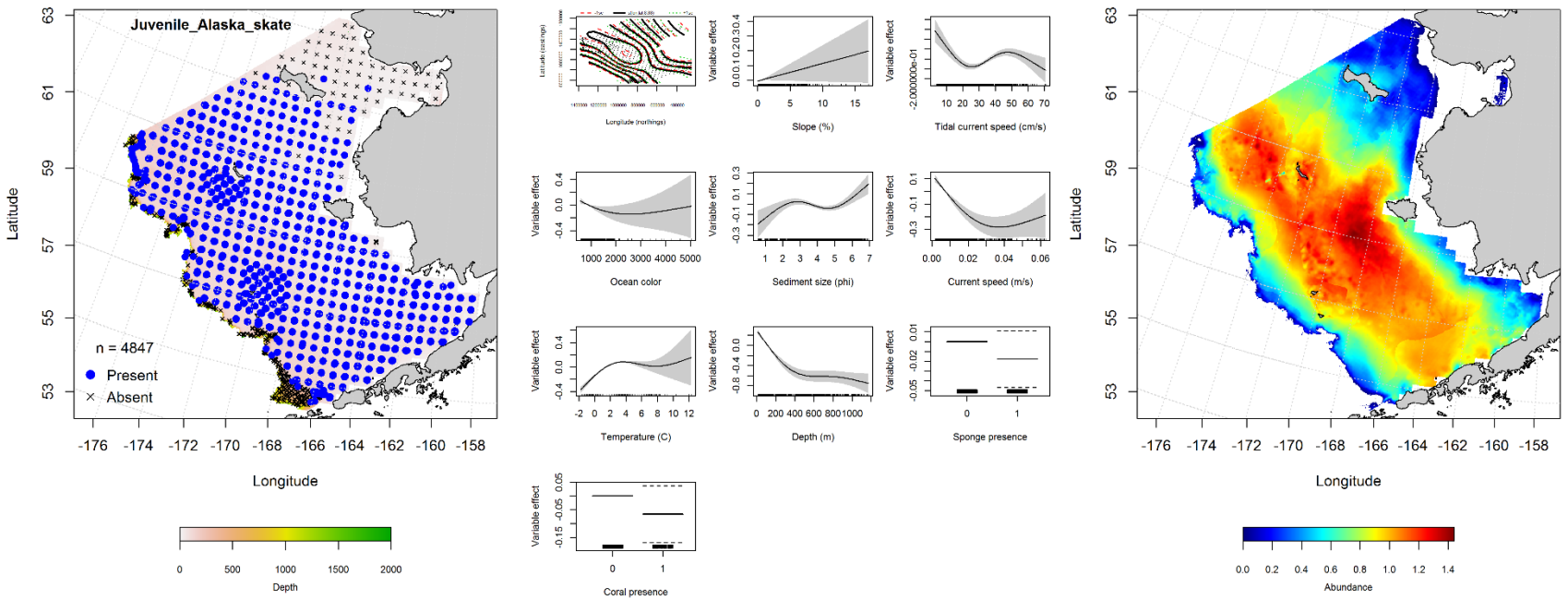

Figure 141. -- Distribution of juvenile Alaska skate in 1999-2014 RACE-GAP summer bottom trawl surveys (left panel) alongside effects of retained habitat covariates in the best-fitting generalized additive model (GAM; center panel) predicting spatial distribution of abundance (CPUE, right panel) across the eastern Bering Sea.

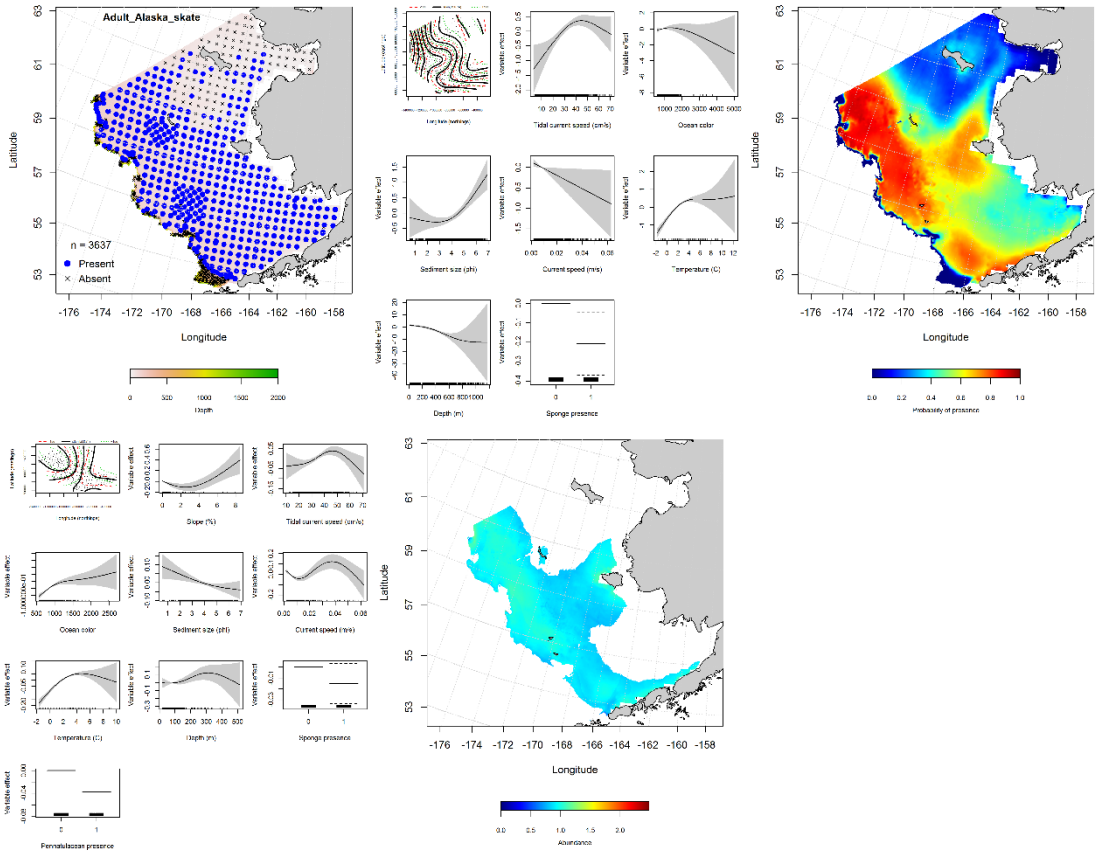

Figure 142. -- Distribution of adult Alaska skate in 1999-2014 RACE-GAP summer bottom trawl surveys conducted in the eastern Bering Sea (upper left panel) and the effects of retained habitat covariates in the best-fitting generalized additive model (GAM) of presence-absence (upper center panel) spatially predicting the probability of their presence (upper right panel); the best-fitting abundance GAM (lower left panel) conditionally predicts adult Alaska skate catch-per-unit-effort (CPUE) at sites where the optimum threshold for probability of presence was met or exceeded (lower center panel).

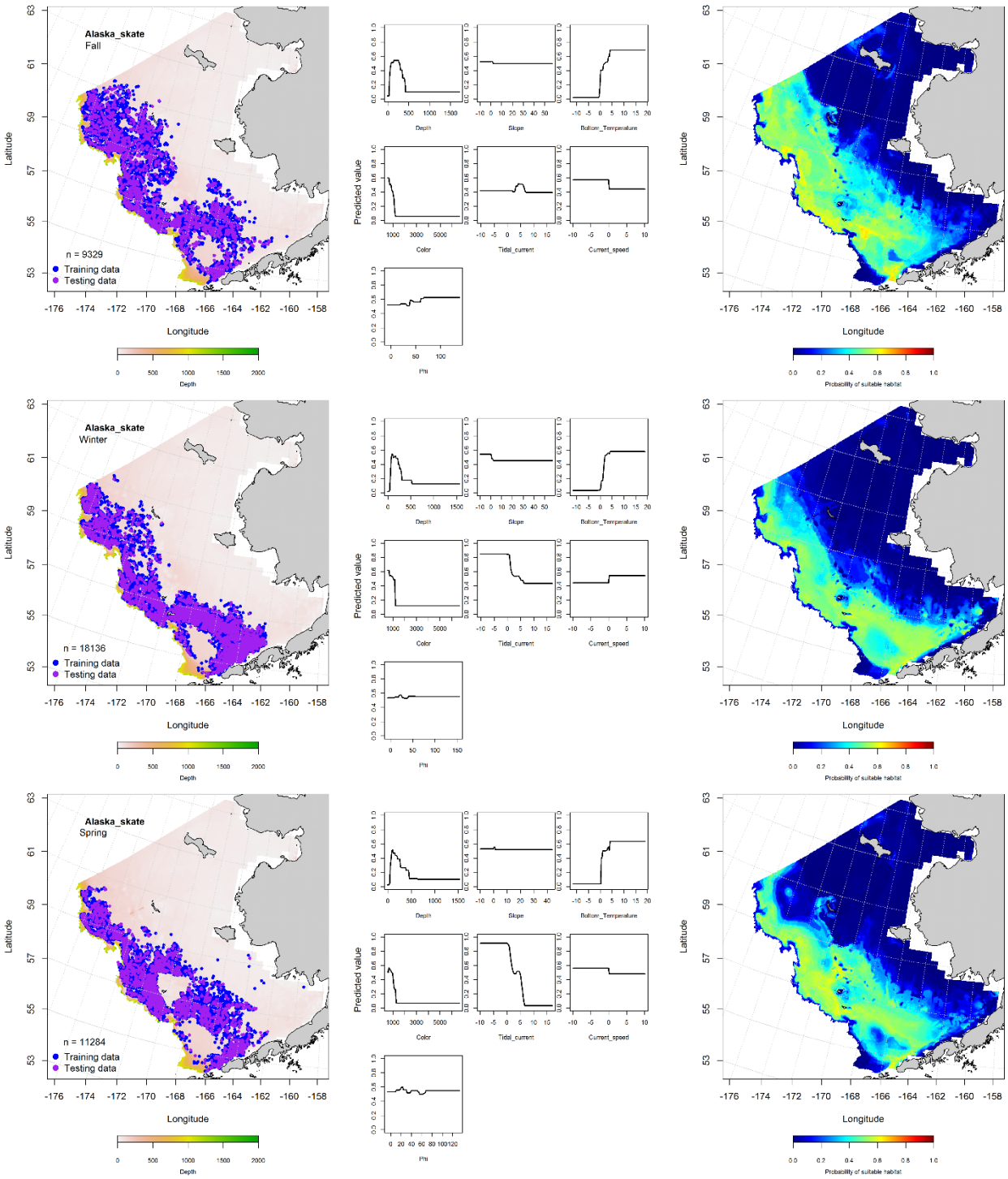

Figure 143. -- Locations of Alaska skate in fall (October-November; top row), winter (December-February; middle row), and spring (March-May; bottom row) commercial fisheries catches (2003-2013) from the eastern Bering Sea (left-hand column). Blue points were used to train the MaxEnt model (center column) predicting the probability of suitable habitat (right-hand column) and the purple points were used to validate the model.

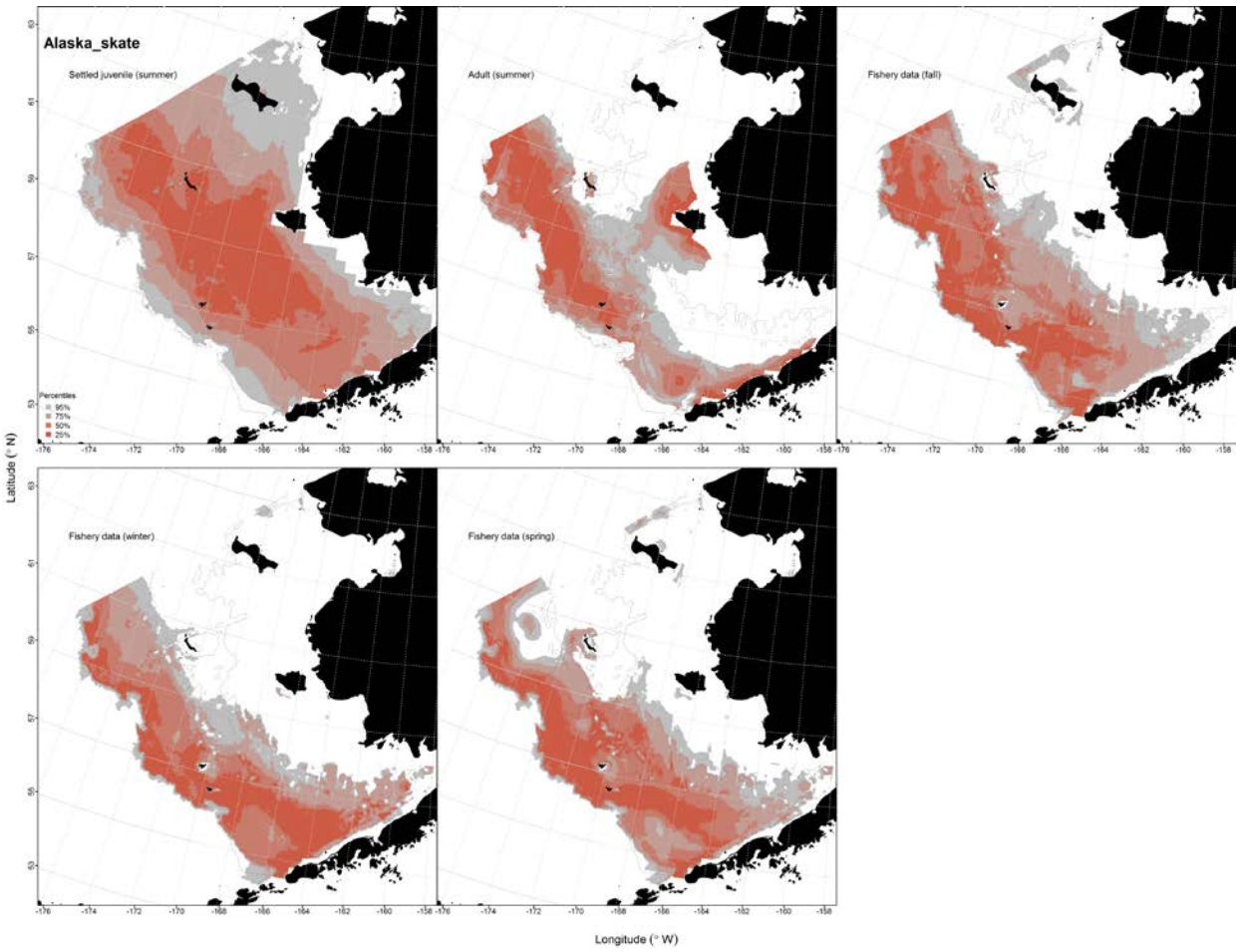

Figure 144. -- Essential fish habitat (EFH) predicted for juvenile and adult Alaska skate (upper left and middle panels) from RACE-GAP summertime bottom trawl surveys (1999-2014) and predicted from presence in commercial fishery catches (2003-2013) from fall (upper right panel), winter, and spring (bottom two panels) in the eastern Bering Sea.

Invertebrates

Southern Tanner crab (*Chionoecetes bairdi*)

Summertime distribution of southern Tanner crab from RACE-GAP bottom trawl surveys of the eastern Bering Sea -- Southern Tanner crabs occurred in RACE-GAP summer bottom trawl surveys of the EBS (1982-2014) from the inner shelf in Bristol Bay to the outer shelf in the northern Bering Sea (Fig. 145). Their distribution in the EBS was modeled using a standard GAM of abundance

data from the bottom trawl survey. The most significant habitat covariates retained in the best-fitting GAM were geographic location, sediment grain size, and bottom depth. Model effects were highest in the southwestern portion of the EBS, increased with decreasing sediment grain size and decreased with increasing bottom depth. Capture depths for this species ranged from ca. 20 m to greater than 700 m. The highest abundances were predicted in the southwestern and central portions of the middle and outer shelf. Using the training data set, this model explained more than half (54.2%) of the deviance in their CPUE data ($r^2 = 0.54$); the model fit to the test data was the same ($r^2 = 0.54$).

Seasonal distribution of southern Tanner crab in commercial fishery catches from the eastern Bering Sea -- Southern Tanner crab were observed in fall, winter, and spring commercial fishery catches primarily on the middle and outer shelf of the EBS and with slightly greater prevalence in the southern portion of the survey area (Fig. 146). MaxEnt models used to predict the probability of suitable habitat for this species determined that bottom depth, ocean productivity, sediment grain size, and bottom temperature were consistently among the most important covariates predicting their potential habitat in all three seasons. The combined relative importance of these four predictor terms ranged from 78.3% in spring to 83.1% in fall and the probability of potential habitat was highest in waters ca. 100 m deep with moderate ocean productivity, coarser sediments, and bottom temperatures greater than 0°C. Model fits to the training data were outstanding (AUC = 0.91-0.96) and the proportion of cases correctly classified was high (83-90%). Model validation was successful (AUC = 0.82-0.90) and predictions based on the test data correctly classified for 82 to 90% of predicted cases.

Essential habitat maps and conclusions for southern Tanner crab (*Chionoecetes bairdi*) in the eastern Bering Sea -- Results of the species distribution modeling for southern Tanner crab from RACE-GAP summer bottom trawl surveys and seasonal commercial fishery observer data were transformed into EFH maps (Fig. 147). The distribution of predicted EFH generally covered the middle and outer shelf o the EBS with the notable exception of EFH on the inner shelf in Bristol Bay. Southern Tanner crab EFH extends from the Alaska Peninsula northward to the U.S.-Russia Convention Line. Core

habitat for this species (top 25% of predictions) was found mostly over the middle and outer shelf of the southwestern portion of the survey area.

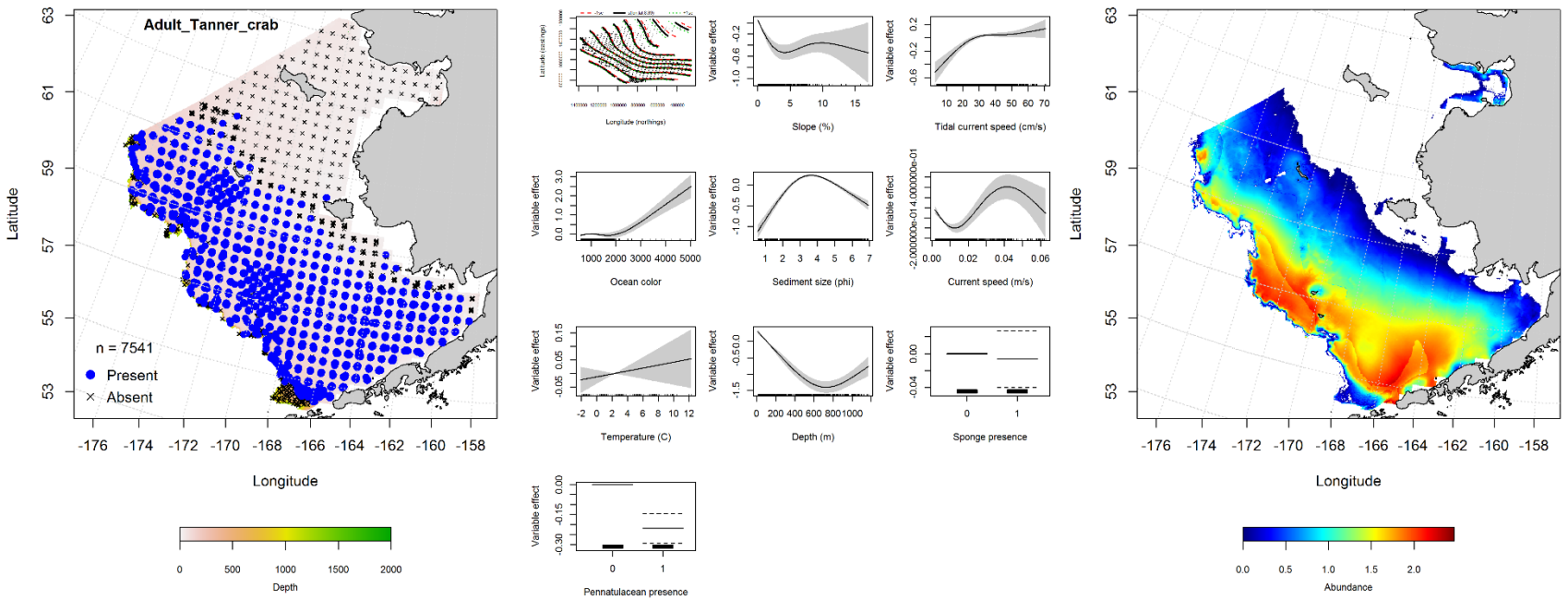

Figure 145. -- Distribution of southern Tanner crab in 1982-2014 RACE-GAP summer bottom trawl surveys (left panel) alongside effects of retained habitat covariates in the best-fitting generalized additive model (GAM; center panel) predicting spatial distribution of abundance (CPUE, right panel) across the eastern Bering Sea.

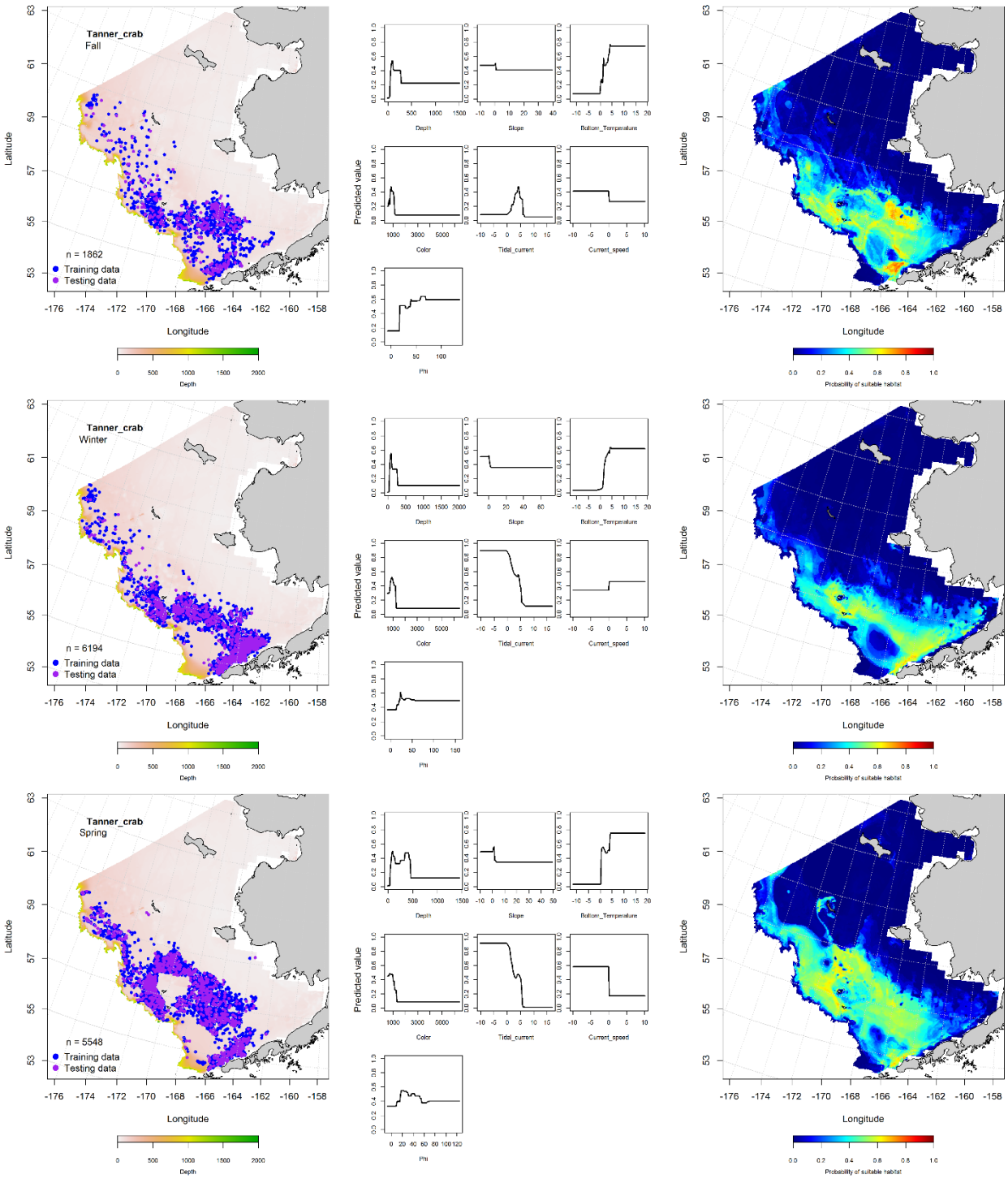

Figure 146. -- Locations of southern Tanner crab in fall (October-November; top row), winter (December-February; middle row), and spring (March-May; bottom row) commercial fisheries catches (2003-2013) from the eastern Bering Sea (left-hand column). Blue points were used to train the MaxEnt model (center column) predicting the probability of suitable habitat (right-hand column) and the purple points were used to validate the model.

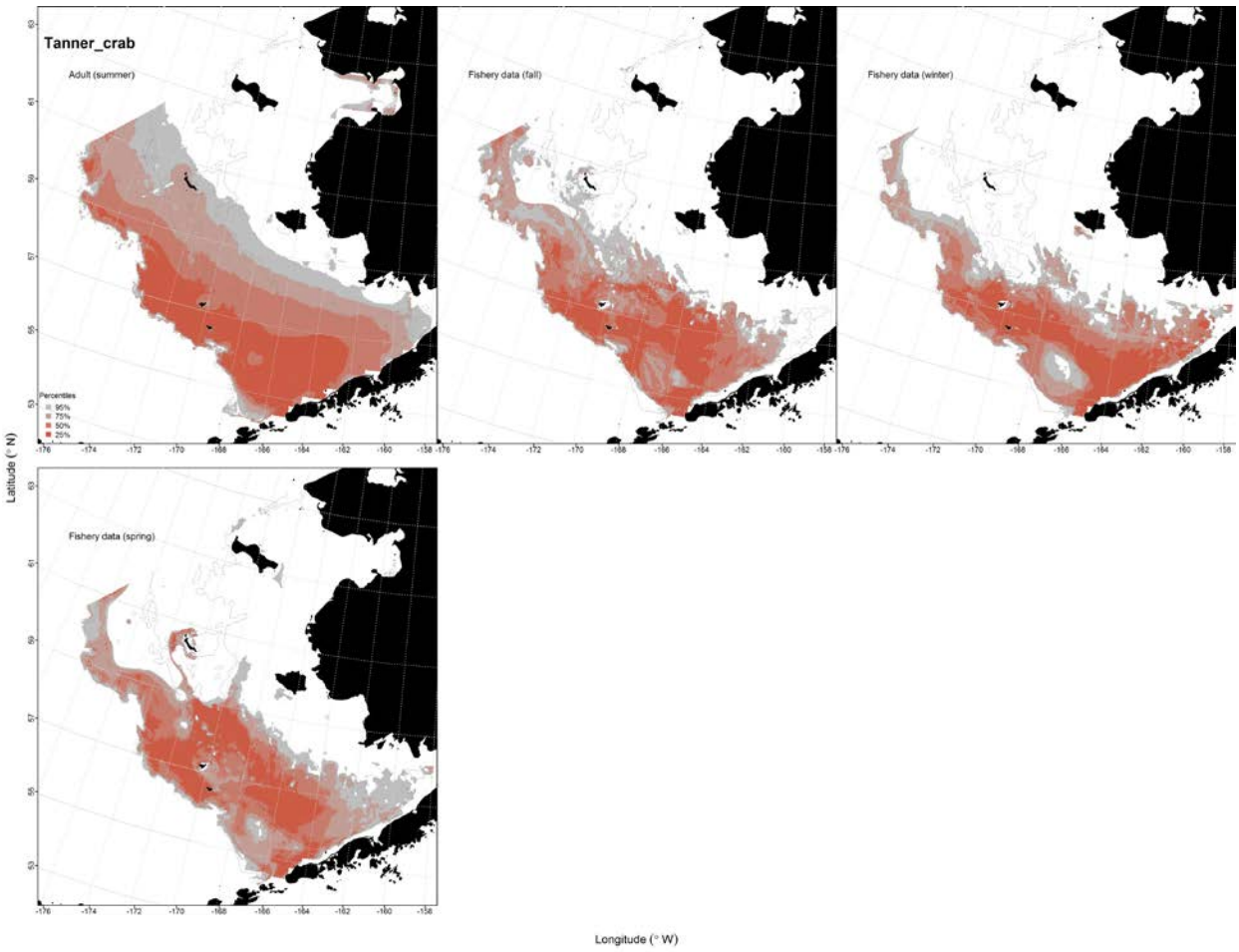

Figure 147. -- Essential fish habitat (EFH) predicted for southern Tanner crab (upper left panel) from RACE-GAP summertime bottom trawl surveys (1982-2014) and predicted from presence in commercial fishery catches (2003-2013) from fall, winter, and spring (remaining three panels) in the eastern Bering Sea.

Snow Crab (*Chionoecetes opilio*)

Summertime distribution of snow crab from RACE-GAP bottom trawl surveys of the eastern Bering Sea -- Snow crabs occurred in RACE-GAP summer bottom trawl surveys of the EBS (1982-2014) from the inner to the outer shelf and from the Alaska Peninsula and Bristol Bay to Norton Sound and the U.S.-Russia Convention Line (Fig. 148). Snow crab distribution in the EBS was modeled using a standard GAM on abundance data from the bottom trawl survey. The most significant habitat covariates retained in the best-fitting GAM were geographic location, bottom current speed, and bottom

temperature. Model effects were highest in the northern portion of the EBS, increased with decreasing sediment grain size and bottom temperature. Capture depths for this species ranged from ca. 10 m to nearly 800 m. The highest abundances were predicted along the U.S.-Russia Convention Line north of St. Matthew and west of St. Lawrence Islands. Using the training data set, this model explained 60.9% of the deviance in their CPUE ($r^2 = 0.61$); the model fit to the test data was slightly less ($r^2 = 0.6$).

Seasonal distribution of snow crab in commercial fishery catches from the eastern Bering Sea -- Snow crab were observed in fall, winter, and spring commercial fishery catches on the middle and outer shelf of the EBS (Fig. 149). MaxEnt models used to predict the probability of suitable habitat for this species determined that bottom depth, bottom temperature, and ocean productivity were consistently among the most important covariates predicting their potential habitat in all three seasons. The combined relative importance of these three predictor terms ranged from 66.7% in spring to 94.9% in winter and the probability of potential habitat was highest in waters ca. 200 m deep with bottom temperatures ca. 5°C and moderate ocean productivity. Model fits to the training data ranged from excellent to outstanding (AUC = 0.87-0.91) and the proportion of cases correctly classified was high (80-84%). Model validation was successful (AUC = 0.78-0.84) and predictions based on the test data correctly classified for 78 to 84% of predicted cases.

Essential habitat maps and conclusions for snow crab (*Chionoecetes opilio*) in the eastern Bering Sea -- Results of the species distribution modeling for snow crab from RACE-GAP summer bottom trawl surveys and seasonal commercial fishery observer data were transformed into EFH maps (Fig. 150). The distribution of predicted snow crab EFH extended from the southern to the northern bound of the survey area for both data sources, but covered a greater proportion of the inner shelf when predicted from the summer bottom trawl data. Core habitat (top 25% of predictions) in summertime was in the northern part of the survey area, while in the fall, winter, and spring commercial catches it was along the axes of the middle and outer shelf which corresponds to where much of the pollock fishery effort is directed.

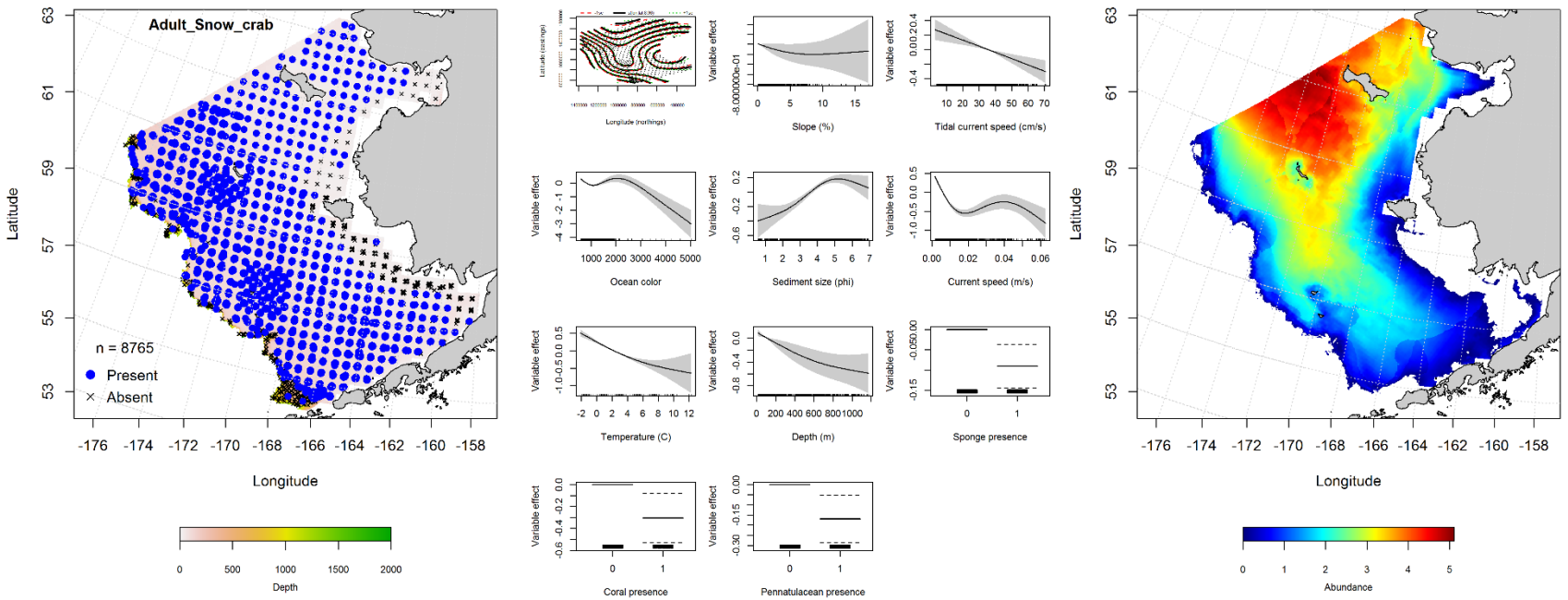

Figure 148. -- Distribution of snow crab in 1982-2014 RACE-GAP summer bottom trawl surveys (left panel) alongside effects of retained habitat covariates in the best-fitting generalized additive model (GAM; center panel) predicting spatial distribution of abundance (CPUE, right panel) across the eastern Bering Sea.

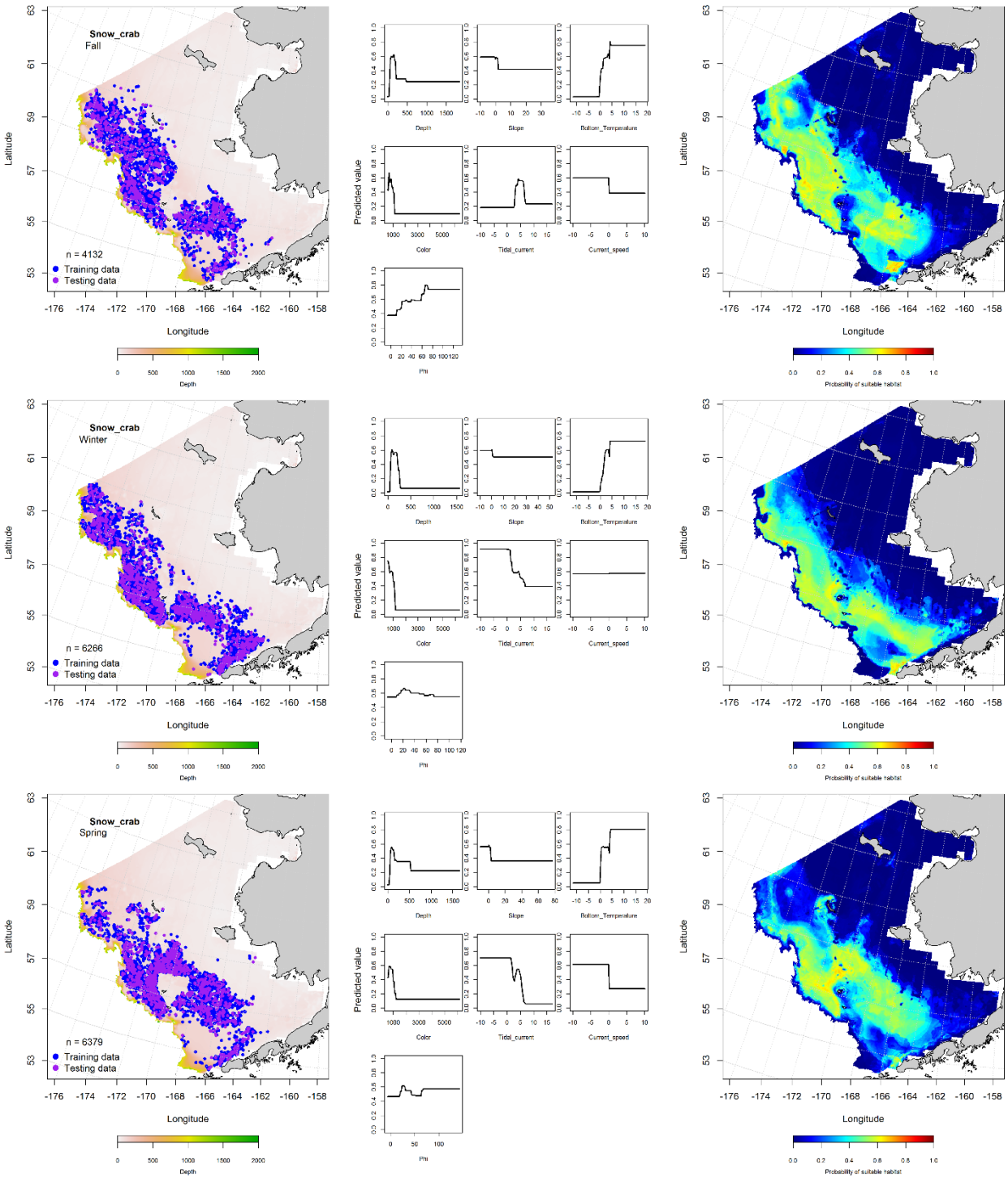

Figure 149. -- Locations of snow crab in fall (October-November; top row), winter (December-February; middle row), and spring (March-May; bottom row) commercial fisheries catches (2003-2013) from the eastern Bering Sea (left-hand column). Blue points were used to train the MaxEnt model (center column) predicting the probability of suitable habitat (right-hand column) and the purple points were used to validate the model.

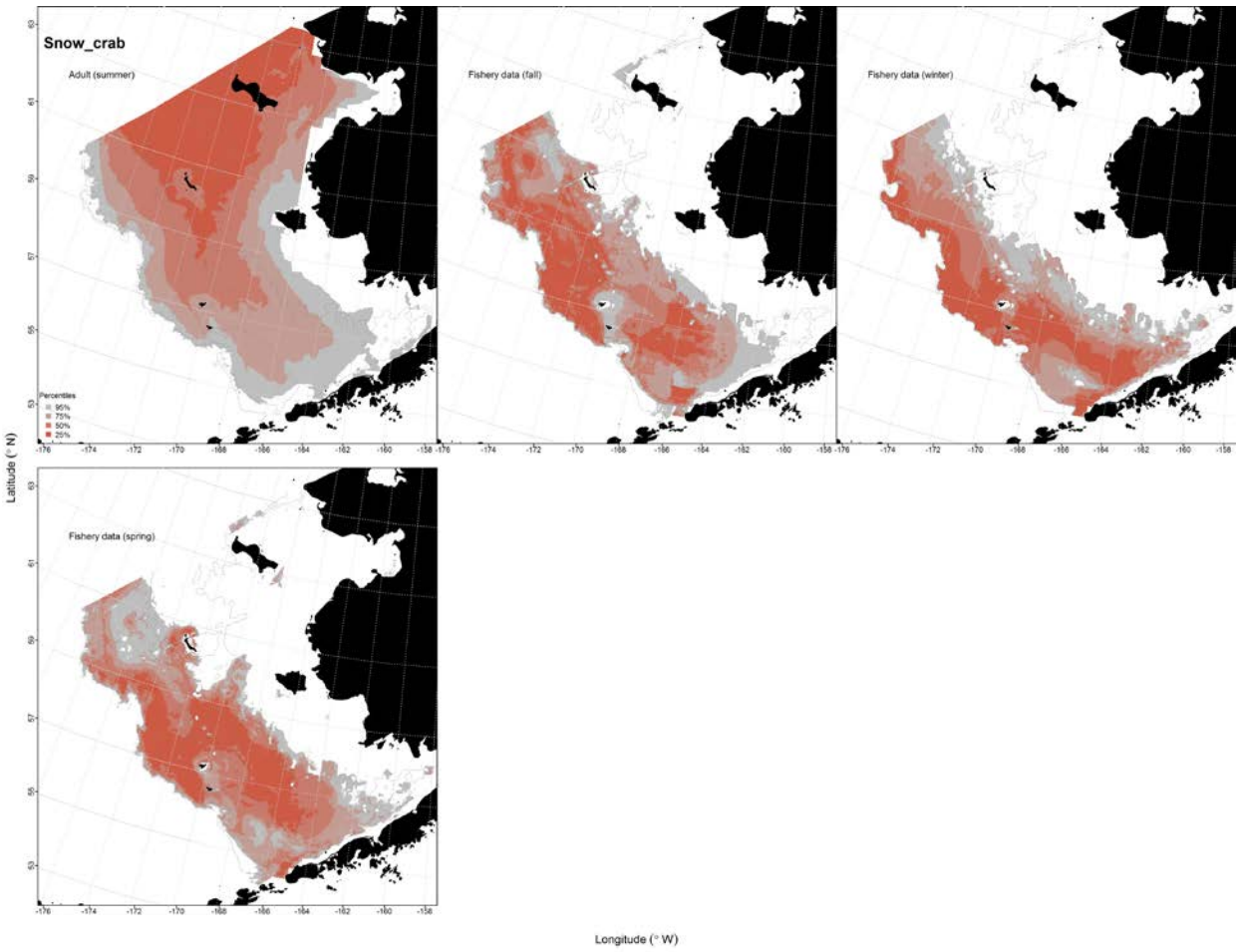

Figure 150. -- Essential fish habitat (EFH) predicted for snow crab (upper left panel) from RACE-GAP summertime bottom trawl surveys (1982-2014) and predicted from presence in commercial fishery catches (2003-2013) from fall, winter, and spring (remaining three panels) in the eastern Bering Sea.

Red King Crab (*Paralithodes camtschaticus*)

Summertime distribution of red king crab from RACE-GAP bottom trawl surveys of the eastern Bering Sea -- Red king crab were primarily distributed over the inner and middle shelf of the central and southern EBS in RACE-GAP summer bottom trawl surveys (1982-2014) as well as in Norton Sound (Fig. 151). An hGAM identified the habitat covariates that describe the distribution of red king crab. The most significant predictor variables retained in the best-fitting presence-absence GAM were geographic location, sediment grain size, and tidal current maxima. Their predicted probability of

presence was highest on the inner shelf in Norton Sound and Bristol Bay over optimally coarser sediments and increasing tidal maxima. This GAM explained 59.3% of the deviance in their distribution data, was an outstanding model fit to the training data (AUC = 0.96), and correctly classified 89% of predicted cases. Model validation was successful (AUC = 0.95) and also correctly classified 89% of predicted presence-absence cases. Abundance of red king crab was predicted at locations where the threshold probability of occurrence (0.28) established in the presence-absence GAM above was met or exceeded. The most important habitat covariates describing distribution from their conditional abundance were geographic location, tidal current maxima, and bottom depth. Predicted CPUE was highest in Norton Sound and Bristol Bay at around 60 m depth over increasing tidal maxima. This conditional abundance GAM explained just 43.1% of the deviance in their CPUE at these sites ($r^2 = 0.43$). The model fit to the test data in the validation step was less ($r^2 = 0.37$).

Seasonal distribution of red king crab in commercial fishery catches from the eastern Bering Sea -- Red king crab were observed in fall, winter, and spring commercial fishery catches on the middle shelf near Bristol Bay and around the Pribilof Islands (Fig. 152). MaxEnt models used to predict the probability of suitable habitat for this species determined that sediment grain size, bottom current speed, and bottom depth were consistently among the most important covariates predicting their potential habitat in all three seasons. The combined relative importance of these three predictor terms ranged from 65.2% in fall to 86.5% in winter and the probability of potential habitat was highest over fine sediments, low bottom current speeds, and shallow depths. Model fits to the training data were outstanding (AUC = 0.94-0.99) and the proportion of cases correctly classified was high (86-95%). Model validation was successful (AUC = 0.87-0.95) and predictions based on the test data correctly classified for 87 to 90% of predicted cases.

Essential habitat maps and conclusions for red king crab (*Paralithodes camtschaticus*) in the eastern Bering Sea -- Results of the species distribution modeling for red king crab from RACE-GAP summer bottom trawl surveys and seasonal commercial fishery observer data were transformed into EFH

maps (Fig. 153). The distribution of red king crab EFH from the RACE-GAP summer bottom trawl surveys included habitat in Norton Sound. The commercial observer data did not appear to extend into this area so the EFH predicted from those data was constrained to Bristol Bay. Core habitat (top 25% of predictions) in both cases tended to occur in relatively shallow water (< 100 m) in the southern portion of the survey area with Norton Sound being the notable exception to geographic location.

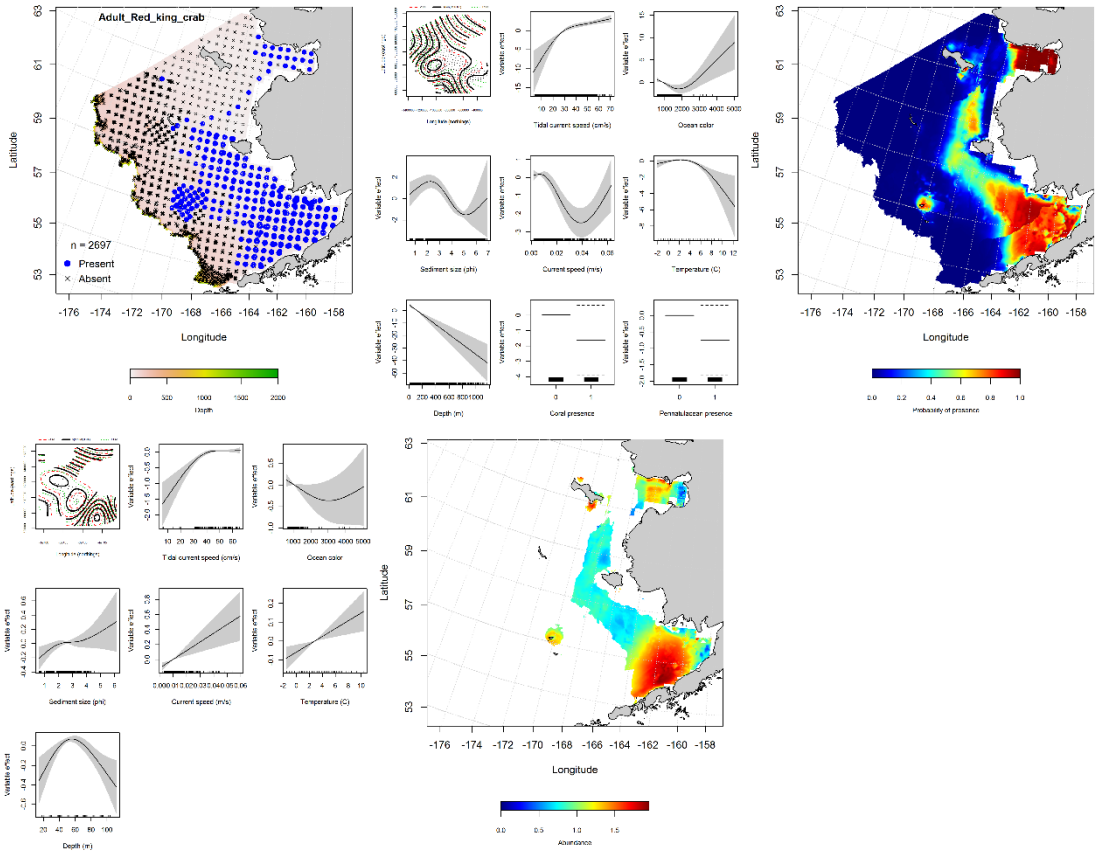

Figure 151. -- Distribution of red king crab in 1982-2014 RACE-GAP summer bottom trawl surveys conducted in the eastern Bering Sea (upper left panel) and the effects of retained habitat covariates in the best-fitting generalized additive model (GAM) of presence-absence (upper center panel) spatially predicting the probability of their presence (upper right panel); the best-fitting abundance GAM (lower left panel) conditionally predicts red king crab catch-per-unit-effort (CPUE) at sites where the optimum threshold for probability of presence was met or exceeded (lower center panel).

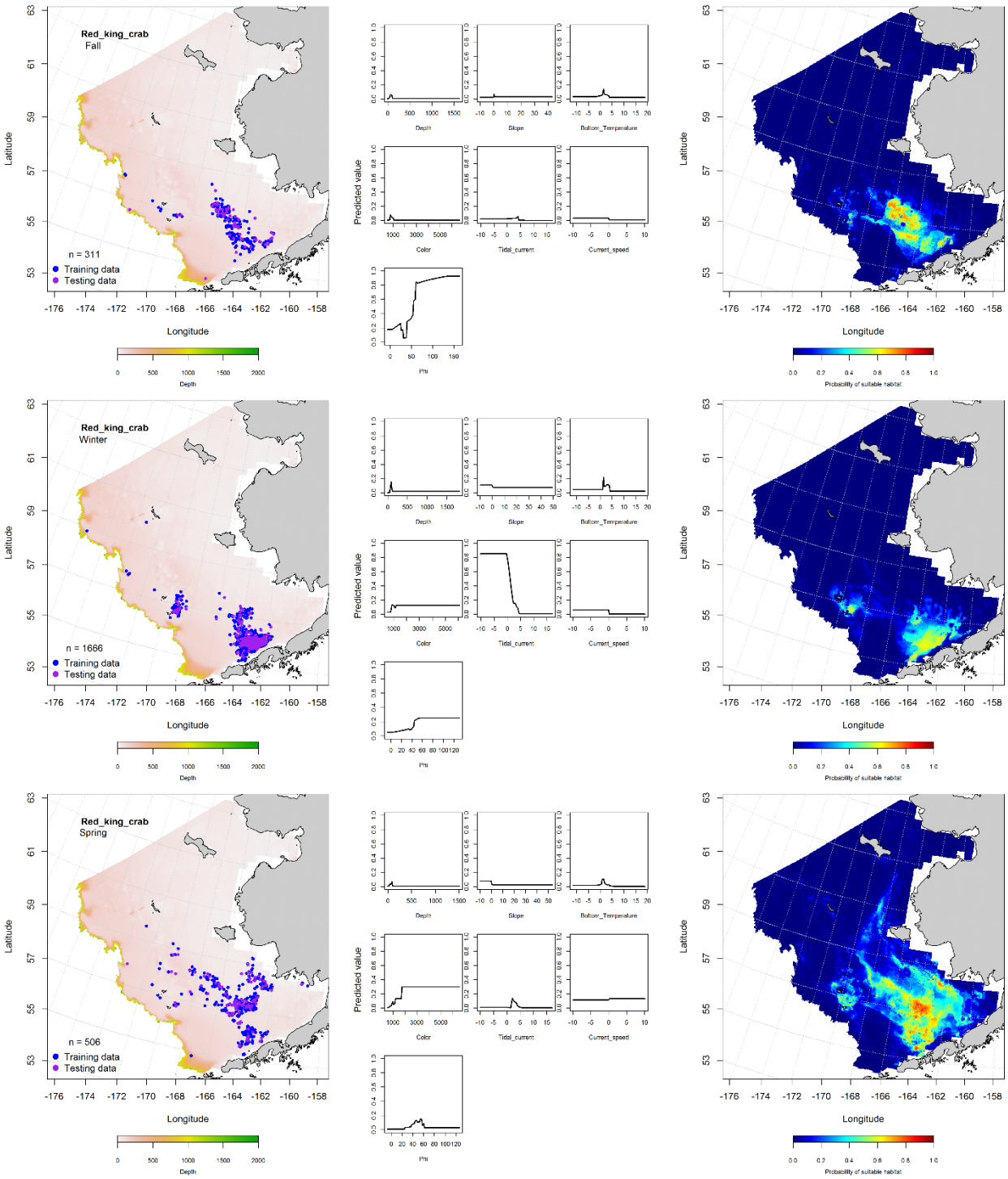

Figure 152. -- Locations of red king crab in fall (October-November; top row), winter (December-February; middle row), and spring (March-May; bottom row) commercial fisheries catches (2003-2013) from the eastern Bering Sea (left-hand column). Blue points were used to train the MaxEnt model (center column) predicting the probability of suitable habitat (right-hand column) and the purple points were used to validate the model.

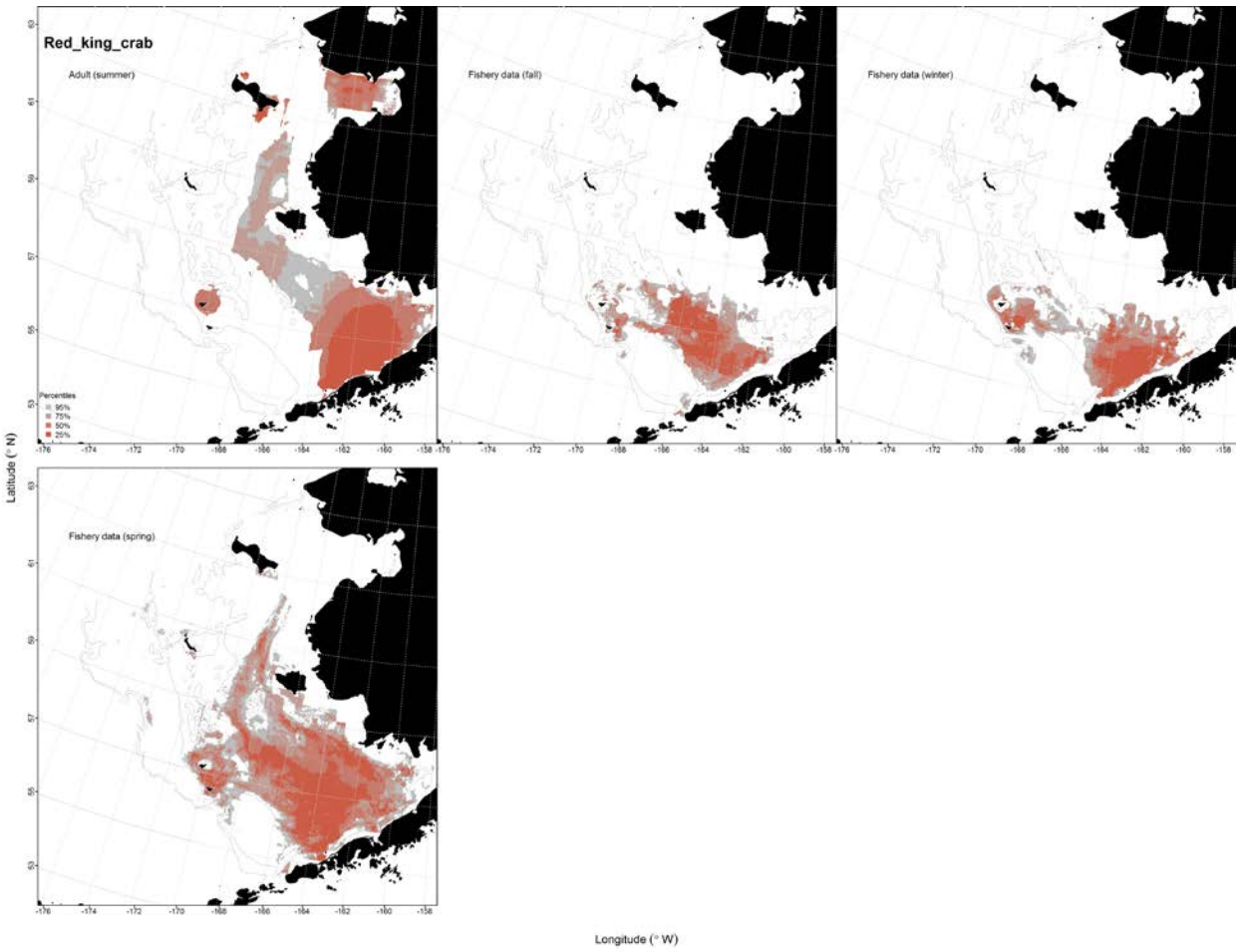

Figure 153. -- Essential fish habitat (EFH) predicted for red king crab (upper left panel) from RACE-GAP summertime bottom trawl surveys (1982-2014) and predicted from presence in commercial fishery catches (2003-2013) from fall, winter, and spring (remaining three panels) in the eastern Bering Sea.

Blue King Crab (*Paralithodes platypus*)

Summertime distribution of blue king crab from RACE-GAP bottom trawl surveys of the eastern Bering Sea -- Blue king crab distribution was centered around the Pribilofs and St. Matthew Island in RACE-GAP summer bottom trawl surveys of EBS (1982-2014) and also occurred in the northern Bering Sea north and east of St. Lawrence Island (Fig. 154). An hGAM was used to model the distribution of this species in the EBS and the most significant predictor variables retained in the best-fitting presence-absence GAM were geographic location, tidal current maxima, and sediment grain size.

Probability of blue king crab presence was highest between the Pribilofs and St. Matthew Island over coarser sediments and lower maximum tidal currents. This GAM explained 52.7% of the deviance in their distribution data, was an outstanding model fit to the training data (AUC = 0.95), and correctly classified 89% of predicted cases. Model validation was successful (AUC = 0.95) and also correctly classified 88% of predicted presence-absence cases. Abundance of blue king crab was predicted at locations where the threshold probability of occurrence (0.13) established in the presence-absence GAM above was met or exceeded. The most important habitat covariate describing distribution from their conditional abundance was geographic location. Predicted CPUE was highest in western portion of the survey area. This conditional abundance GAM explained just 32.2% of the deviance in their CPUE at these sites ($r^2 = 0.32$). The model fit to the test data in the validation step was less ($r^2 = 0.23$).

Seasonal distribution of blue king crab in commercial fishery catches from the eastern Bering Sea – Blue king crab were observed in fall, winter, and spring commercial fishery catches around the Pribilofs and St. Matthew Island (Fig. 155). MaxEnt models used to predict the probability of suitable habitat for this species determined that ocean productivity, bottom temperature, and bottom depth were consistently among the most important covariates predicting their potential habitat in all three seasons. The combined relative importance of these three predictor terms ranged from 81.7% in winter to 86.1% in spring and the probability of potential habitat was highest when ocean productivity was ca. 500 $g \cdot C \cdot m^{-2} \cdot day^{-1}$, bottom temperature ca. 0°C, and at shallower depths (< 100 m). Model fits to the training data were outstanding (AUC = 0.93-0.98) and the proportion of cases correctly classified was high (88-93%). Model validation was successful (AUC = 0.91-0.92) and predictions based on the test data correctly classified for 91 to 92% of predicted cases.

Essential habitat maps and conclusions for blue king crab (*Paralithodes platypus*) in the eastern Bering Sea -- Results of the species distribution modeling for blue king crab from RACE-GAP summer bottom trawl surveys and seasonal commercial fishery observer data were transformed into EFH maps (Fig. 156). The distribution of blue king crab EFH from the RACE-GAP summer bottom trawl

surveys as well as the commercial observer data included areas around St. Lawrence Island in the northern Bering Sea as well as EFH along the middle and outer shelf of the EBS between the U.S.-Russia Convention Line and the Alaska Peninsula. Core habitat (top 25% of predictions) in all seasons was found primarily between 100 and 200 m depths along the middle shelf.

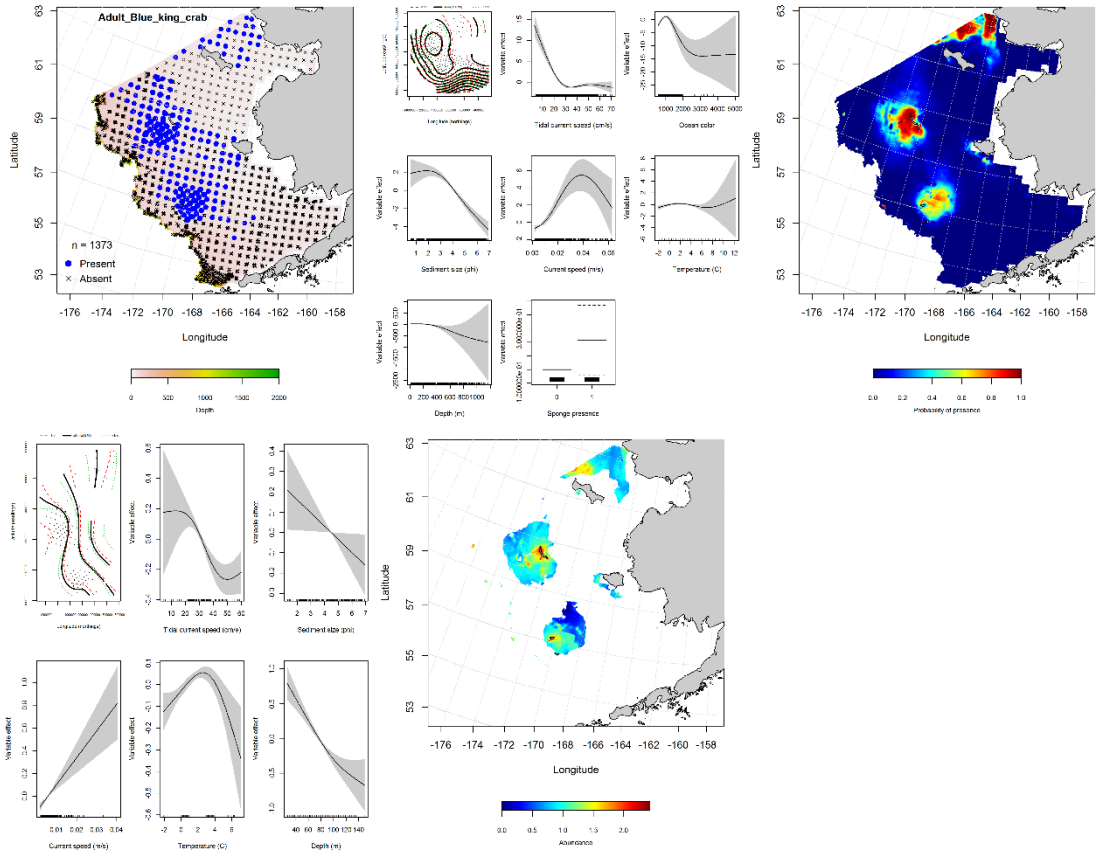

Figure 154. -- Distribution of blue king crab in 1982-2014 RACE-GAP summer bottom trawl surveys conducted in the eastern Bering Sea (upper left panel) and the effects of retained habitat covariates in the best-fitting generalized additive model (GAM) of presence-absence (upper center panel) spatially predicting the probability of their presence (upper right panel); the best-fitting abundance GAM (lower left panel) conditionally predicts blue king crab catch-per-unit-effort (CPUE) at sites where the optimum threshold for probability of presence was met or exceeded (lower center panel).

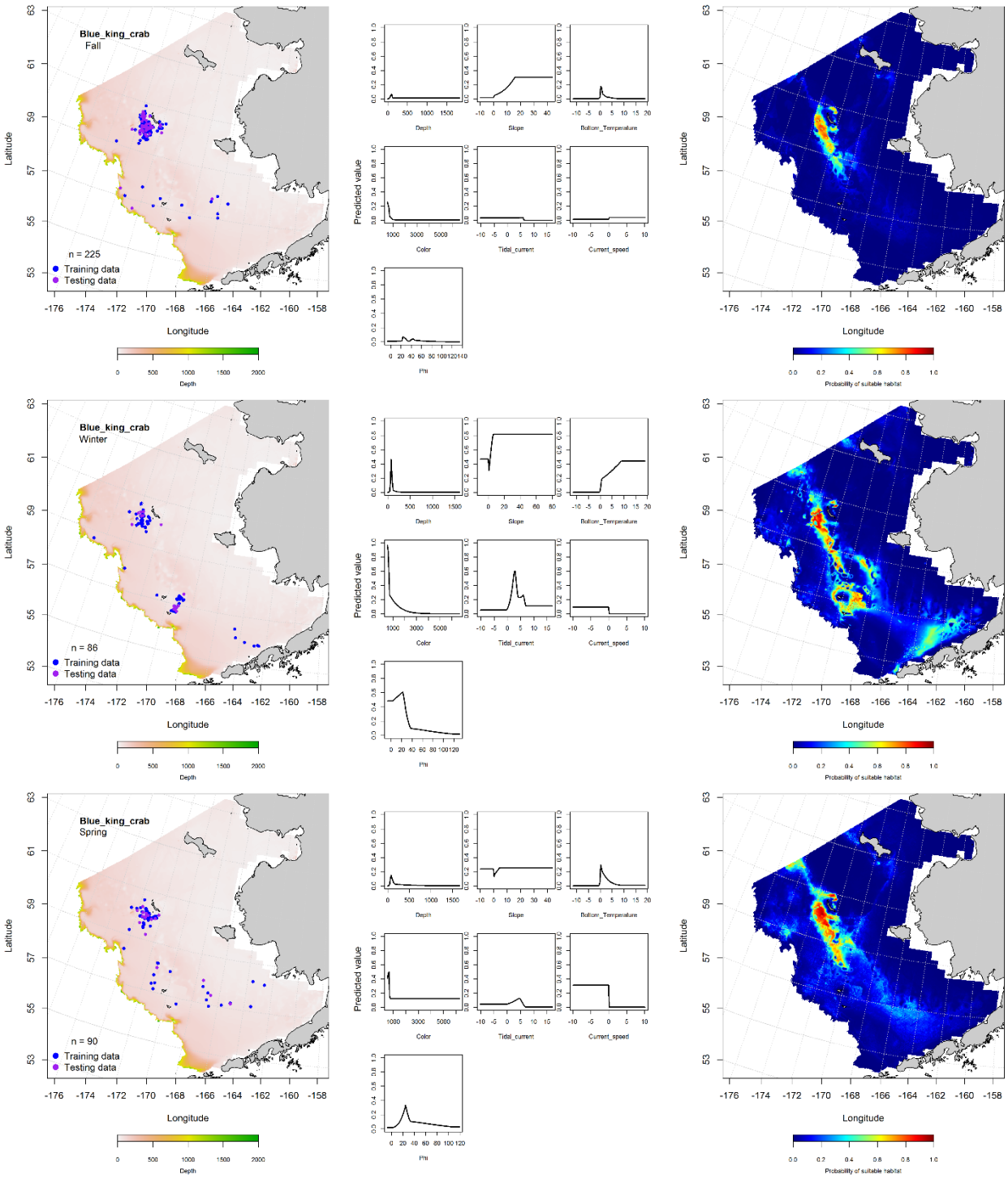

Figure 155. -- Locations of blue king crab in fall (October-November; top row), winter (December-February; middle row), and spring (March-May; bottom row) commercial fisheries catches (2003-2013) from the eastern Bering Sea (left-hand column). Blue points were used to train the MaxEnt model (center column) predicting the probability of suitable habitat (right-hand column) and the purple points were used to validate the model.

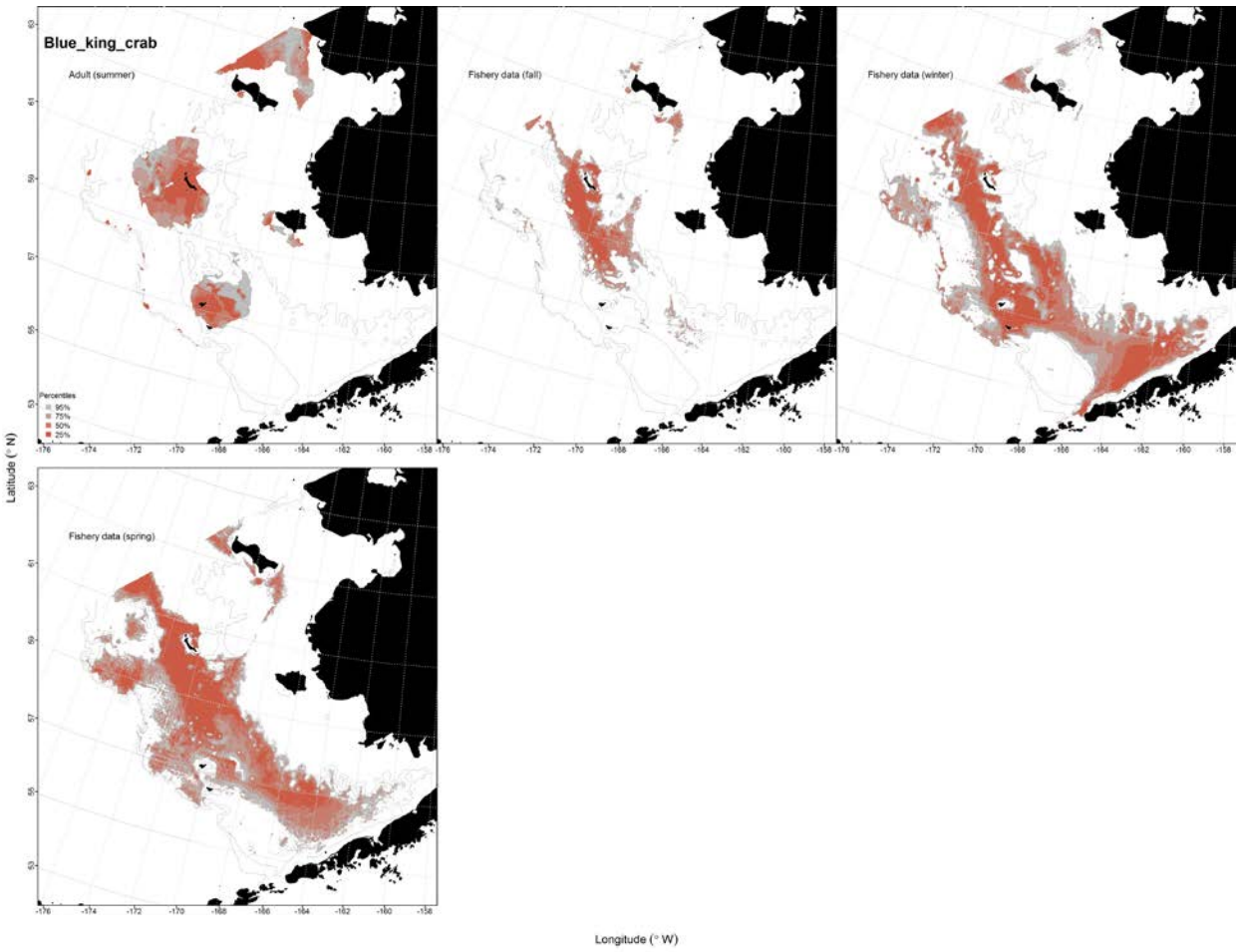

Figure 156. -- Essential fish habitat (EFH) predicted for blue king crab (upper left panel) from RACE-GAP summertime bottom trawl surveys (1982-2014) and predicted from presence in commercial fishery catches (2003-2013) from fall, winter, and spring (remaining three panels) in the eastern Bering Sea.

Octopus Unidentified

Summertime distribution of octopus unidentified from RACE-GAP bottom trawl surveys of the eastern Bering Sea -- Unidentified octopus were observed in fall, winter, and spring commercial fishery catches primarily along the outer shelf of the EBS (Fig. 158). MaxEnt models used to predict the probability of suitable habitat for this species determined that bottom depth and bottom temperature were consistently among the most important covariates predicting their potential habitat in all three seasons. The combined relative importance of these two predictors ranged from 75.7% in winter to 80.6% in fall

and the probability of potential habitat was highest at ca. 5°C bottom temperatures but at differing bottom depths in different seasons. Peak model effects in fall were at depths ca. 200 m while in winter and spring the peak effects were at both 200 and ≥ 500 m. Model fits to the training data were outstanding (AUC = 0.93-0.97) and the proportion of cases correctly classified was high (86-91%). Model validation was successful (AUC = 0.84-0.88) and predictions based on the test data correctly classified for 84 to 88% of predicted cases.

Essential habitat maps and conclusions for unidentified octopus in the eastern Bering Sea -- Results of distribution modeling for unidentified octopus from RACE-GAP summer bottom trawl surveys and seasonal commercial fishery observer data were transformed into EFH maps (Fig. 159). The distribution of their EFH extended from the Alaska Peninsula and Bristol Bay in the south to the U.S.-Russia Convention Line in the north and over the inner, middle, and outer shelf of the EBS. Core habitat (top 25% of predictions) in all seasons was found primarily in waters ≥ 200 m deep along the outer shelf.

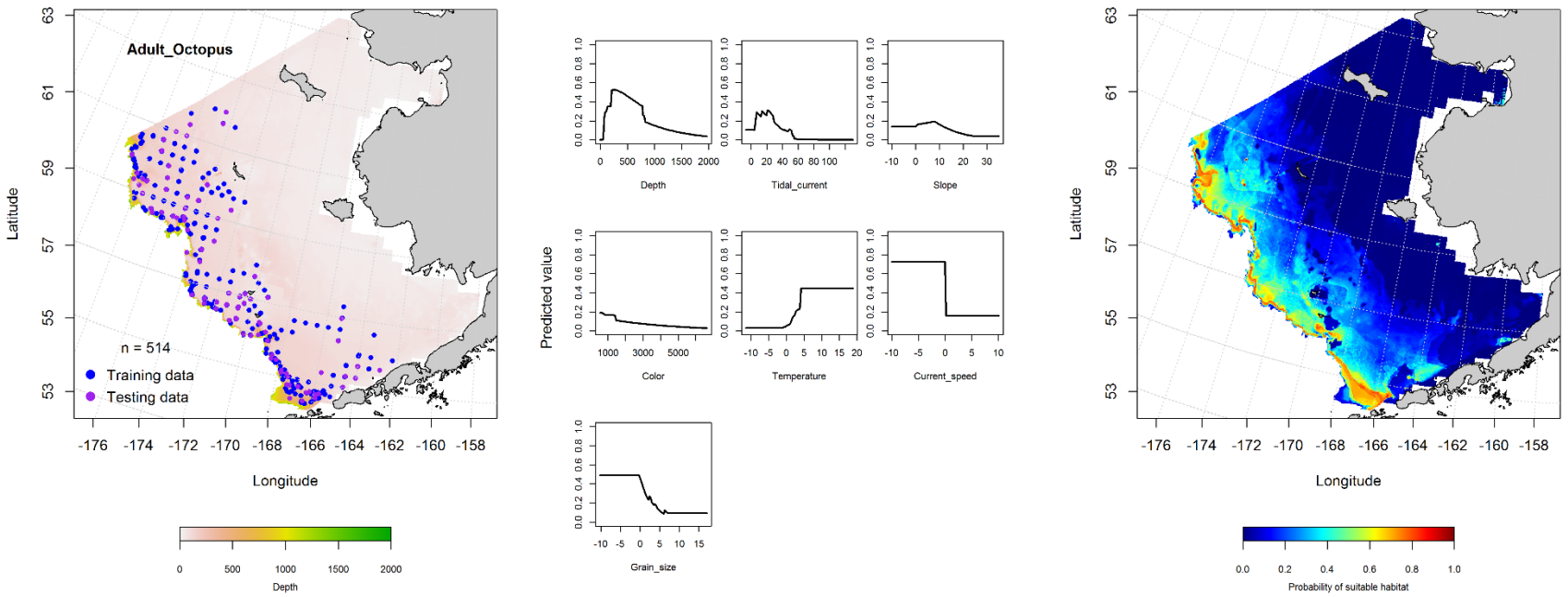

Figure 157. -- Presence of unidentified octopus in summertime RACE-GAP bottom trawl surveys (1982-2014) of the eastern Bering Sea (left panel) with training (blue dots) and testing (purple dots) data sets indicated alongside the maximum entropy model (MaxEnt) effects (center panel) and the MaxEnt spatial predictions of the probability of suitable unidentified octopus habitat (right panel).

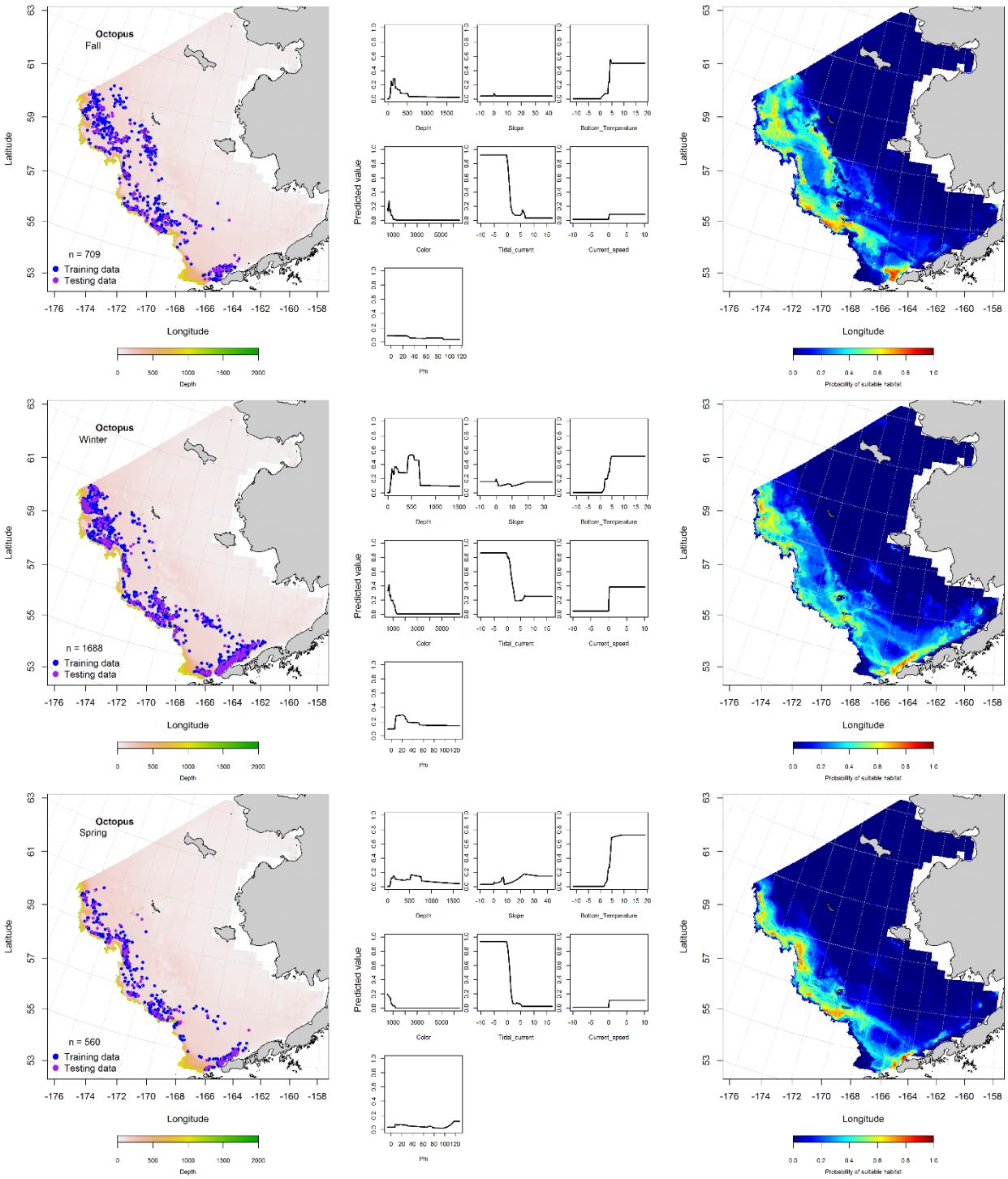

Figure 158. -- Locations of unidentified octopus in fall (October-November; top row), winter (December-February; middle row), and spring (March-May; bottom row) commercial fisheries catches (2003-2013) from the eastern Bering Sea (left-hand column). Blue points were used to train the MaxEnt model (center column) predicting the probability of suitable habitat (right-hand column) and the purple points were used to validate the model.

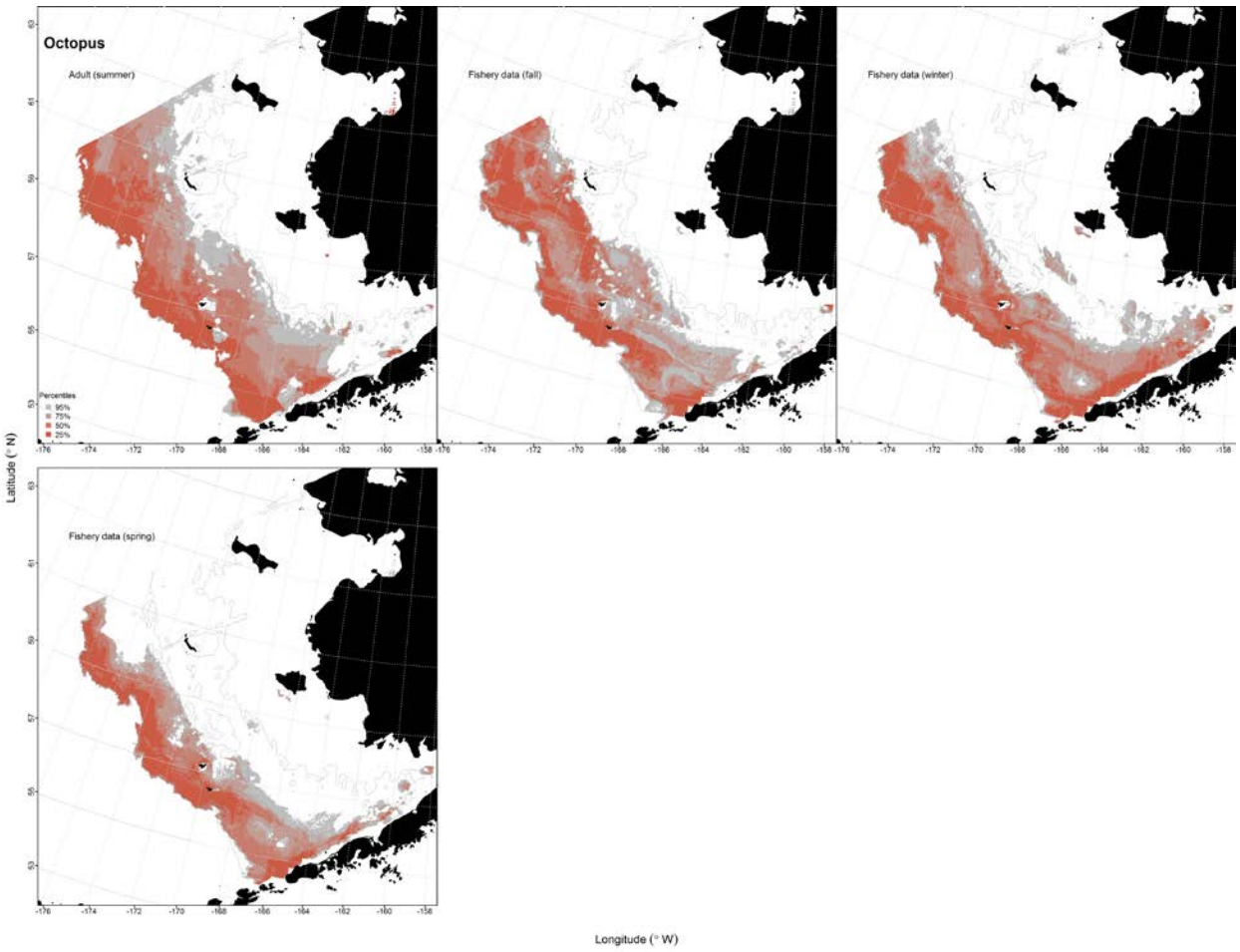

Figure 159. -- Essential fish habitat (EFH) predicted for unidentified octopus (upper left panel) from RACE-GAP summertime bottom trawl surveys (1982-2014) and predicted from presence in commercial fishery catches (2003-2013) from fall, winter, and spring (remaining three panels) in the eastern Bering Sea.

ACKNOWLEDGMENTS

The authors are grateful to Megan Prescott for her diligence and work on the bathymetry layers for each region. This project was funded by the Alaska Fisheries Science Center/Alaska Regional Office (AKRO) Habitat Research Program. We thank John V. Olson and Steve Lewis in AKRO for providing data from the Alaska fisheries observer program. We thank Al Hermann for providing ROMS model outputs. We thank all of the vessel companies, ship's crews, sea-going scientists, and observers who collected these data. Finally, the authors are grateful to Bob Foy, Jerry Hoff, Elaina Jorgensen, Stan Kotwicki, Bob Lauth, Michael Martin, Dan Nichol, Duane Stevenson, and Cynthia Yeung who reviewed and greatly improved this manuscript.

CITATIONS

Abookire, A. A. 2006. Reproductive biology, spawning season, and growth of female rex sole (*Glyptocephalus zachirus*) in the Gulf of Alaska. Fish. Bull., U.S. 104(3):350-359.

Abookire, A. A., and B. J. Macewicz. 2003. Latitudinal variation in reproductive biology and growth of female Dover sole (*Microstomus pacificus*) in the North Pacific, with emphasis on the Gulf of Alaska stock. J. Sea Res. 50(2):187-197.

Alverson, D. L., and W. T. Pereyra. 1969. Demersal fish explorations in the northeastern Pacific Ocean – An evaluation of exploratory fishing methods and analytical approaches to stock size and yield forecasts. J. Fish. Res. Bd. Can. 26:1985-2001.

Behrenfeld, M. J., and P. G. Falkowski. 1997. Photosynthetic rates derived from satellite-based cholorphyll concentration. Limnol. Oceanogr. 42(1):1-20.

Bio, A. M. F., P. De Becker, E. De Bie, W. Huybrechts, and M. Wassen. 2002. Prediction of plant species distribution in lowland river valleys in Belgium: Modelling species response to site conditions. J. Biogeog. 11:2189-2216.

Buckley, T.W., A. Greig, and J. L. Boldt. 2009. Describing summer pelagic habitat over the continental shelf in the eastern Bering Sea, 1982-2006. U. S. Dep. Commer., NOAA Tech. Memo. NMFS-AFSC-196, 49 p.

Bush, K., W. Donaldson, M. Dorn, G. Eckert, H. Fitch, R. J. Foy, W. Gaeuman, B. Garber-Yonts, J. Gasper, T. Hamazaki, D. Pengilly, A. E. Punt, L. Rugolo, M. S. M. Siddeek, W. Stockhausen, D. Stram, B. J. Turnock, and J. Zheng. Stock assessment and fishery evaluation report for the king and Tanner crab fisheries of the Bering Sea and Aleutian Islands Regions, 828 p. North Pacific Fisheries Management Council, Anchorage, AK.

Chilton, E. (A.). 2007. Maturity of female northern rockfish *Sebastes polyspinis* in the central Gulf of Alaska. Alaska Fish. Res. Bull. 12:264-269.

Chilton, E. A. 2010. Maturity and growth of female dusky rockfish (*Sebastes variabilis*) in the central Gulf of Alaska. Fish. Bull., U.S. 108(1):70-79.

Cooper, D. W., K. R. Maslenikov, and D. R. Gunderson. 2007. Natural mortality rate, annual fecundity, and maturity at length for Greenland halibut (*Reinhardtius hippoglossoides*) from the northeastern Pacific Ocean. Fish. Bull., U.S. 105(2):296-304.

Cooper, D. W., S. F. McDermott, and J. N. Ianelli. 2010. Spatial and temporal variability in Atka mackerel female maturity at length and age. Mar. Coast. Fish.: Dynam. Manage. Ecosys. Sci. 2(1): 329-338.

Cragg, J.G. 1971. Some statistical models for limited dependent variables with application to the demand for durable goods. Econometrica 39:829-844.

Cutler, R. D., T. C. Edwards, K. H. Beard, A. Cutler, K. T. Hess, J. Gibson, and J. J. Lawler. 2007. Random forests for classification in ecology. Ecology 88(11):2783-2792.

Danielson, S., E. Curchitser, K. Hedstrom, T. Weingartner, and P. Stabeno. 2011. On ocean and sea ice modes of variability in the Bering Sea. J. Geophys. Res. 116:C12034.

De Forest, L., J. T. Duffy-Anderson, R. A. Heintz, A. C. Matarese, E. C. Siddon, T. I. Smart, and I. B. Spies. 2014. Taxonomy of the early life stages of arrowtooth flounder (*Atheresthes stomias*) and Kamchatka flounder (*A. evermanni*) in the eastern Bering Sea, with notes on distribution and condition. Deep-Sea Res. II 109:181-189.

DeLong, E. R., D. M. DeLong, and D. L. Clarke-Pearson. 1988. Comparing the area under two or more correlated receiver operating characteristic curves: a nonparametric approach. Biometrics 44(3):837-845.

Ebert, D. A., W. D. Smith, D. L. Haas, S. M. Ainsley, and G. M. Cailliet. 2007. Life history and population dynamics of Alaskan skates: providing essential biological information for effective management of bycatch and target species. Final Report to the North Pacific Research Board, Project 510. North Pacific Research Board, 1007 W. 3rd Ave., STE 100, Anchorage, AK 99501.

Egbert, G. D., and S. Y. Erofeeva. 2002. Efficient inverse modeling of barotropic ocean tides. J. Atmos. Ocean. Tech. 19(2):183-204.

Elith, J., J. R. Leathwick, and T. Hastie. 2008. A working guide to boosted regression trees. J. Animal Ecol. 77(4):802-813.

Elith, J., S. J. Phillips, T. Hastie, M. Dudik, Y. E. Chee, and C. J. Yates. 2011. A statistical explanation of MaxEnt for ecologists. Diversity Distrib. 17:43-57.

Jordan, D. S., and B. W. Evermann. 1898. The fishes of North and Middle America: a descriptive catalogue of the species of fish-like vertebrates found in the waters of North America, north of the Isthmus of Panama. Part II. Bull. U.S. Natl. Mus. 47: i–xxx, 1,241-2,183.

Hastie, T. J., and R. J. Tibshirani. 1990. Generalized Additive Models. Monogr. Stat. Appl. Prob. 43, 338 p.

Hoff, G. R., and L. L. Britt. 2011. Results of the 2010 eastern Bering Sea upper continental slope survey of groundfish and invertebrate resources. U. S. Dep. Commer., NOAA Tech. Memo. NMFS-AFSC-224, 300 p.

Hosmer, D. W., and S. Lemeshow. 2005. Multiple Logistic Regression. John Wiley and Sons, Inc.

Knight, C. A., C. C. Cheng, and D. A. DeVries. 1991. Adsorption of alpha-helical antifreeze peptides on specific ice crystal planes. Biophys. J. 59:409-418.

Kotwicki, S., J. K. Horne, A.E. Punt, and J. N. Ianelli. 2015. Factors affecting the availability of walleye pollock to acoustic and bottom trawl survey gear. ICES J. Mar. Sci. 72(5):1425-1439.

Kumar, S., and T. J. Stohlgren. 2009. Maxent modeling for predicting suitable habitat for threatened and endangered tree *Canacomyrica monticola* in New Caledonia. J. Ecol. Nat. Environ. 1(4):94-98.

Lauth, R. R. 2011. Results of the 2010 eastern and northern Bering Sea continental shelf bottom trawl survey of groundfish and invertebrate fauna. U. S. Dep. Commer., NOAA Tech. Memo. NMFS-AFSC-227, 256 p.

Lauth, R. R., and J. Conner. 2014. Results of the 2011 eastern Bering Sea continental shelf bottom trawl survey of groundfish and invertebrate fauna. U. S. Dep. Commer., NOAA Tech. Memo. NMFS-AFSC-266, 176 p.

Lozier, J. D., P. Aniello, and M. J. Hickerson. 2009. Predicting the distribution of Sasquatch in western North America: Anything goes with ecological niche modelling. J. Biogeog. 36(9):1623-1627.

Matarese, A. C., D. M. Blood, S. J. Picquelle, and J. L. Benson. 2003. Atlas of abundance and distribution patterns of ichthyoplankton from the Northeast Pacific Ocean and Bering Sea ecosystems based on research conducted by the Alaska Fisheries Science Center (1972-1996). U.S. Dep. Commer., NOAA Professional Paper, NMFS-1, 281 p.

Matta, M. E. 2006. Aspects of the life history of the Alaska skate, *Bathyraja parmifera*, in the eastern Bering Sea. M.S. thesis, Univ. Washington, Seattle, WA.

Mecklenburg, C.W., T. A. Mecklenburg, and L. K. Thorsteinson. 2002. Fishes of Alaska. Am. Fish. Soc. Bethesda, MD. 1,037 p.

Orr, J. W., and S. Hawkins. 2008. Species of the rougheye rockfish complex: resurrection of *Sebastes melanostictus* (Matsubara, 1934) and a redescription of *Sebastes aleutianus* (Jordan and Evermann, 1898) (*Teleostei: Scorpaeniformes*). Fish. Bull., U. S. 106(2):111-134.

Orr, J. W., and A. C. Matarese. 2000. Revision of the genus *Lepidopsetta* Gill, 1862 (*Teleostei: Pleuronectidae*) based on larval and adult morphology, with a description of a new species from the North Pacific Ocean and Bering Sea. Fish. Bull., U. S. 98(3):539-582.

Phillips, S. J., R. P. Anderson, and R. E. Schapire. 2006. Maximum entropy modeling of species geographic distributions. Ecol. Model. 190(3-4):231–59.

Potts, J., and J. Elith. 2006. Comparing species abundance models. Ecol. Model. 199:153-163.

R Core Development Team. 2013. R: A language and environment for statistical computing. R Foundation for Statistical Computing, Vienna, Austria. URL: http://www.R-project.org/.

Robinson, L. M., J. Elith, A. J. Hobday, R. G. Pearson, B. E. Kendall, H. P. Possingham, and A. J. Richardson. 2011. Pushing the limits in marine species distribution modelling: lessons from the land present challenges and opportunities. Glob. Ecol. Biogeogr. 20(6):789-802.

Rooper, C. N. 2008. An ecological analysis of rockfish (*Sebastes* spp.) assemblages in the North Pacific Ocean along broad-scale environmental gradients. Fish. Bull., U.S. 106(1):1-11.

Rooper, C. N., M. F. Sigler, P. Goddard, P. Malecha, R. Towler, K. Williams, R. Wilborn, and M. Zimmermann. 2016. Validation and improvement of species distribution models for structure forming invertebrates in the eastern Bering Sea with an independent survey. Mar. Ecol. Prog. Ser. 551:117-130.

Rooper, C. N., M. Zimmermann, M. M. Prescott, and A. J. Hermann. 2014. Predictive models of coral and sponge distribution, abundance, and diversity in bottom trawl surveys of the Aleutian Islands, Alaska. Mar. Ecol. Prog. Ser. 503:157-176.

Sagarese, S. R., M. G. Frisk, R. M. Cerrato, K. A. Sosebee, J. A. Musick, and P. J. Rago. 2014. Application of generalized additive models to examine ontogenetic and seasonal distributions of spiny dogfish (*Squalus acanthias*) in the Northeast (US) shelf large marine ecosystem. Can. J. Fish. Aquat. Sci. 71(6): 847–877.

Sigler, M. F., C. N. Rooper, G. R. Hoff, R. P. Stone, R. A. McConnaughey, and T. K. Wilderbuer. 2015. Faunal features of submarine canyons on the eastern Bering Sea slope. Mar. Ecol. Prog. Ser. 526:21-40.

Smith, K. R., and R. A. McConnaughey. 1999. Surficial sediments of the eastern Bering Sea continental shelf: EBSSED database documentation. U.S. Dep. Commer., NOAA Tech. Memo. NMFS-AFSC-104, 41 p.

Spies, I., T. K. Wilderbuer, D. G. Nichol, and K. Aydin. 2014. Assessment of the arrowtooth flounder stock in the eastern Bering Sea and Aleutian Islands, *In* Stock assessment and fishery evaluation report for the 2014 Bering Sea Aleutian Islands groundfish fishery. North Pacific Fishery Management Council, P.O. Box 103136, Anchorage, AK.

Stahl, J. P., and G. H. Kruse. 2008. Spatial and temporal variability in size at maturity of walleye pollock in the eastern Bering Sea. Trans. Am. Fish. Soc. 137(5):1543-1557.

Stark, J. W. 2004. A comparison of the maturation and growth of female flathead sole in the central Gulf of Alaska and south-eastern Bering Sea. J. Fish Biol. 64(4):876-889.

Stark, J. W. 2007. Geographic and seasonal variations in maturation and growth of female Pacific cod (*Gadus macrocephalus*) in the Gulf of Alaska and Bering Sea. Fish. Bull., U.S. 105(3):396-407.

Stark, J. W. 2012(a). Female maturity, reproductive potential, relative distribution, and growth compared between arrowtooth flounder (*Atheresthes stomias*) and Kamchatka flounder (*A. evermanni*) indicating concerns for management. J. Appl. Ichthyol. 28(2):226-230.

Stark, J. W. 2012(b). Contrasting maturation and growth of northern rock sole in the eastern Bering Sea and Gulf of Alaska for the purpose of stock management. N. Amer. J. Fish. Manage. 32(1):93-99.

Stauffer, G. 2004. NOAA protocols for groundfish bottom trawl surveys of the Nation's fishery resources. U. S. Dep. Commer., NOAA Tech. Memo. NMFS-F/SPO-65, 205 p.

Stevenson, D. E., and G. R. Hoff. 2009. Species identification confidence in the eastern Bering Sea shelf survey (1982-2008). AFSC Processed Rep. 2009-04, 46 p. Alaska Fish. Sci. Cent., NOAA, Natl. Mar. Fish. Serv., 7600 Sand Point Way NE, Seattle, WA 98115.

Tenbrink, T. T., and T. W. Buckley. 2013. Life-history aspects of the yellow Irish lord (*Hemilepidotus jordani*) in the Eastern Bering Sea and Aleutian Islands. Northwest. Natural. 94(2):126-136.

Tenbrink, T. T., and C. E. Hutchinson. 2009. Age, growth, and mortality of the plain sculpin, *Myoxocephalus jaok*, in the eastern Bering Sea. North Pacific Research Board Project Final Report. North Pacific Research Board,1007 W 3rd Ave STE100, Anchorage, AK 99501.

Tenbrink, T. T., and T. K. Wilderbuer. 2015. Updated maturity estimates for flatfishes (Pleuronectidae) in the eastern Bering Sea, with implications for fisheries management. Mar. Coast. Fish. Dy. Manage. Ecosys. Sci. 7:474–482.

Venables W. N., and B. D. Ripley. 2002. Modern Applied Statistics with S. Fourth Edition. Springer Science+Business Media, New York, N.Y.

Wakabayashi, K. 1989. Studies on the fishery biology of yellowfin sole in the eastern Bering Sea. [In Jpn., Engl. Summ.]. Bull. Far Seas Fish. Res. Lab. 26:21-152.

Wakabayashi, K., R. G. Bakkala, and M. S. Alton. 1985. Methods of the Japan demersal trawl surveys, p. 7-29. In R. G. Bakkala and K. Wakabayashi (Editors), Results of cooperative Japan groundfish investigations in the Bering Sea during May-August 1979. Int. N. Pac. Fish. Comm. Bull. 44.

Watson, D. F., and G. M. Philip. 1985. A refinement of inverse distance weighted interpolation. Geo-processing 2(4):315-327.

Wood, S. N. 2006. Generalized Additive Models: An Introduction with R. Chapman and Hall/CRC, Boca Raton, FL. 392 p.

Zimmermann, M. 1997. Maturity and fecundity of arrowtooth flounder, *Atheresthes stomias*, from the Gulf of Alaska. Fish. Bull., U.S. 95(3):598-611.

Zimmermann, M., and J. L. Benson. 2013. Smooth sheets: How to work with them in a GIS to derive bathymetry, features, and substrates. U. S. Dep. Commer. NOAA Tech. Memo. NMFS-AFSC-249, 52 p.

Zuur, A. F., E. N. Ieno, N. J. Walker, A. A. Saveliev, and G. M. Smith. 2009. Mixed Effects Models and Extensions in Ecology with R, 574 p. Springer-Verlag, New York, NY.

RECENT TECHNICAL MEMORANDUMS

Copies of this and other NOAA Technical Memorandums are available from the National Technical Information Service, 5285 Port Royal Road, Springfield, VA 22167 (web site: *www.ntis.gov)*. Paper and electronic (.pdf) copies vary in price.

AFSC-

356 CSEPP, D. J., D. C. HONEYFIELD, J. J. VOLLENWEIDER, and J. WOMBLE. 2017. Estuarine distribution, nutritional and thiaminase content of eulachon (*Thaleichthys pacificus*) in Southeast Alaska, with implications for Steller sea lions, U.S. Dep. Commer., NOAA Tech. Memo. NMFS-AFSC-356, 56 p.

355 M. M. MUTO, V. T. HELKER, R. P. ANGLISS, B. A. ALLEN, P. L. BOVENG, J. M. BREIWICK, M. F. CAMERON, P. J. CLAPHAM, S. P. DAHLE, M. E. DAHLHEIM, B. S. FADELY, M. C. FERGISON, L. W. FRITZ, R. C. HOBBS, Y. V. IVASHCHENKO, A. S. KENNEDY, J. M. LONDON, S. A. MIZROCH, R. R. REAM, E. L. RICHMOND, K. E. W. SHELDEN, R. G. TOWELL, P. R. WADE, J. M. WAITE, and A. N. ZERBINI. 2017. Alaska marine mammal stock assessments, 2016, 366 p. NTIS No. PB2017-102381

354 HELKER, V. T., M. M. MUTO, K. SAVAGE, S. TEERLINK, L. A. JEMISON, K. WILKINSON,and J. JANNOTT. 2017. Human-caused mortality and injury of NMFS-managed Alaska marine mammal stocks, 2011-2015. U.S. Dep. Commer., NOAA Tech. Memo. NMFS-AFSC-354,112 p. NTIS No. PB2016102765.

353 CONNER, J., D. G. NICHOL, and R. R. LAUTH. 2017. Results of the 2015 eastern Bering Sea continental shelf bottom trawl survey of groundfish and invertebrate resources,154 p. NTIS No. PB2017-102385.

352 CONNER, J., and R. R. LAUTH. 2017. Results of the 2016 eastern Bering Sea continental shelf bottom trawl survey of groundfish and invertebrate resources,159 p. NTIS No. PB2017-102386.

351 GODDARD, P., R. E. WILBORN, C. N. ROOPER, K. WILLIAMS, and R. TOWLER. 2017. Results of the 2012 and 2014 underwater camera surveys of the Aleutian Islands, 505 p. NTIS No. PB2017-102387.

350 CONNER, J., D. E. STEVENSON, and R. R. LAUTH. 2017. Results of the 2014 eastern Bering Sea continental shelf bottom trawl survey of groundfish and invertebrate resources, 154 p. NTIS No. PB2017-102195.

349 von SZALAY, P. G., N. W. RARING, C. N. ROOPER, and E. A. LAMAN. 2017. Data Report: 2016 Aleutian Islands bottom trawl survey. U.S. Dep. Commer., NOAA Tech. Memo. NMFS-AFSC-349, 161 p. NTIS No. PB2017-102170.

348 BARBEAUX, S. J. 2017. Visualization of ontogenetic and interannual distributional shifts of groundfish from the Alaska Fisheries Science Center eastern Bering Sea bottom trawl survey, 1982-2015, 330 p. NTIS No. PB2017-102169.

347 BARBEAUX, S. J., D, FRASER, L. W. FRITZ, and E. A. LOGERWELL. 2017. Cooperative multispecies acoustic surveys in the Aleutian Islands, 57 p. NTIS No. PB2017-102168.

346 GEARIN, P. J., S. R. MELIN, R. L. DELONG, M. E. GOSHO, and S. J. JEFFRIES. 2017. Migration patterns of adult male California sea lions (*Zalophus californianus*), 27 p. NTIS No. PB2017-102167.

345 KONDZELA, C. M., J. A. WHITTLE, S. C. VULSTEK, HV. T. NGUYEN, and J. R. GUYON. 2017. Genetic stock composition analysis of chum salmon from the prohibited species catch of the 2015 Bering Sea walleye pollock trawl fishery and Gulf of Alaska groundfish fisheries, 65 p. NTIS No. PB2017-101434.